"Analysing the Role of *Short Stop* during the Formation of Synaptic Terminals in *Drosophila melanogaster*"

Dissertation
zur Erlangung des Grades
Doktor der Naturwissenschaften

Am Fachbereich Biologie
Der Johannes Gutenberg-Universität Mainz

Michael Mende
Geboren am 29.01.1974
in Abidjan, Elfenbeinküste

Mainz, März 2004

Tag der mündlichen Prüfung: 07 Juni 2004

CHAPTER INDEX

FIGURE INDEX

TABLE INDEX

1. INTRODUCTION

1.1. Significance of synapses for the function of the nervous system

The nervous system is a complex organ composed of distinct cell types with numerous functions. Sensory neurones mediate perception of information. Interneurones integrate and process this information. Integration and processing lead eventually to a coordinated stimulation of muscles and glands, mediated by motor neurones and neurosecretory cells, respectively. Within this system glial cells have supportive functions, including the maintenance of the ionic milieu of nerve cells and the modulation of neuronal activity (Araque et al., 1999).

Neurones do not function in isolation, the different neuronal cell types are organised into circuits. Neurones form long processes (axons) making specific contacts with other nerve cells, muscles or glands. Neurones use a conserved mechanism for signalling within the cell: the action potential, a large, all-or-none, regenerative electrical event (Albright et al., 2000). The points of contact at which these electrical messages are passed on to other neurones, muscles or glands are the synapses (Sherrington, 1906). Two types of synapses are known: the electrical synapse (gap junction) and the chemical synapse. Several lines of evidence suggest that at most synapses within circuits, signalling between neurones - synaptic transmission - is chemical in nature (Albright et al., 2000). In the signal-sending (presynaptic) neurone incoming action potentials trigger opening of voltage gated calcium channels. Transiently inflowing calcium modifies certain presynaptic molecules, which in turn mediate fusion of presynaptic vesicles with the cell membrane. These vesicles contain and release neurotransmitters which diffuse across the synaptic cleft and bind to postsynaptic receptors. These receptors translate the message back into an electrical signal by inducing ion currents across the membrane. Depending on the type of receptor channel the inflowing ions can be of different charges. This will determine whether transmission is excitatory or inhibitory. Synapses do not merely transduce signals. By converting an electrical signal into chemical

information and back into an electrical signal, they represent sites for signal modulation and filtration. This property of signal processing is essential for the regulation of information flow within neuronal circuits. It is prerequisite for neural circuits to function appropriately in the mature brain and an essential feature underlying phenomena like learning and memory. The study of synapses and synapse formation is therefore essential for the understanding of how neuronal circuits develop and function.

A significant number of gene products and transmitters localised at the synapse have been described so far (Albright et al., 2000; Goda and Davis, 2003; Murthy and De Camilli, 2003; Prokop, 1999, and citations therein). These synaptic components comprise molecules involved in synaptic architecture (e.g. clustering of synaptic elements, adhesion or shape), molecules conferring the electrical properties to cell membranes (e.g. voltage gated ion channels), releasable transmitters and neuropeptides, proteins involved in transmitter metabolism, components required for regulation of the synaptic vesicle cycle, metabotropic and ionotropic receptors for transmitters and neuropeptides, and components involved in signalling and second messenger pathways. Many of these components are specific to or enriched at synapses and can therefore be used as marker molecules for the visualisation of synapses. For example, antibodies to the vesicle proteins Synaptotagmin (Syt, Littleton et al., 1993a; Littleton et al., 1993b) and Synapsin (Syn, Klagges et al., 1996), the clustering molecule Disc large, (DLG, Budnik et al., 1996), and the adhesion molecule Fasciclin II (FasII, N-CAM homologue; Grenningloh, 1991; Halpern et al., 1991) were used as synaptic markers in the course of this study.

1.2. Problem leading up to this work

It becomes apparent that much is known about synaptic function and the factors involved therein. However, the mechanisms underlying the structural differentiation of synapses and the precise assembly of functional synaptic components during development remain poorly understood.

The differentiation of synapses encompasses the following regulatory steps (Albright et al., 2001; Chiba, 1999; Prokop, 1999; Sanes and Lichtman, 1999):

- Target recognition: the correct contacts need to be established

- Consolidation of contact: once the right target has been reached the terminal has to remain in contact with its counterpart through installation of appropriate adhesion properties. Interactions between pre- and postsynaptic sides as well as intrinsic developmental mechanisms initiate the arborisation of the terminal through remodelling of the cytoskeleton.

- Functional differentiation: functional proteins are precisely arranged at the synapse, thus establishing the pre-and postsynaptic apparatus of transmission.

In order to understand the development of the neuronal circuits it is necessary to clarify the cellular and molecular mechanisms that give neurones the ability to establish and differentiate these precise and selective connections with their specific synaptic partners. To do so, one needs to identify the structural and molecular components required at the developing synapse and the gene regulatory events that provide them. This requires convenient models in which the differentiating synapse is accessible to combinations of experimental and genetic manipulations.

Essential insights into synaptic development were obtained from work on the vertebrate neuromuscular junction (NMJ; Sanes and Lichtman, 1999). For instance, molecules promoting synapse formation have been identified, some of which derive presynaptically (some Agrin isoforms and Neuregulin, Campagna et al., 1995; Rüegg and Bixby, 1998), others postsynaptically (e.g. Agrin isoforms and S-Laminin; Campagna et al., 1995; Noakes et

al., 1995), acting as organisers for the post- or presynaptic partner, respectively (Patton et al., 1998). However, the NMJ is a very special synapse. Mechanisms underlying the formation of the NMJ do not necessarily apply to all types of synapses. Therefore more models are required. Other types of synapses that have been established as models are glutamatergic synapses of the CNS (Garner et al., 2002), hippocampal cultures (Ahmari et al., 2000; Dalva et al., 2000; Rao et al., 2000), ribbon synapses of vertebrate retina (Allwardt et al., 2001; Ruether et al., 2000; Schmitz et al., 2000), synaptic contacts in the cerebellum (Hall et al., 2000; Scheiffele et al., 2000), or neurones of the autonomous nervous system (Ernsberger and Rohrer, 1999). However, in contrast to the vertebrate NMJ, so far very little insights have been gained from any of these models for the structural differentiation of synapses.

1.3. *Drosophila melanogaster* as a model system for studying the cellular and molecular mechanisms of synaptic development

Also invertebrate synapses have been established successfully as model system for the analysis of synaptic development, such as the neuromuscular system of *Caenorhabditis elegans* (Broadie and Richmond, 2002; Brockie and Maricq, 2003; Richmond and Broadie, 2002) and *Drosophila melanogaster* (Chiba, 1999; Keshishian et al., 1996). For several reasons *D. melanogaster* is a suitable organism for the investigation of molecular mechanisms underlying synapse formation. Genetic analysis, i.e. access to genes involved in synapse formation, is efficient. The genome of *D. melanogaster* has been entirely sequenced (Adams et al., 2000). Specific mutations and transgenic flystocks for a high number of so far described genes are made available through particular databases (Ashburner, 1989; Budnik and Gramates, 1999; FlyBase, 1999). The analysis of double and triple mutations allows one to define functional interactions between different genes (see Chapter 3.6.1. CA *Dcdc42*^{V12}*;shot*). Another experimental genetic tool in *D. melanogaster* is the Gal4/UAS system for targeted gene expression (Brand and Perrimon, 1993). It allows the expression of optional genes in defined cell types. The system was applied in this study in order to vary expression levels of certain factors involved in synapse formation in subsets of motor neurones. It was further used to express membranous cell marker proteins for the purpose of visualising these subsets of cells exclusively. The principle of the method is outlined in Chapter 2.1.4. Phenotypic characterisation of embryos genetically manipulated through

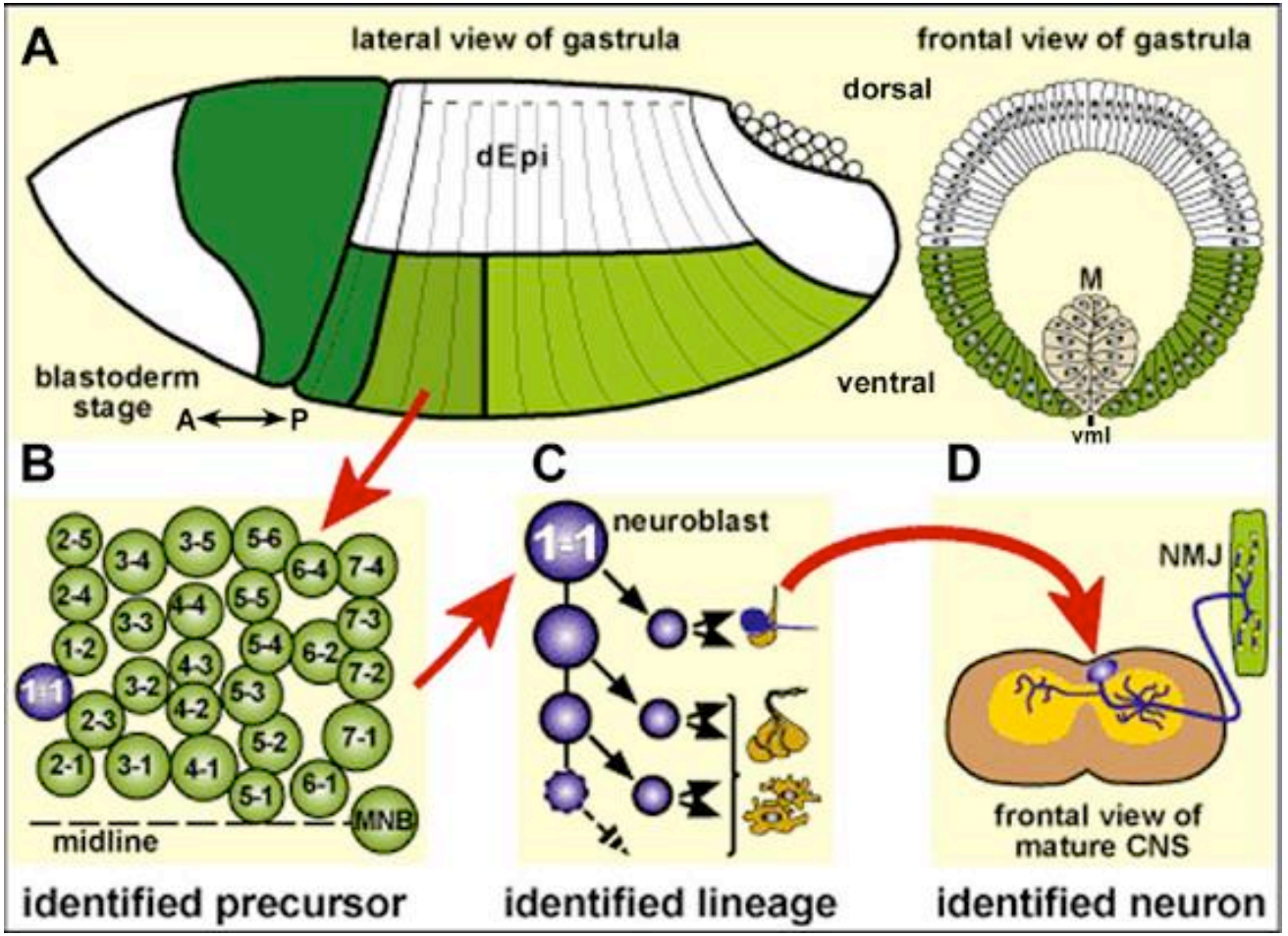
A
lateral view of gastrula
frontal view of gastrula
dorsal
dEpi
M
ventral
vml
blastoderm stage
A
P
B
C
D
1-1
neuroblast
NMJ
midline
MNB
frontal view of mature CNS
identified precursor
identified lineage
identified neuron

mutation or targeted expression of genes can be used to test *in vivo* functions of putative molecules during synaptogenesis (Brand and Dormand, 1995; Broadie et al., 1993; Prokop et al., 1996; Wolf et al., 1998).

D. melanogaster has the advantage of insects, where individual cells can be identified and examined with single cell resolution (Figure 1.1). The development of *D. melanogaster* nervous system has been thoroughly characterised and its morphology extensively studied (Bate and Martínez-Arias, 1993; FlyBase, 1999; Weigmann et al., 2003). In combination with different tools which are available to visualise specific morphological aspects, such as antibodies and markers, genetic approaches can be employed to analyse the development and structural properties of various parts of the nervous system, for example the motor neurones (Keshishian et al., 1996), the peripheral nervous system (PNS, Gao et al., 1999), and the CNS axon pattern (Landgraf et al., 2003).

Figure 1.1: *Drosophila* neurones can be analysed at the identified cell level. The *Drosophila* CNS originates from the neuroectoderm (dark, middle, and light green areas in A, giving rise to CNS in head, thorax and abdomen, respectively; Segment borders are indicated by vertical lines, dEpi dorsal epidermis) lying on either side of the ventral midline (vml; M mesoderm). Within the neuroectoderm a subset of cells assume neuronal stem cell properties and delaminate internally. As a result, stereotyped arrays of neuroblasts (NBs) form directly dorsal to the ventral ectoderm. At about stage 11 (6 hours after egg laying) a full complement of 30 NBs becomes visible in each segment (numbered circles in B). Each NB is unique in terms of its position, time of formation and pattern of gene expression and undergoes NB specific cell devisions, giving rise to a reproducible number of neurones and/or glia cells (example shown for blue NB 1-1, C). Single neurones within these lineages can be identified and individually monitored or manipulated (D; colour code: brown, cortex; orange, neuropile; green, muscle; NMJ neuro muscluar junction). A-P indicates the anterior-posterior axis. Source: http://www.prokop.biologie.uni-mainz.de/

For several reasons this work has focused on the *Drosophila* embryo as a model system: The origin of many identifiable neurones can be traced back, allowing integrated evaluation of early and late developmental events. Studies in the embryo allow the investigation of mechanisms underlying synapse formation when neuronal contacts are established *de novo*. Additionally, phenotypes of embryonic lethal mutations can be analysed.

Several model synapses for the study of synapse formation in the embryo have been established to date. The best characterised synapse in *D. melanogaster* so far is the NMJ (Budnik and Gramates, 1999; Chiba, 1999; Keshishian et al., 1996). NMJs are experimentally easily accessible due to their peripheral localisation. The reproducible and invariant NMJ pattern, that results from specific projections of each motor neurone per hemisegment to one or more muscle fibres (Figure 1.2; Landgraf et al., 1997; Sink and Whitington, 1991), serves as a strong readout for genetic and experimental work. This, in conjunction with the overall organisation of the fly allows observation of the same sequence of events repeated many times within a single animal, which facilitates the quantitative analysis of the development of identified motor neuronal projections. However, the NMJ has the disadvantage, that mechanisms underlying the structural differentiation of neuronal postsynapses cannot be studied. Moreover, with the exception of neuropeptides and potential neuromodulators, glutamate appears to be the only neurotransmitter at the NMJ (Johansen et al., 1989). Synapses in the CNS are known to have an essentially higher variety of neurotransmitters (Prokop, 1999). Thus, mechanisms underlying synaptogenesis in non-glutamatergic terminals can only be studied at synapses of the CNS. In contrast to the NMJ, central synapses are difficult to access. Central synapses are localised in high density within the neuropile, which is enwrapped by the cell body containing cortex (Figure 1.2). Nonetheless, different strategies to access central synapses of individual neurones or subsets of neurones are available. Genetic mosaic analysis for example allows the visualisation of individual synapses and projections of subsets of neurones within the CNS, and revealed that pre- and postsynaptic compartments are restricted to specific segments of *Drosophila* central neurones (Löhr et al., 2002). Primary cell cultures of *Drosophila* embryos on the other hand, provide higher cellular resolution and accessibility of *in vivo* dyes and imaging markers (Küppers et al., 2002).

Several of the techniques mentioned above have led to the identification of a number of cellular mechanisms involved in axonal growth and guidance (Bate and Broadie, 1995; Chiba, 1999) and allowed the description of synaptic function in considerable detail (Broadie, 1999; Prokop, 1999; Rodesch and Broadie, 2000; Wucherpfennig et al., 2003). In contrast, only little is known about synapse formation in *D. melanogaster.*

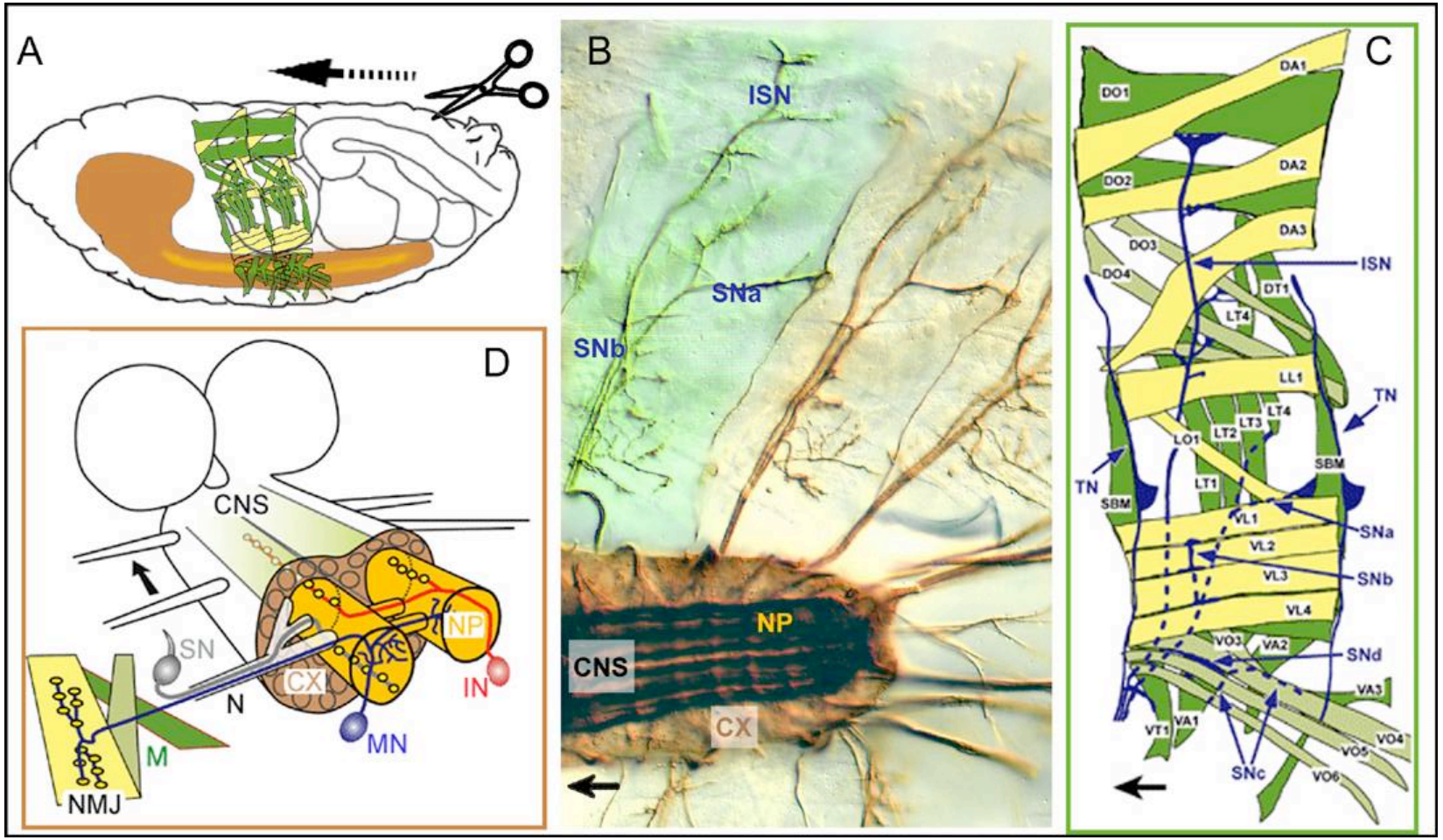
A
B
C
D
ISN
SNa
SNb
NP
CNS
CX
DA1
DO1
DA2
DO2
DA3
DO3
DO4
DT1
LT4
LL1
TN
LT3
LT2
LO1
SBM
LT1
VL1
VL2
VL3
VL4
SNd
VO3
VA2
VA3
VT1
VA1
VO4
VO5
VO6
SNc
CNS
SN
N
M
NMJ
MN
IN

So far, it is known that the basic components of the presynaptic machinery assemble independently of intercellular communication but localise properly only in response to inducing signals from the postsynaptic site. This was for example shown using mutant embryos, which lack all or a considerable part of their muscles. In these embryos the assembly of the NMJ presynaptic active zone occurs independently of the target cell but the synaptic localisation of the active zone requires a potential muscle derived *mef2* (*myocyte enhancer factor 2*)- dependent retrograde signal (Prokop et al., 1996).

Other studies used mutations that specifically affected presynaptic cells. It was shown that when delaying innervation, early developmental events at the postsynaptic side, involving the expression of functional glutamate receptors or cell adhesion molecules FasIII and Connectin, still occur. Also, following denervation, the electrical and contractile properties of the muscle still develop. However, the differentiation of mature postsynaptic properties and synaptic patterning requires the presence of a functional motor neurone (Broadie and Bate, 1993a; Broadie and Bate, 1993b; Featherstone et al., 2000), as is the case in vertebrates (though through different mechanisms, Hall and Sanes, 1993).

Figure 1.2: Localisation of CNS, muscles and synapses in the late embryo of *D. melanogaster*. A latereal view of a stage 17 embryo, highlighting the CNS (orange) and muscles of two hemi-segments (green). Anterior is to the left, dorsal to the top. Upon cutting open along the dorsal midline (dotted arrow), opening flat each side and removing the inner organs, the CNS and nerve patterns are revealed as shown in B for a real specimen at late stage 17 stained with the *Drosophila* N-CAM homologue Fasciclin II (nomenclature see below). The hemisegment highlighted in green is represented as scheme in C. Muscles (green/yellow) represent single fibres which are named individually (black in white boxes; see Landgraf et al., 1997) and innervated by reproducible nerve branches (blue). Dorsal muscles are innervated by the intersegmental nerves (ISN), lateral and ventral muscles by segmental nerves (SN), respectively. The transverse nerve (TN) is a mixed motor and sensory projection with efferent axons that innervate muscle fibres in mid body wall regions. D shows details of the central nervous system (CNS); Interneurons (IN) and motor neurons (MN) lie in the cell body layer of the CNS (cortex, CX), sensory neurons (SN) in the periphery. All send processes towards the synaptic neuropile (NP). Efferent motorneurons project through segmental nerves (N) towards muscles (M) where they form neuromuscular junctions (NMJ). Black arrows indicate anterior. Picture C modified from Landgraf et al., 2003, pictures B and D modified from http://www.prokop.biologie.uni-mainz.de/index.html.

Other reported studies attempted to describe the molecules and mechanisms behind the aggregation and alignment of pre- and postsynaptic components at the precisely opposed sites of the synapse. Proteins in the membrane-associated guanylate kinases (MAGUKs) family for example have clustering function at glutamatergic synapses. They are composed of a number of modular domains involved in protein-protein interactions, such as PDZ repeats (first discovered in **P**SD95/SAP90, **D**lg, and **Z**O1), src homology 3 (SH3) domain, a HOOK domain, and a guanylate kinase-like (GUK) domain. The MAGUKs potentially link the cytoskeleton, components involved in transmission and membrane spanning proteins, which bind to similar complexes on the other side of the synaptic cleft (Budnik et al., 1996; Thomas et al., 2000; Thomas et al., 1997).

Despite the finding of some aspects of synapse formation, the mechanisms underlying the organisation of structural and functional components at the differentiating synapse or synaptic compartment remain unresolved. One key player has been described recently, the Plakin family member protein Short stop (Shot, also known as Kakapo or Groovin; Prokop et al., 1998b). As detailed in the next Chapter, Shot is essential for the structural formation of synapses in the *Drosophila* embryo. Understanding the role of Shot during synaptogenesis will therefore shed more light onto the mechanisms underlying synapse formation.

1.4. *Short stop* phenotypes and its relevance for synapse formation

Embryos carrying loss of function mutations of *shot* display various phenotypes, amongst them some of pivotal interest in the context of synapse formation: motor neuronal and sensory axons stall before reaching their target sites (Lee et al., 2000a; Lee and Luo, 1999; vanVactor et al., 1993), motor neuronal terminals do not expand and fail to assemble appropriate numbers of presynaptic structures (Prokop et al., 1998b), and *shot* mutant motor neuronal sidebranches in the CNS or dendrites of sensory neurones are reduced in size (Gao et al., 1999; Prokop et al., 1998b). Furthermore, the transmembrane adhesion molecule FasII is incorrectly localised along neuronal processes. At the ultrastructural level, electron dense material within presynaptic terminals is found missing, and a specific type of sensory neurones (scolopidial neurones) display disorganised microtubule cytoskeleton (Prokop et al., 1998b). Hence, Shot influences both cytoskeletal organisation and localisation of transmembrane proteins. Interestingly, the *shot* mutant phenotype affects neuronal growth during the phase of pathfinding/target recognition and synaptic differentiation likewise. It either plays two independent roles in both contexts or it is an essential player during the transition phase from the growth cone structure to local branching and arborisation into presynaptic structures of the mature terminal. Understanding the function of Shot seems an opportunity to reveal mechanisms underlying the organisation of structural and functional proteins during the different phases of synapse formation.

Shot has also been found to affect non-neuronal tissues, like the epidermis or the trachea (Gregory and Brown, 1998; Lee and Kolodziej, 2002a; Strumpf and Volk, 1998). Shot is potentially the largest gene in the fly genome, covering more than 69 kbp (Adams et al., 2000). The properties of the transcript place Shot into the Spectraplakin family of proteins (Fuchs and Karakesisoglou, 2001; Gregory and Brown, 1998; Röper et al., 2002; Strumpf and Volk, 1998). Running from N- to C- terminus the main domains of Shot comprise an Actin Binding Domain (ABD), a Plakin domain (that is present in all known isoforms), a Spectrin repeat domain constituting the central Dystrophin-like Coil, two EF Hand calcium binding motifs and a Gas2 homology domain (see Figure 1.3). Shot has close mammalian homologues called MACF1 (Human Microtubule and Actin Cross Linking Factor 1, also known as ACF7,

Macrophin and four others; Karakesisoglou et al., 2000; Leung et al., 1999; Röper et al., 2002) and BPAG1/dystonin (Bullous Pemphigoid AntiGen 1, neural isoform to the mouse *dystonia musculorum* gene; Bernier et al., 1995; Brown et al., 1995; Guo et al., 1995). Members of the Spectraplakin family of proteins are generally believed to orchestrate cellular development and maintenance by linking factors like microfilaments, microtubules, intermediate filaments, cell-adhesion molecules and others (for review see Leung et al., 2002). Indeed the Gas2 homology domain and the ABD of Shot and its mammalian homologue MACF1 are capable of associating with Tubulin and Actin in culture, respectively. Furthermore, the N-terminus of both proteins can bind these respective cytoskeletal components directly *in vitro* (Karakesisoglou et al., 2000; Leung et al., 1999). However, given the complexity of phenotypes seen in *shot* mutant embryos (see above), its additional domains, its enormous size, the variety of different splice versions (Gregory and Brown, 1998; Lee et al., 2000a), and the precedents set by other members of the Plakin family, its molecular interactions would be expected to involve a larger palette of binding partners, and each cellular or developmental context could potentially involve distinct forms of interactions. The discovery of molecules which interact with Shot during the processes leading to formation of synapses or synapse compartments will enhance the understanding of Shot (and MACF1) function at the molecular level.

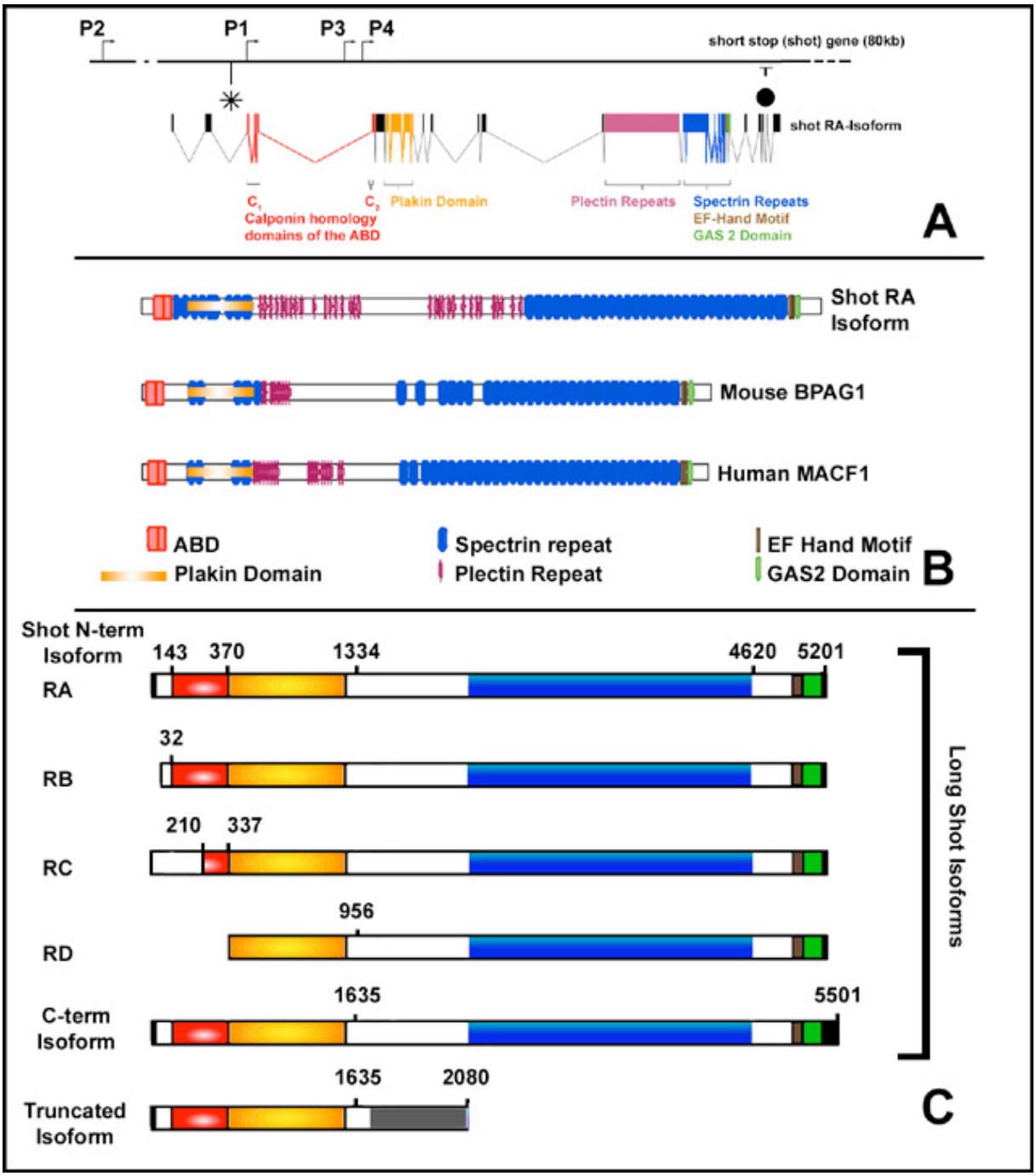
P2
P1
P3
P4
short stop (shot) gene (80kb)
shot RA-Isoform
C1
C2
Calponin homology
domains of the ABD
Plakin Domain
Plectin Repeats
Spectrin Repeats
EF-Hand Motif
GAS 2 Domain
A
Shot RA
Isoform
Mouse BPAG1
Human MACF1
ABD
Plakin Domain
Spectrin repeat
Plectin Repeat
EF Hand Motif
GAS2 Domain
B
Shot N-term
Isoform
RA
143
370
1334
4620
5201
RB
32
RC
210
337
RD
956
C-term
Isoform
1635
5501
Truncated
Isoform
1635
2080
Long Shot Isoforms
C

Figure 1.3: *shot* gene structure and protein isoforms. The *shot* gene is shown in A. It is located on chromosome 2 and has been mapped cytogenetically to 50C6-11. The boxes indicate the exons transcribed for Shot isoform RA (Ensembl Gene Annotation CG18076). Small arrows show alternative starts of transcription (P2, P1, P3, P4). Different alternative transcripts are not shown. Colour of the exons reflect the protein domains encoded as shown in B and C. Names of the different domains encoded are written below. ✳ indicates site of P-element insertion in the *shot* mutant allele $shot^{kakP2}$, • indicates the mutational event that was reported to cause alterations within the last 280 amino acids of the $shot^{V104}$ mutant protein (see chapter 3.1; Strumpf and Volk, 1998). The Shot protein and its mammalian homologues (BPAG1, MACF1) are shown in B (modified from Röper et al., 2002). The strucural domains which are highly conserved are shown in coloured boxes. Running from N-to C-terminus one finds the actin binding domain (ABD) consisting of two Calponin homology domains (see A), the common Plakin domain, the Plectin repeat domain, the Spectrin (or Dystrophin) repeat domain, EF Hand Ca^{2+} binding motifs and the GAS 2 domain. C shows simplyfied cartoons (used as reference henceforth in this study) of some of the predicted isoforms encoded by the *shot* gene. Four different N-terminal sequences have been identified (Lee et al., 2000a), containing complete (RA and RB), partial (RC) or no ABD (RD). Alternative splicing can lead to variances in the length of the coiled-coil sequence following the Plakin domain. Alternative splicing at the C-terminal domain generates additional diversity or truncated isoforms. The numbers at the barcodes refer to the amino acid residues at the junction of the different protein domains for each isoform depicted.

1.5. Aims of this study and brief summary of its outcome

The aim of this study is to investigate the function of the Spektraplakin protein Shot during the structural differentiation of synaptic terminals in *D. melanogaster*. Spectraplakins are proposed to exert their functions through multiple protein interactions mediated by their different modular domains. Here, I tried to pinpoint those Shot protein domains, which are required for the formation of synaptic terminals. To this end I used several cell biological approaches: Different independently isolated *shot* mutant alleles, for which molecular information about the mutational events is partially available, were analysed using several markers for synaptic proteins. Additionally, different tagged Shot protein domains were misexpressed in neuronal tissues using the UAS/Gal4-system and their localisation studied. Also, immunohistochemical studies using antibodies specific to different Shot protein domains were carried out. Furthermore, I intended to unravel binding partners of Shot protein domains and investigate the way they interact with Shot. So far, I carried out a yeast-two hybrid screen. Moreover, I followed an alternative strategy, in which synapses of mutant embryos were analysed, which were previously reported to display early developmental phenotypes reminiscent of *shot* mutant embryos.

Indeed, the different approaches used in this work suggest Shot to make use of its different domains in different developmental contexts and that the N-terminus of Shot is essential for the formation of synaptic terminals. In addition, the strategies I used uncovered several interaction candidates, which provide a sound basis for further investigation into the machinery underlying the structural differentiation of synaptic terminals.

2. MATERIALS AND METHODS

2.1. Fly genetics and Cellbiology

2.1.1. Fly stock maintenance

Fly stocks were maintained in vials containing standard *Drosophila* food media (Greenspan, 1997). Stocks maintained at 25°C were transferred to fresh vials every two weeks and the ones maintained at 18°C were transferred every 4-5 weeks.

2.1.2. Fly stocks

Fly stocks used for the work of this thesis are listed in Table 2.1. A considerable number of mutant alleles studied in this thesis were homozygous embryonic lethal. In order to keep these fly stocks viable, conventional balancer chromosomes were used (FlyBase, 1999; Greenspan, 1997).

Table 2.1.: List of all flystocks used.

Name and Genotype	Origin	Reference
Balancer 2nd Chromosome *CyO Kr-UAS-GFP (**CyO**^{gr})/Dr*	Mainz-Stock Collection	O. Vef
Balancer 3rd Chromosome *Tm3 Kr-UAS-GFP/D* *w¯;CyOStar/Pm*	All Mainz Stock Collection	O. Vef
Double balancer *Fm7 Kr-UAS-GFP(**FM7**^{gr})/M ;* ***CyO**^{gr}/ScO*	A. Prokop	
Deficiencies: *Df(2L)E55, rdo[1] hk[1] Lar[E55] pr[1]/CyO* *Df(2L)TW50,cn(1)/CyO,Dp(2;2)M(2)m (+)* *Df(2L)TW158, cn[1] bw[1]/CyO* *Df(2L)VA23,noc(Sco)pr(1)/CyO* *Df(2R)HK1/ **CyO**^{gr}*	Bloomington Stock Centre Bloomington Stock Centre Bloomington Stock Centre Bloomington Stock Centre A. Prokop	(Prokop et al., 1998b)
PS Integrin mutant allele:		

mys^{XG43}*/FM7*	A. Prokop	
shot mutant alleles:		
shot^{el3}***/CyO***^{gr}	A. Prokop	(Prokop et al., 1998b)
shot^{HG25}***/CyO***^{gr}	A. Prokop	(Prokop et al., 1998b)
shot^{kakP2}***/CyO***^{gr}	Bloomington Stock Centre	(Lee et al., 2000a)
shot^{SF20}***/CyO***^{gr}	A. Prokop	(Prokop et al., 1998b)
shot^{91K}***/CyO***^{gr}	A. Prokop	(Prokop et al., 1998b)
shot^{3}***/CyO***^{gr}	Bloomington Stock Centre	(Lee et al., 2000a)
shot^{V104}***/CyO***^{gr}	T. Volk	(Strumpf and Volk, 1998)
shot^{V168}***/CyO***^{gr}	T. Volk	(Strumpf and Volk, 1998)
Gal4-Stocks:		
Dopadecarboxylase-(DDC)-Gal4	Mainz Stock Collection	(Li et al., 2000)
UAS-CD8-GFP; even-skipped (eve)^{RN2E}*-Gal4*	N. Sanchez-Soriano	
Cyo/if;eve^{RRK}*-Gal4/Tm6b*	A. Prokop	(Baines et al., 1999)
elav^{C155}*-Gal4*	Mainz Stock Collection	(Lin and Goodman, 1994; Luo et al., 1994)
MJ94-Gal4/Fm7;syn^{97}	A. Prokop	(Joiner and Griffith, 2000)
OK6-Gal4	N. Sanchez-Soriano	
UAS-CD8-GFP; Stripe-Gal4/Tm6b	T. Volk	(Strumpf and Volk, 1998)
Mz-VUM-Gal4	Mainz Stock Collection	(Ito et al., 1995)
24B-Gal4	Mainz Stock Collection	
UAS-Stocks		
UAS-Cdc42^{N17}	E. Martin-Blanco	(Luo et al., 1994)
UAS-Cdc42^{V12}	E. Martin-Blanco	(Luo et al., 1994)
UAS-GFP-Cdc42^{V12}	A. Chiba	
UAS- GFP-Cdc42^{WT}	A. Chiba	
Pin/Cyo; UAS-CD8-GFP	R. Löhr	(Lee and Luo, 1999)
UAS-DPxnIR2-1	R. Yagi	
UAS-DPxnIR2-7	R. Yagi	
UAS-DPxn^{GFP} (2nd Chromosome)	R. Yagi	
UAS-DPxn^{GFP} (3rd Chromosome)	R. Yagi	
UAS-Drac^{N17}	E. Martin-Blanco	(Luo et al., 1994)

UAS-Drac^{V12}	E. Martin-Blanco	(Luo et al., 1994)
UAS-DRac1GAP^{WT}/CyO^{gr}	S. Sotillos	(Sotillos and Campuzano, 2000)
UAS-DRac1GAP$^{\Delta EIE}$	S. Sotillos	(Sotillos and Campuzano, 2000)
UAS-DRac1GAP^{R417Q}	S. Sotillos	(Sotillos and Campuzano, 2000)
Wildtype Oregon R	Mainz Stock Collection	(Lindsley, 1992)

Table 2.1.: List of all flystocks used.

The majority of the mutant alleles used here were carried over a green balancer chromosome (a balancer chromosome carrying a P-element insertion that drives the expression of the *Aequorea victoria* Green Fluorescent Protein [GFP] under the control of a specific promoter, Chalfie et al., 1994; Yeh et al., 1995). Thus a homozygous mutation in an embryo could be identified by selection against green fluorescence emission (527 nm wavelength) upon excitation at wavelength of 490 nm.

2.1.3. Virgin collection and genetic crosses

For genetic crosses it is of importance to use virgin female flies. Upon hatching, females are separated from males, transferred and kept in a new vial. Therefore, collection has to occur before the flies become fertile: at least every six hours, if stocks are kept at 25°C, at least every 12 hours if kept at 18°C.

For setting up crosses between two strains, female virgins were always crossed to males of the other strain and allowed to mate for 2 days. If the embryos of this cross were needed for antibody staining the flies were then placed in a vial for egg laying and, if the progeny of the cross were needed for subsequent crosses, the parent flies were allowed to lay eggs in standard vials and removed when enough larvae were produced.

2.1.4. Ectopic gene expression in embryos and larvae

For a number of experiments the *Gal4/UAS* System (Brand and Perrimon, 1993) was used for tissue targeted expression. This system requires on the one hand flies that express the yeast transcriptional activator *Gal4* under the regulation of an endogenous promoter (driver stock), and on the other hand flies that carry a transgene of interest whose expression is regulated by the *Gal4* Upstream Activation Sequence (*UAS*; *UAS* stock). When the driver and *UAS* stock are crossed together, the transgene of interest is expressed in the same pattern as the *Gal4* protein. Thus, ectopic expression of the transgene depends on the enhancer that regulates *Gal4* expression.

Transgenes expressed were coding for wildtype or mutant isoforms of proteins of interest. In cases where the GFP tagged membranous marker molecule CD8 was expressed simultaneously for the visualisation of the Gal4-driving cells, embryos could be selected for green fluorescence emission (see 2.1.2.).

2.1.4.1. Localisation of GFP tagged DCdc42 isoforms in *shot* mutant background

These crosses were set up in order to study the localisation of misexpressed GFP-tagged isoforms of the small GTPase DCdc42 in *shot* mutant background (see Results, Chapter 3.6.1.).

The first cross combined mutant allele $shot^{SF20}$ with eve^{RRK}-*Gal4*, from the resulting F1 generation flies were selected against the markers *irregular facets* (*if*) and GFP (see Chapter 2.1.2.), resulting in a population of genotype shown in the black box.

(i) P ♀ $\frac{shot^{SF20}}{CyO^{gr}}$ ***X*** ♂ $\frac{CyO;\ eve^{RRK}\text{-}Gal4}{if\quad Tm6b}$ ➔ $\boxed{\frac{shot^{SF20};\ eve^{RRK}\text{-}Gal4}{CyO\qquad +}}$

P, Parental generation
F1; first filial generation

F1

The second cross was set up in parallel and combined the *shot* mutation kak^{SF20} with *UAS*-GFP-$Cdc42^{V12}$. Flies of the progeny were selected against the balancer CyO (black box).

(ii) P ♂ $\frac{shot^{SF20}}{CyO^{gr}}$ ***X*** ♀ $\frac{+;\ UAS\text{-GFP-}DCdc42^{V12}}{+\ \ UAS\text{-GFP-}DCdc42^{V12}}$ ➔ $\boxed{\frac{shot^{SF20};\ UAS\text{-GFP-}DCdc42^{V12}}{+\qquad +}}$

F1

Virgin females of one F1 generation were crossed to males of the other F1 generation. Embryos from this cross were selected for *shot* mutant phenotype (no hatching) and GFP-tagged construct expression (see Chapter 2.1.2.) and dissected as described in Chapter2.1.7.2.:

➔ **(iii)**

$\boxed{\frac{shot^{SF20};\ UAS\text{-GFP-}DCdc42^{V12}}{shot^{SF20}\qquad eve^{RRK}\text{-}Gal4}}$

This crossing scheme was applied as well to study localisation of misexpressed *UAS*-GFP-$DCdc42^{WT}$ in kak^{SF20} mutant background.

2.1.4.2. Generation of *mys/shot* double mutant

mys;shot double mutants were established in order to study the localisation of Shot and *Drosophila* Paxillin (DPxn) at the myotendineous junction (Chapter 3.5.1.). Both mutations were first crossed to double balancer flies, crosses (i) and (ii), before being combined (iii). After each cross the flies were selected for the genotypes indicated in the black boxes.

(i) P ♂ $\frac{shot^3}{CyO^{gr}}$ **X** ♀ $\frac{FM7^{gr}; CyO^{gr}}{M \quad ScO}$ ➔ $\boxed{\frac{FM7^{gr}; shot^3}{♂ \quad ScO}}$ F1

(ii) P ♂ $\frac{FM7^{gr}; CyO^{gr}}{M \quad ScO}$ **X** ♀ $\frac{mys^{XG43}}{Fm7}$ ➔ $\boxed{\frac{mys^{XG43}; CyO^{gr}}{FM7^{gr} \quad +}}$ F1

(iii) ♂ F1(i) **X** ♀ F1 (ii) ➔ $\boxed{\frac{mys^{XG43}; shot^3}{FM7^{gr} \quad CyO^{gr}}}$

2.1.4.3. Recombination of *Df(2L)VA23* with *UAS-DPxn^{GFP}*

Both the deficiency *Df(2L)VA23* and the UAS-construct *UAS-DPxn^{GFP}* are localised on the second chromosome. In order to be able to express GFP-tagged DPxn in the background of *Df(2L)VA23* (see Chapter 3.5.2.) it was necessary to combine the deficiency with *UAS-DPxn^{GFP}*. All crosses were carried out in *white$^-$* background (w^-). This mutation causes adult flies to have white eyes instead of red. The UAS-construct, however, carries a so-called *miniwhite* gene (w^+), which reverses the eye-phenotype. Hence, flies carrying the construct can be addressed by the red colour of their eyes. The deficiency *Df(2L)VA23* affects amongst others the gene *Scutoid* (Sco; see Table 2.1.). This dominant marker disrupts the Scutellar bristle pattern (FlyBase, 1999), allowing the recognition of flies heterozygous for the deficiency. In the following crossing scheme, flies resulting from the individual crosses were selected for the genotypes indicated in the black boxes.

(i) P $\frac{w^-; Df(2L)VA23}{w^- \quad CyO^{gr}}$ **X** $\frac{w^-; UAS\text{-}DPxn^{GFP}(w^+)}{Y \quad UAS\text{-}DPxn^{GFP}(w^+)}$ ➔ $\boxed{\frac{w^-; UAS\text{-}DPxn^{GFP}(w^+)}{w^- \quad Df(2L)VA23}}$ F1

At this step it is important to only use female *Df(2L)VA23/UAS-DPxn^{GFP}* flies for the next cross, because recombination occurs only within the germline of females (at random; Greenspan, 1997).

(ii) P $\frac{w^-; UAS\text{-}DPxn^{GFP}(w^+)}{w^- \quad Df(2L)VA23}$ **X** $\frac{w^-; CyO^{Star}}{Y \quad Pm}$ ➔ $\boxed{w^-; \frac{Df(2L)VA23,\ UAS\text{-}DPxn^{GFP}(w^+)}{CyO^{Star}}}$

Flies resulting from cross (ii) were selected for recombination, i.e. Sco and red eyes (w^+) and CyO. Cross (iii) stabilises the recombinant chromosome over a *CyO^{gr}* balancer.

(iii) P $w^-; \frac{Df(2L)VA23,\ UAS\text{-}DPxn^{GFP}(w^+)}{CyO^{Star}}$ **X** $\frac{Df(2L)VA23}{CyO^{gr}}$

➔ $\boxed{w^-; \frac{Df(2L)VA23,\ UAS\text{-}DPxn^{GFP}(w^+)}{CyO^{gr}}}$

Virgin flies from this newly established stock were crossed against the Gal4-driver line *eve*^{RN2E}*-Gal4,* in order to express GFP-tagged DPxn in the motor neurones aCC and RP2 in the *DPxn* deficient background.

(iv) P w^-; $\underline{Df(2L)VA23,\ UAS\text{-}DPxn^{GFP}(w^+)}$ **X** $\underline{+;\ +;}\ \underline{eve^{RN2E}\text{-}Gal4}$
CyO^{gr} +; +; Tm6b

➔ w^-; $\underline{Df(2L)VA23,\ UAS\text{-}DPxn^{GFP}(w^+);}\ \underline{eve^{RN2E}\text{-}Gal4}$
+ +

Recrossing of flies selected against the two balancer CyO^{gr} and *Tm6b* yielded amongst others the genotype shown below (v). These specimens could be selected by the strong phenotype of the deficiency and strong GFP expression due to two copies of *eve*^{RN2E}*-Gal4* (see above, Chapter 2.1.4.).

(v) ➔ $\underline{+};\ \underline{Df(2L)VA23,\ UAS\text{-}DPxn^{GFP};}\ \underline{eve^{RN2E}\text{-}Gal4}$
$+\ \ Df(2L)VA23,\ UAS\text{-}DPxn^{GFP}\ \ eve^{RN2E}\text{-}Gal4$

2.1.5. Embryo collection

To collect embryos, flies were placed in a vial containing apple juice with 2% Agar. To ensure that most embryos of one batch were synchronised in their development, flies were allowed to lay eggs for not longer than one to four hours. The egg lays were aged at 18°C, 25°C, or 29°C until the appropriate stage (staging according to) (Hartenstein, 1988). The eggs were subsequently dechorionised with 7,5% commercial bleach (sodium hypochloride) for about two minutes followed by a thorough wash with dH_2O. The embryos were then ready for further processing: either vivisection or fixation following whole mount preparation protocols (see Chapter 2.1.6.). In the first case, embryos of the appropriate stage were taken out of the water and transferred onto a block of apple juice agar using blunt forceps.

2.1.6. Whole mount preparation of 0-to 17hr embryos

The dechorionised and washed embryos are transferred into an Eppendorf tube containing PBS/Formaldehyde/Heptane in a ratio of 9/1/10, respectively. The embryos were left shaking in the solution for twenty minutes. The solution forms two layers; the lower layer is fixative, the upper layer is Heptane. The embryos come to lie at the interface of the two layers. The Heptane becomes saturated with the fixative, allowing it to penetrate the hydrophobic vitelline membrane surrounding the embryos. After incubation, the aqueous (bottom) layer was removed, replaced by methanol and the tube was vigorously agitated for twenty seconds. Due to this treatment, the vitelline membrane splits open and the fixed embryos fall to the bottom of the tube. Subsequently, the Heptane, methanol and the interface containing the vitelline membranes is removed and the devitellinised embryos are washed at least three times with methanol. The methanol washes are necessary to remove all traces of Heptane, which can interfere with the binding of antibodies. Embryos are either kept in

methanol at -20°C for extended storage, or rehydrated by removing the methanol and applying three washing steps of 5 minutes and one wash of 40 minutes with PBT, in order to proceed with antibody staining.

2.1.7. Hand dissection of living embryos and larvae

To gain better access of antibodies to inner tissues (cuticle is formed from stage 17 onwards), it is possible to hand dissect living embryos prior to fixation. Mutants and controls can be dissected and processed on the same slide, ensuring identical treatment throughout all analytical steps.

2.1.7.1. Hand dissection of stage 16 embryos (modified from Patel, 1994)

Dissection was carried out on specially prepared microscope coverslips (22x22mm). Using a drop of oil the prepared coverslip was adjusted to a microscope slide. A ring of silicone sealant was placed along the edges of the coverslips and allowed to dry. A small square of double stick tape was cut (~0.7cm square) and stuck on one side of the cover slip inside the silicon ring.

Using blunt forceps, about six to one dozen preselected stage 16 dechorionised embryos were placed dorsal up on the double stick tape, their anterior oriented to the top of the coverslip. The well was then filled with Broadie and Bate medium (B&B; Broadie, 2000). Sequentially, the embryos were then taken out of their vitelline membrane by introducing a pulled out pointed glass needle (see Appendix I, Chapter 6.7.3.) at flat angle into the posterior end until the tip was penetrating the anterior pole and the specimen carefully lifted up, always keeping them well below the meniscus of the liquid. Whereas the vitellin membrane stays glued on the double stick tape, the embryos can be moved to an area of clean glass and gently pushed against it, orienting their anterior to the top. The embryos stick to the surface. Using the needle the embryos were dissected flat, cutting along the dorsal midline and folding down the body walls against the glass surface. A needle with broken off tip connected to a rubber tube with mouth piece was used to remove the gut in order to expose the underlying CNS by applying gentle blows (avoiding bubbles). The dissected embryos were then fixed by exchanging the preparation buffer with fixative solution (see Appendix I, Chapter 6.6.). Exchange of the solutions was always carried out without letting the meniscus of the liquid touch the dissections. Fixation was allowed for forty minutes to one hour at room temperature. The dissections were then washed three times ten minutes with PBT followed by another one hour incubation in PBT at room temperature. Fixation, washing steps and the following antibody staining procedure were carried out in a humid chamber.

2.1.7.2. Hand dissection of stage 17 embryos (modified from Broadie, 2000; Prokop et al., 1996; Rohrbough et al., 1999)

With the formation of the cuticle at late stage 16, early stage 17 embryos lose their ability to stick on a clean glass surface. It is therefore necessary to perform vivisection. To this end, Histoacryl glue is used to attach the specimen to the surface. The glue is applied

through a broken off glass capillary, gently blowing into the attached flexible rubber tube. The glue polymerises upon contact with the buffer liquid.

For the dissection a drop of B&B medium was applied in the middle of the Sylgard coated coverslip (see Appendix I, Chapter 6.7.2.), which was previously fixed with a drop of oil to a microscope slide. With blunt forceps about 10 to 50 preselected stage 17 dechorionised embryos were transferred into the buffer solution. The embryos were then attached by their anterior and posterior pole to the Sylgard surface, thereby stretching them slightly. Using sharpened tungsten wires (see Appendix I, Chapter 6.7.1.) the embryos were cut open. The gut was then removed as described in chapter 2.1.7.1., and the body walls were folded down and glued to the Sylgard surface. The application of glue was kept to a minimum amount, touching the edges of the body walls only. The dissected embryos were then fixed by exchanging the preparation buffer with fixative solution (see Appendix I, Chapter 6.6.). Exchange of the solutions was always carried out without letting the meniscus of the liquid touch the dissections. Fixation was carried out for forty minutes to one hour at room temperature. The dissections were then washed three times ten minutes with PBT followed by another one hour incubation in PBT at room temperature. Fixation, washing steps and the following antibody staining procedure were carried out in a humid chamber.

2.1.7.3. Hand dissection of third instar larvae (modified from Ranjan et al., 1998)

Climbing third instar larvae were dissected by placing them dorsal or lateral side up on a small Petri dish with a thin layer of Sylgard resin in B&B medium. The larvae were pinned down anteriorly and posteriorly with small tungsten wire pins, giving them a “healthy stretch”, i.e. as wide as possible but without damaging the tissue through stress. Larvae were then cut along the dorsal or lateral midline using microscissors. With forceps the body walls were stretched out and pinned at the edges. After removing the viscera with forceps, the segmentally repeated larval body wall muscles and the innervating nerve fibers were clearly visible. Following a one hour fixation, the filleted larvae were washed briefly with PBT, freed from the Sylgard by removing the pins and transferred to a PBT containing Eppendorf tube. Mutant larvae and wildtype controls were processed in the same Eppendorf tube. In order to be able to distinguish between them, mutant larvae were marked by removing the mouth hooks and the posterior spiracles using microscissors. Mouth hooks and spiracles were removed from wildtype controls only prior to mounting (see Chapter 2.1.9.). In the Eppendorf tube the dissected larvae were washed with PBT three times 15 minutes, and incubated in PBT for another hour at room temperature. The dissections were then ready for antibody staining procedures.

2.1.7.4. Dissection of larval CNSs (modified from Patel, 1994)

The larvae were initially washed with water to remove adherent yeast. The larvae were dissected in B&B medium in a glass depression well. To remove the CNS one pair of forceps was used to grab the mouth hooks and a second to grab the middle of the larva. The body was pulled apart longitudinally. The CNS and the imaginal discs remain attached to the mouth hooks. The larval body was discarded and excess tissue (part of the viscera and imaginal discs) removed with forceps from the mouth hooks and attached CNS. By grabbing the mouth hooks with forceps, the dissected brains were rapidly transferred into an Eppendorf tube containing the fixative solution. Fixation was carried out for 20 minutes, followed by three

washes in PBT for ten minutes and a subsequent PBT incubation at room temperature for one hour. The PBT incubation perforates the membranes, allowing better antibody penetration into the fixed tissues. Prior to mounting (Chapter 2.1.9.) the mouth hooks were removed from the CNS using sharpened tungsten wires (see Appendix I, Chapter 6.7.1.).

2.1.8. Antibody staining

The primary antibody of appropriate dilution (see Table 2.2.) was added to dissected specimens, following the removal of PBT. The primary antibody was incubated overnight or weekend at 4°C, or at room temperature for three hours. Afterwards, the preparations were washed with PBT three times for 15 minutes each. The secondary antibody (coupled with fluorescent dye, Biotin or Alkaline Phosphatase) of appropriate dilution was added and incubated for two hours at room temperature. The secondary antibody was then washed off with PBT three times 15 minutes each. At this stage the preparations were treated differently depending on the type of conjugate being used i.e. fluorescence (see Chapter 2.1.8.1.), Biotin (see Chapter 2.1.8.2.) or Alkaline Phosphatase (see Chapter 2.1.8.3.).

If double or triple stains were performed, the other primary antibody/ies were incubated sequentially, with three PBT washing steps of 15 minutes following each antibody incubation. The primary antibodies had to be generated in different animals, in order to provide distinct epitopes to the secondary antibodies. The secondary antibodies (supplied preabsorbed against epitopes from respective animals to rule out unspecific cross reaction) were applied simultaneously.

Primary antibodies	Animal raised in	Dilutions used in µl	Supplier/Reference
anti-22C10(Futsch)	mouse	1 in 10	C. Klämbt
anti-CD8	rat	1 in 10	Caltech Laboratories
anti-Disc large (Dlg)	mouse	1 in 10	Developmental Studies Hybridoma Bank (DSHB) (Budnik et al., 1996)
anti-Drosophila Paxillin (DPxn)	rabbit	1 in 400	R. Yagi, (Yagi et al., 2001)
anti-Fasciclin II (FasII)	mouse	1 in 10	DSHB, (Halpern et al., 1991)
anti-GFP	rabbit	1 in 250	Clontech Laboratories, Inc.
Fitc-conjugated anti-Horseradish Peroxidase (HRP)	rabbit	1 in 400	Jackson Immuno Research Laboratories
Anti-Paxillin (pax)	mouse	1in100	BD Biosciences – Transduction Laboratories, Lexington, USA
anti-$Shot^{204}$	rabbit	1 in 100	See Chapter 2.2.
anti-$ShotKak^{Gas2}$	guinea pig	1 in 100	T. Volk, (Strumpf and Volk, 1998)
anti-Synapsin (Syn)	mouse	1 in 10	DSHB, (Klagges et al., 1996)
anti-Synaptotagmin (Syt)	rabbit	1 in 10000	(Littleton et al., 1993a)
anti-Tubulin (Tub)	mouse	1 in:500	Sigma Aldrich, Inc.
Secondary antibodies	**Animal raised in**	**Dilutions used in µl**	**Reference/Supplier**
Alkaline Phosphatase conjugated: anti-rabbit anti-mouse anti-guinea pig	goat	1 in 250	Jackson Immuno Research Laboratories
Biotinylated: anti rabbit anti-mouse	goat	1 in 250	Jackson Immuno Research Laboratories
Fitc-conjugated (also preabsorbed): anti-rabbit anti-mouse	goat	1 in 250	Jackson Immuno Research Laboratories
Cy3-conjugated (also preabsorbed): anti-rabbit anti-mouse anti-guinea pig	 goat goat donkey	1 in 250	Jackson Immuno Research Laboratories
Cy5-conjgated (also preabsorbed): anti rabbit anti-mouse	goat	1 in 250	Jackson Immuno Research Laboratories

Table 2.2.: List of antibodies used, with the dilutions chosen for staining reactions. All primary antibodies were diluted in PBT with 0,1% Sodium Azide to prevent bacterial growth. The secondary antibodies were diluted in PBT only.

2.1.8.1. Fluorescence staining

After secondary antibody incubation and PBT washes, the preparations were briefly rinsed with PBS. For storage, whole mount embryos were kept in dark at –20°C in 70% Glycerol in PBS. To observe under the fluorescence microscope the embryos were mounted in Vectashield fluorescent mounting media (Vector Laboratories, Burlingame, USA). The flat preparations and brain dissections were mounted differently (see 2.1.9.).

2.1.8.2. Biotin Staining

DAB staining was done when the secondary antibody used was conjugated with Biotin resulting in a brown colour reaction upon staining. The AB complex (from the Vector ABC Elite kit-Vector laboratories) was prepared by adding 4µl each of solution A and B to 300µl of PBT and left shaking for 20 minutes. The two components form a complex of Biotin and Streptavidin coupled to horseradish peroxidase, which helps to amplify the signal. The AB complex was then added to preparations and incubated at room temperature for 20 minutes after which the AB complex was rinsed with PBT two to three times. Subsequently, DAB solution with freshly added hydrogen peroxide (final concentration of 0.1%) was added to the preparation. The reaction was allowed to take place for two to three minutes then stopped by rinsing with PBT two to three times.

2.1.8.3. Alkaline Phosphatase staining

This staining was done when the secondary antibody used was an Alkaline Phosphatase conjugated one, giving a blue/black colour reaction upon staining. After incubation of the secondary antibody the embryos were rinsed with AP detection buffer briefly two to three times. Then in another Eppendorf cap containing 1ml of AP detection buffer 3µl of BCIP and 6.6µl NBT were added. This constituted the staining solution for the Alkaline Phosphatase reaction. This solution was added to the preparations and allowed to develop for 15-20 minutes depending on the intensity of staining. When the staining was weak, the reaction was prolonged up to 1hour. The reaction was then stopped by rinsing the stained preparations with PBT and then fixed in 10% formaldehyde solution in PBT for 15 minutes. After fixing, the preparations were rinsed in Methanol for 20 minutes followed by a PBT and then a PBS rinse. Stained embryos were then stored in 70% Glycerol in PBS. Flat preparations were mounted different (see Chapter 2.1.9.). For double staining procedures, preparations were first subjected to DAB and then Alkaline Phosphatase staining.

2.1.9. Mounting of preparations

Stage 17 preparations were cut off the preparation slide with a razor blade splinter (held between a pair of forceps) and transferred to a clean microscope slide. Flat preparations of stage 16 embryos were embedded on the same slide on which they were dissected after

removal of the silicon ring and the double stick tape. Flat preparations of third instar larvae and dissected larval brains were transferred to a new clean microscope slide. For embedding a small drop of 70% glycerol or Vectashield fluorescent mounting medium (Vector Laboratories; only if labelled with fluorescent antibodies) was used. The coverslips were sealed with commercial nail polish.

2.1.10. Analysis of embryos and documentation

The analysis of preparations was carried out on an Axioplan microscope mainly using Normaski optics. Preparations labelled with fluorescent dyes were documented with a Leica TCS confocal microscope or Zeiss Axiophot microscope. The digital pictures were analysed using Leica Scanware and/or using Adobe Photoshop 5.1-7.0 software (Adobe Systems, Mountain View, CA). Non fluorescent images were digitally recorded with a CCD video camera (Sony 3 CCD color video camera). For clarity, different focal planes were combined into one picture using Adobe Photoshop 5.1-7.0 . Muscles, motor neurone branches, axons and growth cones were measured on scanned or recorded images using several functions within the Photoshop and NIH Image software (http://rsb.info.nih.gov/nih-image/). The Wilcoxon-Mann-Whitney Test was chosen as statistic method in different comparative experiments (Chapter 3.2. and Chapter 3.5.2.), because it is a non-parametric (distribution free) test, generally used to compare two independent groups of sample data (Bärlocher, 1999). The WMW-test uses ranks of the data rather than their raw values to calculate the statistic. Since this test does not make distribution assumption, it is regarded to be less powerful as for example the parametric Students t-test. Therefore it is suggested to use the significance value $p = 0.05$ as critical value: Differences observed in numbers obtained for two independent groups are not to be regarded as statistically significant, i.e. greater than would be expected by chance, if the significance level exceeds the value of $p = 0.05$. Calculations were carried out using StatView or Sigma-Stat software.

2.2. Generation of an antibody specific for Shot

Antibodies specific to a protein of interest can be generated by immunising animals (i.e. injecting the protein into animals and retrieving the serum after the immune response) with either the entire protein or oligopeptide fragments. Proteins or oligopeptides can be produced in bacterial cells using specific expression vectors. Oligopeptides can also be produced by chemical peptide synthesis. Large proteins such as Shot (see Introduction, Chapter 1.3.) are difficult to express in bacterial cells, and are not suited for protein isolation and purification protocols, and protein injection into animals (Eurogentec, personal communication). Therefore, chemical synthesis of oligopeptides representing potentially antigenic regions of the Shot protein were chosen here for the immunisation of animals. Further, using this strategy, the antigenic regions could be chosen specifically from the N-terminal part of the protein (essentially of interest for this study, see Results, Chapter 3.5.). Potentially antigenic sequences within the N-terminal region of Shot were predicted using Vector NTI 7 software. Two sequences, both within the Actin binding domain of Shot, were chosen for peptide synthesis:

Antigen code EP011203: H_2N-DWRKARNDRPRERLEC-$CONH_2$ (16 amino acids)

Antigen code EP011204: H_2N-LDPEDVDTNEPDEKSC-$CONH_2$ (15 amino acids)

Both synthesis of the antigens and immunisation of animals was carried out by EUROGENTEC (Eurogentec Bel S.A., Herstal, Belgium). The schedule of immunisation (immunisation program DE01369) consisted of the injection of the two synthesised oligopeptides into each of two rabbits (Code of animals: SA611 and SA612) followed by four rounds of boost every 28 days. Antisera were retrieved from the animals two weeks after the last boost. Partial volumes of the sera were used for a small scale affinity purification against both epitopes, yielding about 1,1mg/1,2ml of antibodies purified against antigen EP011203 and antigen EP011204, respectively.

2.2.1. Western Analysis

Western blot analysis was carried out, in order to assess whether the produced antibodies recognise their epitopes.

2.2.1.1. Protein extraction from third instar larvae

Ten larvae, that were ectopically expressing GFP tagged N-terminal domains of Shot (PAG, see Chapters 2.3.3.1. and 3.3.), were transferred into an Eppendorf tube containing 50µl 1x Lämmli buffer. Using an Eppendorf pistil, the larvae were crashed and afterwards incubated at 100°C for 15 minutes. The extracted proteins in Lämmli buffer were either used directly for SDS gel application or kept at -20°C. In case the larva-protein suspension had been stored frozen, the mixture was heated up anew for five minutes at 100°C before being applied on the gel.

2.2.1.2. SDS polyacrylamide gel electrophoresis (PAGE)

SDS-PAGE is a standard method for separation of proteins according to their molecular weight (Sambrook et al., 2001). The proteins are first denatured with DTT (Dithiothreitol) and SDS (Sodium dodecyl sulfate), which cause disruption of the intra- and intermolecular disulfide-, hydrogen- and hydrophobic bonds, respectively. The proteins lose their tertiary and quaternary structure and become masked by a surplus of negative charges. Hence, in an electrical field, the separation of the molecules in mixture within the gel mainly occurs according to their molecular weight.

Extracted proteins from larvae were separated in 5% of acrylamide in the stacking gel (this collecting, rough matrix simplifies the passage of the proteins into the gel), and 8% of acrylamide in the separation gel (see Appendix I, Chapter 6.5.). The gels were made freshly for each application. To begin with, two clean glass plates were placed in the casting stand. Two spacers were placed between both glass plates, one on each side. The assembly was tightened and fixed within the gel casting stand. The components for the separation gel were mixed together and the mixture was poured, filling about three quarter of the volume between the glass plates. Then a comb was placed in front of the outer glass plate and the separation

gel mixture was poured to only a few inches below the teeth of the comb. The gel was overlaid with water saturated butanol to exclude air from the gel while polymerising. When the gel had polymerised the butanol layer was discarded and the components for the stacking gel were mixed. The mixture was then poured to fill the remaining space between the glass plates. The comb was then placed between the glass plates so that the teeth of the comb were completely immersed in the stacking gel solution. The gel was left polymerising.

When the gel had polymerised, it was transferred within the glass sandwich to the gel chamber apparatus. Electrode buffer was added and the comb was removed. The wells were then washed using a syringe with electrode buffer to prevent the remains of the stacking gel solution to polymerise. Samples were then loaded, the gel was run at 20mA for approximately one hour (until gel front reached bottom of gel).

The Gel was then dismantled by first removing the spacers from the glass plate sandwich. The upper glass plate was levered away from the remaining assembly. The gel was rinsed with distilled water, one corner of the gel was notched to allow orientation, and the gel was transferred into the Coomassie staining solution. Within this solution the gel was carefully separated from the second glass plate. The gel was stained for two hours. The gel was then transferred into destaining solution and incubated therein. By replacing the destaining solution the gel was first destained to a degree that the efficiency of the separation of the protein extraction could be assessed. In case of successful SDS-PAGE, the gel was destained entirely and directly used for western blotting.

2.2.1.3. Western blotting

Proteins were transferred from the gel to a polyvinylidene fluoride (PVDF) microporous membrane in a semi-dry system using a graphite electroblotter (Fastblot B34, Biometra, Göttingen).

Two sheets of Whatman 3mm filter paper of size accurate to the gel were presoaked in anode buffer I solution and placed in the centre of the graphite anode electrode plate. One Whatmann filter paper was presoaked in anode buffer II solution and placed on top of the first two sheets of filter paper. The PVDF membrane was then placed on top of the filter papers. Then the gel was placed on top of the membrane, and was overlaid with three filter papers presoaked in cathode buffer solution. To ensure an even transfer of the proteins, air bubbles were removed by carefully rolling a pipette over the surface of each paper layer of the stack. The cathode plate cover was then placed on top of the assembled transfer stack. The blotting was carried out for one hour at 5mA/cm² of the gel. The blot was then dismantled and the membrane was incubated for five minutes in Ponceau-S Red solution in order to visualise the proteins and assess the efficacy of the blotting procedure. The membrane was washed after Ponceau-incubation with distilled water. Using clean scissors, the marker lanes were separated from the remaining blot and left drying. The remaining protein lanes were separated by cutting though the bands. Each half of the protein lane was notched and labelled to allow orientation and identification, and then destained by incubation for twenty minutes in PBS at room temperature. Each half was assessed with different antibodies, i.e. one half to immunodetect the GFP tag of the overexpressed construct with a GFP specific antibody, the other half to immunodetect the overexpressed construct with the newly generated Shot antibody. By aligning the two halved protein lanes back together one can deduce whether the visualised bands come from the same protein.

2.2.1.4. Immunodetection on the blotted membrane

After the PBS wash the membranes were incubated over night in blocking solution (PBT with 10% milk powder and 3%BSA). The membranes were then incubated with the primary antibody in PBS with 5% milk powder for two hours. The blots were washed three times for five minutes in PBS before the secondary Alkaline Phosphatase coupled antibody was applied (in PBS, with 5% milk powder) for one hour. This was followed by two washing steps of five minutes in PBS and one of ten minutes in TBS (Chapter 6.5.). The proteins were then visualised by incubating the membranes in ten ml TBS containing 145µl NBT and 75µl BCIP (Chapter 6.5.), which constitutes the staining solution for Alkaline Phosphatase reaction. The staining was allowed to develop for 15-30 minutes, depending on the intensity of the staining. The reaction was stopped by washing the membranes in water. The blotted membranes were then dried on Whatmann filter paper.

2.3. Molecular Biology

Chemicals (Chapter 6.1.), Kit-systems (Chapter 6.2.), Enzymes (Chapter 6.3.), Equipment (Chapter 6.4.), Other Materials (Chapter 6.7.), Bacterial and Yeast strains (Chapter 6.8. and 6.9., respectively), Vectors (Chapter 6.10.), Oligonucleotides (Chapter 6.11.), DNA/protein markers and quantifying standards (Chapter 6.12.), Buffers and media (Chapter 6.5.) are detailed in Appendix I.

2.3.1. Generally applied methods

2.3.1.1. Sterilisation of solutions and utensils

Media, solutions, buffers and utensils were autoclaved at 2 bar, 120°C for 20 minutes. Thermolabile solutions were sterilised by filtration using a 0.2µm filter. Glasware was sterilised at 1 bar, dry heat (90°C) over the weekend.

2.3.1.2. Photometric measurements

Concentration and purity of dsDNA in solution was assessed by measuring the absorption at 260nm and 280nm using disposable cuvettes. dsDNA with an absorption quotient (A_{260}nm/A_{280}nm) of 1.8-2.0 was regarded as clean. Alternatively, the concentration of PCR-products and plasmid-DNA-solutions was assessed by comparing the band intensity with that of DNA markers of known concentration after simultaneous agarose gel electrophoresis (see Chapter 2.3.3.4.).

2.3.1.4. Optic density (OD) of bacterial and yeast cultures

Bacterial and yeast growth was measured at a wavelength of 600nm in 2ml disposable plastic cuvettes, using the original, sterile medium as reference. Bacteria and yeast are still in a logarithmic growth phase when an OD_{600} of 0,7-0,8 or ≥1, respectively, is measured.

2.3.2. Bacteriological methods

2.3.2.1. Cultivation of bacteria

Frozen cells of appropriate strain were thawed and left on ice for ten minutes. 200µl aliquots were plated onto 90mm selective LB-agar plates, which were incubated at 37°C overnight. Single colonies were used to inoculate 5ml LB selective medium and left shaking for six to eight hours or over night at 37°C, 300rpm. These cultures were then used to either inoculate liquid cultures of larger volume or to establish long term glycerol stocks. For glycerol stocks of *E.coli*, 245µl of 80% glycerol was added to 800µl cultured cells in a safe lock Eppendorf tube. The cells were immediately shock frozen in liquid nitrogen. The glycerol stocks were kept at -80°C.

2.3.2.2. Making of competent cells

Electrocompetent cell were made as described elsewhere (Sambrook et al., 2001). In brief, two times 500ml of LB-standard medium were each inoculated with 100µl of an overnight culture of appropriate *E.coli* strain and left shaking at 37°C, 300rpm until an OD_{600} of 0,7-0,8 was reached. Before sedimentation (GS-3 rotor, Sorvall centrifuge, 15 minutes at 4°C, 4000rpm) the cell suspension was left on ice for 20 minutes. The sedimented cells were resuspended in 500ml ice cold sterile distilled H_2O, and subjected to another round of centrifugation. The supernatant was discarded and the cell pellets were pooled in 250ml ice cold sterile distilled H_2O. After an additional round of centrifugation (15 minutes at 4°C, 3000rpm), the pellets were resuspended in 20ml ice cold sterile 10% glycerol (in sterile distilled H_2O), followed by centrifugation at 4°C, 3000rpm, 20 minutes (Eppendorf centrifuge, rotor number 19776). The sedimented cells were taken up in two ml ice cold sterile10% glycerol and aliquoted in volumes of 50-100µl in safe lock Eppendorf caps. The aliquots were shock frozen in liquid nitrogen and stored at -80°C. The treated cells can be stored up to six months without loosing their competence.

All steps were carried out at sterile conditions. The cells were kept cold at all times. Chemocompetent cells were made and generously provided by other members of the laboratory, following general protocols described elsewhere (Sambrook et al., 2001).

2.3.2.3. Transformation of competent cells

Chemocompetent cells: Frozen competent cells were thawed and left on ice for ten minutes. 1µl of a 1:10 diluted ligation reaction or an equivalent of 0.1-50ng DNA was added. After incubation of the mixture for 30 minutes on ice the cells were heat shocked for 30 seconds at 42°C. The samples were left on ice for a couple of minutes before preheated (37°C, 500µl) standard liquid LB medium was added. The samples were then left in a 37°C shaking waterbath for one hour. Finally 200µl aliquots were plated onto 90mm selective LB plates, which were incubated overnight at 37°C.

Electrocompetent cells: Frozen competent cells were thawed and left on ice for ten minutes. One to five µl of the DNA sample (<100ng) to be transformed was cooled on ice[i]. After adding the cold DNA the cell suspension was transferred to a precooled quartz cuvette. The cuvette was placed in the electroporation chamber of a pulse apparatus (EasyjecT, Prima, EQUIBIO, Peqlab, Labotec, Wiesbaden) and the electrical impulse was triggered off (capacity 25µF, resistance factor 200, voltage 2,5kV). Directly after the electroporation, 200µl of preheated (37°C) standard liquid LB medium were added. The transformation was then transferred to a clean safe lock Eppendorf tube and left shaking at 37°C and 300rpm for 40 minutes. This incubation time allows the cells to express the resistance providing genes, enabling them to grow on the selection agar medium onto which they were plated thereafter and kept overnight at 37°C.

2.3.3. Mating-based Yeast Two-Hybrid Screening

The yeast two-hybrid system allows the detection of protein-protein interactions (Emery, 2002; Gietz and Woods, 2002; Stanyon and Finley, 2000). The assay is based on the fact that many eukaryotic trans-acting transcription factors are composed of physically separable, functionally independent domains. Such regulators often contain a DNA-binding domain (BD) that binds to a specific enhancer-like sequence, in yeast referred to as the upstream activation site (UAS, see also Chapter 2.1.4.). One or more activation domains (AD) direct the RNA-polymerase II complex to transcribe the gene downstream of the UAS. Both the BD and the AD are required to activate a gene. Normally, as in the case of the native yeast GAL4 protein, the two domains are part of the same protein. If physically separated by recombinant DNA technology and expressed in the same host cell, the BD and AD peptides do not directly interact with each other and thus cannot activate the responsive genes. However, if the BD and the AD can be brought into close physical proximity in the promoter region, the transcriptional activation function will be restored. In principle, any AD can be paired with any BD to activate transcription, with the BD providing the promoter specificity. In a yeast two-hybrid assay, a bait gene is expressed as a fusion of the GAL4-BD (bait-BD), while another gene or cDNA is expressed as a fusion to the GAL4-AD (prey/cDNA-AD;) (Chien et al., 1991; Fields and Song, 1989). When bait and library fusion proteins interact, (the bait-)BD and (prey-)AD are brought into proximity, activating transcription of downstream reporter genes. Hence, with the use of this system, interactions between two proteins can be tested, novel protein interactions identified (known bait against cDNA library)

[i] It is important to reduce the volume of DNA to a minimum, since salts in the solution might interfere with the electroporation of the nucleotide acid into the cells

and interacting domains defined. Through the sequence of the cDNA in the AD-expression vector, one has immediate access to the genes encoding the interacting proteins.

Traditional yeast two-hybrid screening is based on co-transformation or sequential transformation of yeast competent cells with a BD-bait fusion plasmid and an AD-cDNA fusion plasmid. Despite the numerous successes with this method (Stanyon and Finley, 2000 and citations therein), the conventional screening procedure is described as being fairly labour-intensive (BioTechniques, 2000): The preparation of the plasmid DNA to be used in subsequent transformations of the two-hybrid cDNA library is tedious and time consuming, and the transformation efficiency is relatively low and varies greatly with the growth conditions and strain of the yeast cells.

To circumvent the constraints of the traditional yeast two-hybrid screening, an alternative screening approach based on yeast mating procedure has been developed, described, and made commercially available (BioTechniques, 2000; Harper et al., 1993; CLONTECH, MATCHMAKER Two-Hybrid System 2, PT1030-1, Clontech Laboratories, Inc, Palo Alto, CA, USA) and has been used in this study.

Basis of the yeast mating system is that *Saccharomyces cerevisiae* cells grow persistently as either haploid cells or as diploid cells. The haploid cells are either **a** or α mating types, depending on which allele (**a** or α) occupies the transcriptionally active mating type locus, *MAT*. When cells of opposite mating types, which secrete different pheromones, detect the opposite cell type's pheromones and then make physical contact with each other under nutrient rich growth conditions, the haploid cells mate to form **a**/α diploid cells. In the mating-based screening approach the bait plasmid and cDNA library are first introduced separately into yeast cells of opposite mating types by transformation. The bait and cDNA plasmids are then brought together into one cell by mating. The resulting diploid cells are selected by the presence of the prototrophic markers from both plasmid types. In the mating-based screen applied here, the selection for the prototrophic reporters was imposed simultaneously to increase the stringency of the screen.

In the course of this study, the construction and quality control of the library, phenotype verification of the yeast strains, the transformation of the bait-BD and cDNA-AD constructs into the appropriate yeast strains, test for autonomous reporter gene activation, the yeast mating, and the verification (cotransfection of bait- and prey vector into AH109) of the positive candidates was kindly carried out by A. Ahle in the collaborating laboratory of T. Böckers at the Institute for Anatomy, University of Münster, Germany. The construction of the bait-BD constructs (Mainz) and the analysis of the putative positive clones, i.e. β-galactosidase colony-lift filter assay (Münster), plasmid isolation from yeast (Münster and Mainz), transformation of *E.coli* with plasmid isolated from yeast, plasmid extraction from *E.coli*, isolation of the cDNA-AD vector through restriction digest analysis, and sequence analysis (all Mainz) was carried out by the author.

2.3.3.1. Construct fusion genes

Four fusion gene constructs were generated:

(i) Actin Binding Domain (ABD) of *shot* in pAS2-1
(ii) Plakin (PT) domain of *shot* in pAS2-1
(iii) ABD and PT domain (PAT) of *shot* in pAS2-1
(iv) C-terminal *shot* domain containing the GAS2 homology (GT) in pAS2-1

The domains were chosen on the basis of the GAL4/UAS study performed earlier (see Chapters 2.1.4. and 3.3.). The respective domains were kindly provided in pNB40 (PAT and PT; for pNB40 vector see Brown and Kafatos, 1988) and pUAST (GT; for pUAST vector see Brand and Perrimon, 1993) vectors by A. Subramanian of the collaborating laboratory of T. Volk, Department of Molecular Genetics, the Weizmann Institute, Rehovot, Israel. Since no restriction sites in the test domains were compatible with the pAS2-1 vector (see Appendix I, Chapter 6.10.), the gene fragments to be tested were generated by High Fidelity (HF-) PCR with appropriate restriction sites incorporated into the primers, respecting or not interfering with the reading frame (see Chapter 6.11.).

2.3.3.2. Generation of primers

The primers were designed using an oligonucleotide calculator freely accessible in the internet (http://www.basic.nwu.edu/biotools/oligocalc.html), and verified for unique binding using two independent align tools (Vector NTI 7 software, *align* at http://www2:igh.cnrs.fr/bin/align-guess.cgi, Person et al., 1997). The primers for construction of the fusion genes were produced and purified by BioSpring, Frankfurt, Germany (http://www.biospring.de). Primers for sequencing reactions were produced by GenTech (Mainz, Germany). The individual primers are listed in Appendix I, Chapter 6.11.

2.3.3.3. Polymerase Chain Reaction (PCR)

The PCR allows the amplification of nucleic acids. A DNA template is denatured by heat, and specific primers anneal to the separated sites on opposite template strands. The primers are present in great excess over the template. Therefore annealing conditions are chosen that restrict primer binding only to sites that are highly homologous to the oligonucleotides. After annealing, the primers are each extended in the 5'-3' direction by temperature stable DNA polymerase to yield overlapping copies of the original template. PCR is a cyclic process, i.e. the three distinct steps of denaturation, primer annealing, and extension are repeated many times, leading to exponential accumulation of nucleotide fragments during subsequent rounds of amplification. However, the exponential phase of product accumulation is not indefinite, after a certain number of cycles product accumulation reaches a plateau.

To circumvent misinterpretation of the template during the PCR, high quality DNA polymerases should be used in combination with accurate buffer, polymerase stabilising proteins and proof reading enzymes. Here, the TripleMaster PCR Kit (Eppendorf, Wesseling-Berzdorf, Germany) was used to amplify the fusion gene fragments. The Kit's enzyme mix contains the DNA *Taq* polymerase, a polymerase enhancing factor and three distinct proof reading enzymes, all working synergistically in the supplied buffer mixture.

The PCR was run in a total reaction volume of 50µl

Concentration in PCR mixture	Component
1x	High Fidelity buffer
2mM	dNTPs
~200pmol	Primer X
~200pmol	Primer Y
~200ng	Template
1,5U	Enzyme mix
x µl to final volume	H_2Obidest

Table 2.3: High Fidelity PCR set up

The reaction was first heated for five minutes at 94°C to initiate denaturation of the template, followed by 30 cycles with 30 seconds at 94°C to denature the DNA, one minute at the lower basic melting temperature of both primers used, e.g. 56°C in the PCR for *shot* PAT (see Appendix I, Chapter 6.11.), allowing the primers to anneal to the single-stranded template, and four minutes at 72°C to extend the second strand in 5'-3' direction (polymerisation should be carried out for approx. one minute per every 1000bp of length of target DNA). The reaction was then left at 72°C for 40 minutes to allow the reannealing process to be completed. The reactions were kept at 4°C or frozen for long term storage.

2.3.3.4. Agarose gel electrophoresis

Agarose gel electrophoresis allows the separation of a mixture of nucleotide acids in an electrical field. 0.7-1% standard agarose gels (depending on the length of nucleic acids to be separated or viewed) were applied to test the efficiency of PCR reactions (Chapter 2.3.3.3.), estimate DNA concentrations, test for ligation reaction efficiency (Chapter 2.3.3.9.), or to analyse restriction enzyme analysis (Chapters 2.3.3.7., 2.3.3.16.), using 1x TAE as gel- and running buffer. The gels contained 0.5µg ethidium bromide in order to visualise the applied DNA samples under short wave UV-light. Loading dye was added to each sample. The gels were run at 90V. Pouring and handling of gels was done as described elsewhere (Sambrook et al., 2001).

2.3.3.5. Cloning of the PCR amplified *shot* gene fragments

The restriction sites incorporated by the respective primers into the amplified *shot* gene fragments were not directly accessible for restriction enzymes (too short 5'–sequence extension). The PCR products first had to be inserted into an intermediate vector before subsequent restriction enzyme digestion, purification and ligation into the pAS2-1 vector containing the BD-sequence. At this step, the TOPO TA cloning Kit (Invitrogen), was used. The Kit allows the direct insertion of *Taq* polymerase-amplified PCR products into the provided vector pCRII TOPO. The *Taq* polymerase has a non-template dependent terminal transferase activity which adds a single deoxyadenosine (A) to the 3' ends of PCR products.

The supplied linearised vector has single overhanging 3' deoxythymidine (T) residues. This allows PCR inserts to be ligated efficiently with the vector using the ligation activity of a topoisomerase I (in the supplied vector reaction mixture).

The cloning of the PCR fragments was carried out according to the manufacturer's manual. In brief, 2µl of fresh PCR product were added to 2µl sterile water and 1µl TOPO vector solution, resulting in 5µl reaction volume. The reaction was gently mixed and left incubating for maximal five minutes. 1µl of supplied salt solution was added and mixed for ten minutes in order to stop the reaction. The mixture was left on ice. 2µl of the TOPO cloning reaction were added to a vial of freshly thawed chemocompetent cells and gently mixed, without pipetting. The cells were then left on ice for 30 minutes before applying the heat shock (see Chapter 2.3.2.3.).

125µl of transformation solution was spread out onto LB-plates containing 100µg/ml ampicillin. The plates were incubated over night at 37°C. 10 colonies were then picked from the plate and cultured in liquid LB medium containing 100µg/ml ampicillin for six to eight hours at 37°C. Subsequently, the DNA plasmids were isolated (see Chapter 2.3.3.6.).

2.3.3.6. Isolation of plasmid DNA from bacteria

For clean and high yield plasmid DNA isolation the QIAprepSpin Miniprep Kit was used (Qiagen GmbH, Hilden, Germany). The procedure was followed as outlined in the manufacturer's manual, with the exception that plasmid elution was carried out with 55µl 70°C warm sterile water instead of the suggested TE-buffer. This choice was taken to keep the concentration of salts low, as too high salt concentrations might interfere with the enzyme activity in subsequent procedures, such as restriction enzyme digests.

2.3.3.7. Restriction enzyme digestion of plasmid DNA

Restriction enzyme digestion was carried out to isolate the *shot* domain inserts from the TOPO plasmid using enzymes that recognise the unique restriction sites introduced by the respective primers. Isolation of the *shot* domain inserts had best results when a sequential double digestion was carried out, precipitating the samples with ethanol (see Chapter 2.3.3.6.) after the first digestion step. In general, 80µl reaction volumes were chosen, containing 30µl of isolated plasmid, 40µl sterile water, 8µl of appropriate buffer and 2µl of respective digestion enzyme. For the restriction enzymes XmaI, SalI and NdeI the reactions were carried out at 37°C for approx. three hours. Digestions were stopped by incubating the mixture for 20 minutes at 65°C, denaturing the digestion enzymes. SfiI digestions were carried out at 50°C for approx. three hours. SfiI is not temperature sensitive, reactions were therefore stopped by keeping them at 4°C. Entire digestions were loaded on a 0.7% agarose gel (see Chapter 2.3.3.4.), and in case of successful digestion, the bands of interest, representing the *shot* gene fragments, were cut out and processed according to a gel purification protocol (see Chapter 2.3.3.8.).

pAS2-1 Vectors, into which the inserts were to be ligated after purification were digested under the same respective conditions and subsequently agarose gel purified (Chapter 2.3.3.8.).

2.3.3.8. Gel purification of restriction enzyme digestions

Digested *shot* gene fragments were gel purified using the QIAquick Gel Extraction Kit (Qiagen GmbH, Hilden, Germany), following the Kits protocol. The DNA was however eluted with 70µl 70°C warm sterile water instead of 50µl supplied elution buffer.

2.3.3.9. Ligation of digestion products into plasmid vector pAS2-1

Ligation was carried out in 20µl reactions containing approximately 300ng pre-digested pAS2-1 vector DNA, 100ng GT or ABD insert, 200ng PT insert, or 250ng PAT insert, respectively, 2µl T_4-ligase buffer and 1µl T_4-ligase. The ligation was run at 16°C overnight.

Verification of the efficiency of the ligations was carried out by digestion reactions with EcoRV for the PAT and GT domains, and BglII for the PT domain. EcoRV digestion resulted in three expected distinct bands, BglII in two distinct bands. 2µl of ligation reaction was mixed with 1µl enzyme and 2µl of appropriate buffer in a total reaction volume of 20µl for 2 hours at 37°C. The digestion was then loaded on a 0.7% agarose gel.

2.3.3.10. Amplification of the bait-BD vectors

Bait-BD vectors were amplified in *E.coli* RRI electrocompetent cells as described above. Plasmid DNA from 40ml overnight LB cultures was isolated using the GenElute Plasmid Midi-Prep Kit from Sigma (Sigma-Aldrich Chemie GmbH, München, Germany), following the manufacturer's protocol. The plasmid DNA was taken up in 500µl elution buffer. The DNA was ethanol precipitated as described previously. The precipitated DNA was taken up in 200µl sterile water.

2.3.3.11. Sequencing

Sequencing reactions were performed using the Sanger enzymatic method (Alberts et al., 1994; Ansorge et al., 1989). The method is based on the termination of the elongation step of the sequencing reaction by random incorporation of differentially fluorescently labelled dideoxynucleotides (ddNTPs). This results in a mixture of differentially labelled strands of distinct length, depending on the timepoint the respective ddNTP has been incorporated. The strands are separated by acrylamide gel electrophoresis. The fluorescently labelled fragments are detected by a CCD camera (charged coupled device) upon laser beam excitation at the end of the gel.

Inserts within pAS2-1 were sequenced to verify their sequence accuracy and to verify that the insertion of the fragments did not cause frameshifts. Per sequencing reaction 800ng-1µg of DNA template were used (due to large size of the vector; usually one takes about 500ng) in addition to 10pmol respective primer and 4µl Big Dye Terminators (contains dNTPs, fluorescently labelled ddNTPs and the polymerase; supplied by GENterprise at the Institute of Molecular Genetics, Mainz, Germany) in a total reaction volume of 20µl using required volume of sterile water.

The sequencing was programmed for 30 cycles of: (i) 96°C for 15 seconds, denaturing the DNA template(s), (ii) 55°C for 4 minutes, allowing annealing of the primer and its extension until a ddNTP gets incorporated. The lower temperature (instead of 72°C for optimal enzyme function) allows the polymerase to incorporate the chemically modified ddNTPs in the time window given.
Sequencing was stopped by keeping the reaction at 4°C.

Afterwards, the reaction was ethanol precipitated as described earlier. The dried pellet was sent to GENterprise (Institute of Molecular Genetics, Mainz, Germany) for further processing and detection of the sequence on an automated sequencer. Obtained sequences were analysed using Vector NTI7 software.

pAS2-1 vectors with correctly incorporated bait sequences were transformed into the appropriate yeast strains (Y187, see Appendix I, Chapter 6.9.) and tested for autonomous reporter gene activation. The bait-constructs containing the PAT and GT domain, respectively, activated the reporter gene autonomously, i.e. without the presence of the AD-prey sequence. These vector constructs were discarded from the yeast two-hybrid screen. The bait-constructs containing the ABD and the PT domain showed no autonomous reporter gene activation. Therefore Yeast two-hybrid screening was proceeded with these two constructs only. As mentioned above (see Chapter 2.3.3.), the transformation of the bait-constructs, the test for autonomous reporter gene activation and the yeast mating was kindly carried out by A. Ahle in the collaborating laboratory of T. Böckers at the Institute for Anatomy, University of Münster, Germany. The mating reactions were plated out and cultivated on selective synthetic dropout (SD) agar plates (see Chapter 2.3.3.13.).

2.3.3.13. Cultivation of yeast cells

Yeast colonies growing on SD agar plates deficient for the nutrients Trp, Leu, Ade, and His were streaked out on new SD/-Trp/-Leu/-His/-Ade agar plates (-Trp/-Leu to reveal diploid yeast cells, His and Ade as the first reporter genes for interaction). These established masterplates were incubated colony side down at 30°C until the yeast colonies reached approximately 2 mm in diameter. The masterplates were then sealed with Parafilm for long term storage (~ two months) at 4°C.

The colonies on the masterplates were assayed for expression of the *MEL1* reporter gene (β-Galactosidase) in a Colony-lift Filter Assay (see Chapter 2.3.3.24.).

If positive, the respective colonies were picked from the masterplate and grown in 5ml SD/-Leu/-Trp/-His/-Ade (to maintain selective pressure on the positive interacting cDNA-AD plasmid) at 30°C, 300rpm, for subsequent isolation of plasmids.

2.3.3.14. Colony-lift Filter Assay

The procedure followed the protocol given in the CLONTECH MATCHMAKER2 manual (http://www.bdbiosciences.com/clontech/). In brief, for each masterplate to be tested for *MEL1* reporter gene expression, sterile Whatman #5 filter (VWR, Darmstadt, Germany) were presoaked with Z buffer/X-gal solution (see Appendix I, Chapter 6.5.). Using forceps, clean, dry filter were placed over the surface of the plate of colonies to be assayed. Through gentle rubbing with a round non-sharp tool (sterile glass pipette) a colony print was obtained on the filter. Holes were poked through the filter in asymmetric positions to orient the filter to

the agar. The filter was then transferred colonies facing up to a pool of liquid nitrogen, where it was submerged for ten seconds. Thereafter the filter was left to thaw at room temperature. This freeze/thaw treatment permeabilises the cells. The filter was then placed colony side up on the Z buffer/X-gal presoaked filter and incubated at 30°C for 30 minutes to four hours (maximum). β-galactosidase producing colonies turn blue: the enzyme cleaves X-gal, releasing dibromodichloroindigo (Sambrook et al., 2001).

2.3.3.15. Plasmid isolation from yeast

Plasmid DNA isolated from yeast is often contaminated by yeast genomic DNA, and is therefore not suitable for restriction enzyme analysis and sequencing. Hence, it first needs to be isolated form yeast and transformed into *E.coli* to be further processed.

The 20-24 hour cultures were centrifuged down at 3000rpm for five minutes at room temperature. The supernatant was discarded and the pellet resuspended in the residual liquid by vortexing. The suspension was then transferred to a clean safe lock Eppendorf tube. 200µl of yeast lysis solution were added, followed by addition of 200µl of phenol/chloroform/isoamyl alcohol (25/24/1) and approximately 300µg of acid-washed glass beads (to destroy the cells; Sigma-Aldrich Chemie GmbH, München, Germany). The suspension was then mixed by vortexing for two minutes followed by ten minutes centrifugation at 14000rpm at room temperature. The supernatant was transferred to a fresh Eppendorf tube and ethanol precipitated as mentioned earlier. The dried pellet was taken up in 20µl TE buffer and stored at -20°C. Plasmid DNA isolated from yeast could only be transformed into electrocompetent *E.coli* RRI cells (see Chapter 2.3.2.3.).

2.3.3.16. Large scale plasmid DNA isolation from bacteria

Plasmid DNA isolated from yeast contains both the bait- and prey bearing vector. Hence, bacteria transformed with the plasmid DNA isolated from the positive two-hybrid interaction candidates contained either of the two vectors. In order to identify the prey-AD vector, restriction digestion followed by gel analysis (bait-BD and prey-AD show differential restriction patterns) was carried out for plasmid DNA isolated from at least four of the bacterial transformants from positive two-hybrid interaction candidates.

For isolation of plasmid DNA from a high number of individual cultures, a rapid plasmid isolation protocol established by A. Ahle (Institute for Anatomy, University of Münster, Germany) was followed:

3-5ml of previously master plated over night cultures were centrifuged for four minutes at 15000rpm in an Eppendorf tube. The supernatant was discarded and the pelleted cells were resuspended in 100µl resuspension buffer. After resuspension, 200µl lysis buffer were added, and the preparation was quickly mixed by inverting the tube gently a couple of times (too vigorous shaking might lead to shearing of bacterial chromosomal DNA). Immediately after, 200µl neutralisation buffer were added, in order to neutralise the reaction and adjust the high salt concentration necessary for the separation of the plasmid DNA from other cellular components. The suspension was then centrifuged for ten minutes at full speed (15000rpm) and the supernatant transferred into clean Eppendorf tubes. The plasmid DNA was then isolated from the supernatant by DNA precipitation. Two and a half volume of 100% ethanol, and 1/10th volume of 3M sodium acetate (pH 5,2) were added to the supernatant, followed by 30 minutes centrifugation at 4°C at full speed. The alcohol was discarded and the DNA pellet

was washed by adding 500µl 70% ethanol and centrifugation for five minutes at full speed. The alcohol was discarded and the DNA pellet was spin vacuum dried. The dried pellet was taken up in 20µl sterile water containing 1mg/ml RNase.

Restriction analysis was carried out using double digestions of the unique restriction sites recognised by the enzymes EcoRI and XhoI. 10µl isolated plasmid in sterile water containing RNase were digested with 0,5µl of each enzyme, 4µl Y^+Tango buffer (to yield 2x Y^+Tango buffer) and 5µl sterile water in a total reaction volume of 20µl for a maximum of two hours at 37°C. The digestions was then analysed in a 1% agarose gel (see Chapter 2.3.3.4.).

2.3.3.17. Identification of putative interaction partners of the distinct Shot domains

Bacterial colonies containing a prey-AD vector (see Chapter 2.3.3.16.) were amplified (see Chapter 2.3.2.1) and plasmid DNA was isolated according protocol described in Chapter 2.3.3.6. Thereafter the inserted cDNA fragment within the prey-AD vector was sequenced as described in Chapter 2.3.3.11. Obtained sequences were analysed using Vector NTI7 software and submitted to basic local alignment search tools (BLAST; Altschul et al., 1990), provided by the Berkeley Drosophila Genome Project (http://www.fruitfly.org/blast/) and the National Centre for Biotechnology Information (NCBI; http://www.ncbi.nlm.nih.gov/blast).

3. RESULTS

Synapse formation is a key event during the development of neuronal circuits. It comprises the establishment and maintenance of synaptic contacts, shaping of synaptic terminals and localisation and assembly of synaptic components. Little is known about genes and gene functions underlying mechanisms of synaptogenesis. In *Drosophila*, the Spectraplakin protein family member Shot, a close homologue of mammalian MACF1 and BPAG1 was found to be one of the few factors with synaptogenic function (Prokop et al., 1998b). *shot* mutant phenotypes cause structural defects at embryonic synapses. Specifically, *shot* mutations affect late motor axonal growth, shape acquisition of the presynaptic motor terminal at the NMJ, the assembly of presynaptic specialisations, and the formation of motor neuronal side branches in the CNS. Shot is predicted to execute its function through multiple interactions with other proteins (Röper et al., 2002). In order to approach the functionality of Shot at the genetic, cell biological and molecular level, several series of experiments were carried out in the context of this thesis.

First, different *shot* mutant alleles were analysed phenotypically (Chapter 3.1.) to find out whether the different phenotypes described for *shot* mutant embryos can be isolated genetically from others. This way it was intended to test the assumption that Shot is organised into modular domains responsible for different kinds of molecular interactions. Different allelic classes would provide an ideal starting point for structure functional studies.

Second, it was tested whether growth cones of *Drosophila* embryos can be used as potential assay structures for the visualisation of cytoskeletal components at a subcellular level (see Chapter 3.2.). This approach was taken to improve the resolution of the *shot* mutant analyses. Furthermore, growth cones could provide an ideal structure for the analysis of the subcellular localisation of intrinsic Shot protein or misexpressed domains of Shot.

Third, different domains of Shot were misexpressed in *Drosophila* neurones (see Chapter 3.3.). On the one hand these neurones were assayed for potential dominant negative phenotypes. On the other hand, the subcellular localisation of the different Shot domains were analysed. Such studies were carried out to complement the mutant analyses mentioned above and to select domains which were the most reasonable to be taken for yeast-two-hybrid screens for Shot interactors.

Fourth, the subcellular localisation of different antisera raised against different Shot domains was tested (see Chapter 3.4.) in order to complement mutant analyses as well as the

experiments of misexpression of Shot domains. One of the antibodies used was obtained in the context of this thesis and was raised against an N-terminal domain of Shot.

Fifth, yeast-two-hybrid screens were carried out with two N-terminal Shot domains in order to uncover potential Shot interactors and thus to gain first insights into the molecular context of these Shot domains (see Chapter 3.5.).

Sixth, one of the 13 candidate interactors obtained in the yeast-two-hybrid screen, the gene DPaxillin, was investigated genetically. This way it could be demonstrated that the screen obtained the right type of candidate genes.

Finally, a genetic approach was chosen as an alternative strategy to identify potential Shot interaction molecules. Synapses of mutant embryos were analysed, which were reported previously to display motor neuronal stall phenotypes, i.e. early developmental phenotypes reminiscent of *shot*. This strategy uncovered connections between Rho-GTPases and Shot, which were analysed in further detail (see Chapter 3.6.).

3.1. Comparative morphological study of different *shot* mutant alleles

shot mutations affect essential aspects of synapse formation: Neuronal phenotypes during the late embryonic differentiation period involve, amongst others, stall of outgrowing motor neurones, reduced neuromuscular terminals and failure to grow motor neuronal side branches in the CNS (Lee et al., 2000a; Löhr et al., 2002; Prokop et al., 1998b; vanVactor et al., 1993). Further neuronal phenotypes include reduced dendritic arbours of multidendritic peripheral sense organs, malformation of the scolopidial sense organs, and wrong compartmentalisation of a specific isoform of the N-CAM-homologous transmembrane protein Fasciclin II (Gao et al., 1999; Prokop et al., 1998b). Phenotypes have also been described for non-neuronal tissues (see Introduction). For example, mutations in *shot* affect the cytoskeletal organisation at muscle attachment sites, resulting in disruption of tendon cells upon mechanical stress through muscle contraction (Prokop et al., 1998b; Strumpf and Volk, 1998). Shot is a member of the Spectraplakin family of proteins. Members of this family are believed to orchestrate cellular development and maintenance by linking combination of factors such as cytoskeletal elements and cell adhesion molecules via their distinct domains (Leung et al., 2002; Röper et al., 2002). A large quantity of *shot* mutant alleles is available,

and it was expected, that a considerable number of these alleles represent hypomorphic mutations. If different domains of Shot are responsible for different types of molecular interactions, it should be possible to isolate some phenotypes genetically from others through mutations affecting only certain parts of the gene. In order to test this possibility, phenotypic analyses of a number of *shot* mutant alleles were carried out.

Of the alleles tested, four were isolated in independent ethylmethane sulfonate (EMS; usually causing point mutations) mutagenesis experiments ($shot^{el3}$, $shot^{91K}$, $shot^{HG25}$, $shot^{SF20}$) and were previously reported to affect synapse formation (Prokop et al., 1998b). The other alleles tested are *shot* mutants that have been studied in different developmental contexts: The alleles $shot^{kakP2}$ (P-element insertion mutagenesis experiment) and $shot^{3}$ (isolated in a diepoxybutane mutagenesis experiment) have been reported to affect late motor axonal growth (Lee et al., 2000a). $shot^{V104}$ and $shot^{V168}$ have been studied in the context of epidermal muscle attachment cell differentiation (Gregory and Brown, 1998; Strumpf and Volk, 1998). Molecular information about mutational events is so far not available for the alleles $shot^{3}$, $shot^{el3}$, $shot^{91K}$, $shot^{HG25}$ and $shot^{SF20}$. However, $shot^{3}$ is reported to be a *shot* null mutant (Lee et al., 2000a). More molecular information about mutational events is available for $shot^{kakP2}$, $shot^{V168}$ and $shot^{V104}$. In $shot^{kakP2}$, a P-element insertion between the third and fourth exon of the *shot* gene (Figure 1.3) is thought to disrupt transcription of the N-terminal region of Shot (Lee et al., 2000a). $shot^{V168}$ and $shot^{V104}$ were isolated in X-ray mutagenesis experiments and the mutational events were reported to lead to premature translational termination of Shot (Strumpf and Volk, 1998; $shot^{V168}$: T. Volk, personal communication). All *shot* mutant alleles mentioned cause embryonic lethality, and all except $shot^{kakP2}$ have been reported to lead to muscle detachment phenotypes in late stage 17 (Prokop et al., 1998b, and observations not shown).

Initially, I analysed the *shot* mutant alleles at stage 16, visualising the motor neuronal projections with anti-FasII. Because of facilitate accessibility, the analyses focussed on motor neurones contacting the ventral muscle area (Figure 3.1.A). At stage 16, wildtype projections of the segmental nerve b (SNb) reach the ventral lateral muscle VL1 (Landgraf et al., 1997; Figure 3.1.A). Shortly after having exited the CNS, projections of the segmental nerves c and d (SNc/d) defasciculate from the SNb and intersegmental nerve (ISN) and reach towards their ventral oblique target muscles (Figure 1.2., Figure 3.1.A). In contrast, all tested *shot* mutant alleles except $shot^{V168}$ show a stall phenotype for the projections of the SNb, c and d (Figure 3.1.B-G). Strongest stall phenotype was observed for alleles $shot^{91K}$, $shot^{HG25}$ and $shot^{SF20}$, where the SNb hardly reaches muscle VL4, and SNc and d stall shortly after defasciculating

from the other segmental nerves. In the *shot* mutant alleles $shot^{kakP2}$ and $shot^{el3}$ a weaker stall phenotype is observed. Here the growth cones of SNb motor neurones are found at the level of muscles VL2 and VL3, and SNc and d projections grow out further into the ventral most muscle area as compared to those found in $shot^{91K}$, $shot^{HG25}$ and $shot^{SF20}$. Interestingly, the two alleles, which are known to have mutations affecting different regions of the Shot protein reveal divergent phenotypes. While a stall phenotype is observed in $shot^{kakP2}$, the mutant allele $shot^{V168}$ shows a wildtypic pattern of ventral projections. The mutational events in the different regions of the *shot* gene seem to have diverse consequences for Shot function.

Subsequently, the *shot* mutant alleles were studied at late embryonic stage 17 (see Chapter 2.1.7.). At this stage, wildtype motor neurone terminals have branches on their target muscles and display varicosities of about 1 µm diameter (called boutons; Figure 3.2.A, D-F). Boutons can be visualised with antibody stains against synaptic markers, like the presynaptic proteins Synapsin (Syn) and Synaptotagmin (Syt), or the postsynaptic protein Disc Large (Dlg; Figure 3.2A, D, E and F). Motor neuronal projections can be visualised with antibodies specific to cell adhesion molecules, such as FasII (see above), with anti-Futsch (Futsch is also known as 22C10, a MAP1B homologue; Figure 3.2.B) or with the Horseradish Peroxidase antibody (recognises specifically an epitope presented by a membraneous glykosylated protein found exclusively on the surface of all neuronal cells and male reproductive tissue, Fabini et al., 2001; Figure 3.2.D). The motor neuronal projections and terminals are found in reproducible, precise and invariant patterns in each hemisegment of the embryo (see Chapter 1.3.), facilitating the comparison between wildtype and *shot* mutant morphology.

In almost all *shot* mutant embryos studied, NMJs in all muscle locations display branches reduced in length and boutons appear reduced in number and size (Figures 3.3 and 3.4). Whereas some alleles exhibit an almost complete absence of NMJs ($shot^{91K}$, $shot^{HG25}$, $shot^{SF20}$ and $shot^{3}$), others show less severe phenotypes ($shot^{el3}$ and $shot^{kakP2}$). Only two *shot* mutant alleles showed no obvious NMJ phenotype at all ($shot^{V104}$ and $shot^{V168}$).

Taking the studies of stage 16 and stage 17 embryos together, it is possible to divide the *shot* mutant alleles into two groups on the basis of the motor neuronal phenotypes observed: Alleles in the first group have normal motor neuronal projection patterns and motor terminals ($shot^{V104}$ and $shot^{V168}$). Alleles in the second group exhibit disrupted motor neuronal patterns and boutons of reduced number and size (alleles $shot^{el3}$, $shot^{91K}$, $shot^{HG25}$, $shot^{SF20}$, $shot^{kakP2}$ and $shot^{3}$). As mentioned earlier, mutational events particularly in the first group have been reported to affect the C-terminal region of Shot. In contrast, $shot^{kakP2}$, exhibiting stall phenotype and reduced NMJ, is known to have a mutational event affecting the N-terminal of

Shot. Moreover, *shot*^{kakP2} is the only mutant allele known so far that does not display a muscle detachment phenotype (see above). Thus, the domains at the opposed ends of the Shot protein seem to be required in different cellular and probably functional contexts: especially the N-terminus seems to be essential for Shot synaptogenic function. The mutant alleles *shot*^{el3}, *shot*^{91K}, *shot*^{HG25}, *shot*^{SF20} and *shot*^{3} display synaptic as well as epidermal phenotypes, suggesting that mutational events might affect domains at the two opposed termini of Shot or domains with functions in both synaptic and epidermal context.

Stage 17 embryos of *shot* mutant alleles revealed further divergence in parameter values in the analysis of other neuronal phenotypes. As shown in Figure 3.2, antibodies specific to HRP and Futsch not only allow NMJs but also peripheral sensory neurones to be visualised. The peripheral neurones in each hemisegment of *Drosophila* wildtype embryos are grouped into dorsal, lateral and ventral clusters (Hartenstein, 1988). The neurones within each cluster can be further classified on the basis of their dendrite morphology (Gao et al., 1999): external sensory (*es*) neurones and scolopidial (*sc*) neurones, each containing a single dendrite; bipolar dendrite (*bd*) neurones, each with two simple unbranched dendritic projections; and multiple dendrite (*md*) neurones with extensive arborisation. The neurones are thought to function as touch receptors or proprioreceptors to sense body surface tension or deformation (Bodmer and Jan, 1987). With the exception of *shot*^{kakP2}, preliminary results indicate that all *shot* mutant alleles that were previously found to affect synapse formation have scolopidial neurones with reduced dendritic projections (Figure 3.5; Prokop et al., 1998b). Furthermore, arborisations in multiple dendrite neurones are reduced and the projections appear deformed (Figure 3.6). Although *md* dendritic projections in *shot*^{kakP2} also appear deformed their arborisation is more extensive. Hence, the P-element insertion that possibly disrupts the transcription of the N-terminal region of the protein in *shot*^{kakP2} does not seem to abolish Shot function required for dendrite integrity of *md* and *sc* peripheral sensory neurones. This or these functions are however severely disrupted in *shot*^{91K}, *shot*^{HG25}, *shot*^{SF20} and *shot*^{3}.

Similar to the phenotypes observed for *md* and *sc* sensory neurones, defects in the dendritic projections of bipolar dendrite sensory cells were found differential in *shot*^{91K}, *shot*^{HG25}, *shot*^{SF20} and *shot*^{3} as compared to *shot*^{kakP2} in initial experiments (Figure 3.6): In wildtype embryos the dendrites of *bd* cells are found within the anterior-posterior borders of each hemisegment. *shot*^{91K}, *shot*^{HG25}, *shot*^{SF20} and *shot*^{3} mutant *bd* dendrite projections appear thinner and longer, partially extending beyond the anterior-posterior borders (Prokop et al., 1998b). In the mutant allele *shot*^{kakP2} the projections of the *bd* sensory neurones seem normal.

Since *shot*^{kakP2} does not seem to affect dendritic projections of the PNS, the effect of the P-element insertion in this mutant on dendritic projections of motor neurones of the CNS was assessed subsequently. The motor neuronal dendrites are located and densely packed within the neuropile. For clear access to dendrite arborisation, it is necessary to visualise only a subset of motor neurones. This can be achieved by either labelling individual motor neurones with the lipophilic dye DiI (Prokop et al., 1998b) or by targeted expression of cell membrane markers using the Gal4/UAS-system (see Chapter 2.1.4.). Targeted expression of the cell marker CD8-GFP was chosen in this experiment in order to visualise *Vum* (*V*entral *U*npaired *M*edian)-motor neurones in the background of *shot*^{kakP2} (Löhr et al., 2002) and the motor neurones aCC and RP2 in the background of *shot*^{SF20} (mainly to reproduce findings of DiI labelled *shot* mutant motor neurones and to serve as reference for further comparative studies, see Chapter 3.6.; Figure 3.7).

Expression of the cell membrane marker can be targeted to the motor neurones aCC and RP2 by placing the *Gal4* gene under the control of the enhancer to the gene *even skipped* (*eve*), which is active in the stage 17 CNS solely in these motor neurones (and the interneurone pCC; *eve*^{RRK}-Gal4; Baines et al., 1999). Dendritic projections of CD8-GFP expressing aCC and RP2 motor neurones were found severely reduced in *shot*^{SF20} mutant embryos (Figure 3.7C), confirming earlier findings using the DiI labelling method (Prokop et al., 1998b). Per neuromere, the *Vum*-Gal4 driver line expresses Gal4 in 12-14 paired cells and 3 unpaired Vum motor neurones located in the ventral midline (Landgraf et al., 2003). In the recombinant *shot*^{kakP2};UAS-CD8-GFP (Löhr et al., 2002) dendrites of the *Vum-Gal4*-positive motor neurones seemed reduced, suggesting the N-terminal region of Shot to be required for motor neuronal dendrite formation in the CNS. However, the recombinant showed only very weak CD8-GFP expression. The misexpression of CD8-GFP in the background of *shot*^{kakP2} will be repeated in order to confirm the preliminary results obtained in this experiment.

The parameter values of different *shot* mutant alleles were finally assessed for CNS patterning phenotypes, using the markers FasII and Dlg. Anti-Dlg staining in the CNS of stage 17 embryos is found throughout the entire neuropile and, usually at higher levels, in motor neuronal nerve roots (Figure 3.8, arrow head). In embryos of *shot*^{91K}, *shot*^{HG25}, *shot*^{SF20} and *shot*^{3}, but not in *shot*^{kakP2} embryos, this distinction is gone (Figure 3.8). Further, it was observed that Dlg accumulates ectopically along commissures of the CNS midline in *shot* mutants positive for the nerve root phenotype. Hence, the localisation of Dlg in the nerve roots requires a functional domain other than those, which are potentially disrupted in *shot*^{kakP2}.

Anti-FasII stains a set of longitudinal fibre tracts of reproducible and constant pattern within the synaptic neuropile of stage 16 and stage 17 wildtype embryos (Landgraf et al., 2003; Figure 3.9). The overall pattern of the longitudinal tracts in the CNS does not seem to be affected in all *shot* mutant embryos studied. However, FasII fails to stay in the nerve but spreads into the nerve roots of *shot* mutant motor neurones (Figure 3.9). The specific localisation of the N-CAM homologue FasII is affected in all *shot* mutants that also show stall and NMJ phenotypes, but not in $shot^{V104}$ and $shot^{V168}$. Therefore, like the synaptic and axonal growth phenotypes, the mislocalisation of FasII seems to correlate with mutational events disrupting the N-terminus of Shot.

The results of the comparative study of *shot* mutant alleles are summarised in table 3.1 and in Figure 3.10. The phenotypic analysis of the *shot* mutants revealed that the different alleles show different combinations and/or degrees of phenotypes. The mutations in the different alleles might affect distinct domains of the Shot protein. On the basis of their neuronal phenotype, such as late axonal growth, NMJ formation and synaptic marker localisation, *shot* mutant alleles can be classified into separate groups: $shot^{V104}$ and $shot^{V168}$ (light blue frame in Table 3.1 and Figure 3.10) have an intact nervous system, $shot^{kakP2}$, $shot^{el3}$, $shot^{91K}$, $shot^{HG25}$, $shot^{SF20}$ and $shot^{3}$ have defects to different degrees (orange frame in Table 3.1 and Figure 3.10). The neuronal function of Shot might be referred to the N-terminus and central regions of Shot, since both $shot^{V104}$ and $shot^{V168}$ are known to have mutations disrupting the C-terminus of the protein. Indeed, Shot function seems to involve distinct forms of molecular interactions with its numerous domains in each cellular and developmental context.

	$shot^{el3}$	$shot^{kakP2}$	$shot^{SF20}$	$shot^{91K}$	$shot^{HG25}$	$shot^{3}$	$shot^{V104}$	$shot^{V168}$
NMJ reduced	+[#]	+	++	++	++	++	O	O
MTJ disrupted[$]	+	O	+	+	+	+	+	+
Scolopidia disrupted	n.d.	O	+	+	+	+	n.d.	n.d.
CNS dendrites reduced	+[#]	(+)	+	+[#]	+[#]	+	n.d.	n.d.
PNS MD reduced	+/o	+/o	+	+	+	+	O	n.d.
FasII mislocalisation	n.d.	+	+	+	+	+	O	O
Syn mislocalisation	n.d.	O	O	O	(+)	O	O	O
Syt mislocalisation	n.d.	+	+	(O)	+	+	O	O
Dlg (CNS) mislocalisation	n.d.	O	+	+	+	+	n.d.	n.d.
Stage 16 stall phenotype	+	+	++	++	++	++	n.d.	O

Table 3.1: Summary of phenotypes observed for the *shot* mutant alleles kak^{el3}, kak^{91K}, kak^{HG25}, kak^{SF20}, kak^{P2}, $shot^{3}$, kak^{V168} and kak^{V104}. For details see text. O: wildtypic phenotype; +: mutant phenotype; ++: strong mutant phenotype; n.d.: not determined. Results shown in brackets are preliminary and need to be confirmed with further experiments. NMJ, neuromuscular junction; MTJ, myotendineous junction; CNS, central nervous system; PNS, peripheral nervous system; MD, multi dendritic sensory neurones; FasII, Fasciclin II; Syn, Synapsin; Syt, Synaptotagmin; Dlg, Disc large. *shot* alleles with mutant neuronal phenotypes are highlighted in orange, *shot* alleles with wildtypic neuronal phenotypes are highlighted in light blue. (#, Prokop et al., 1998b, $, Strumpf and Volk, 1998, Prokop et al, 1998b).

Having shown that the N-terminal and central region are essential for synapse formation, it was intended to dissect the molecular basis for Shot activity in more detail by expressing distinct Shot domains in neuronal tissues using the Gal4/UAS-system and studying their localisation. Since Shot is suggested to be involved in time specific organisation of the

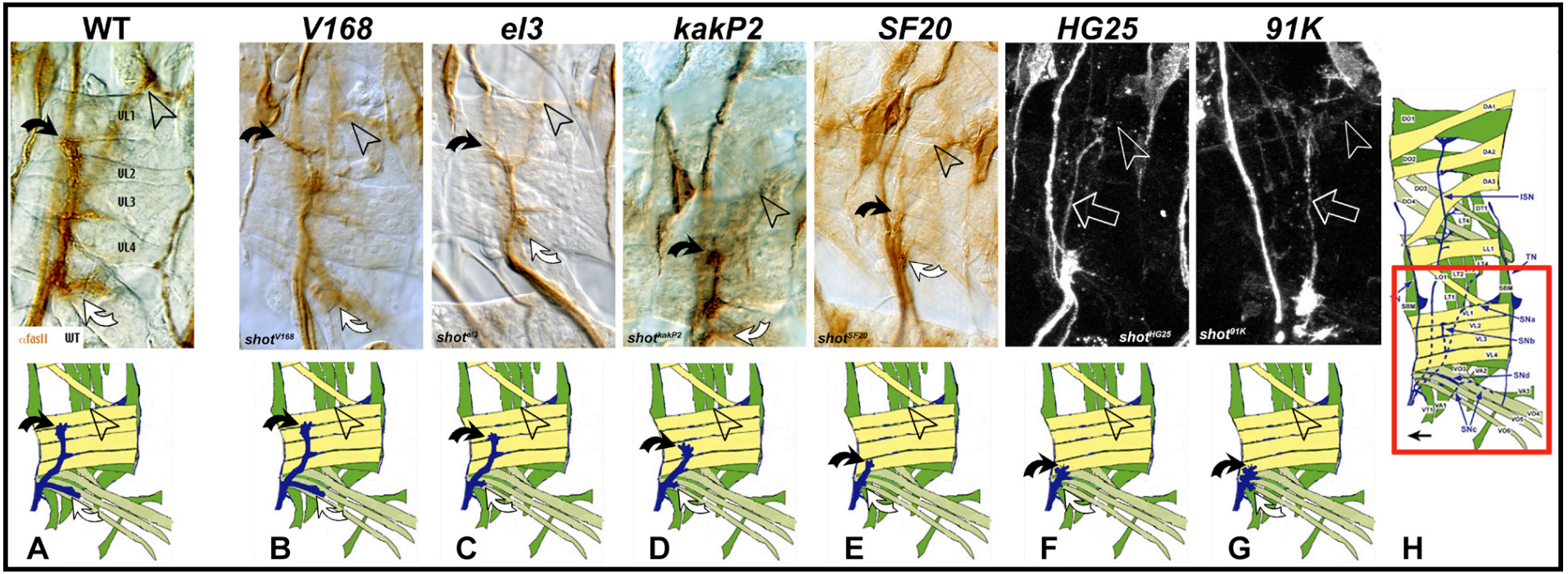
WT
V168
el3
kakP2
SF20
HG25
91K
αfasII WT
shot^V168
shot^el3
shot^kakP2
shot^SF20
shot^HG25
shot^91K
UL1
UL2
UL3
UL4
ISN
TN
SNa
SNb
SNd
SNc
A
B
C
D
E
F
G
H

MT cytoskeleton and its association with the cell cortex, it was further considered to establish a cellular model system, which should allow both the study of Shot protein and Shot domain localisation and the organisation of cytoskeletal elements within neurones.

Figure 3.1.: Motor neuronal projections of most *shot* mutant alleles show stall phenotypes at stage 16. (A-G) Light microscopic view of projections on ventral longitudinal muscles VL1-VL4 (SNb) and ventral oblique muscles (SNc and d; nomenclature as in Landgraf et al., 1997) in the central abdomen of wildtype control (A) and *shot* mutant embryos: $shot^{V168}$ (B), $shot^{el3}$ (C), $shot^{kakP2}$ (D), $shot^{SF20}$ (E), $shot^{HG25}$ (F), and $shot^{91K}$ (G). Specimens were labelled with anti-FasII (A-E, diaminobenzidine; F+G, fluorescent). The lower panel shows cartoons of the ventral muscle area (red box in overview cartoon, H) summarising the phenotypes observed for the respective genotypes. Black bent arrows indicate growth cones of SNb motor neurones, open arrowheads indicate dorsal edges of muscle VL1, white bent arrows indicate projections of SNc and d. In F and G the SNa is visible in the background (open white arrows). Black arrow in (A) points anterior. Stall phenotypes are found for $shot^{el3}$, $shot^{kakP2}$, $shot^{SF20}$, $shot^{HG25}$, and $shot^{91K}$, but not for $shot^{V168}$.

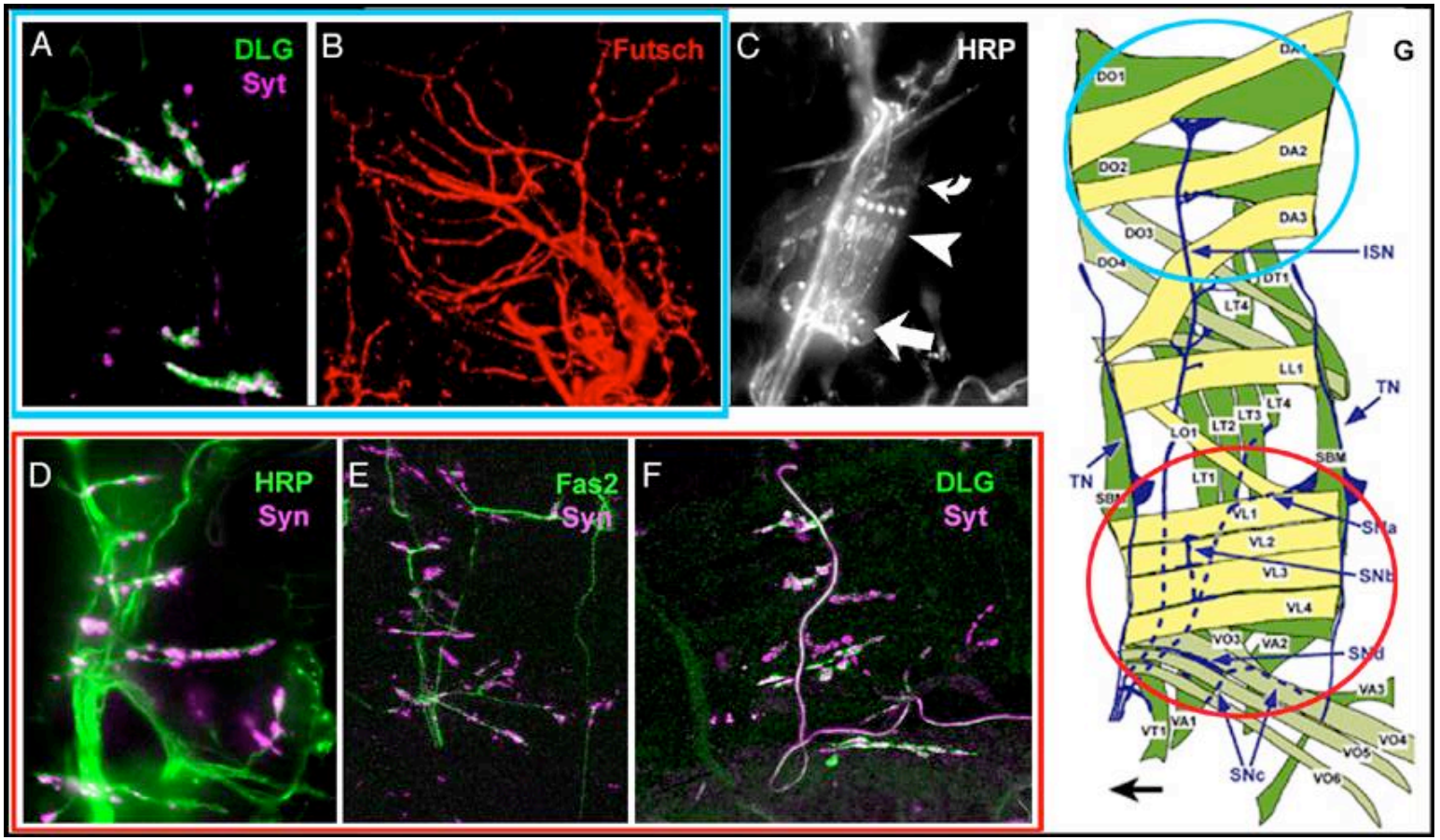
A
DLG
Syt
B
Futsch
C
HRP
D
HRP
Syn
E
Fas2
Syn
F
DLG
Syt
G
DO1
DO2
DO3
DO4
DA1
DA2
DA3
ISN
DT1
LT4
LL1
TN
LT3
LT2
LO1
SBM
LT1
VL1
VL2
VL3
VL4
VO3
VA2
VA3
VT1
VA1
VO4
VO5
VO6
SNc

Figure 3.2.: Examples of structures analysed at late stage 17. A) NMJs in the dorsal muscle field (see blue circle in G), B) multidendritic sensory organs, C) scolopidial sensory organs, D-F) NMJs in the ventral muscle field (see red circle in G); G) shows a schematic representation of all muscles of one abdominal hemi-segment (muscle nomenclature according to Landgraf et al., 1997). Used markers are indicated in colour code top right in each figure: Fas2, fasciclin2 (motoraxons); HRP, horseradish peroxidase (neuronal surfaces), Futsch (neuronal Microtubules); Syn, Synapsin; Syt, Synaptotagmin (Presynapse); DLG, Disc Large (Postsynapse). Motorneuronal terminals at the NMJ show typical thickenings (boutons) revealed by all used markers. Multidendritic sensory organs show characteristic dendritic arborisations extending over the basal surface of the epidermis. Scolopidial sensory organs are characterised by cell bodies of scolopidial neurones (white arrow), which send out thick dendrites, extending into thin cilia (arrow head), which are supported by hollow lymph-filled capsules (bent arrow, see also Figures 3.5 and 3.14).

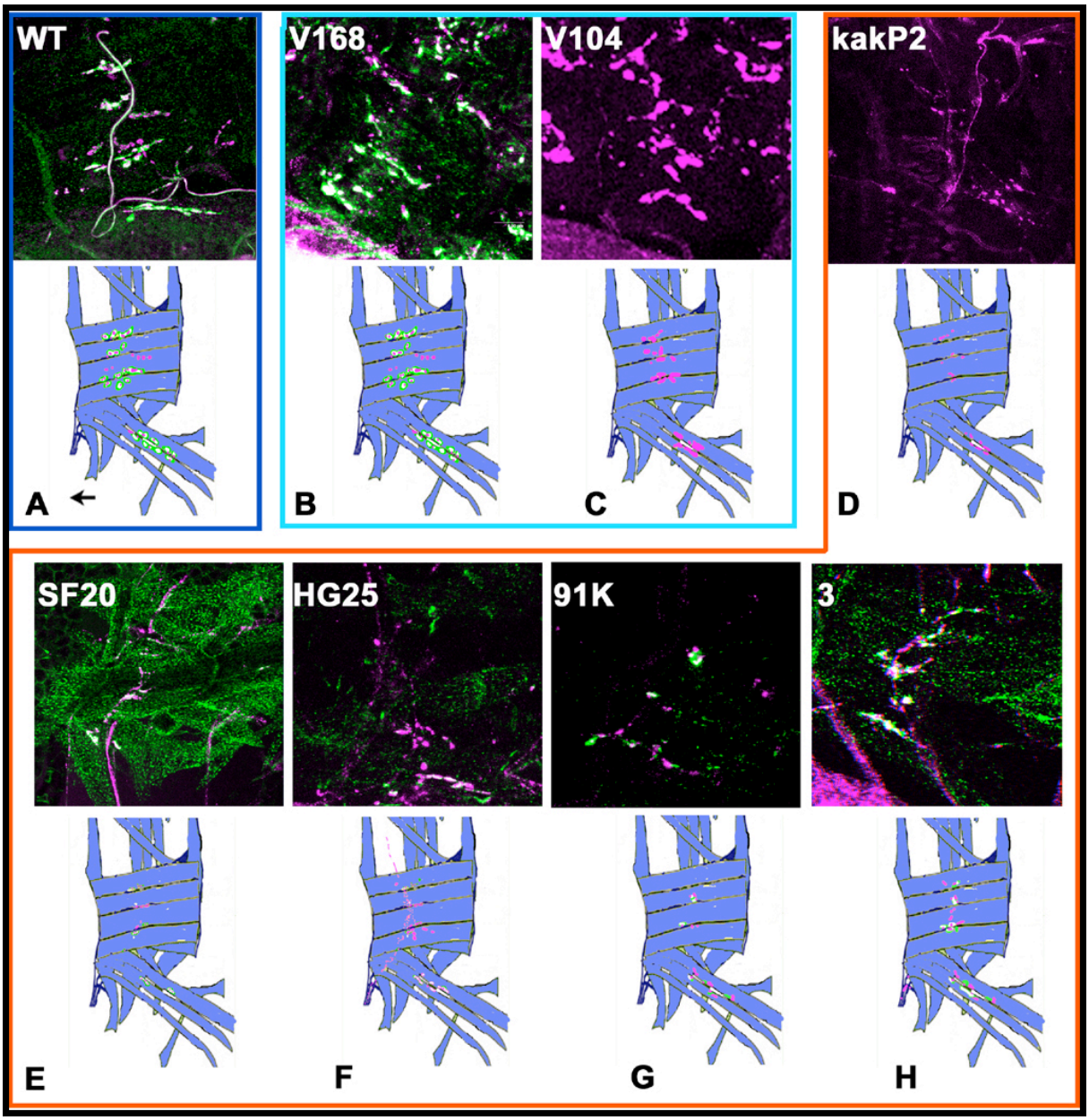
WT
V168
V104
kakP2
A
B
C
D
SF20
HG25
91K
3
E
F
G
H

Figure 3.3: Comparative study of NMJ phenotypes in the ventral muscle field (compare Figure 3.2G). Confocal pictures of NMJs on ventral muscles labelled with anti-Syn (magenta) and anti-Dlg (green) of wildtype control (A) and different *shot* mutant alleles (B-H) at stage 17 are represented together with a schematic interpretation of the phenotype. NMJs are reduced in size in $shot^{kakP2}$, $shot^{SF20}$, $shot^{HG25}$, $shot^{91K}$, and $shot^{3}$ (orange box). In contrast, NMJs in $shot^{V168}$ and $shot^{V104}$ are wildtypic in size (blue boxes). Mutational events in the latter mutant alleles do not seem to disrupt Shot synaptogenic function.

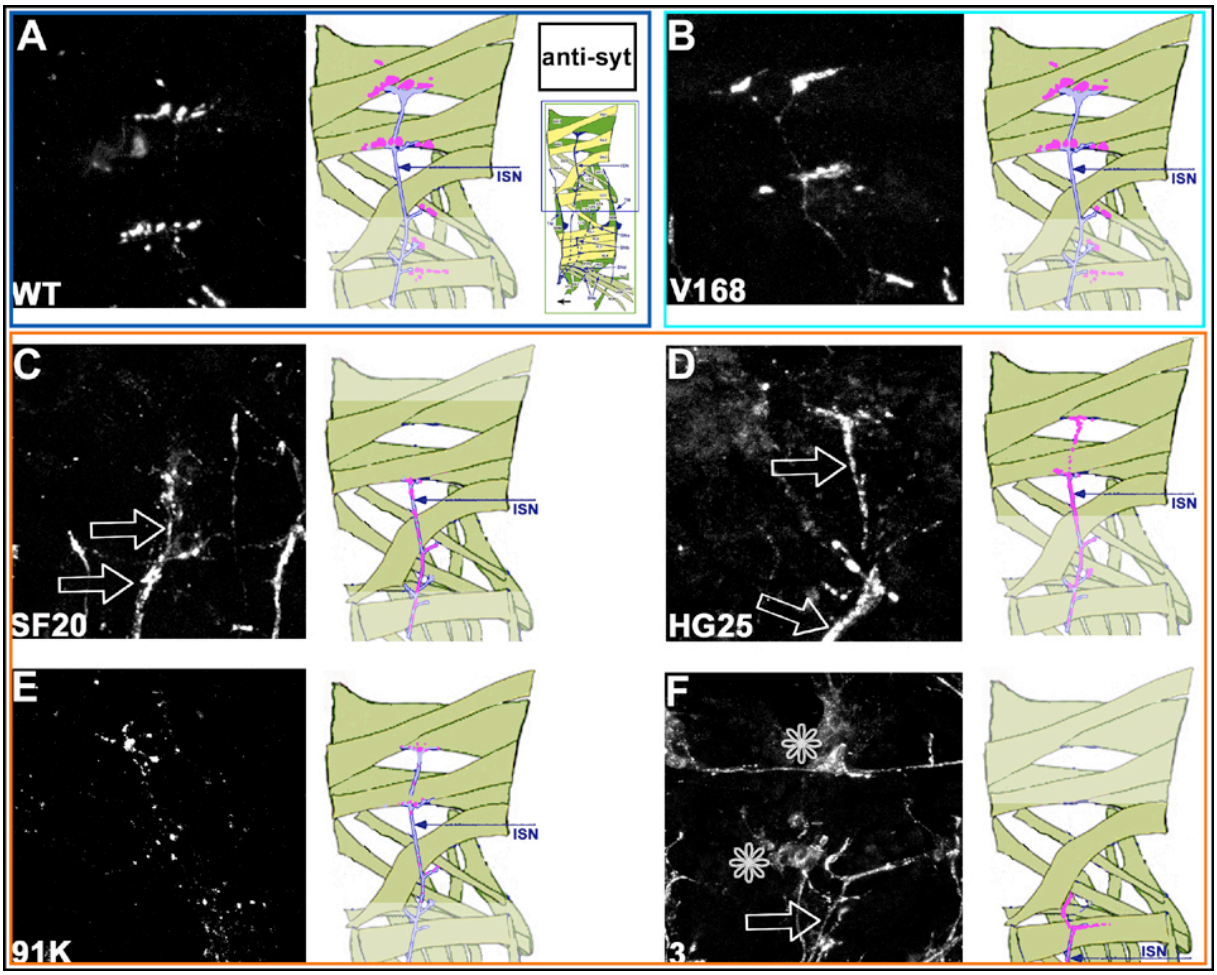
A
anti-syt
ISN
WT
B
ISN
V168
C
ISN
SF20
D
ISN
HG25
E
ISN
91K
F
3
ISN

Figure 3.4: Comparative study of NMJ phenotypes in the dorsal muscle field. Confocal pictures of dorsal most muscle NMJs labelled with anti-Syt in wildtype controls (A) and *shot* mutant alleles (B-F). Comparable to findings shown in Figure 3.3, where NMJs have been stained with different synaptic markers, *shot* mutant alleles $shot^{SF20}$, $shot^{HG25}$, $shot^{91K}$ and $shot^{3}$ have NMJs reduced in number and size while NMJs in $shot^{V168}$ are wildtypic. Interestingly Syt is not restricted to presynaptic sites in most mutant alleles affecting NMJ morphology (exception $shot^{91K}$), but is found mislocalised along axonal processes (white open arrows). Anti-Syt reactivity along processes of peripheral sensory neurones (asterisks) in $shot^{3}$ is probably due to unspecific reaction of the antibody in that particular experiment. In all pictures anterior is to the left. The Syt staining is represented in magenta in the summarising cartoons.

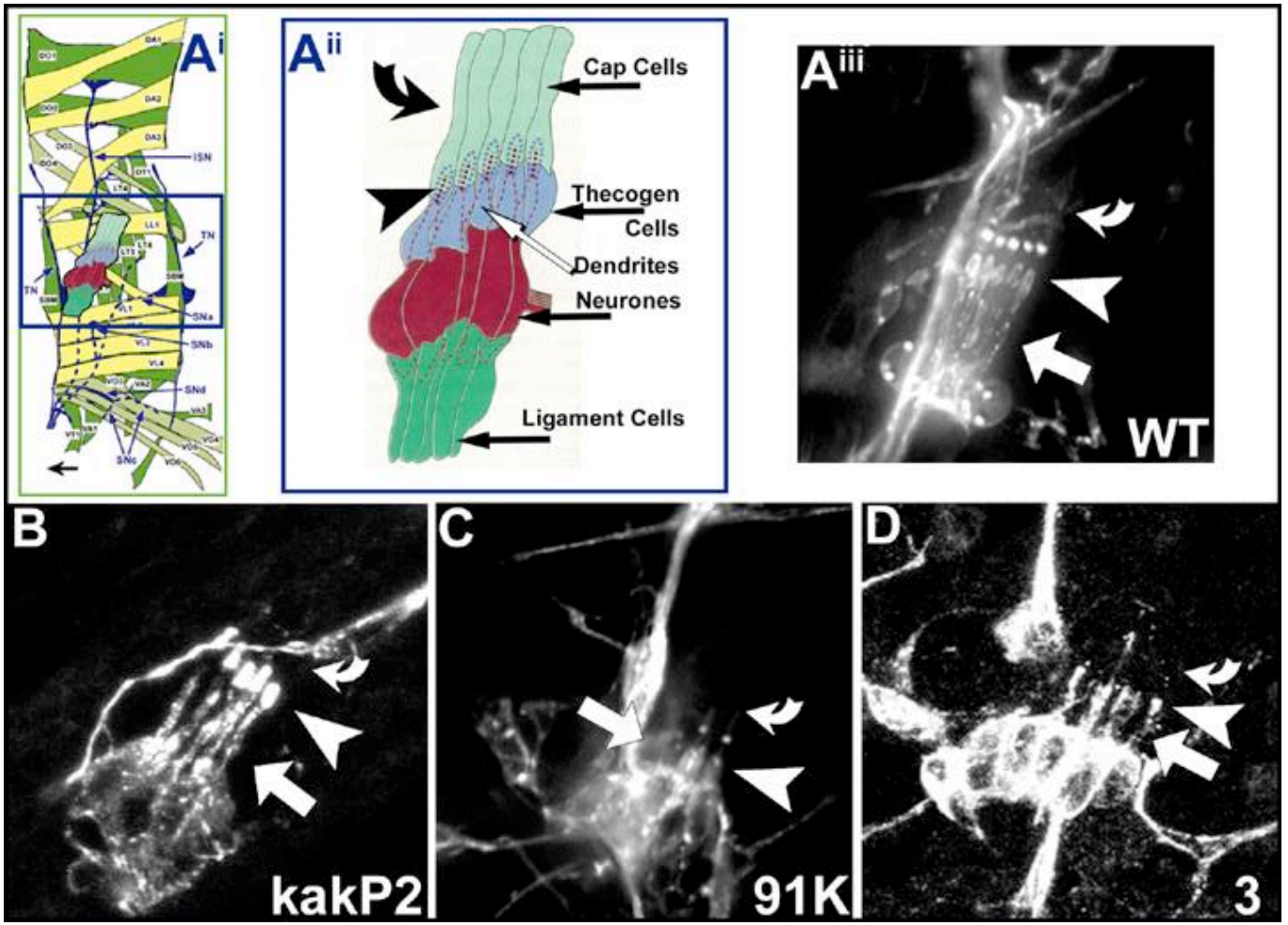
Ai
ISN
TN
SNa
SNb
SNd
SNc
Aii
Cap Cells
Thecogen Cells
Dendrites
Neurones
Ligament Cells
Aiii
WT
B
kakP2
C
91K
D
3

Figure 3.5: Comparative study of scolopidial sensory neurones. Confocal images of Futsch- (B and D) and HRP-labelled (A^{iii} and C) pentascolopidial organs (group of five scolopidia). The pentascolopidial organs are found in the lateral area in each hemisegment (blue box in A^{i}). The sensory neurones are supported by ligament cells, the dendrite enwrapping thecogen cells and the cilia surrounding cap cells (A^{ii}, modified from Campos-Ortega and Hartenstein, 1997). White arrow indicates the dendrites, arrow head points to the ciliary rootlets, bent arrow indicates location of the cilia supporting cap cells. In scolopidia of *shot* mutant alleles $shot^{91K}$ (C), $shot^{3}$ (D), $shot^{HG25}$ and $shot^{SF20}$ (not shown), the thick dendrites appear collapsed towards the somata and ciliary rootlets disaggregated. In contrast, $shot^{kakP2}$ scolopidia still send out dendrites and cilia and ciliary rootlets can be addressed. Scolopidia were observed to be wildtypic in $shot^{VI04}$ mutant alleles (not shown).

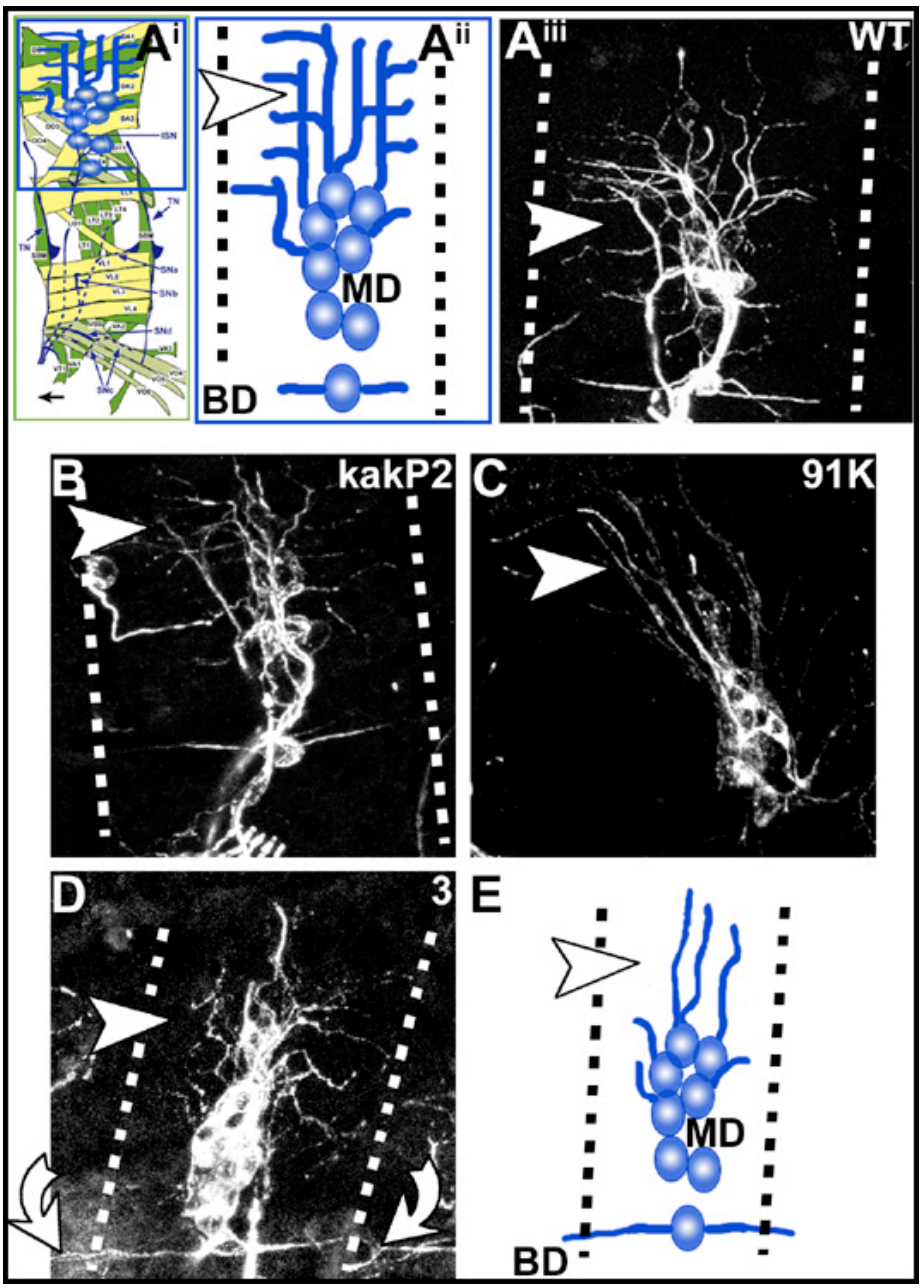
A i
A ii
MD
BD
A iii
WT
B
kakP2
C
91K
D
3
E
MD
BD

Figure 3.6: Comparative study of neuronal phenotypes: bipolar dendrite (*bd*) and multi dendrite (*md*) sensory neurones. Confocal images of Futsch-labelled *bd* and md sensory neurones of wildtype (A^{iii}) and *shot* mutant alleles (B-D). Wildtype and *shot* mutant phenotypes are summarised in A^{ii} and E, respectively. A^{i} depicts localisation of *bd* and *md* in every hemisegments. Arrowheads point to *md* dendritic projections, bent arrows in D indicate the tips of *bd* dendritic projections, dashed lines indicate the segment borders. *md* dendrite projections appear deformed and arborisations are reduced in $shot^{91K}$ (C), $shot^{3}$ (D), $shot^{HG25}$ and $shot^{SF20}$ (not shown). $shot^{kakP2}$ *md* projections (B) seem less affected. Similarly, *bd* neurone projections appear thinner and elongated in $shot^{91K}$, $shot^{3}$, $shot^{HG25}$ and $shot^{SF20}$ as compared to $shot^{kakP2}$ mutants (compare B and D). *bd* and *md* projections were observed to be wildtypic in $shot^{V104}$ and $shot^{V168}$ (not shown).

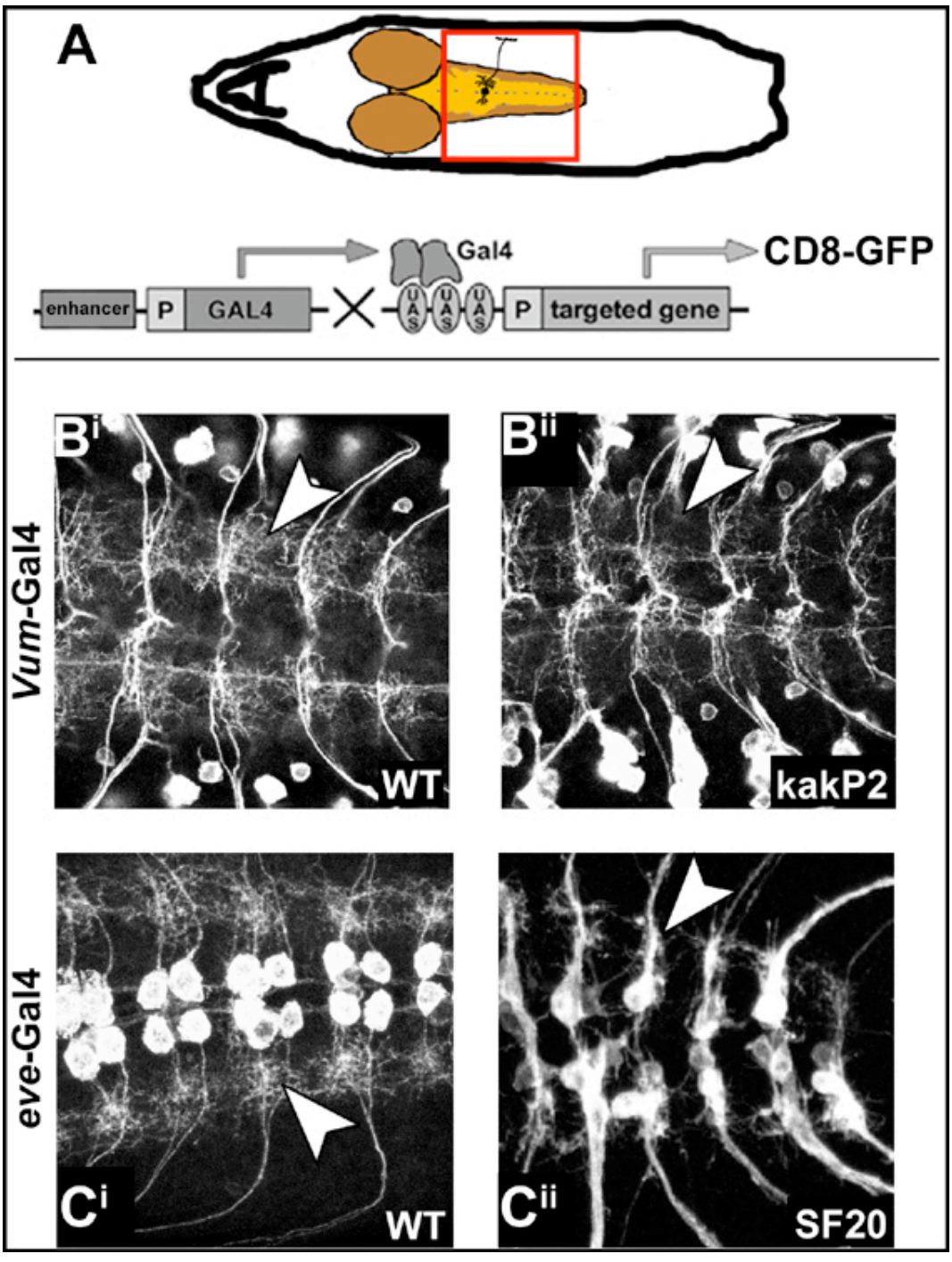
A
Gal4
CD8-GFP
enhancer
P
GAL4
UAS
UAS
UAS
P
targeted gene
Vum-Gal4
Bi
WT
Bii
kakP2
eve-Gal4
Ci
WT
Cii
SF20

Figure 3.7: Comparative study of dendritic arborisation in the CNS. The cell membrane marker CD8-GFP was expressed selectively in *Vum-Gal4*-positive motor neurones (B^{i} and B^{ii}) or aCC/RP2-motor neurones (*eve*^{RRK}-Gal4 driver, C^{i} and C^{ii}) in wildtype (left) and *shot* mutant background (right). Arrowheads point to the dendritic arborisation of the respective motor neurones, which were stained against the overexpressed marker. The confocal images show that dendrites are reduced in both *shot*^{kakP2} and *shot*^{SF20} mutant alleles. The red box in (A) depicts the studied CNS area.

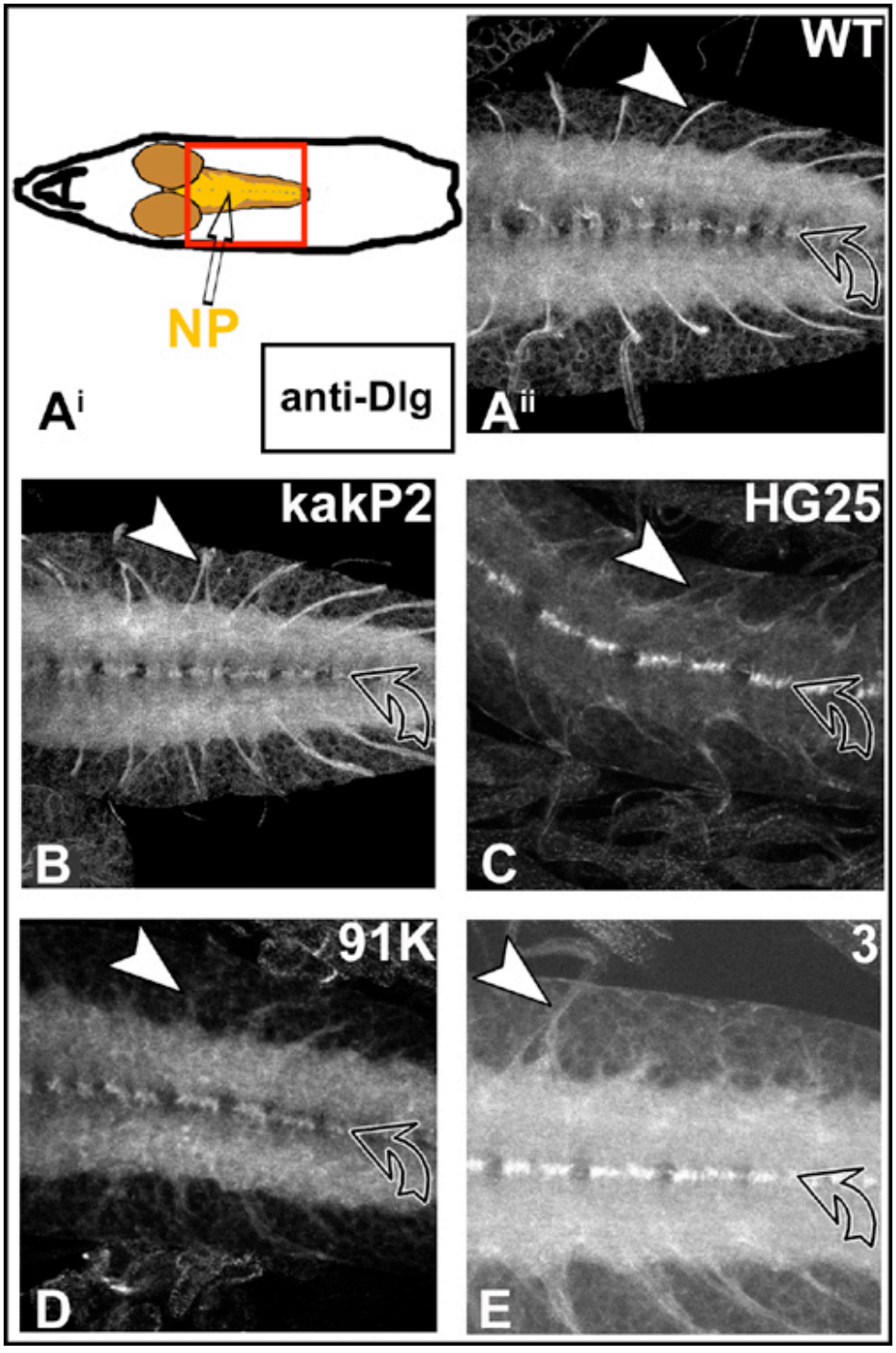
NP
Ai
anti-Dlg
WT
Aii
kakP2
B
HG25
C
91K
D
3
E

Figure 3.8: Comparative study of Dlg pattern in the CNS. Confocal images of CNS of wildtype (A^{ii}) and *shot* mutant (B-E) embryos at stage 17 stained with anti-Dlg. The red box in Ai shows the area of the CNS pictured in the studies. Dlg was found mislocalised in nerve roots (arrowheads) and commissures (bent arrows) in $shot^{HG25}$ (C), $shot^{91K}$ (D), $shot^{3}$ (E) and $shot^{SF20}$ (not shown), but not in $shot^{kakP2}$ embryos. NP: neuropile.

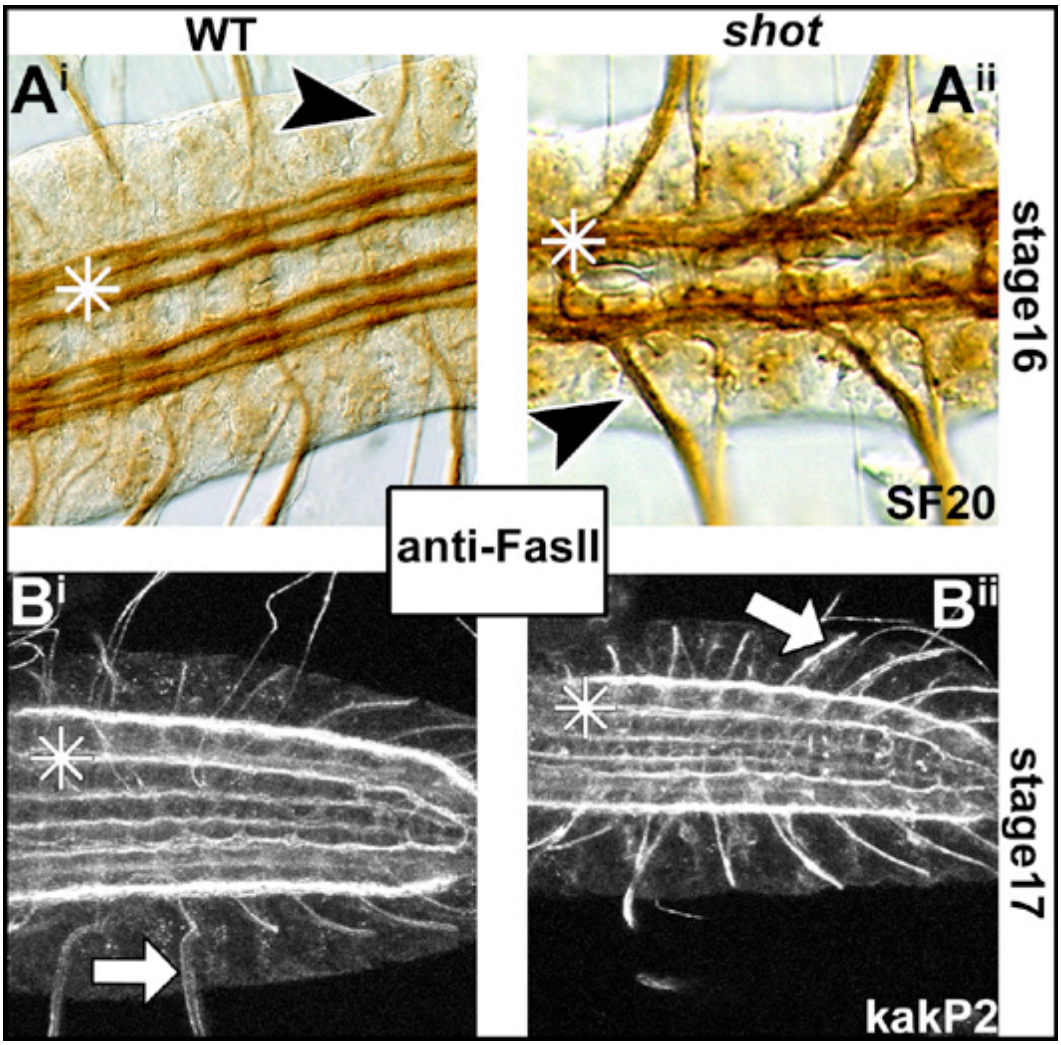
WT
shot
A^i
A^ii
stage16
SF20
anti-FasII
B^i
B^ii
stage17
kakP2

Figure 3.9: Comparative study of FasII pattern in the CNS. Light microscopic (A) and confocal (B) images of wildtype (i) and *shot* mutant (ii) embryos. Stage 16 embryos were stained with diaminobenzidine, stage 17 with fluorescent dyes. The pattern of the longitudinal FasII positive tracts (✳) were not affected in *shot* mutant alleles $shot^{SF20}$ (A^{ii}), $shot^{kakP2}$ (B^{ii}), $shot^{91K}$, $shot^{3}$ and $shot^{HG25}$ (not shown). However, FasII was found mislocalised into the nerve roots (arrowheads in A, white arrows in B) of motor neurones in all of these alleles. $shot^{V104}$ and $shot^{V168}$ nerve roots and longitudinal tracts were wildtypic (not shown).

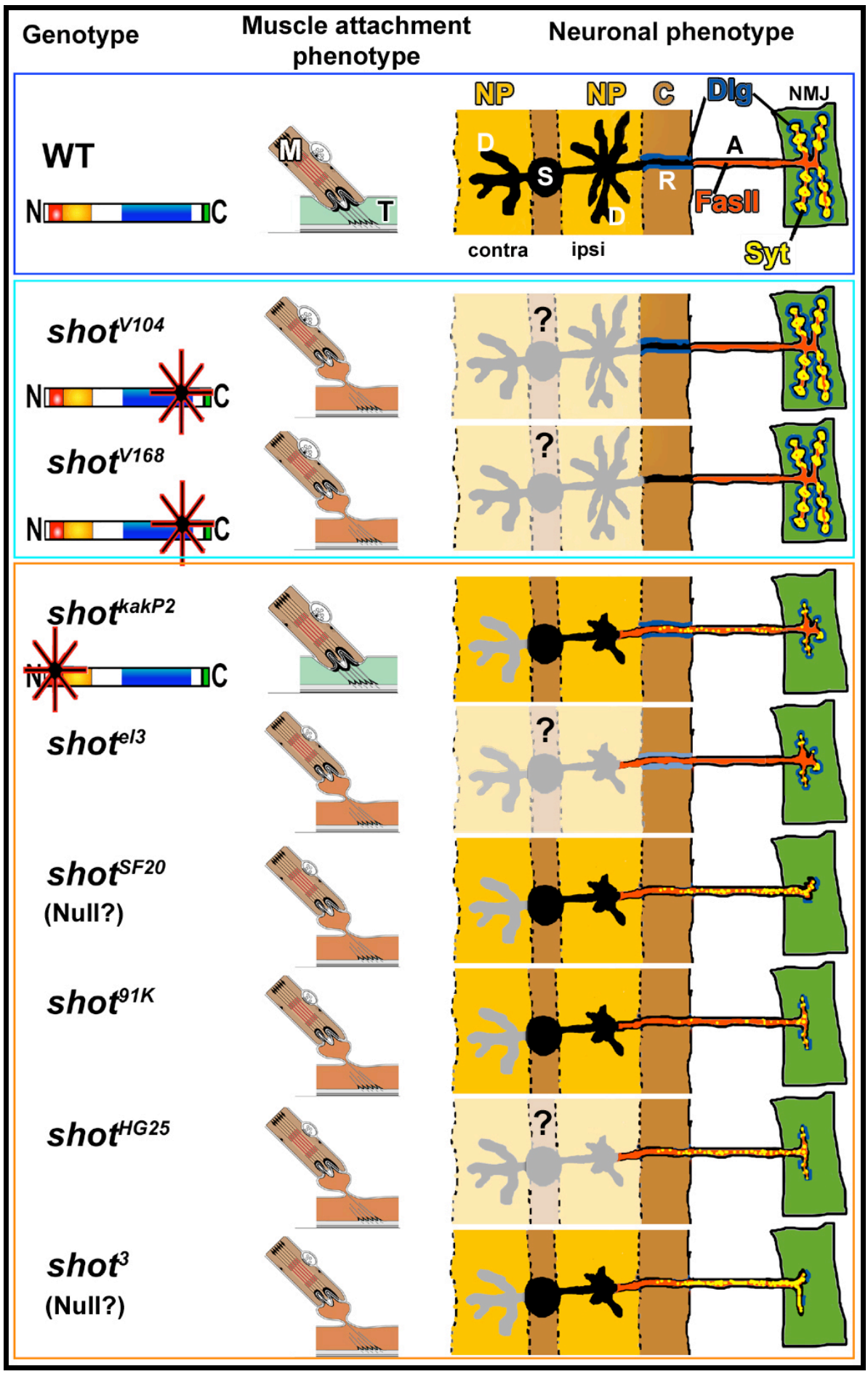
Genotype
Muscle attachment phenotype
Neuronal phenotype
WT
N
C
M
T
NP
NP
C
Dlg
NMJ
D
S
R
A
D
FasII
contra
ipsi
Syt
shotV104
shotV168
?
shotkakP2
shotel3
shotSF20
(Null?)
shot91K
shotHG25
shot3
(Null?)

Figure 3.10: Schematic summary of *shot* mutant phenotypes. *shot* mutant alleles affecting neuronal differentiation and in particular synapse formation are framed in orange (compare Table 3.1). The light blue frame highlights the *shot* mutant alleles that do not affect neuronal differentiation. Genotype: list of the investigated *shot* mutant alleles; asterisks in bar diagrammes (compare Figure 1.3 for details) indicate the potential N- or C-terminal position of the mutations in some of the alleles (for details see text). Muscle attachment phenotype: Many *shot* mutant alleles cause aberrations of the cytoskeleton in tendon cells (T), which get torn apart upon contraction of the attached muscles (M; for details of the graph see Figure 3.26 and Prokop et al., 1998b). Neuronal phenotype: graph illustrates a motor neurone with its soma (S) at the midline of the CNS, dendrites (D) in the ispi- and contralateral neuropile (NP), its primary neurite passing through the cortex (C; where it contributes to the nerve root, R) and forming the peripheral axon (A), which terminates on its target muscle (NMJ). Different phenotypes were observed in different alleles: accumulation of Disc large (DLG) in nerve roots is affected by most alleles; Fasciclin II (Fas2) is usually excluded from nerve roots whereas this compartmentalisation is abolished by most *shot* mutant alleles; most *shot* mutant alleles cause reduction of neuromuscular terminals or dendrites (? indicates non-investigated cases); most *shot* mutant alleles cause the presynaptic marker Synaptotagmin (Syt) to be mislocalised in axons. Based on the distribution of phenotypes we hypothesise that N-terminal domains of Shot play an essential role in neuronal differentiation.

3.2. *shot* mutants show defects in the organisation of the cytoskeleton in outgrowing motor neurones

As shown in Chapter 3.1., the N-terminal and central region of Shot seem to be required for synapse formation. The function of the C-terminus of Shot potentially involves proper epidermal muscle attachment cell differentiation (Strumpf and Volk, 1998). Only little is known about the molecular basis for the activity of the distinct protein regions. Several studies have suggested that *shot* functions as a cytoskeletal element with Actin- and Microtubule (MT) binding, organising and cross-linking properties (Gregory and Brown, 1998; Leung et al., 1999; Strumpf and Volk, 1998). The ABD and MT binding domains of the N-terminus of MACF1, the mammalian homologue of Shot, were shown to form direct interactions with microfilaments and MTs, respectively (Karakesisoglou et al., 2000). A direct binding between the C-terminal Gas2 domain and α-Tubulin has been demonstrated in a yeast two-hybrid assay (Lee and Kolodziej, 2002b). Growth and maintenance of the motor neuronal terminal are likely to involve the cytoskeletal elements Actin and Tubulin (Intermediate Filaments are found missing in insects; Weber et al., 1991). The arrangements of cytoskeletal elements can hardly be studied at the mature *Drosophila* NMJ on lightmicroscopic level due to its small size at late embryonic stages. However, at earlier stages of NMJ formation, namely just before the transition phase from axonal growth to target recognition and synaptic differentiation the tips of motor neurones still display growth cone-like structures. It has been shown in other animal systems that the cytoskeleton is accessible within growth cone structures (Challacombe et al., 1997; Dent et al., 1999; Lin and Forscher, 1995; Lu et al., 1997).

Drosophila motor neuronal growth cones were analysed in an attempt to find out whether they can be used as an appropriate model to study the *in situ* arrangements of cytoskeletal proteins. Studies at subcellular level would advance the understanding of Shot function by allowing description of growth cone morphology and cytoskeletal arrangements in wildtype as compared to *shot* mutant background, and by assessing the localisation of intrinsic Shot and misexpressed Shot domains with respect to the cytoskeletal elements.

Motor neurones of stage 16 embryos were labelled with anti-HRP (see Chapter 3.1.). Simultaneously applied antiserum to the β-Tubulin subunit revealed strong staining of MTs along axonal shafts. Within the growth cone structure, the β-Tubulin antibody showed

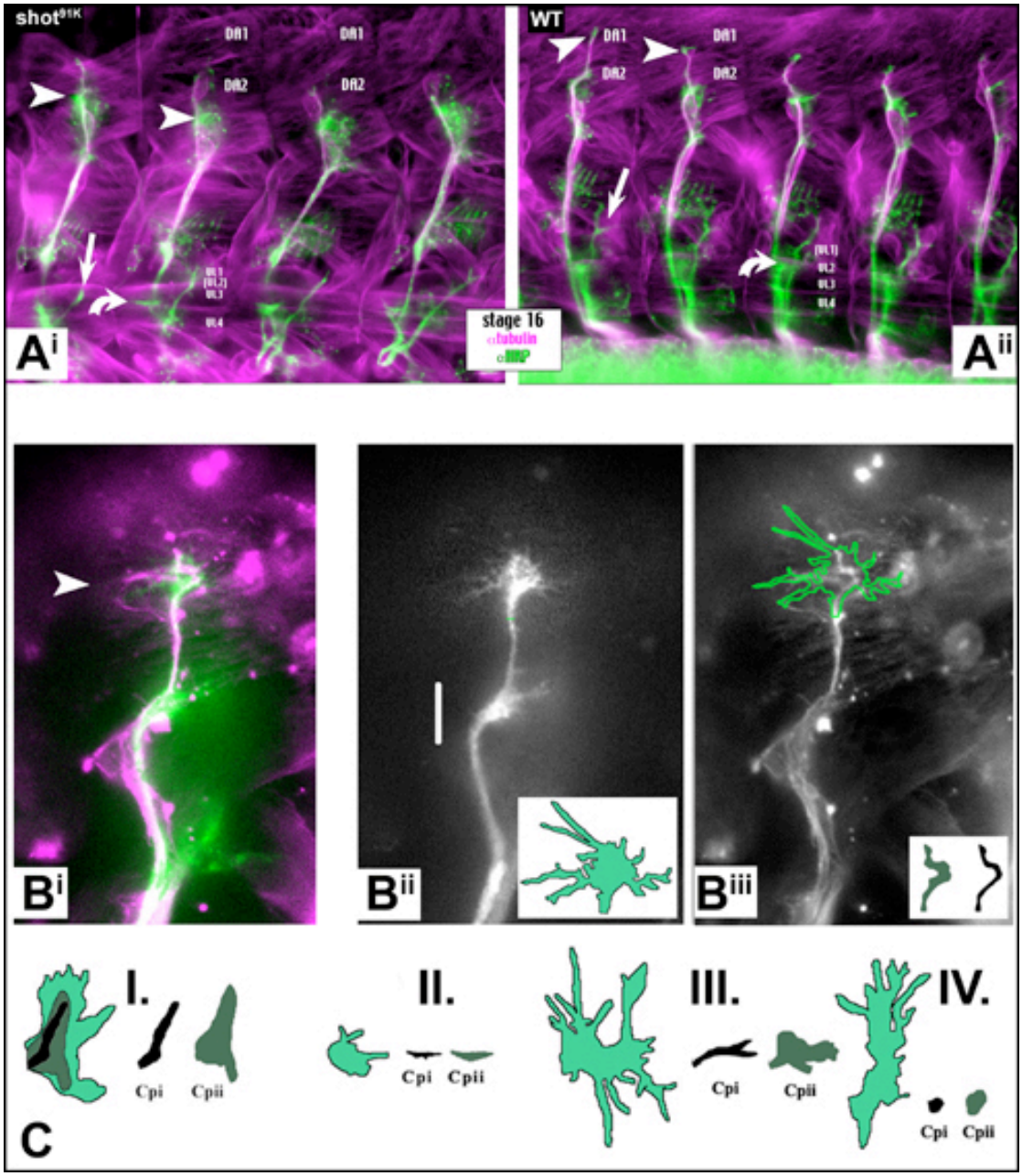
shot3IK
DA1
DA2
DA1
DA2
WT
DA1
DA2
DA1
DA2
stage 16
α-tubulin
α-MAP
Ai
Aii
Bi
Bii
Biii
I.
Cpi
Cpii
II.
Cpi
Cpii
III.
Cpi
Cpii
IV.
Cpi
Cpii
C

strongly stained MTs in the centre, which were surrounded by a small area of weaker stained MTs (Figure 3.11). Similar MT organisation has been reported for other growth cone systems, e.g. for cultured chicken dorsal root ganglion neurones (Challacombe et al., 1997) or bag cell neurones of *Aplysia* (Suter and Forscher, 1998). According to Challacombe et al. (1997), the central core of MTs represents stable MT bundles, while dynamic MT bundles compose the surrounding, weaker stained area.

Motor neuronal growth cones of ISNs were best visible within the surrounding tissue. On the basis of confocal images, the perimeter of ISN growth cones and subcellular MT organisation were traced, by starting and finishing at the transition point of the axon shaft into the growth cone structure, using Adobe Photoshop Software. To quantify the degree of growth cone and MT complexity, the perimeter and area were measured using NIH Image Software. Subsequently, the P2A value (square of perimeter divided by the area), a well established parameter for the complexity of growth cones (Bowie and Young, 1977; Hall et al., 2000), was calculated. The higher the P2A value, the more or longer filopodia are formed, or, as for the MT organisation, the more MT bundles are dispersed within the growth cone structure. Additionally, the percentage of the growth cone area filled out by MTs was calculated in order to establish a relationship between both parameters.

Figure 3.11: Measurement of growth cone and subcellular MT complexity in stage 16 embryos. (A) lightmicroscopic images showing an overview of opened flat *shot*^{91K} mutant (A^{i}) and wildtype (A^{ii}) stage 16 embryos. Motor neurones were stained with anti-HRP (green), MT were labelled with anti-β-tubulin (magenta). Confocal images were taken of ISN motor neuronal growth cones (B^{i}; white arrow head), and the perimeter of the growth cone was traced (B^{ii}). Within the growth cone area, the perimeter of the stable MT bundles (shown in black) and of the entire visible MTs within the growth cone (shown in grey) was traced (B^{iii}). The respective perimeter and area of the growth cone, the stable MT bundles (Cpi) and of the entire visible MT (stable and dynamic MT bundles, Cpii) were measured and the degree of complexity was calculated using a well established parameter (see text). C shows examples of traced growth cones and MTs of *shot* mutant (I and II) and wildtype (III and IV) embryos. Measurements were carried out in blind tests in order to circumvent biased evaluations. Anterior is to the left. Scale bar in B^{ii}, 10 µm. White arrows point to the tip of the SNa, bent white arrows point to the tip of the SNb. Muscle nomenclature according to Landgraf et al., 1997.

P2A values for growth cone, stable MT bundles (P2Ai) and total MT (stable plus dynamic MT; P2Aii) of wildtype ISN projections as compared to those of the *shot* mutant alleles $shot^{HG25}$, $shot^{SF20}$ and $shot^{91K}$, respectively, are presented in table 3.2. Embryos were precisely staged (see Chapter 2.1.5.) and all dorsal motor neuronal projections in these embryos were observed to reach similarly far into the periphery (Figure 3.11 A^{i} and A^{ii}). Nonetheless, the growth cone morphologies of ISNs were observed to differ remarkably even within two adjacent hemisegments of the same embryo, which is expressed in the high deviation numbers obtained for the P2A values measured. These values possibly also result from further problems encountered during the documentation and measurement of growth cones and cytoskeletal organisations therein:

i) The method applied to trace the growth cone perimeter as well as the perimeter of the MT bundles showed to be very tedious, which restricted the possibilities to increase the sample number.

ii) High background of Tubulin-staining in the surrounding tissue often impaired the accessibility to the MT bundles within the growth cone structures (see Figure 3.11.A, growth cones of the ISN were often found to stall at the height of *md* sensory neurones).

iii) *Drosophila* growth cones are very small structures, which are not always completely labelled. This leaded to further errors in the measurement of growth cone perimeters.

iv) The growth cones of the ISNs represent several growth cones at a time (growth cones of the motor neurones aCC, RP2 and Q). Hence, it was not possible to carry out the measurements at single cell resolution, and differences in P2A-values of individual growth cones escape the detection.

Therefore, the results presented have to be considered carefully. However, they might reflect that Shot function influences the organisation of the dynamic MT in motor neuronal growth cones. The results would also imply that Shot function within the growth cone exceeds organisation of the dynamic MT, since reduced P2A values obtained for dynamic MT bundles (P2Aii) not necessarily lead to reduced degrees of growth cone complexity (P2A), as observed in $shot^{91k}$ (see Table 3.2). Furthermore, the results would suggest that different mutant alleles of *shot* have the tendency to influence the cytoskeleton differentially. This would be in agreement to findings in the comparative morphological studies described in Chapter 3.1., where different mutant alleles were found to display divergent degrees and combinations of phenotypes (see table 3.1). As postulated in Chapter 3.1., the display of

different mutant phenotypes suggest Shot to exert its function through a variety of interactions mediated by its distinct domains.

	n ISN-growth cone	P2A±SD	P2Ai	P2Aii	%of aii in a
shot^{HG25}	22	93,32±45,99	36,49±31,9	37,54±29,54	22,34±20,76
wildtype-Control	19	101,15±39,13	37,57±30,18	33,98±21,39	21,99±20,32
WMW-test		p=0,403	p=0,895	p=0,9166	p=0,895
shot^{SF20}	16	45,19±13,19	53,49±21,8	44,34±27,9	13,13±9,45
wildtype-control	22	97,57±47,4	45,36±23,68	49,58±22,3	25,13±9,8
WMW-test		p=0,0006	p=0,8825	p=0,0413	p=0,0023
shot^{91K}	12 (6)	85,02±34,35	(32,21±19,18)	(27,98±5,58)	4,5±6
wildtype-control	16	106,43±61,76	40,5±14,37	32,37±9,11	16,45±7,8
WMW-test		p=0,516	(p=0,416)	(p=0,0024)	p=0,0005

Table 3.2: Summary of the mean values measured for complexities of ISN growth cones (P2A), core MT bundles (P2Ai), and dynamic MT (P2Aii) in the *shot* mutant embryos *kak*^{HG25}, *kak*^{SF20}, *kak*^{91K} and respective wildtype controls. Statistical significance of the different data was calculated using the Wilcoxon-Mann-Whitney-Rank test (WMW-test; see Chapter 2.1.10.). aii, area of stable and dynamic MT perimeter; a, area of the growth cone perimeter. SD, standard deviation. *shot*^{HG25} showed no differences in growth cone or MT P2A values, respectively, as compared to wildtype. The allele *shot*^{SF20}, however, revealed to have a reduced growth cone P2A value. Furthermore, differences in the MT organisation could be observed: A smaller P2Aii value was calculated, and less MTs were found within the growth cone area. Yet, the P2Ai value was not significantly different to that in wildtype. Thus, the organisation of the stable MT bundles did not seem to be affected. Similar findings were obtained for the mutant allele *shot*^{91k}. Here, too, the P2Aii was smaller than in wildtype, and less MTs were found within the growth cone area. As in *shot*^{SF20}, the organisation of the stable MT bundles did not appear to be different to that found in wildtype. Interestingly, in contrast to *shot*^{SF20}, *shot*^{91k} did not show significant differences in the P2A value as compared to wildtype. Though differences can be observed for the MT organisation, the degree of complexity of growth cones did not seem to be reduced in this *shot* mutant allele. The results presented have to be considered with care, since the growth cone system revealed disadvantages outlined in the text.

The disadvantages of the growth cone system encountered could be circumvented by the use of new available constructs (UAS-Actin-GFP, Sepp and Auld, 2003; Verkhusha et al.,

1999; UAS-Tubulin-GFP, Grieder et al., 2000). The targeted expression of these constructs would allow the analyses of cytoskeletal organisations within growth cones to be carried out at single cell level. However, there was no time to repeat these experiments on the basis of the new tools in the course of this thesis.

In order to dissect the molecular basis for Shot activity it was instead considered to misexpress different tagged Shot domains in neuronal tissues of third instar larvae. The localisation of the different domains could allow assumptions about the nature of molecular interactions of Shot.

3.3. N- but not C-terminal domains of Shot localise at presynaptic sites of NMJs

As shown earlier, Shot seems to influence the organisation of the cytoskeleton in outgrowing motor neurones (Chapter 3.2.). It might further be, that Shot has the tendency to influence the growth cone shape independently of cytoskeletal arrangements. This would be in agreement with results presented in Chapter 3.1., which bring forward the notion, that mutations in different *shot* alleles might affect the function of distinct Shot domains, giving rise to the varieties of phenotype combinations observed in the different *shot* alleles. Transgenic flies carrying different domains of Shot tagged with GFP or TAP-tag were used to study the molecular nature and specific protein-protein interactions of these domains. The Shot protein contains distinct structural domains, which are highly conserved (Figure 1.3). Three different Shot domains, placed under the control of UAS, were used to create transgenic flies (work carried out by Arul Subramanian and Talila Volk; Subramanian et al., 2003): The first construct contains both the ABD and the Plakin domain (PAT; amino acids 1-1202 in the long isoform A of Shot - see Figure 1.3), the second comprises the Plakin domain alone (PT; amino acids 379-1202) and the third includes EF Hand motifs and the GAS2 homology domain (GT; amino acids 4842-5272). Expression of these domains was driven by the Gal4-driver lines *elav-Gal4* (Lin and Goodman, 1994; Luo et al., 1994), *eve-Gal4* (Baines et al., 1999), *DDC-Gal4* (Landgraf et al., 2003; Li et al., 2000), *Vum-Gal4* (Landgraf et al., 2003), and *MJ94-Gal4* (Joiner and Griffith, 2000; Figure 3.12). All Gal4-lines used drive Gal4 expression at late larval stages, allowing the analysis of Shot-construct localisation in third instar larvae (dissection at this stage is far easier than at late embryonic stages, see

Chapter 2.1.7., and due to the much larger body size, the resolution for subcellular studies is much better). Strongest expression was observed for the Plakin domain, the construct bearing the C-terminal domains was expressed at lowest levels. The different Shot domains were found to localise differentially in all misexpression studies applied.

Misexpression of the constructs in motor neurones using *elav-Gal4* as driver, resulted in the localisation of both N-terminal domains (PT and PAT) in somata, axons and at NMJs (Figure 3.13). The C-terminal domain, on the other side, was found in somata, in axons and within branches of NMJs, however excluded from presynaptic sites, as revealed by simultaneous staining for presynaptic Syt. Thus, both PAT and PT, but not GT are localised at presynaptic sites of motor neurones. This suggests N-terminal domains to display specific protein-protein interactions with factors at the NMJ. Differential localisation of the domains was also observed in neuronal cells other than motor neurones (Figure 3.14). Within peripheral multidendritic sensory neurones GT localised evenly along the dendritic branches, whilst both PAT and PT localised in small clusters. The cluster localisation was observed to coincide with small swellings found in dendritic protrusions (not shown). These structures have so far not been described in detail. Besides other possible explanations, they could represent sites from which secondary and tertiary projections branch off the main dendritic tract (Gao et al., 1999; Grueber et al., 2002) or transport vesicles within the branches. In scolopidial sensory organs, GT was found to localise in the somata and the dendritic protrusions of the sensory cells. The N-terminal constructs were found in the somata as well, but not along the dendritic protrusions. Rather the domains were detected at the tip of the dendrites and in the capsules of the sensory cells. Interestingly, both the dendrite protrusions and structures within the capsules were reported to be affected in *shot* mutant embryos (Prokop et al., 1998b ; see Figure 3.5). Thus, the constructs are found at sites of Shot action, suggesting that the specific localisations reflect protein-protein interactions with accurate Shot interaction partners.

Expression of the constructs using *eve*^{RRK}*-Gal4* as driver resulted in similar differential localisations of the respective domains as observed in motor neurones with *elav-Gal4* driven construct expression. PAT was found in the nuclei and in boutons of NMJs. PT localised in nuclei, somata, axons and in boutons of NMJs. GT localised comparable to PT in somata, axons and additionally in peripheral terminal branches, but was excluded from boutons (Figure 3.15). Though both N-terminal constructs were found at presynaptic sites, only PT was found in axonal projections. This suggests that PT has the tendency of interacting with different partners in distinct cellular compartments. It could also be argued that the axonal

localisation of PT might reflect unspecific localisation due to diffusion or transport of the ectopic protein fragment. However, PT would then be expected to also localise within the peripheral terminal branches, which is not the case in Gal4-expressing driver lines tested (see also below).

In peripheral projections of larvae with *DDC-Gal4-* and *Vum-Gal4*-driven expression of the constructs, the N-terminal domains were found in boutons, with PT additionally localising in axonal tracts (Figures 3.16 and 3.17). GT was found in axonal tracts only. The localisation pattern obtained in the CNS was also similar to previous findings (*eve-Gal4*). Interestingly, both N-terminal constructs additionally localised in a varicous pattern along the neuropile, clearly reflecting only a subpattern of projections targeted by these Gal4-driver lines (compare Landgraf et al., 2003). It was not yet possible to determine whether this localisation reflects potential pre- or postsynaptic sites. Since both Gal4-driver lines contain peptidergic neurones, the results might reflect localisations of the respective constructs in specific neurone types, compared to *eve-Gal4*, where only motor neurones are stained. In *eve-Gal4*, PT was detected in axons of central projections only.

MJ94-Gal4 mediated Shot-construct expression confirmed the differential localisation of the three Shot domains observed in *elav-Gal4* driving peripheral sensory neurones (Figure 3.18). In this line however, PAT is detected exclusively in the nucleus. On the one hand, the nuclear export of the misexpressed domain could be inefficient in this GAL-driver line due to lower expression levels. On the other hand, as can be assumed for the experiments with the other Gal4-driver lines, the localisation presumably reflects cleaved tag that generally targets to the nuclei (Subramanian et al., 2003).

The studies with the different Shot domains show that PAT and PT, but not GT, are capable of driving the specific localisation of the respective domains to presynaptic sites especially at the NMJ. This suggests that GT does not bind to proteins that are highly localised in synapses. Alternatively, synaptic proteins that may form a complex with this domain may be engaged in existing protein complexes and are therefore not accessible to the exogenous C-terminal domain. The Plakin domain shares presynaptic localisation with both, the PAT and the C-terminal domain, whereas there were clear differences in the axonal localisation. The Plakin domain is found in all Shot isoforms (Röper et al., 2002). It is therefore likely that the Plakin domain is binding to a variety of factors, and that each interaction depends on the subcellular (and possibly developmental) context of the cell. Since the Plakin domain in conjunction with the ABD (PAT) has the tendency to localise more

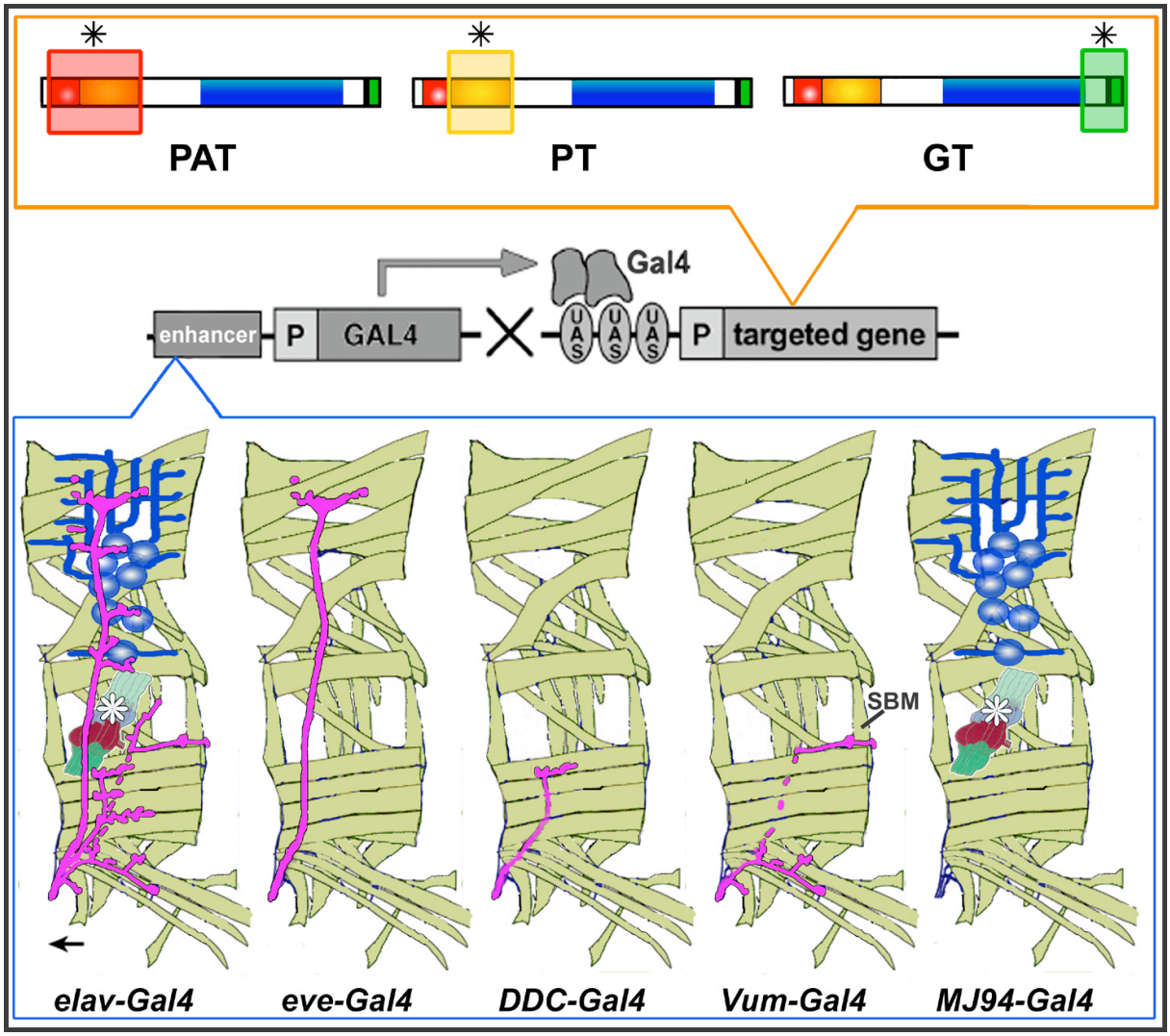
PAT
PT
GT
Gal4
enhancer
P
GAL4
UAS
UAS
UAS
P
targeted gene
SBM
elav-Gal4
eve-Gal4
DDC-Gal4
Vum-Gal4
MJ94-Gal4

specifically to presynaptic sites, it is possible that the ABD is targeting the localisation of the Plakin domain to this particular cellular compartment.

None of the domains tested showed a dominant-negative effect when misexpressed, suggesting that the proteins to which they bind are not present in limited amount. In scolopidial neurones, the differential localisation was found to cover distinct cellular compartments affected in *shot* mutants. This suggests that the observed localisations reflect true wildtype Shot interactions. However, the localisation of the distinct domains can result from inappropriate interactions. In order to rule this out and to confirm the results obtained in the misexpression study, antibodies raised against specific domains of Shot were applied in wildtype third instar larvae.

Figure 3.12: Schematic summary of the peripheral expression pattern of different Gal4 lines used to misexpress distinct tagged Shot domains. The Shot constructs (orange box, top) comprised the ABD and Plakin domain (PAT), the Plakin domain alone (PT) and a C-terminal domain covering the EF-Hand motifs and GAS2 homology (GT; The respective domains are indicated in the bar code with ✳; For a more detailed map of the gene see Figure 1.3). The Gal4-lines (blue box) used to misexpress these domains were the panneuronal driver *elav-Gal4* (all motor neurones and sensory neurones, *md* and *bd* shown in blue, *sc* marked by asterisk; for clarity only a fraction of sensory neurones is shown), *eve-Gal4* (motor neurones of the dorsalmost muscles aCC and RP2, see also chapter 3.1.), *DDC-Gal4* (expresses Gal4 in 9-11 neurones per abdominal hemisegment -not shown- plus one efferent neuromodulatory projection to muscle VL1), *Vum-Gal4* (see also chapter 3.1.; displays per abdominal hemisegment 12-14 cells, amongst which are the cells projecting to the ventral oblique and segment border muscle SBM shown in the graphic. Additionally *Vum-Gal4* drives Gal4 expression in three unpaired efferent *Vum* neurones per segment, for clarity not shown in the graphic), and *MJ94-Gal4* (chemosensory neurones of the CNS - not shown - and the majority of sensory peripheral neurones, for clarity only a fraction of sensory neurones is shown). Black arrow points anterior.

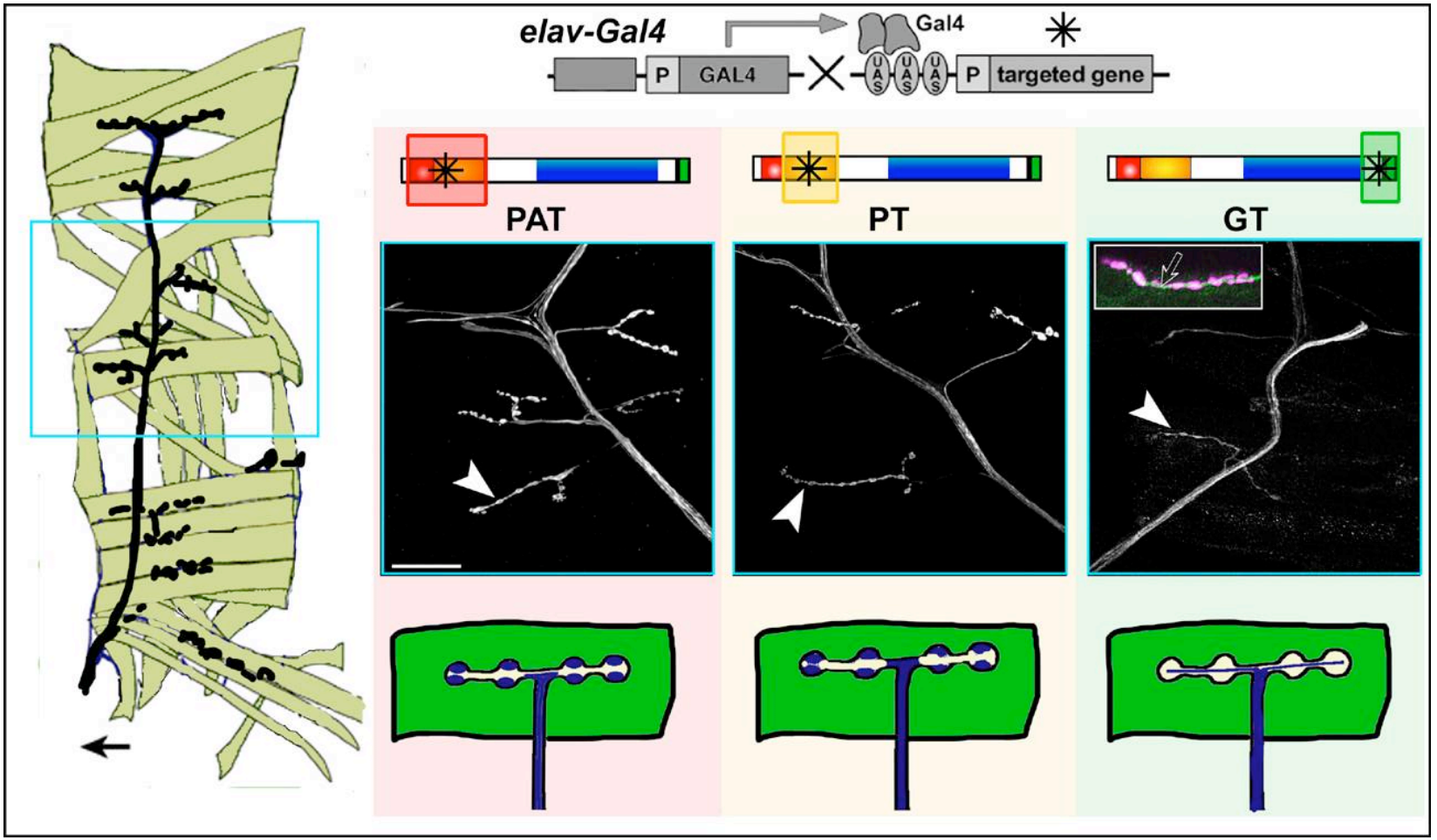
elav-Gal4
Gal4
P
GAL4
UAS
UAS
UAS
P
targeted gene
PAT
PT
GT

Figure 3.13: ***Elav-Gal4*** **driven expression of distinct Shot constructs in motor neurones reveals differential localisation of the respective protein domains. Confocal images of PAT (red) PT (yellow) or GT (green) in misexpressing motor neurones (labelled with TAP-tag binding rabbit IgG). Both N-terminal domains localise in boutons and axonal projections. The C-terminal domain is found in axonal projections and branches only, as revealed by double stain with anti-Syt (in magenta in the enlarged picture of the anterior motor neuronal projection on muscle 4, white arrowhead; the open arrow points to the green stained GT construct). The localisation of the distinct domains is summarised in the cartoons in the lower row (blue: respective construct; green: muscle). The cartoon on the left shows the imaged area. The black arrow points anterior. White bar 40µm.**

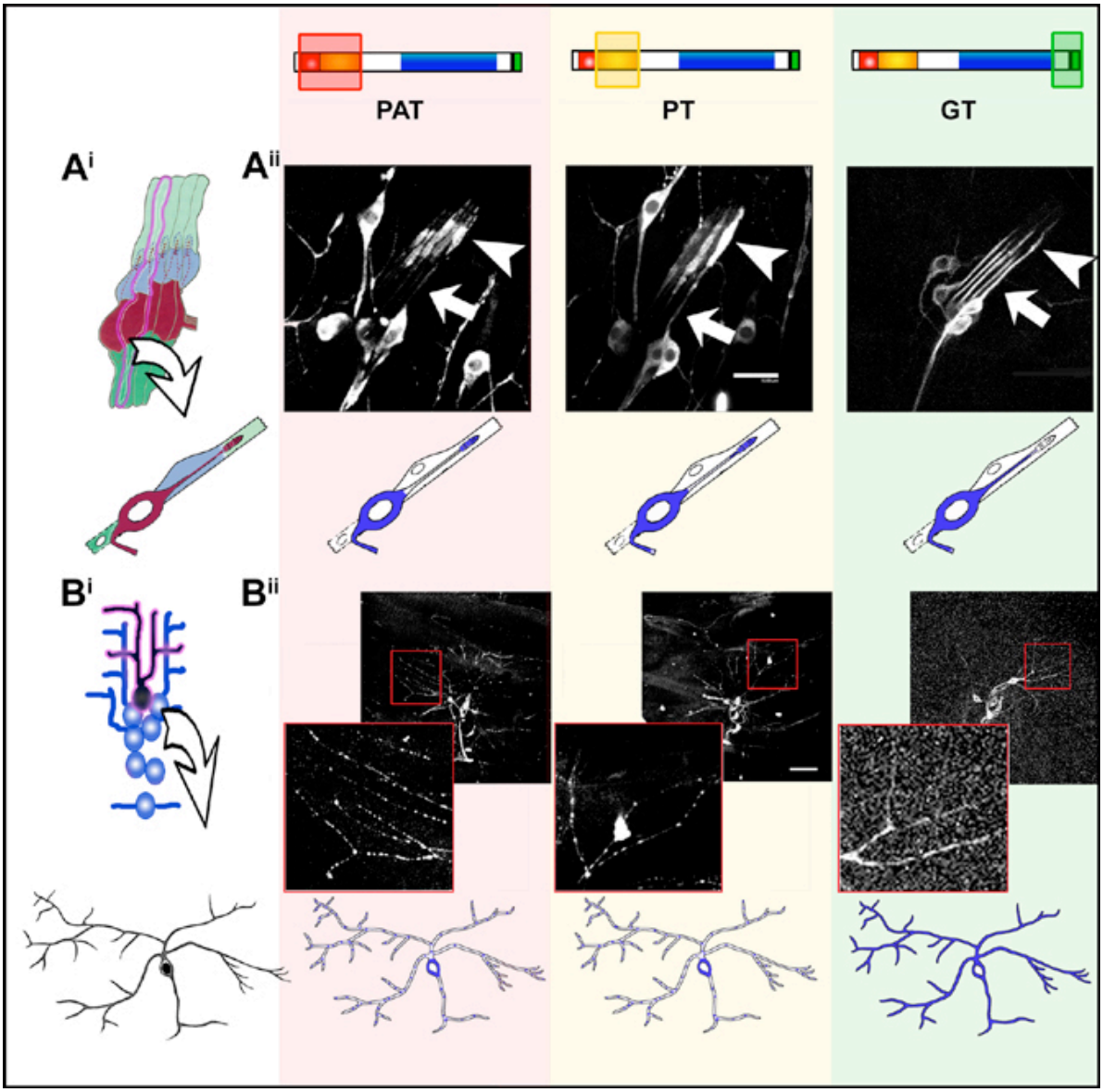
PAT
PT
GT
Ai
Aii
Bi
Bii

Figure 3.14: *Elav-Gal4* driven expression of Shot constructs PAT, PT and GT in peripheral sensory neurones. Background colour code as in Figure 3.13. A^{i} and B^{i} show schematic representations of the respective sensory organs depicted. Confocal pictures of the distinct Shot domains labelled with rabbit IgG in *sc* organs (Aii; Bar 8μm) and *md* sensory cells (Bii; Bar 40 μm) are shown. In *sc* cells, both N-terminal domains localise to somata and capsules (arrowheads), while the C-terminal domain is found in somata and dendrite shafts (arrows). Bottom row of pictures in B^{ii} are enlargements of the *md* dendritic projections outlined by the red squares. In these projections, the N-terminal domains PAT and PT are found in little clusters. In contrast, GT localises evenly along the dendrites. In the cartoons below the confocal pictures the localisation of the constructs is represented in blue.

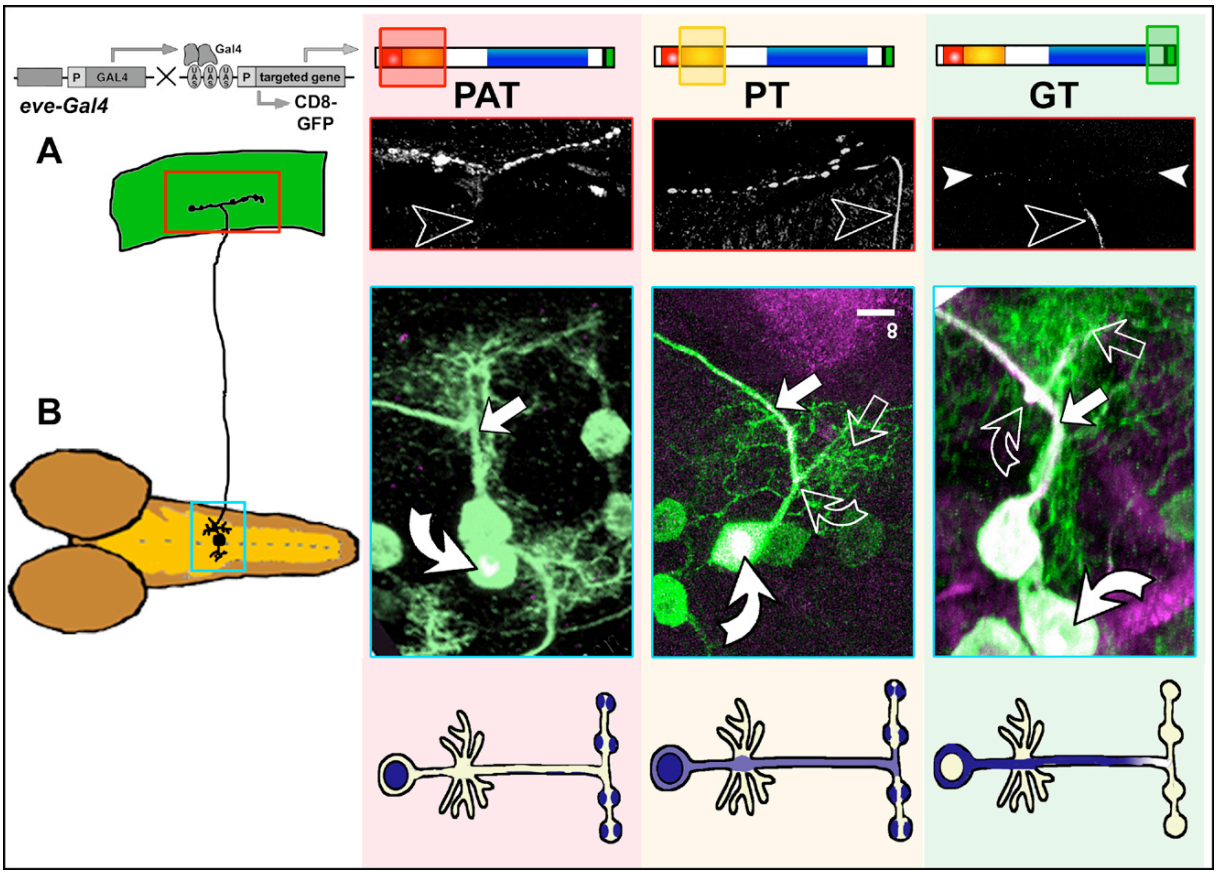
Gal4
P
GAL4
P
targeted gene
eve-Gal4
CD8-
GFP
A
B
PAT
PT
GT

Figure 3.15: Misexpression of the Shot constructs driven by *eve-Gal4* results in differential localisation of the respective domains in motor neurones aCC and RP2. Confocal images of motor neuronal projections are shown in A, of cell bodies and central dendrites are shown in B. The constructs were detected with rabbit IgG (magenta in B). In order to visualise the construct expressing cells, the membranous marker CD8-GFP was co-expressed and detected with anti-GFP antibody (green in B, not shown in A). In the motor neuronal projections, PAT is found exclusively in the boutons. PT is found in boutons as well, but further localises in axonal tracts (open arrowheads). GT is found in the axonal tracts but is excluded from the NMJs (area of the NMJ is indicated by the small arrowheads). In the CNS (B), PT and GT were detected in axons (arrow) and the somata (bent open arrows) but both domains were not observed within the dendrites (open arrow). PT and PAT, but not GT, were found in the nuclei (bent arrow). Bar 8µm. Colour code of the summarising cartoons as above.

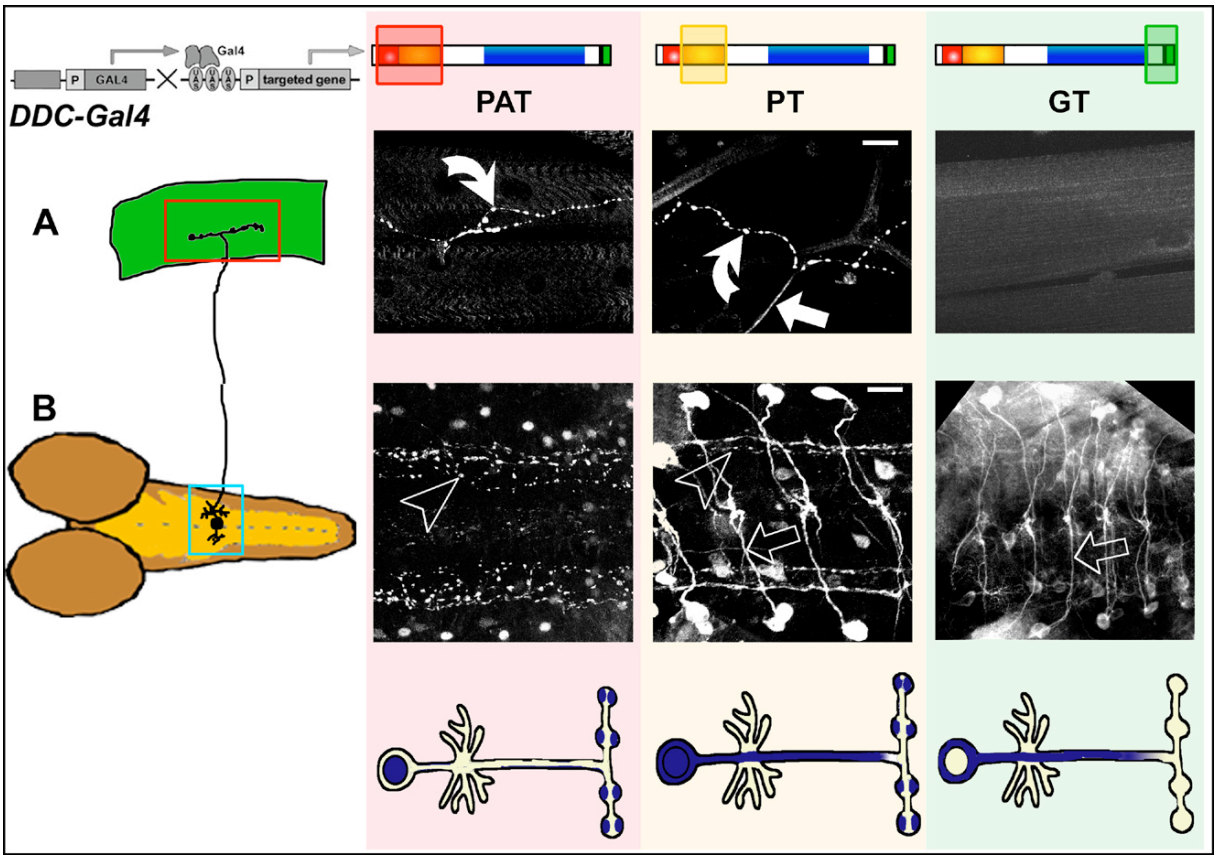
Gal4
P
GAL4
P
targeted gene
DDC-Gal4
A
B
PAT
PT
GT

Figure 3.16: *DDC-Gal4* driven expression of PAT, PT and GT. The misexpressed domains were detected with rabbit IgG. Peripheral projections are depicted in A, localisation of the domains in the CNS is shown in B. Similar to results presented in Figure 3.15 PAT and PT localise synaptically (bent white arrows). PT was additionally found in axonal tracts (white arrow). GT was hardly detectable in the periphery. In the CNS however, PT and GT were found in somata and axonal tracts (B, open arrows). As in neurones with *eve*-mediated expression, neither PT nor GT could be detected in dendritic branches (not shown; however, dendrites of DDC-neurones are fairly small and misexpressed constructs might have escaped detection). PAT and PT are localised in varicous patterns along the neuropile (open arrowheads). It is unclear, whether this localisation is pre- or postsynaptic. Bars in A and B are 20 µm. Colour code as above.

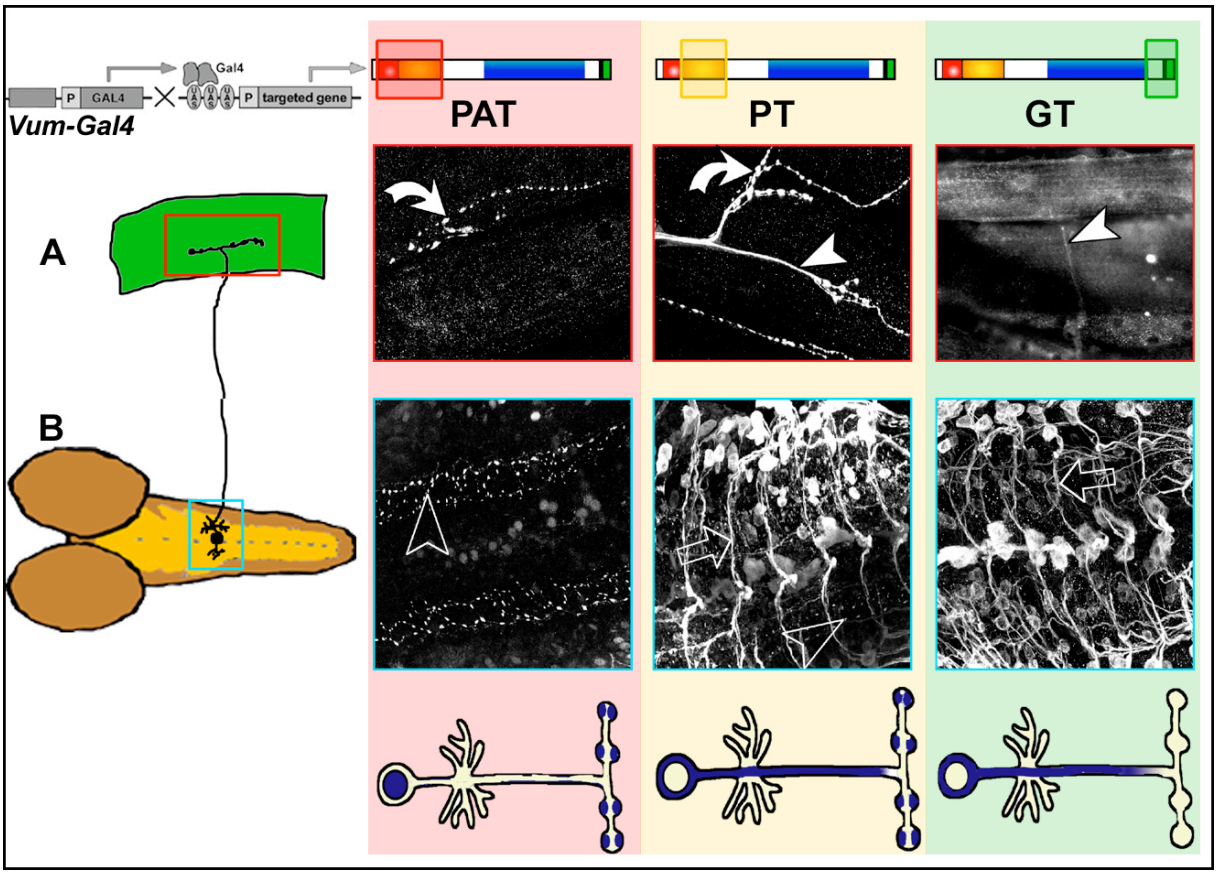
Gal4
P
GAL4
P
targeted gene
Vum-Gal4
A
B
PAT
PT
GT

Figure 3.17: Misexpression of the different Shot constructs with *Vum-Gal4*. Confocal images of peripheral (A) and central projections (B) are shown. The domains were detected with rabbit IgG in synapses (PAT, bent arrows; open arrowheads in the CNS) or axonal tracts (GT, white arrowheads; open arrow in the CNS) or both (PT), confirming previous results with other Gal4-drivers. Colour code as above.

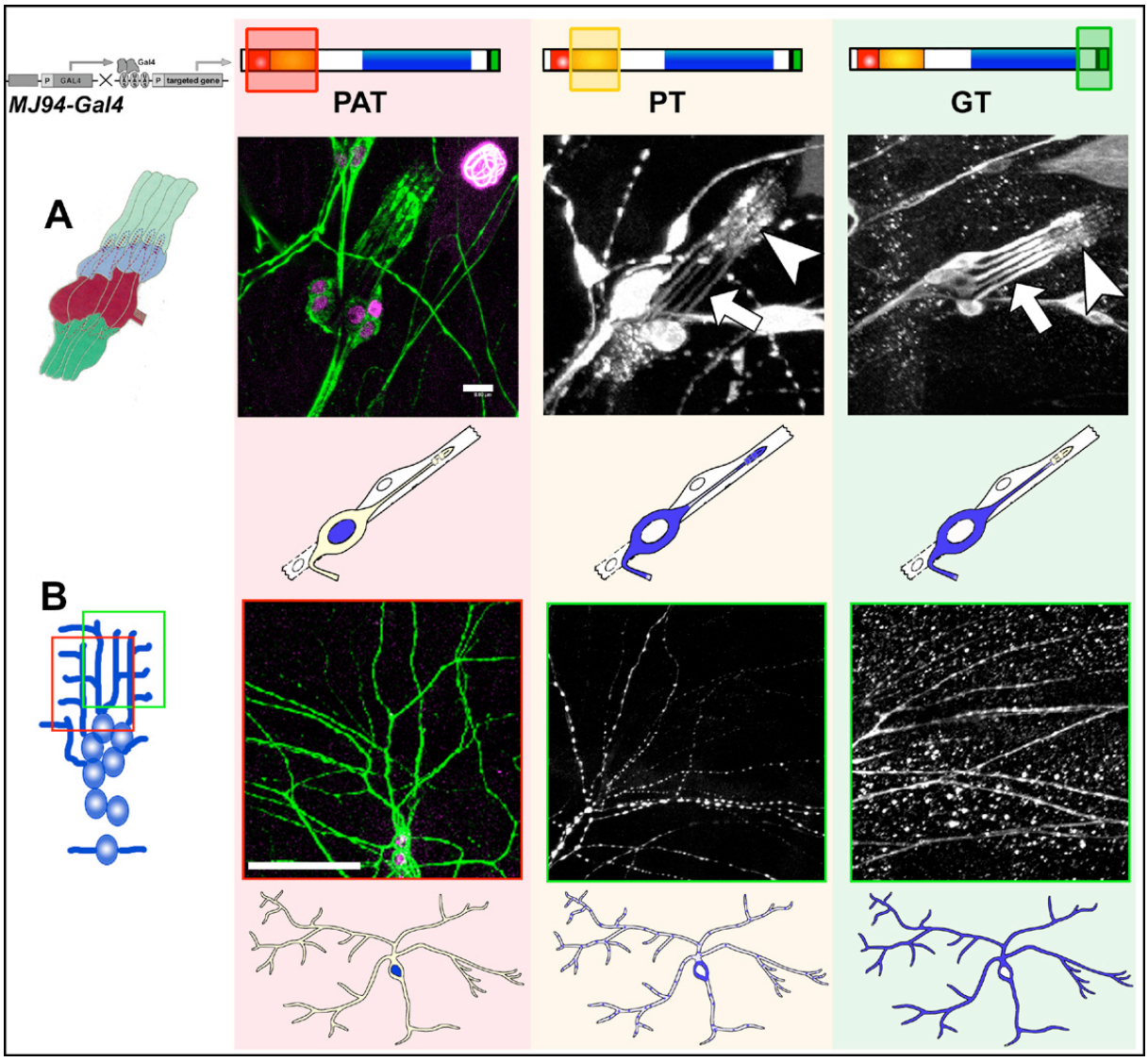
Gal4
P
GAL4
P
targeted gene
MJ94-Gal4
PAT
PT
GT
A
B

Figure 3.18: Localisation of the three different Shot domains in peripheral sensory neurones following *MJ94-Gal4* mediated expression. PAT (in magenta) and PT were detected with rabbit IgG, the C-terminal domain was tagged with GFP and was therefore additionally labelled with anti-GFP. To visualise the PAT-construct expressing cells, the membraneous marker CD8-GFP was co-expressed and labelled with anti-CD8 (green). The coloured boxes in the *md*-neurones cartoon depict the approximate area shown in the confocal images. PAT was detected exclusively in nuclei (see text). PT was found only weakly in the *sc*-dendritic protrusions (A; arrow). It was mainly detected in somata and capsules (arrowhead). GT localised in somata and *sc*-dendrites only. As in elav mediated expression (Figure 3.14), PT was found in clusters along the *md*-sensory projections (B). GT was found to be more evenly distributed. Bar in A 8 µm, in B 40 µm. Colour code as above.

3.4. Immunohistochemical study using anti-sera to different domains of the Shot protein

The results from the misexpression experiments with the different Shot domains tempt to speculate that the N-terminal ABD and Plakin homology are good candidate domains mediating Shot function during synapse formation. In order to verify these results in neurones with no artificial transgene expression the localisation of antibodies raised against specific domains of Shot were analysed in wildtype third instar larvae.

Two specific antibodies have thus far been published (see Figure 3.19). Using an oligopeptide covering the amino acids 3450-4950 (includes the Gas2 Homology; amino acid positions refer to the Shot-RE isoform, Ensembl, CG18067-RE) as epitope, Strumpf and Volk (1998) generated an antibody that specifically recognises all long isoforms of Shot (Lee et al., 2000a; Strumpf and Volk, 1998, out of simplicity further referred to as anti-Shot^{Gas2}). A polyclonal antibody specific to the N-terminal domain of Shot (anti-Shot^{NB}) was generated by Gregory and Brown (1998), using amino acids 2-341 as epitope, which cover most of the ABD and the region upstream from it. The latter antibody was only available as non-purified serum and proved to be insufficient for immunohistochemical studies (not shown), in contrast to existing studies with the purified antiserum (Prokop et al., 1998b). In order to carry out the experiment with an antibody specific to the N-terminal region of Shot, in particular to the ABD, a new polyclonal antibody was generated in the context of this thesis using two oligopeptides covering the amino acids 312-325 (EP011203, out of simplicity referred to as Shot^{203}) and 342-355 (EP011204, Shot^{204}) as epitopes. Both epitopes lie within the ABD and were selected on the basis of the potential antigenic character of their sequences as predicted using Vector NTI 7 software. The sequences were sent to EUROGENTEC (Eurogentec Bel S.A., Herstal, Belgium) for generation of synthetic peptides and subsequent injection into rabbits (see Chapter 2.2.). The antiserum obtained was purified with both epitopes, respectively (likewise carried out by Eurogentec). First histochemical studies revealed that best staining was obtained with antiserum purified with the epitope Shot^{204} (see later for details). Next, it was tested whether anti-Shot^{204} recognises the epitope within the ABD *in vitro*. In a Western Blot assay the antibody was probed against protein extracts gained from third instar larvae that pan-neuronally misexpressed GFP tagged PAT (using *elav-Gal4* as driver). The protein Blots were separated along the protein lanes and tested independently

with anti-Shot^{204} and anti-GFP (see Chapter 2.2.1.3.). As shown in Figure 3.20, both antibodies labelled the misexpressed GFP-tagged N-terminal domain of Shot. Thus, anti-Shot^{204} is able to recognise its epitope within the ABD.

To further test the specificity of anti-Shot^{204}, the serum was used to stain embryos at stage 17. Wildtype and *shot*^{3} null mutant embryos (Lee et al., 2000a) were used in these experiments. In wildtype embryos anti-Shot^{204} was detected in tendon cells, trachea and very weakly in the capsule structures of scolopidial sensory neurones (Figure 3.21). The tracheal staining was still visible in *shot*^{3} mutant embryos, and the same observation was made with anti-Shot^{GAS2}, suggesting this epitope to be unspecific (not shown; see also Lee et al., 2000a). In contrast, tendon cells and scolopidial organs were free of anti-Shot^{204} (and anti-Shot^{GAS2}) in *shot*^{3} mutant embryos. Hence, the antibody is specific for Shot protein. Unfortunately, anti-Shot^{204} could not be detected in peripheral projections or NMJs. However, this was also observed previously in staining procedures using the purified serum generated from Gregory and Brown and demonstrated to be due to low levels of native protein at late embryonic stages (Prokop et al., 1998b).

Subsequently, both antibodies were applied to wildtype third instar larvae to compare their staining pattern at the NMJ. The antibodies were applied separately in individual experiments, because each antibody required specific fixation protocols at this larval stage (see Chapter 2.1.7.2. in Material and Methods and Chapter 6.6. in Appendix I). Anti-Shot^{204} was detected in motor neuronal projections and in the boutons of NMJs (Figure 3.22A$^{i/ii}$), showing a staining pattern similar to that obtained in previous studies using anti-Shot^{NB} (which like anti-Shot^{204} was raised against epitopes that lie within the ABD of Shot; Prokop et al., 1998b). In contrast, anti-Shot^{Gas2} did not stain boutons, though it stained motor neuronal axon tracts and branches (Figure 3.22B^{i}). The obtained staining patterns are reminiscent of the results of the misexpression study of the different Shot domains. Thus, only N-terminal antibodies (anti-Shot^{204} and anti-Shot^{NB}) and constructs (PAT and PT) but not the C-terminal construct (GT) and antibodies (anti-Shot^{GAS2}) localise at presynaptic sites. Therefore it seems to be the N-terminus of Shot that interacts with other proteins at presynaptic sites. Given the severe *shot* mutant phenotypes at synaptic terminals, these protein interactions are likely to reflect interactions executed by the native Shot protein.

The differential localisation of the constructs was further confirmed by antibody localisation studies in scolopidial sensory neurones (Figure 3.22). At the late larval stage these specialised sensory organs were stained by anti-Shot^{Gas2} in somata of the sensory neurones and along the dendritic protrusions, almost identical to the localisation observed for the C-

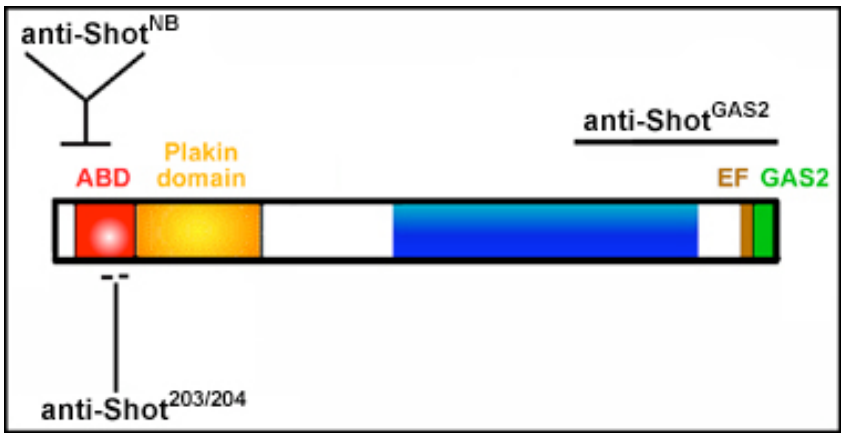
anti-Shot^NB
anti-Shot^GAS2
Plakin
domain
ABD
EF
GAS2
anti-Shot^203/204

terminal domain. Interestingly, at stage 17, anti-Shot^{Gas2} was additionally detected in capsule structures at the dendrite tip, where the misexpressed C-terminal domain was not detected. The localisation of Shot isoforms bearing the C-terminal domain might be shifted in the time course of development, either by following the compartmentalisation of the interacting partner, or by interacting with a new partner. Alternatively, interaction partners might become masked by other protein interactions interfering with the binding of the C-terminal domain and prohibiting antibody detection. Anti-Shot^{204} staining in scolopidial organs was found restricted to the capsules (Figure 3.21.A), which confirms results obtained for the localisation of misexpressed PAT and PT. It further suggests that in scolopidial organs, anti-Shot^{GAS2} detects protein localised through the N-terminal sequences. The N-terminal antibody was not detected in cell nuclei of scolopidia or other neurones. This supports the assumption made earlier, that the localisation of misexpressed PAT in the nuclei of Gal4-positive cells seems to be unspecific.

The newly created antibody represented an additional tool for the study of the different *shot* mutant alleles. Observations made by applying anti-Shot^{204} and anti-Shot^{Gas2} in a subset of *shot* mutant alleles are presented in the next Chapter.

Figure 3.19: Available antisera specific to different Shot domains. The polyclonal rabbit anti-Shot^{NB} was generated using amino acids 2-341 (including most of the ABD) as epitope (Gregory and Brown, 1998). The polyclonal guinea pig anti-Shot^{GAS2} was raised against an epitope covering partially the Dystrophin Coiled Coil structure (blue), the EF Hand motifs (EF) and the GAS2 homology (amino acids 3450-4950; Strumpf and Volk, 1998). Polyclonal anti-Shot$^{203/204}$ were generated in rabbit using the two most epigenic sites within the ABD (amino acids 312-325 and 342-355, respectively, carried out in the context of this work).

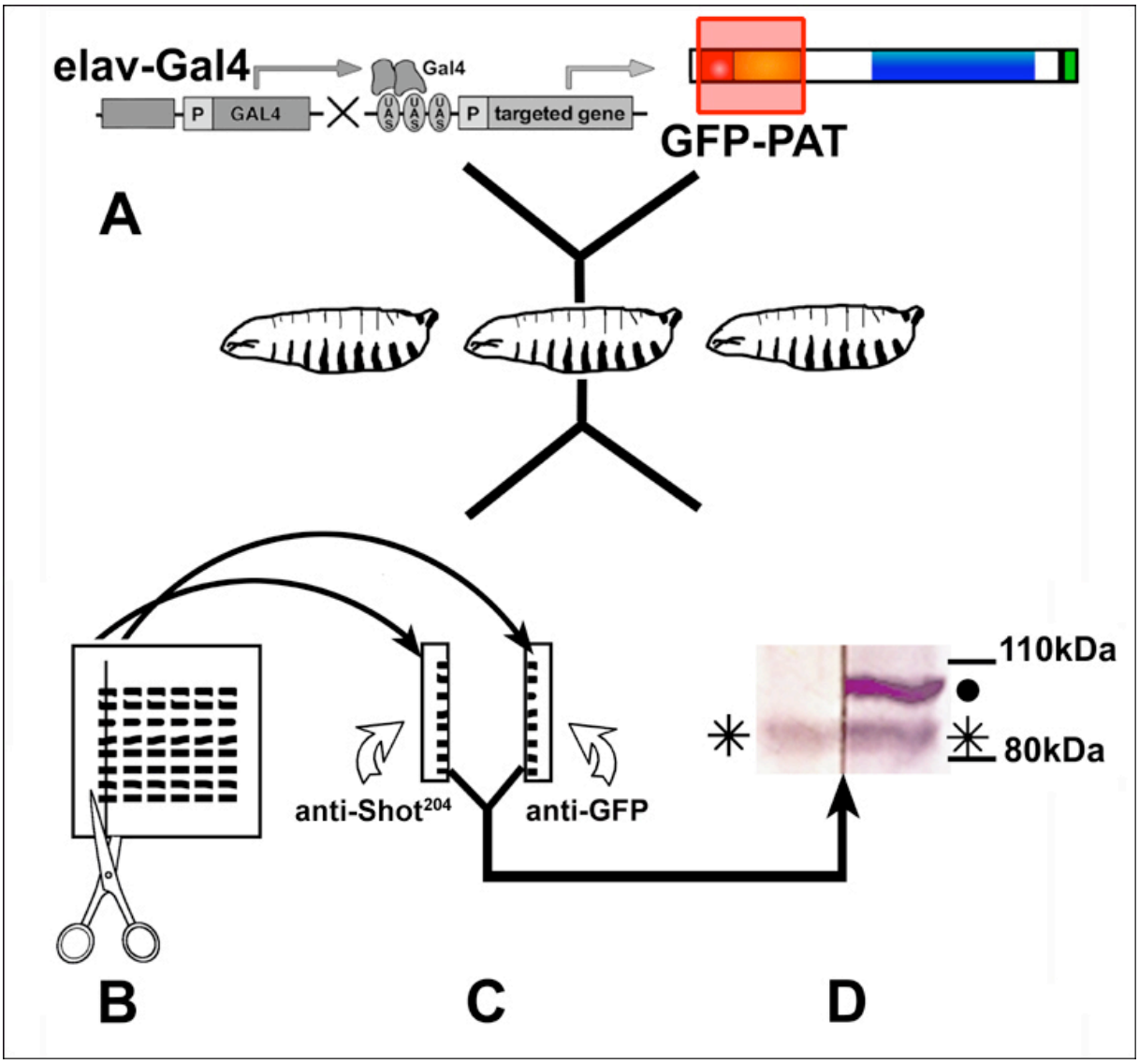
elav-Gal4
Gal4
P
GAL4
UAS
UAS
UAS
P
targeted gene
GFP-PAT
A
anti-Shot204
anti-GFP
110kDa
80kDa
B
C
D

Figure 3.20: Anti-Shot^{204} recognises its epitope within the ABD of Shot *in vitro*. Protein was extracted from GFP-tagged PAT misexpressing third instar larvae (A). The proteins were separated in polyacrylamid gel electrophoresis, blotted, and the protein lanes on the blot halved (B). The half lanes were probed with anti-Shot^{204} or anti-GFP, respectively (C). The halved protein lanes were then realigned (D). Both antibodies recognise the PAG construct (asterisk). An additional unspecific band at about 100kDa is recognised by anti-GFP only (black dot). The numbers on the blot indicate the approximate molecular masses as estimated by standard markers.

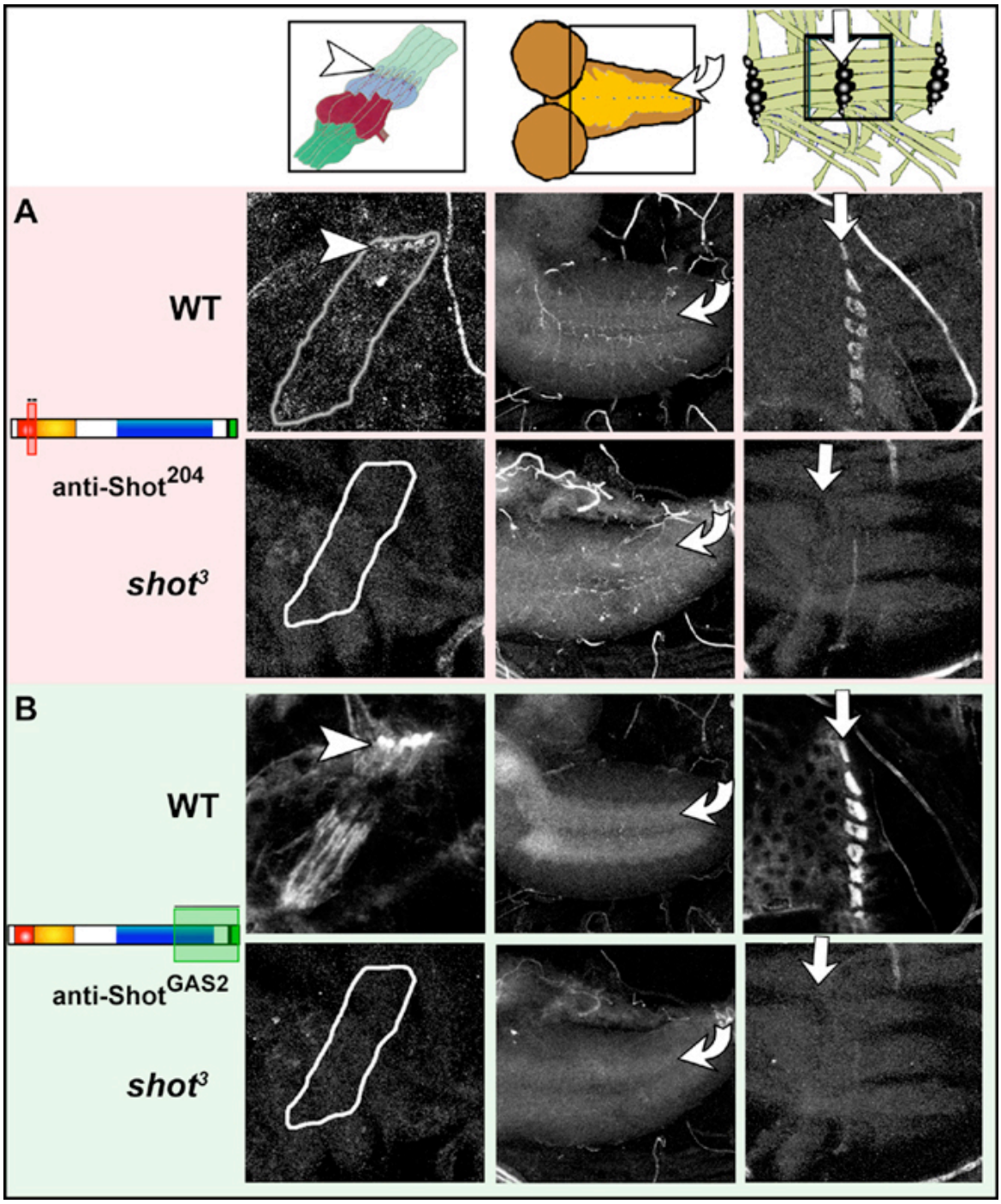
A
WT
anti-Shot204
shot3
B
WT
anti-ShotGAS2
shot3

Figure 3.21: Anti-Shot^{204} and anti-Shot^{GAS2} are specific to Shot. Confocal images of staining with anti-Shot^{204} are shown in A, with anti-Shot^{GAS2} in B. In stage 17 wildtype embryos, both antibodies recognise their epitope in scolopidia (left row of confocal images) and tendon cells (row to the right). While anti-Shot^{Gas2} stains the neuropile specifically, staining in the CNS with anti-Shot^{204} seems rather unspecific (middle row). Labelling with both antibodies is lost in shot null-mutants (shot^{3}, bottom row in A and B, respectively). The frames in the cartoons show the area imaged. Arrowheads point to the capsules of scolopidia, bent arrows to the neuropile and straight arrows to the location of muscle attachment cells of the ventro-lateral muscles.

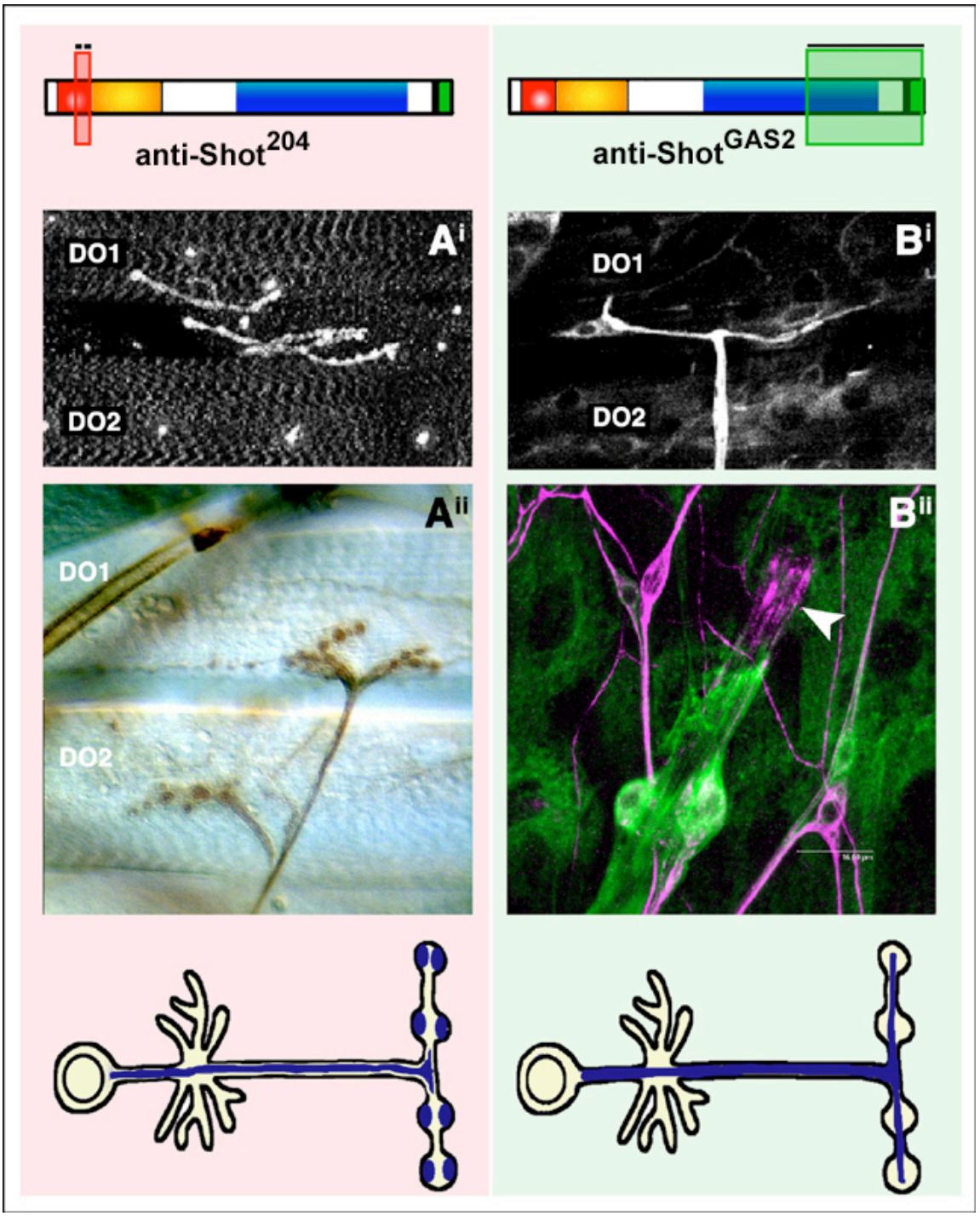
anti-Shot204
anti-ShotGAS2
DO1
DO2
Ai
Bi
Aii
Bii

Figure 3.22: Antibodies to different domains of Shot localise differentially. NMJs of wildtype third instar larvae in A^{i} and A^{ii} were labelled with newly generated anti-$Shot^{204}$ (specific to the ABD). The antibody stains presynaptic sites as well as axonal tracts. In contrast, the antibody specific to the C-terminus of Shot (anti-$Shot^{GAS2}$) is detected in axonal tracts and branches only (B^{i}). These results confirm, that the differential localisation of the distinct misexpressed Shot domains reflect appropriate protein-protein interactions of native Shot protein, and that the N-terminus of Shot is essential for synapse formation. B^{ii} shows anti-$Shot^{GAS2}$ (green) and anti-Futsch (magenta) labelling of scolopidial organs. Note, that in third instar larvae, anti-$Shot^{GAS2}$ shows a different staining pattern than in stage 17 (Figure 3.21B). This could either be due to true changes of the protein localisation or distribution of isoforms, or due to masking of the Shot isotope as a result of protein interactions. A^{i}, B^{i} and B^{ii} are confocal images of fluorescently stained wildtype third instar larvae, A^{ii} is a light microscopic image of diaminobenzidine stained specimen. Arrowhead in B^{ii} points to the scolopidial capsule structures. DO1/2, dorsal oblique muscle 1/2 (Bate and Rushton, 1993).

3.4.1. Analysis of *shot* mutant alleles using antibodies specific to different regions of Shot

Different *shot* mutant alleles display different combinations or degrees of phenotypes (Chapter 3.1.; Gregory and Brown, 1998; Prokop et al., 1998b; Strumpf and Volk, 1998). These differences could be caused by mutational events disrupting diverse domains of Shot or impairing the expression of Shot or Shot isoforms. To test this, the two antibodies anti-Shot^{204} (specific to the Shot N-terminus) and anti-Shot^{Gas2} (specific to the Shot C-terminus; see Figure 3.19) were applied in embryos of *shot* mutant alleles *shot^{kakP2}*, *shot^{el3}* and *shot^{SF20}*. All three *shot* mutant alleles have impaired NMJ formation to different degrees (Chapter 3.1.). The mutant allele *shot^{kakP2}* was chosen for this analysis because molecular information on mutational events is available and its phenotype is restricted to the nervous system (Lee et al., 2000a). *shot^{SF20}* shows severe phenotypes in all tissues studied and was suggested to be a *shot*-Null mutant. Phenotypes in *shot^{el3}* are milder, suggesting *shot^{el3}* to be a strong hypomorphic allele (Chapter 3.1).

As described in Chapter 3.4. both anti-Shot antibodies stain muscle attachment cells (Figure 3.23B and C) and scolopidial sensory neurones (Figure 3.23D and E), but only anti-Shot^{Gas2} labels the neuropile (Figure 3.23A). In all three *shot* mutant alleles tested, staining with anti-Shot^{Gas2} in the neuropile was no longer detectable (Figure 3.23F, K and P). However, in *shot^{kakP2}*, both antibodies were able to detect their epitopes in muscle attachment cells and scolopidia (Figure 3.23G-J). This was surprising, since another N-terminal antibody (anti-shot^{NB}) was reported to fail to stain in *shot^{kakP2}* (Gregory and Brown, 1998). Anti-shot^{NB} was raised against amino acids 2 to 341 (Gregory and Brown, 1998), whereas the epitope used for production of anti-shot^{204} comprises amino acids 342 to 355 (Chapter 2.2.). This strongly suggests, that the mutant allele *shot^{kakP2}*, which represents a P-element insertion into an N-terminal intron of *shot*, affects only the anterior part of the N-terminus. Since *shot^{kakP2}* causes some phenotypes in the nervous system (see Chapter 3.1.), it is a promising candidate allele with the help of which to pinpoint precise domains involved in neurodevelopmental functions of Shot.

In contrast to *shot^{kakP2}*, anti-shot^{204} did not show any staining in muscle attachment sites or scolopidial neurones of *shot^{el3}* mutant embryos (Figure 3.23L and N). However, Shot protein was detected by anti-Shot^{Gas2} in both tissues (Figure 3.23M and O) though at much lower levels than in *shot^{kakP2}* mutant embryos or wildtype control. The residual Shot protein detected might carry out some of its functions, explaining why the phenotypes observed in

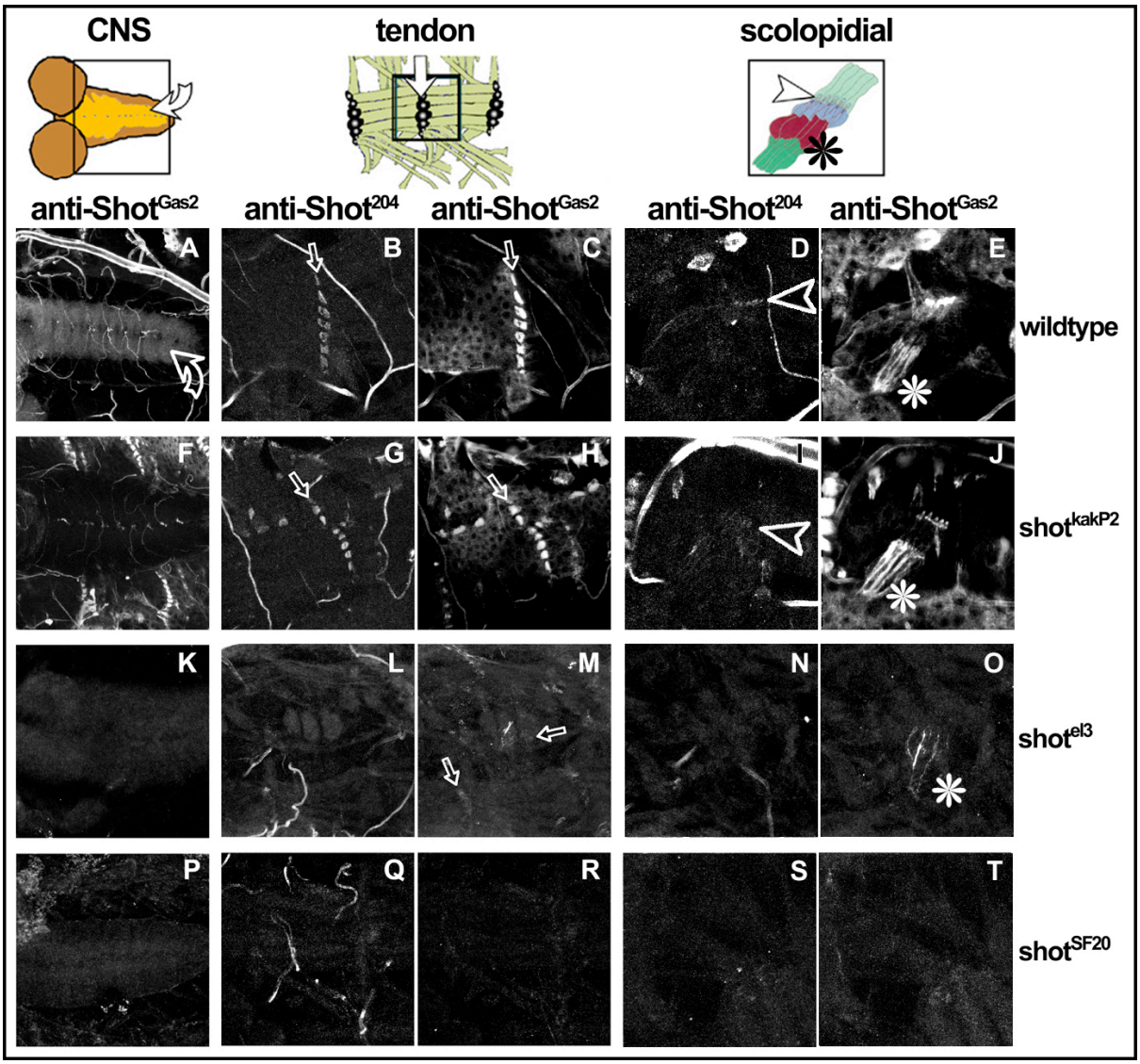
CNS
tendon
scolopidial
anti-Shot^Gas2
anti-Shot^204
anti-Shot^Gas2
anti-Shot^204
anti-Shot^Gas2
A
B
C
D
E
wildtype
F
G
H
I
J
shot^kakP2
K
L
M
N
O
shot^el3
P
Q
R
S
T
shot^SF20

shot^{el3} where found to be milder than in other *shot* mutant alleles (Chapter 3.1.). Yet, the activity of the remaining protein might be too weak or abolished in *shot*^{el3} muscle attachment cells, which were reported to disrupt upon muscle contractions (Prokop et al., 1998b). The phenotype of reduced NMJs observed in *shot*^{el3} (Chapter 3.1.) could be explained by the lack or low levels of N-terminal domains or isoforms of Shot, as revealed by the absence of anti-Shot^{204} labelling.

In *shot*^{SF20} mutant alleles no protein could be detected with either antibody used. The findings that all tissues are free of Shot protein together with the severity of its phenotypes (Chapter 3.1) speak in favour of *shot*^{SF20} being a *shot*-Null mutant allele.

In this immunohistochemical study experiments were only carried out once for *shot*^{el3} and *shot*^{SF20}. The findings in experiments with *shot*^{kakP2} could be confirmed in independent additional trials. Thus, the results obtained for the first two *shot* mutant alleles have to be regarded as preliminary and await further confirmation. Yet, the experiments show that the two available antibodies, anti-Shot^{204} and anti-Shot^{Gas2}, represent exclusive tools for the detailed analysis of *shot* mutant alleles.

Figure 3.23: Mutations in different *shot* mutant alleles appear to affect Shot expression differentially. Embryos at stage 17 of mutant alleles *shot*^{KakP2} (F-J), *shot*^{el3} (K-O) and *shot*^{SF20} (P-T) were stained with anti-Shot^{204} (specific to Shot N-terminal) and anti-Shot^{Gas2} (specific to Shot C-terminal). In wildtype controls anti-Shot^{Gas2} labels the neuropile in the CNS (A; bent arrow), while in the periphery both anti-Shot^{204} and anti-Shot^{Gas2} are found in muscle attachment cells (tendon cells, B and C, respectively; arrows) and scolopidial sensory neurones (D and E, respectively; arrowheads point to the capsule structures, ✱ point to cellbodies). In all three *shot* mutant alleles Shot is no longer detected in the neuropile (F, K and P), but staining is still visible in periphery of *shot*^{KakP2} (G-J). In *shot*^{el3} mutant embryos only C-terminal but not N-terminal staining is weakly detected (L-O). Neither anti-Shot^{204}, nor anti-Shot^{Gas2} show reactivity in *shot*^{SF20} mutant embryos (Q-T). For details see text. The cartoons in the top row show the area depicted in the confocal images. Anterior is to the left.

3.5. Yeast two-hybrid analysis: screening for interaction partners of the N-terminal domains of Shot

It was suggested that the N-terminus of Shot is essential for synapse formation (Chapters 3.1., 3.3., 3.4. and 3.4.1). Shot might act through targeting special factors with its N-terminal domains to the presynaptic compartment. Alternatively, Shot might be required for the organisation of the cytoskeleton (Chapter 3.2.) and is targeted itself to the forming synapse through interactions with its N-terminal domains. In order to detect candidate interactors of Shot mating-based yeast two-hybrid screens were performed using as baits the N-terminal domains of Shot. By uncovering such binding partners at synaptic sites one could gain insights into Shot function during synapse formation and/or unravel novel proteins with potential synaptogenic function. So far, it has been shown that Shot, and its mammalian homologue MACF1 can bind directly to Tubulin and Actin (Karakesisoglou et al., 2000; Lee and Kolodziej, 2002b; Leung et al., 1999). However, precedents set by other members of the Spectraplakin family of proteins (Blake and Kröger, 2000), the enormous size and complexity of Shot, and the wide range of function it executes (Gregory and Brown, 1998; Lee et al., 2000a; Lee and Kolodziej, 2002a; Prokop et al., 1998b; Strumpf and Volk, 1998) suggest that Shot has a larger collection of binding partners.

Different N-terminal Shot domains were introduced into respective Yeast Bait vectors (see Chapter 2.3.3.). These domains comprised the ABD, the Plakin domain (PT), the ABD in conjunction with the Plakin domain (PAT). Also, the C-terminal domain covering the EF-Hand motifs and GAS2 Homology (GT) was prepared in order to be used as a control but also to detect other proteins interacting with Shot, e.g. at other sites of functions. As described in more detail in Chapter 2.3.3., the actual screens were carried out in the laboratories of Tobias Böckers (Institute for Anatomy, University of Münster, Germany) partly in form of visits of the author, whereas cloning and sequencing work was carried out in Mainz.

All four domains were initially tested for auto-inducing activity within the yeast system, i.e. whether the individual Shot-Bait constructs alone were able to activate the expression of the reporter genes. Autonomous activity was detected for the bait constructs bearing the C-terminal domain of Shot (GT) and the ABD in conjunction with the Plakin domain (PAT). Since the resulting background noise would necessarily lead to selection for potential false positive yeast-colonies, it was preferred to refrain from using these baits. Fortunately, the Plakin domain (PT) or ABD alone did not show autonomous activity and were therefore used in mating-based yeast two-hybrid screens against a three million-clone genomic *D.*

melanogaster cDNA prey library. The screen was based on stringent parameters that increase reliability of the obtained candidates (three individual reporter genes; simultaneous selection for the prototrophic reporters; see Chapter 2.3.3.13. for details).

A total of 120 cDNA sequences could be obtained from 128 yeast-clones showing interaction with the Plakin domain. 80 cDNA sequences were retrieved from the 110 clones positive for ABD interaction. Six candidate sequences from the Plakin based screen and seven from the ABD based screen were selected as potential true positive, fulfilling the following criteria: They were obtained as at least two independent clones and their binding to the respective Shot domain could be reconfirmed through reintroduction into yeast for direct yeast two-hybrid analysis. Using *in silico* analysis based on the existing fly genome sequence the genes or annotated open reading frames (ORFs) associated with the 13 sequences were determined (NCBI BLASTn, BDGP BLAST; Altschul et al., 1990; Vector NTI 7 Software; Adams et al., 2000; FlyBase, 1999). Using data based searches, further information about these genes and ORFs was retrieved: Out of the 13 candidate genes five were of completely unknown function showing no obvious homologies, three contained domains with homologies, which might indicate some functional aspects, and five represented cloned genes, of *Drosophila*, which have not been analysed in the context of Shot or synapse formation (Table3.3).

Number of Interacting candidates representing:	ABD	Plakin-domain
Unknown Genes	4	1
Genes with known Homologies	/	3
Cloned *Drosophila* Genes	3	2

Table 3.3: Summary of the 13 yeast two-hybrid candidate genes selected on the basis of the criteria outlined in the text. The number of candidates for unknown genes, genes with known homology and cloned *Drosophila* genes fished with the respective Shot domain are listed. One candidate gene that has been cloned in *Drosophila* was found to interact with both the ABD and the Plakin domain. Amongst the cloned *Drosophila* genes interacting with the Plakin domain is also the candidate gene *Drosophila* Paxillin (DPxn) which was obtained in 11 independent clones (see text).

In the applied yeast two-hybrid screen the two distinct N-terminal Shot domains showed mostly interactions with different candidate proteins. This was taken as a promising indication

for the quality of the screen. However, given the artificial context of yeast two-hybrid assays further independent proof for the protein interactions needs to be obtained. Furthermore, the requirement of the candidate genes for synapse formation has to be shown.

The candidate gene obtained with highest frequency (interacting with the Plakin-domain) was the gene coding for the *Drosophila* LIM domain protein Paxillin (DPxn). *DPxn* has been mapped cytologically to the second chromosome at 37D5-7 (Figure 3.29), it was cloned, sequenced, and antibodies are available detecting the protein at muscle attachments, i.e. sites of Shot localisation and action (FlyBase, 1999; Wheeler and Hynes, 2001; Yagi et al., 2001). It is suggested that its function comprises, amongst others, a cytoskeletal anchoring activity. Based on the existing knowledge and tools, work on DPxn in the context of Shot function and potential involvement in synaptogenesis was the most promising choice to achieve a reasonable amount of data within the framework of this project. Part of this analysis was carried out by our co-laborators. Thus, Arul Subramanian und Talila Volk (Weizmann Institute of Genetics, Rehovot, Israel) studied interaction of N-terminal Shot domains and DPxn in co-transfected SR^{2+} cells. They found co-localisation of both proteins in the cultured cells and were able to co-immunoprecipitate DPxn with the Shot domain from cell-derived protein extract (for details see Appendix II, Chapter 7.1., Figure 7.1). Using N- and C-terminal constructs of DPxn (obtained from Ryohei Yagi; Department of Molecular Biology, Osaka Bioscience Institute, Japan) together with the Shot Plakin domain in yeast two-hybrid assays (carried out in Tobias Böckers laboratory) we were able to pinpoint the N-terminus of DPxn (amino acids 1-347) as the Shot interacting region (for details see Appendix II, Chapter 7.1., Table 7.1).

My own task was the analysis of DPxn function and its potential interaction with Shot via genetic and immunohistochemical studies within *Drosophila* embryos. These studies are described in detail in the following.

3.5.1. Studies of DPxn *in situ*

Two available antisera for Paxillin were used in an attempt to study the localisation of DPxn within *D. melanogaster*. A commercially available monoclonal antibody is directed against the entire Paxillin protein from chicken (anti-pax; for details see Chapter 2.1.8.). A purified polyclonal antibody directed against *Drosophila* Paxillin (anti-DPxn) was generously

provided by Ryohei Yagi (Department of Molecular Biology, Osaka Bioscience Institute, Japan). The antibody was generated using the N-terminal region (amino acids 2-346) as epitope and its specificity for DPxn was confirmed previously (Yagi et al., 2001). Both antibodies were first used in wildtype embryos at stage 17. As shown in Figure 3.24A, staining with anti-pax was observed in tendon cells, muscle tips and dendritic projections of scolopidial sensory neurones, and weakly in the neuropile of the CNS. Similar results were also obtained with polyclonal anti-DPxn (shown for tendon cells and muscles in Figures 3.26 and 3.27). Additionally, and of most interest for this work, anti-DPxn was found to stain axons and motor neuronal terminals (Figure 3.25A, B, E and F; see below). Hence, DPxn was found in tissues positive for Shot localisation and function, i.e. tendon cells, scolopidia, CNS and most importantly, in motor neurones. In order to analyse the specificity of the applied antibodies and of their staining patterns, available databases were screened for mutations disrupting the *DPxn* gene-locus (FlyBase, 1999). Four fly-stocks deficient for the chromosomal area of DPxn, (*Df(2L)TW50*, *Df(2L)VA23*, *Df(2L)TW158* and *Df(2L)E55*; see Chapter 3.5.2 for details; Figure 3.29) were stained with anti-pax (*Df(2L)TW50* and *Df(2L)VA23*, respectively) or anti-DPxn (*Df(2L)VA23* or embryos transheterozygous for the deficiencies *Df(2L)TW158* and *Df(2L)E55*). No staining could be detected in tendon cells, muscles, scolopidial neurones and motor neurones of any of these mutant individuals (see Figures 3.24B and 3.25C, D, G and H). These results show that the deficiencies affect *DPxn* and vice versa that the antibodies detect specific epitopes within these tissues. However, the weak staining of DPxn in the neuropile remained in all cases, suggesting the DPxn-antibodies to cross-react with an unspecific epitope in the CNS (Figure 3.24B).

In order to study potential interactions of Shot and DPxn in embryos, experiments were carried out that focussed on their similar localisation patterns in tendon cells at muscle attachment sites. Tendon cells form a narrow cell junction with the tips of muscles. Whereas Shot is localised exclusively on the side of the tendon cells, DPxn is found on both sides of the cell junction, which complicates the analysis (see Figure 3.26A). To overcome this problem, the localisation of Shot and DPxn was studied in tendon cells of *βPS-Integrin* null mutant embryos (mys^{XG43}) at late stage 17. In mys^{XG43} mutant embryos muscles detach from the tendon cells without disrupting their intracellular organisation (Prokop et al., 1998a). This condition allows clear visual access to the tendon cells (Figure 3.26B). In all mys^{XG43} mutant embryos studied, DPxn was found to co-localise with Shot in a plug like structure on the basal surface of the tendon cell (Figures 3.26D and 3.27A). Hence, there is a considerable probability for DPxn and Shot to interact *in situ* at this site. To test this, the mys^{XG43} mutation

was combined with the *shot*^{3} mutant allele (Chapter 2.1.4.2.). In *mys*^{XG43}*;shot*^{3} double mutant embryos, the muscles detach from the epidermis due to the *mys*^{XG3} mutation. This allows the easy analysis of tendon cells as explained before. In addition, this constellation prevents physical destruction of tendon cells, a typical phenotype of *shot* mutations (compare schemes of muscle attachments in Figures 3.26B and 3.10). Therefore, *mys*^{XG43} and *mys*^{XG43}*;shot*^{3} mutant embryos were stained with anti-DPxn and anti-Shot^{Gas2}. In order to visualise the lateral borders of individual cells within the epidermis, the embryos were further stained with anti-DLG. As shown before, DPxn and Shot are found co-localised in a round plug-like structure in the centre of *mys*^{XG43} mutant tendon cells (Figure 3.27A, Figure 3.26D). In the absence of Shot, i.e. in *mys*^{XG43}*;shot*^{3} double mutant embryos, DPxn still occurs in small dotted accumulations, although they are clearly smaller than in embryos mutant for βPS-Integrins alone. Furthermore, the DPxn-plug is found no longer centred on the basal surface of the muscle-deprived tendon cells. Instead, the DPxn positive plugs have a strong tendency to localise at the cell's fringe, as if they lost anchorage and drifted away from their original position (Figure 3.27B). This suggests that Shot might play a role in cross linking DPxn-containing complexes to the cytoskeletal scaffold.

The results show that DPxn and Shot co-localise in tendon cells, and that DPxn localisation in tendon cells is dependent on the presence of Shot. However, a potential requirement for DPxn during synapse formation was still an open issue. In wildtype embryos at stage 17, staining with both DPxn-antibodies in the neuropile of the CNS turned out to be unspecific. Yet specific DPxn staining could be detected in peripheral axons and at NMJs (Figure 3.25). To further confirm that DPxn is localised at the NMJ, DPxn immunocytochemistry was additionally carried out in wildtype third instar larvae, i.e. at a developmental stage, where strong Shot staining was observed (Figure 3.22) and where synapses are larger and thus their components more abundant. Figure 3.28 shows that both DPxn antibodies detect DPxn in peripheral projections and at NMJs. The localisation of DPxn seems to be presynaptic, since it superimposes only partially with simultaneously labelled DLG, a predominantly postsynaptic marker (Figure 3.28B). Moreover, the DPxn staining seems to be specific, since impaired DPxn expression levels in RNA-interference experiments resulted in reduction of antibody reactivity (see Chapter 3.5.2., Figure 3.33C). Hence, DPxn specifically localises in *Drosophila* motor neuronal projections at embryonic stage 17, when motor neuronal terminals form *de novo* (Figure 3.25), and in third instar larvae, when NMJs expand or undergo structural changes. To find out whether DPxn is also required for the

anti-pax
A
wildtype
B
Df(2L)VA23
M
T

structural differentiation of motorneuronal synapses, a mutational analysis of *DPxn* was carried out as described in the next Chapter.

Figure 3.24: Localisation of DPxn in *Drosophila* embryos at stage 17. In wildtype (A) DPxn is detected with the monoclonal antibody anti-pax in muscle attachment cells (also called tendon cells, T, white arrows), at muscle tips (bent white arrows; M, muscle), in dendrite projections of scolopidial sensory neurones (white arrowheads) and in the neuropile (∗). The fly-deficiency Df(2L)VA23 (B), which is reported to carry a deletion with breakpoints within the *DPxn*-gene locus (FlyBase, 1999, compare Figure 3.29), reveals that the DPxn stain in the neuropile is most likely unspecific (confirmed with other deficiencies; see Figure 3.25).

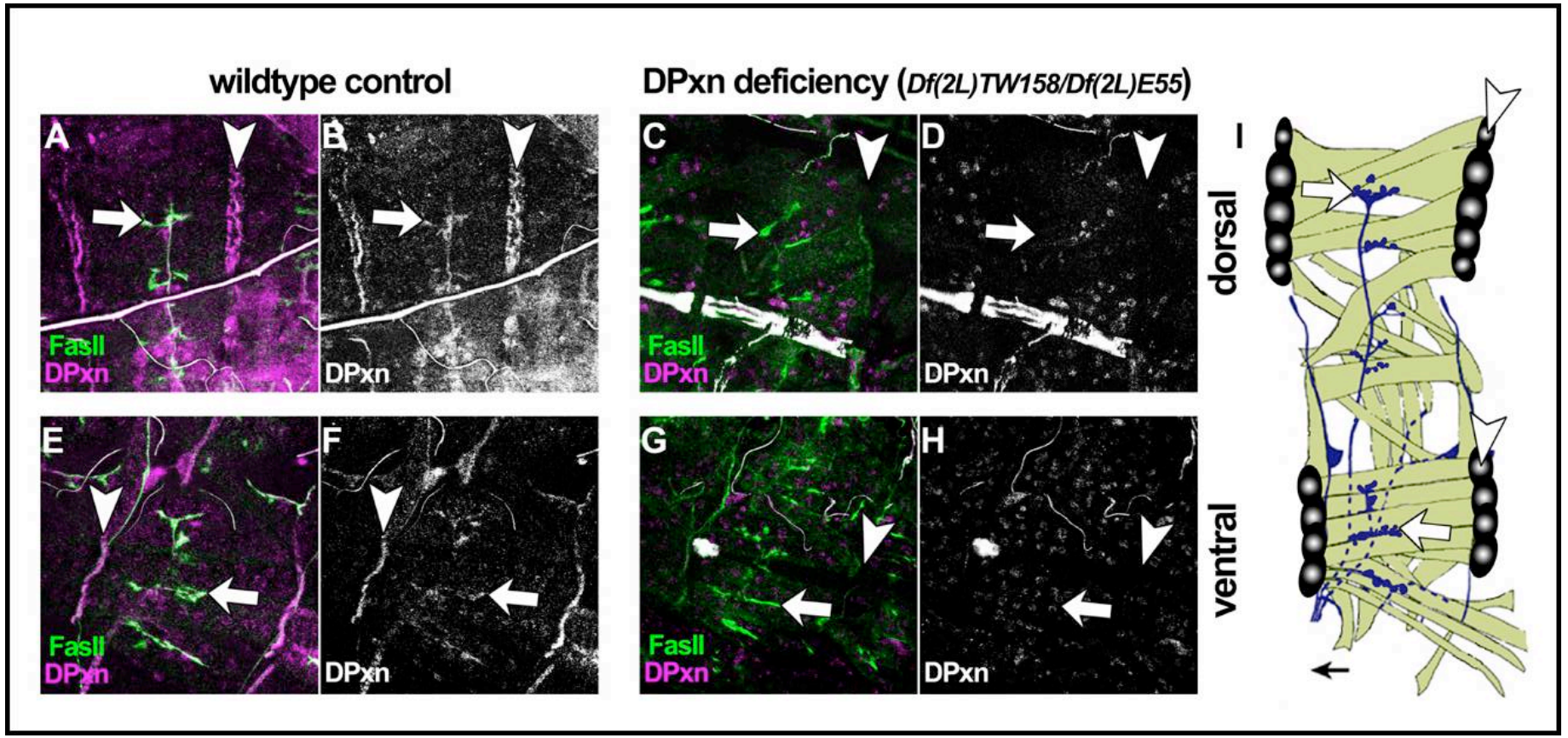
wildtype control
DPxn deficiency (Df(2L)TW158/Df(2L)E55)
A
B
C
D
E
F
G
H
FasII
DPxn
DPxn
dorsal
ventral

Figure 3.25: DPxn is localised in motor neurones and muscle attachment cells. Anti-DPxn labels motor neurones (white arrows) and muscle attachment cells (arrowheads) of wildtype embryos at stage 17 (A and E show dorsal or ventral area, respectively, with anti-DPxn in magenta and anti-FasII in green. For clarity the DPxn stain is shown alone in B and F). Anti-DPxn is not detected in these tissues in *DPxn* deficient embryos (C and D, dorsal area, G and H, ventral area; for details on the used DPxn deficient mutants see Chapter 3.5.2., Figure 3.29), suggesting the antibody staining to be specific. The cartoon (I) shows the areas depicted in the confocal images (compare white arrows and arrowheads). The black arrow points anterior.

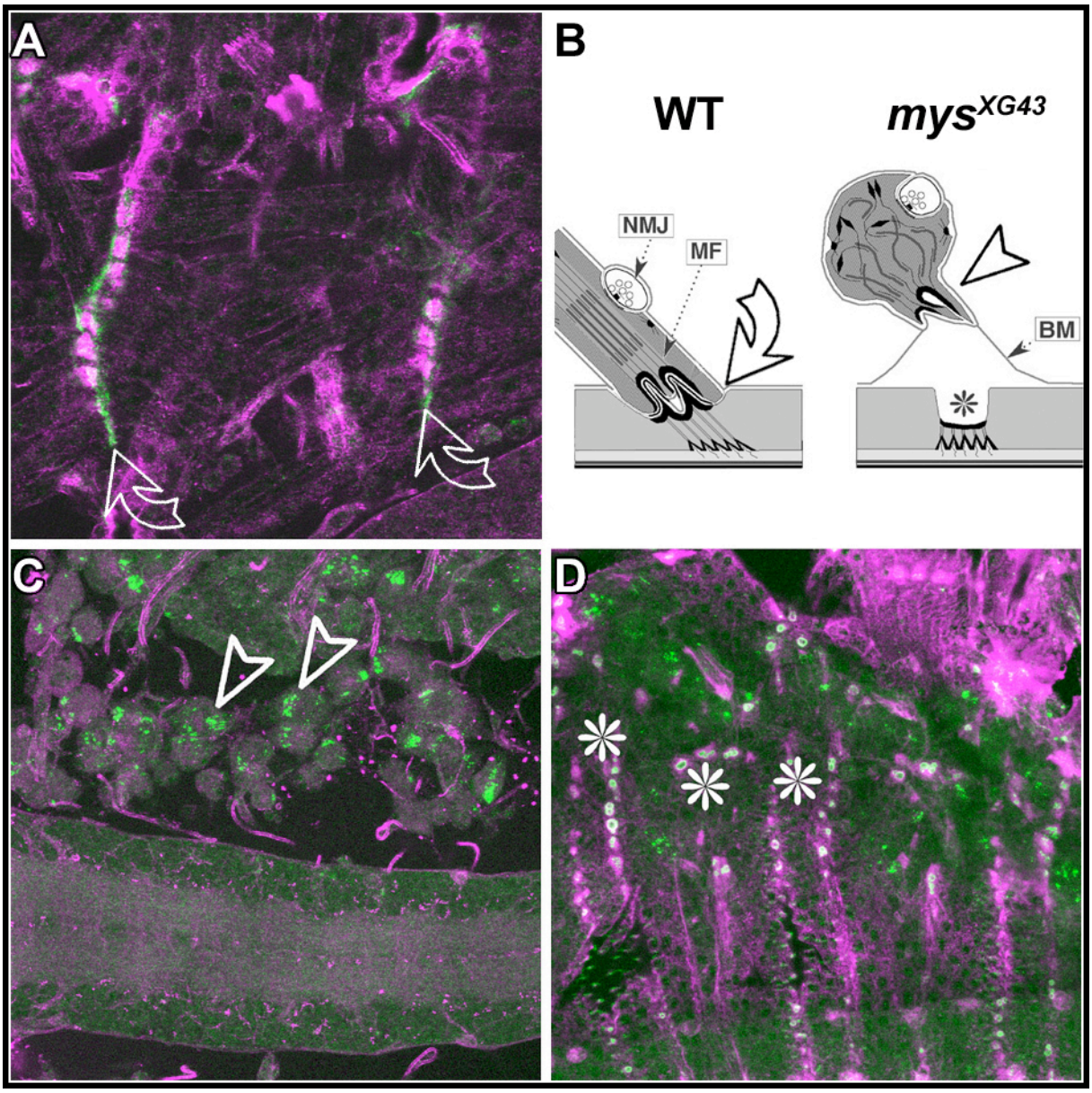
A
B
WT
mys^XG43
NMJ
MF
BM
C
D

Figures 3.26: Localisation of Shot and DPxn in *Drosophila* embryos at stage 17. Wildtype (A) and PS-Integrin mutant embryos (*mys*^{XG43}, C and D) were labelled with anti-DPxn (green) and anti-Shot^{Gas2}. It could not be unequivocally determined whether the DPxn stain in wildtype embryos originated from the muscle tips or tendon cells (bent arrows in A and B). Therefore, *mys*^{XG43} mutant embryos were used, in which muscles detach from the epidermis without disrupting the tendon cells, as shown schematically in B (Source: Prokop et al., 1998b). In the detached muscles, only DPxn can be found (arrowheads in B and C). In tendon cells of *mys*^{XG43} mutants (asterisks in B and D) DPxn is found to co-localise with Shot in the centre of the basal cell surface (D).

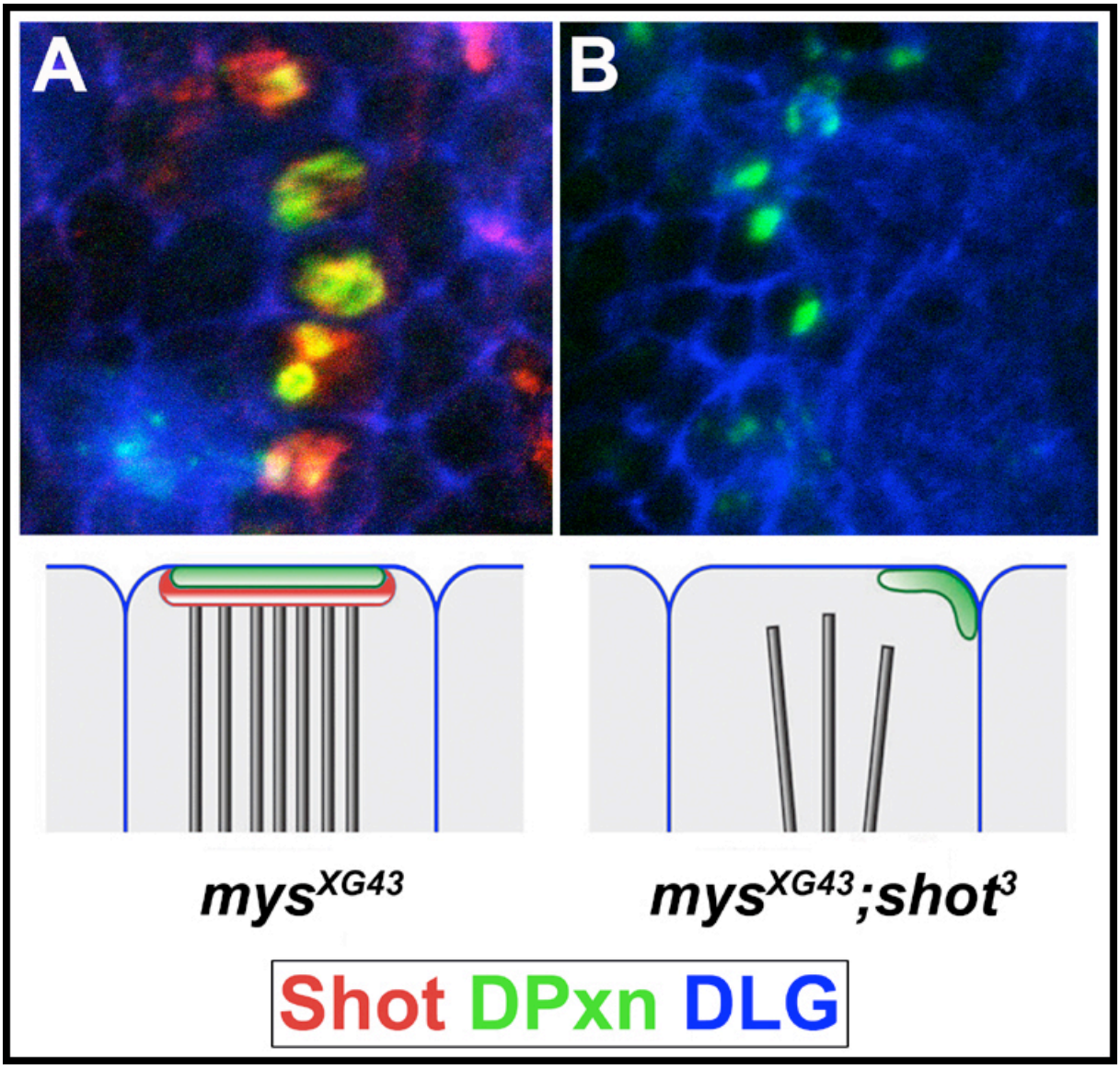
A
B
mys^XG43
mys^XG43;shot^3
Shot DPxn DLG

Figure 3.27: Localisation of DPxn is dependent on the presence of Shot. *mys*^{XG43} (A) and *mys*^{XG43}*;shot*^{3} (B) mutant embryos at stage 17 were labelled with anti-Shot^{Gas2} (red) and anti-DPxn (green). *mys*^{XG43} mutation was used in order to view the outer basal surface of the cells (see text). The cell circumference of the epidermis cells were visualised with anti-DLG (blue). In *mys*^{XG43} mutant embryos, both DPxn and Shot are found in the centre of the tendon cells. In the absence of Shot (*mys*^{XG43};*shot*^{3}), the localisation of DPxn is acentric towards the cell circumferences. The observations are represented in the cartoons (lateral view, basal surface at top), the colour code corresponds to that of the confocal pictures. Microtubules are shown as grey bars.

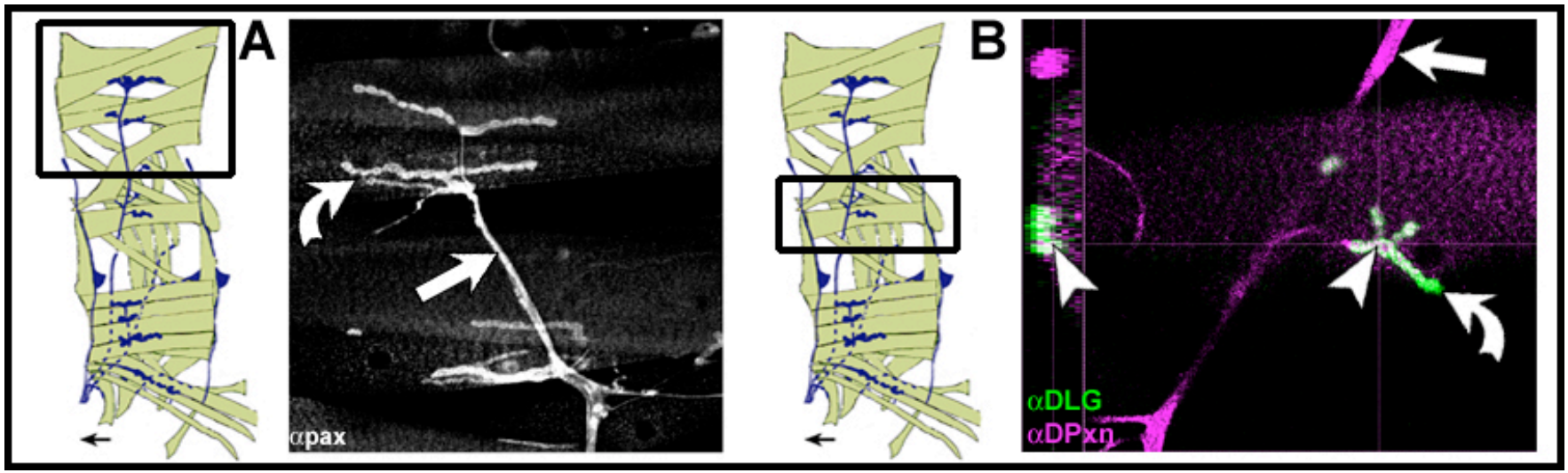
A
αpax
B
αDLG
αDPxn

Figure 3.28: Localisation of DPxn in axons and NMJs in third instar larvae. Both, monoclonal anti-pax (A) as well as polyclonal anti-DPxn (B, magenta) detect DPxn in peripheral projections (arrows) and at wildtype NMJs (bent arrows). Larvae in B were further stained with anti-DLG (green). In cross-sections (indicated by arrowheads) anti-DPxn stain does not cover the entire DLG-positive area, suggesting the DPxn to be presynaptic. The cartoons show the peripheral area depicted in each confocal image; black arrows point anterior.

3.5.2. *DPxn* mutant analysis

To date no specific mutant alleles for the *DPxn* gene are available. Four flystocks, which are deficient for a region of the second chromosome that includes the DPxn gene locus, have been introduced in the previous Chapter. The *Drosophila* mutant *Df(2L)TW50* was reported to have lost a very large region of the second chromosome (cytological map locations 36E4 to 38A6-7; *DPxn* gene locus is located at 37D5-7; see Figure 3.29A), which results in embryonic lethality at early stages. In contrast, the other deficiencies, *Df(2L)VA23*, *Df(2L)TW158*, and *Df(2L)E55* were found to be lethal at late embryonic stages. *Df(2L)VA23* was reported to be deficient for a region 3' of the DPxn gene locus, with a breakpoint of the deficient locus lying within the DPxn gene (FlyBase, 1999; cytological map locations 37B9 to 37D5; Figure 3.29B). The deletion on *Df(2L)TW158* covers almost the same chromosomal region as *Df(2L)VA23*. However, the deleted chromosomal region in *Df(2L)TW158* includes the entire DPxn gene (cytological map locations 37B2 to 37E2; see Figure 3.29A). The deletion in *Df(2L)E55* covers the entire DPxn gene as well. In contrast to *Df(2L)VA23* and *Df(2L)TW158*, sequences that lie 5' of DPxn are additionally deleted (cytological map locations 37D2 to 38A1; see Figure 3.29). In order to investigate the effect of loss of DPxn on NMJ formation animals homozygous for either deficiency (except *Df(2L)TW150*) or transheterozygous for *Df(2L)VA23* and *Df(2L)TW158*, *Df(2L)VA23* and *Df(2L)E55*, or *Df(2L)TW158* and *Df(2L)E55*, respectively, were analysed at late stage 17. As done in previous experiments (see Chapter 3.1.) NMJs were visualised using antibodies specific to presynaptic vesicle trafficking molecules (anti-Syn, anti-Syt), predominantly postsynaptic scaffolding protein (anti-DLG) and pre- and postsynaptic cell adhesion molecules (anti-FasII). All embryos carrying any of the deficiency constellations shared a common phenotype at the NMJ: Their motor terminals have growth cone-like shapes with long filopodia-like protrusions (Figure 3.30B-E). However, the morphological changes observed at the NMJ do not seem to affect synaptic markers: Syn and Syt are found to localise almost normally in motor neurones of all mutant embryos tested. In one of the mutant constellations, homozygous *Df(2L)VA23*, the effect of the deletion on central dendrite formation was assessed by eve^{RNE}*-Gal4* mediated expression of CD8-GFP. Astonishingly, the dendritic projections did not appear severely affected by this deficiency (Figure 3.30H). Most mutant constellations showed a variety of additional phenotypes, including disrupted pattern of the FasII positive fascicle in the CNS and aberrant muscle patterns in the periphery (not shown). Only embryos transheterozygous for either *Df(2L)VA23* and *Df(2L)E55* or *Df(2L)TW158* and

Df(2L)E55 (which show deformed NMJs with long filopodia-like structures; Figure 3.30D and E) did not show these muscle and CNS FasII phenotypes (not shown). Thus, these phenotypes are caused by the deletion of genes lying at either side of the *DPxn* gene locus. Although the chromosomal deletion defined by the overlap between the deficiencies is relatively short, about 18 genes or open reading frames (ORFs) are contained in this region (FlyBase, 1999). Any of these genes or ORFs might cause the observed neuronal phenotypes, although *DPxn* appears to be the best candidate. To test this, the following strategies were followed:

- GFP tagged full length DPxn (GFP-DPxn) was expressed in neuronal tissues of homozygous *Df(2L)VA23* mutant embryos, to assess whether the mutant NMJ phenotype can be rescued[ii].
- Misexpression of DPxn double-stranded RNA (dsRNA) was carried out in order to analyse whether reduced DPxn expression levels lead to phenocopies of mutant motor terminals observed in the deficiency bearing embryos described above.

Flies transgenic for *GFP-DPxn* were generously provided by Ryohei Yagi (Department of Molecular Biology, Osaka Bioscience Institute, Japan). eve^{RN2D+O}-Gal4 mediated misexpression of GFP-DPxn was initially carried out in wildtype background of embryos at late stage 17. To enhance the GFP-signal, the preparations were labelled with anti-GFP antibody. The misexpressed tagged DPxn protein localised specifically at NMJs, revealing that GFP-DPxn reaches the site of potential DPxn activity (Figure 3.31). *GFP-DPxn* transgenic flies could therefore be used in an attempt to rescue the strong NMJ phenotype observed in *Df(2L)VA23* homozygous embryos at stage 17.

In the DPxn rescue experiments GFP-DPxn was expressed pan-neuronally (*elav-Gal4*) or in the motor neurones aCC, RP2 and Qs (combined expression of eve^{RNE}-*Gal4* and *Q-Gal4*), in *Df(2L)VA23*-background. Motor neurones with strong GFP-DPxn expression tended to show less or no filopodial extensions and were of a more compact structure (Figure 3.32). However, a clear rescue of *Df(2L)VA23* motor neuronal phenotypes was not achieved (although in double blind tests 17 out of 26 cases were assigned correctly) and motor neuronal terminals still appeared considerably deformed. It has so far not been possible to develop a strategy to evaluate the observed morphological changes numerically and calculate their statistical relevance. Thus, motor neuronal defects observed in *Df(2L)VA23* are likely to be

[ii] The deficiency *Df(2L)VA23* was the first deletion stock received from public stock centres and, after having discovered that its chromosomal deletion causes motor neuronal phenotypes and lacks DPxn expression, was used for the lengthy genetic recombination crosses required for the rescue experiments; see Chapter 2.1.4.3.

caused by loss of *DPxn* expression, but the rescue approach did not provide strong evidence for this hypothesis.

Therefore, a second approach was used trying to affect DPxn protein levels specifically through targeted expression of double-stranded *DPxn-RNA* (*DPxn-RNAi*; RNAi for RNA interference). RNAi-triggered mechanisms are natural cellular responses induced upon dsRNA invading the cell usually in form of ribonuclear pathogens such as transgenes, transposons, viruses or aberrant single stranded RNA (Bernstein et al., 2001a). Such pathogens are recognised and degraded by proteins of the RNaseIII nuclease family of proteins (Bernstein et al., 2001b). Also 'healthy' single stranded RNA in the cell is destroyed by these mechanisms if it matches the sequence of the triggering dsRNA (such as the RNA that is targeted in RNAi-knock out experiments; Bosher and Labouesse, 2000). Thus, expression of dsRNA results in specific inhibition of gene-expression at the post-transcriptional level.

Different UAS-constructs and respective transgenic fly-strains suitable for *DPxn-RNAi*-experiments were generated and generously provided by Ryu Ueda (Invertebrate Genetics Laboratory, National Institute of Genetics, Shizuoka, Japan). Two copies of *DPxn-RNAi* were expressed in stage 17 embryos using the driver lines eve^{RN2D+O}*-Gal4* (Figure 3.30F; this experiment gave the clearest phenotype, see below), eve^{RNE}*;Uas-Cd8*^{GFP} (Figure 3.31I) and *elav-Gal4* (pan-neuronal, not shown), respectively. Projections and NMJs were visualised using combinations of both anti-FasII and anti-Syt or anti-DLG and anti-Syt (see Chapter 3.1, Figure 3.2). The *DPxn-RNAi* expression in embryos at late stage 17 was found to affect NMJ morphology (Figure 3.30F). Comparable to observations made in embryos deficient for *DPxn*, the terminal branches were observed to elongate into filopodia-like extensions. This suggests the NMJ phenotypes observed in the *DPxn* deficient mutant embryos to be caused by loss of DPxn expression. However, as observed in the *DPxn* deficient embryos, the morphological changes at the NMJ caused by *DPxn-RNAi* expression did not seem to affect the localisation of synaptic proteins: Syt localised within the morphologically affected branches. Furthermore, similar to *DPxn* deficient embryos, it was observed that dendritic projections in the CNS were not reduced (Figure 3.30I), although they approved aberrant in shape. Therefore, so far the structural defects of motor neuronal terminals are the only clear DPxn phenotypes.

The RNA interference experiments were repeated in third instar larvae in order to address the effect of *DPxn-RNAi* on structural differentiation of NMJ at later developmental stages and to assess whether the observed phenotypes are due to reduced DPxn expression levels caused by *DPxn-RNAi*. Targeted gene expression was carried out with two copies of

DPxn-RNAi-constructs driven with the Gal4-lines *OK6-Gal4* (all motor neurones) and *elav-Gal4* (pan-neuronal) in third instar larvae. As done previously, the projections and NMJs were visualised using combinations of either anti-FasII and anti-Syt or anti-DLG and anti-Syt. DPxn protein levels were addressed with anti-pax staining. As revealed by the different applied markers, the targeted *DPxn-RNAi* expression resulted in reduction of DPxn levels (Figure 3.33C) and NMJ malformation (Figure 3.33A-C). Branches of NMJs were longer and in some cases varicosities appeared smaller than in wildtype control larvae. No effects resulting from the *DPxn-RNAi* expression could be observed for the localisation of the synaptic proteins (Figure 3.33A) or trans-membrane adhesion molecules, confirming results from the *DPxn-RNAi* expression at earlier stages. The phenotype was assessed numerically by calculating the ratio between muscle length and the length of the motor neuronal terminal and turned out to be statistically significant (Table 3.4).

Genotype	n (projections)	Marker	Length of muscle/ Length of NMJ	Significance
OK6-Gal4::DPxnRNAi	26	Anti-DLG	3,5±0,8	P=0,002 (Student's t-test)
Wildtype control	18	Anti-DLG	2,4±0,5	
elav-Gal4::DPxnRNAi	10	Anti-FasII	3,45±0,43	P<0,001 (WMW-test)
Wildtype control	6	Anti-FasII	2,46±0,41	

Table 3.4: Ratios of muscle length and the length of NMJs measured in third instar larvae of wildtype or *DPxn-RNAi* expressing motor neurones. The NMJs were visualised using specific synaptic markers (see Figure 3.33A and B). The values measured in the second experimental approach did not follow normal distribution and were therefore subjected to the Wilcoxon-Mann-Whitney- Rank test (WMW-test, see Chapter 2.1.10.) to assess the significance of the measured ratios.

The lower DPxn levels detected with anti-pax in *DPxn-RNAi* expressing larvae confirmed the specificity of the DPxn antibodies in axons and NMJs and revealed, that the observed phenotype is due to reduced DPxn expression levels. Thus, the results strongly suggest DPxn to be required for the structural differentiation of synapses at larval stages.

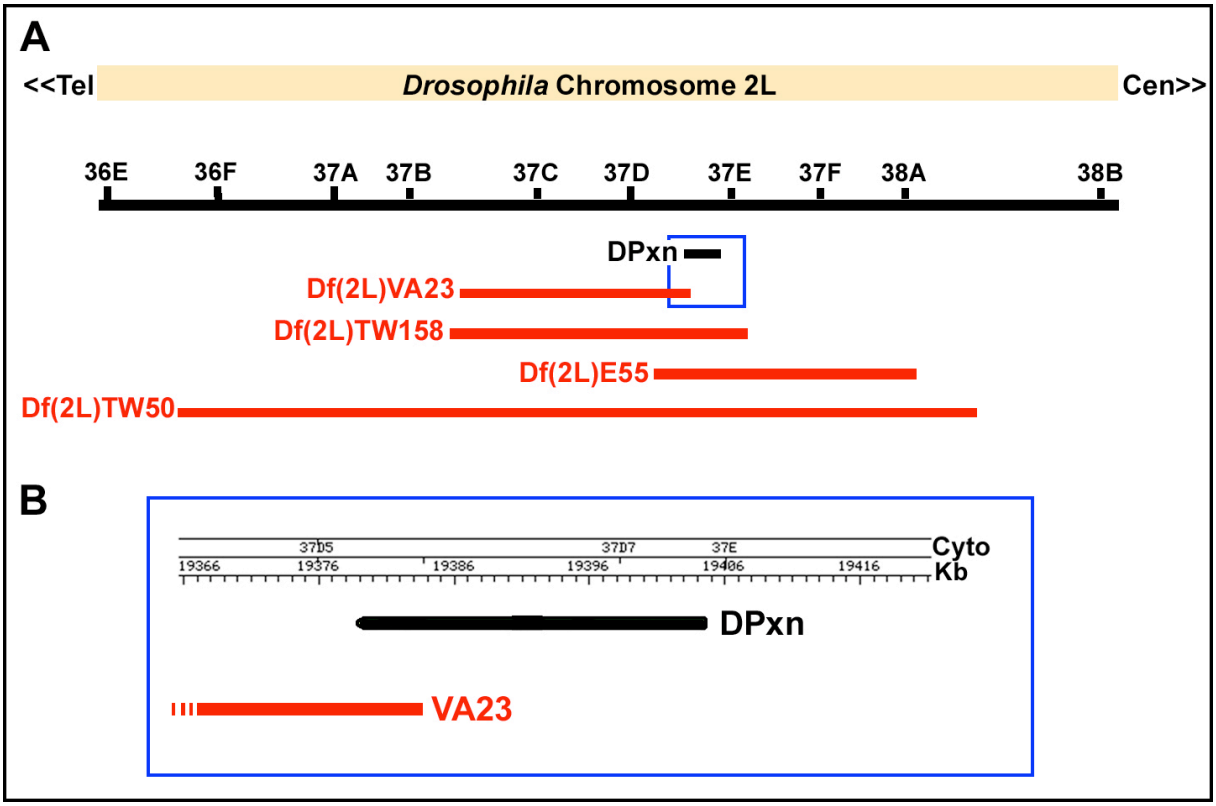
A
<<Tel
Drosophila Chromosome 2L
Cen>>
36E
36F
37A
37B
37C
37D
37E
37F
38A
38B
DPxn
Df(2L)VA23
Df(2L)TW158
Df(2L)E55
Df(2L)TW50
B
37D5
37D7
37E
Cyto
19366
19376
19386
19396
19406
19416
Kb
DPxn
VA23

In summary, an interaction of Shot and DPxn is suggested by the yeast two-hybrid analysis, co-immunoprecipitation, co-localisation in tendon cells and the aberrant localisation of DPxn in tendon cells of *shot* mutant embryos. At late embryonic and late larval stages both proteins localise at NMJs. An early requirement at NMJs is suggested by mutant phenotypes caused by *DPxn* deficiencies *Df(2L)VA23*, *Df(2L)TW158*, and *Df(2L)E55*, which can be mimicked with *DPxn-RNAi* expression. Interestingly, mutant phenotypes of *shot* and *DPxn* are very different: *shot* mutant terminals are reduced, lacking synaptic proteins (which can appear mislocalised in motor axons), whereas *DPxn* mutant terminals are enlarged, leaving synaptic proteins unaffected. Both phenotypes can be interpreted being of opposite nature, providing exciting prospects to speculate about the way they might interact genetically (see Discussion, Chapter 4.2.).

Figure 3.29: Cytological localisation of *DPxn* and of chromosomal regions deleted in the *Drosophila* deficiencies *Df(2L)VA23*, *Df(2L)TW158*, *Df(2L)E55* and *Df(2L)TW50*. An approximate overview over cytological map locations 36E to 38B of chromosome 2L is shown in A. The chromosomal regions deleted by the respective deficiencies are indicated in red (*Df(2L)VA23*: 37B9-37D5; *Df(2L)TW158*: 37B2-37E2; *Df(2L)E55*: 37D2-38A1; *Df(2L)TW50*: 36E4-38A6-7) , the *DPxn* gene is shown as a black bar. Double arrows point to telomere (Tel) or centromere (Cen) of the chromosome. B shows an enlargement of the cytological area at about cytological map location (Cyto) 37D-E (blue box in A). The centromere-directed breakpoint of *Df(2L)VA23* overlaps with the *DPxn* gene. Kb, Kilo base pairs. Source of cytological map locations and Kb numbers: FlyBase, 1999.

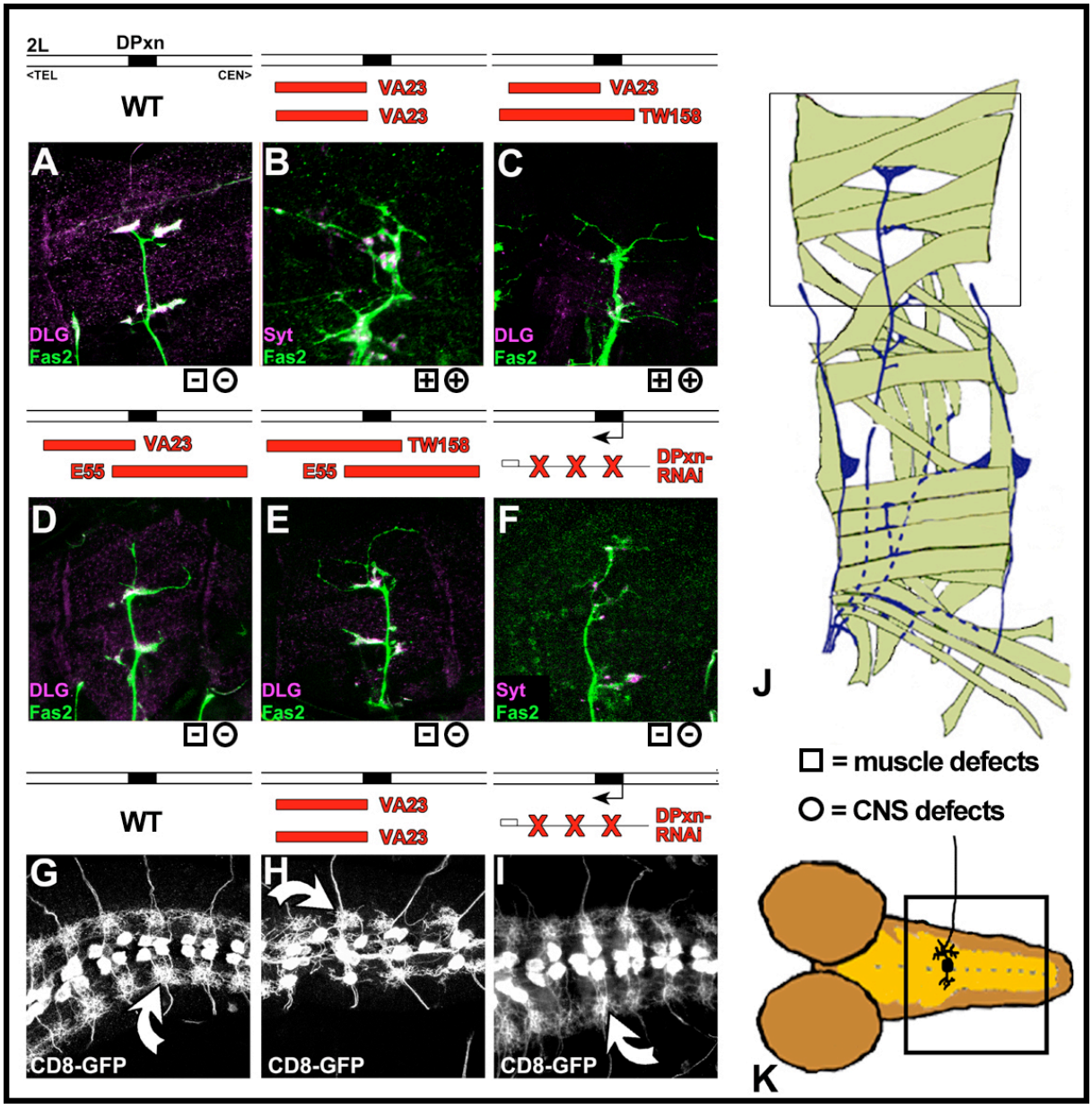
2L
DPxn
<TEL
CEN>
WT
VA23
VA23
VA23
TW158
A
B
C
DLG
Fas2
Syt
Fas2
DLG
Fas2
VA23
E55
TW158
E55
X X X
DPxn-
RNAi
D
E
F
DLG
Fas2
DLG
Fas2
Syt
Fas2
WT
VA23
VA23
X X X
DPxn-
RNAi
G
H
I
CD8-GFP
CD8-GFP
CD8-GFP
J
= muscle defects
= CNS defects
K

Figure 3.30: NMJ malformations in embryos deficient for *DPxn* or with reduced DPxn expression levels at stage 17. A-F) Terminals of motor neurones in wildtype (WT), in specimens with motorneuronal *DPxn-RNAi* expression (driven with eve^{RN2D+O}*-Gal4*; triple X), or in individuals carrying different combinations of deficiencies (red bars indicated above; VA23, *Df(2L)VA23*; TW158, *Df(2L)TW158*; E55, *Df(2L)TWE55*) were labelled with anti-FasII (green). NMJs where additionally stained for synaptic proteins DLG (A and C-E) or Syt (B and F; all shown in magenta). In embryos homozygous for VA23 (B), TW158 or E55 (not shown) or transheterozygous for VA23/TW158 (C), VA23/E55 (D), or TW158/E55 (E), motorneuronal terminals have long filopodia-like branches. The structural defects at the NMJ do not seem to affect the localisation of synaptic proteins such as Syt (unlike the *shot* mutant phenotype). Presence (+) or absence (-) of additional aberrations of the musculature (squares) or the CNS (circles; for details see text) are indicated bottom right and seem to map to genes up-and downstream of DPxn: They are absent in VA23/E55 and TW158/E55 embryos but present in VA23/TW158 or embryos homozygous for any of the deficiencies (only partly shown). The neuronal phenotypes in all deficiencies were found to resemble those of *DPxn-RNAi* misexpressing embryos. Therefore, there is a considerable potential that the NMJ phenotypes observed in embryos deficient for the *DPxn* gene locus are due to loss of DPxn expression. G-I) CD8-GFP expressing central dendritic projections of aCC and RP2 in wildtype- (G) or VA23 (H) background or simultaneously with *DPxn-RNAi* (I) were visualised with anti-GFP. The structural differentiation of dendrites in the CNS appears not to be impaired in *Df(2L)VA23* homozygous or *DPxn-RNAi* misexpressing embryos (bent arrows in H and I). The cartoon in J shows the area depicted in the confocal images A-F, the cartoon in K shows the areas depicted in G-I. Anterior is to the left. TEL and CEN point to the telomere and centromere, respectively, of chromosome 2L.

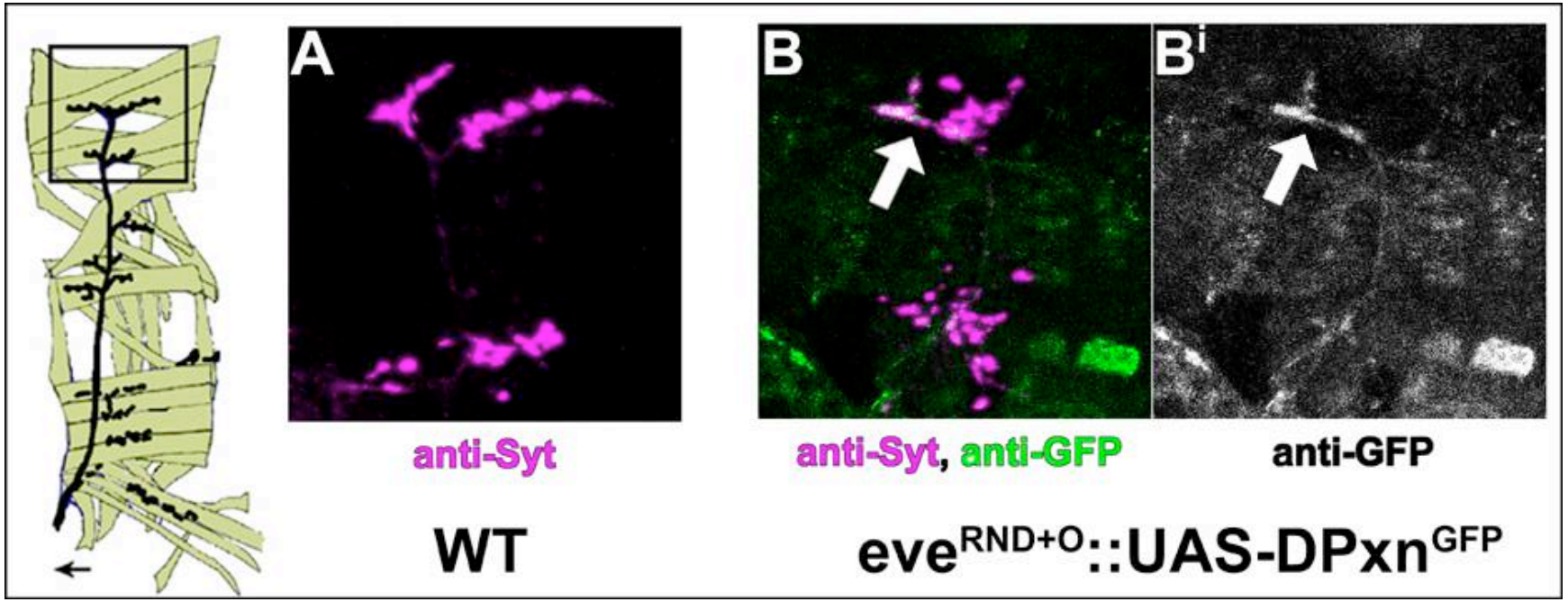
A
B
Bi
anti-Syt
anti-Syt, anti-GFP
anti-GFP
WT
eveRND+O::UAS-DPxnGFP

Figure 3.31: GFP-tagged DPxn misexpressed in neurones localises at NMJs. Expression of the GFP-construct was driven specifically in the motor neurones aCC and RP2 with the *Gal4*-line eve^{RN2D+O}. Stage 17 embryos were labelled with anti-Syt and anti-GFP. Dorsalmost NMJs of wildtype control (WT, A) and GFP-DPxn expressing specimen (B, merged channels, and B^i, GFP-channel only) are shown. The misexpressed construct localises at the NMJ (arrows), but does not cause detectable structural defects. Cartoon to the left shows area depicted in the confocal images. Black arrow points anterior.

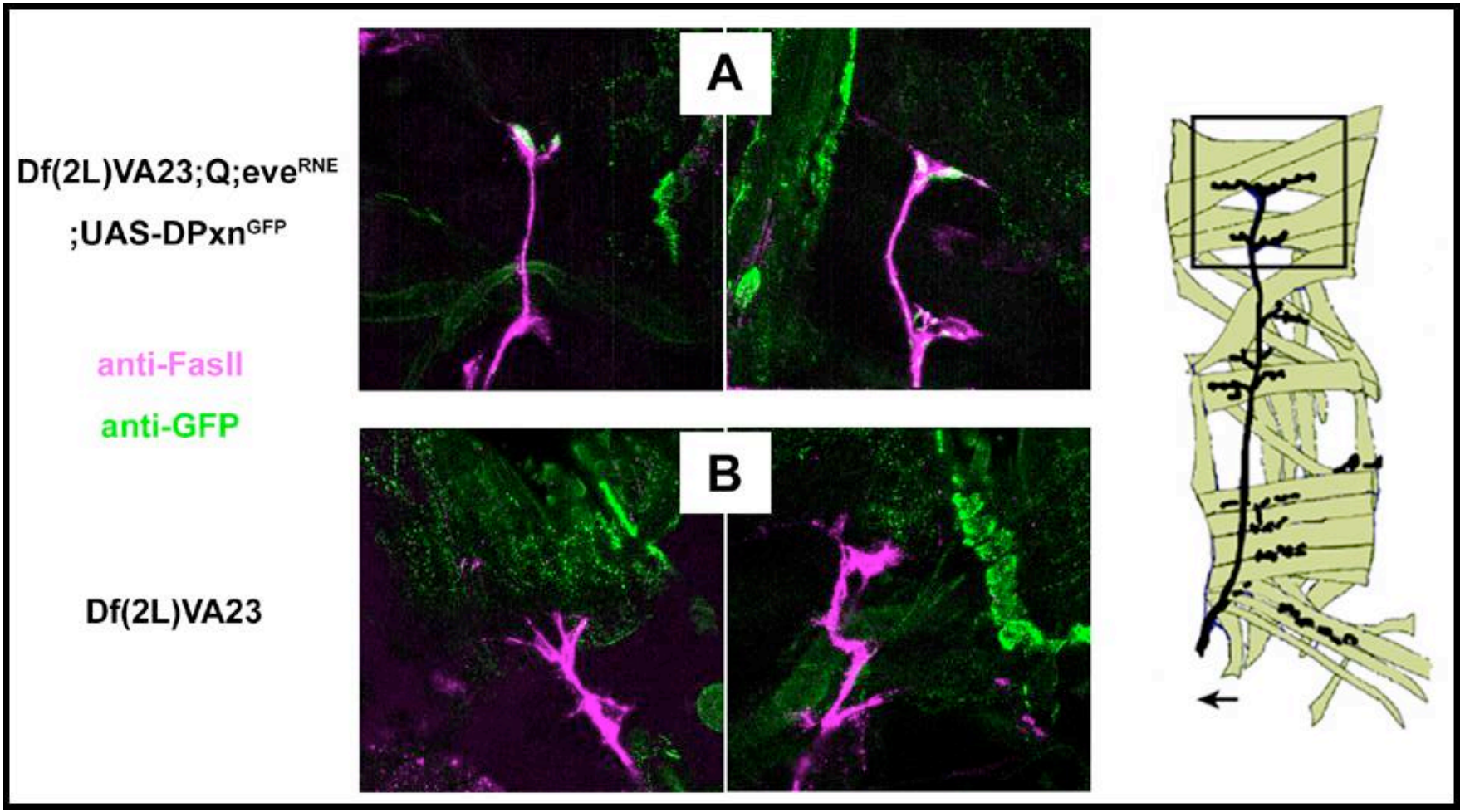
Df(2L)VA23;Q;eve^RNE
;UAS-DPxn^GFP
anti-FasII
anti-GFP
A
B
Df(2L)VA23

Figure 3.32: Rescue attempt of the NMJ phenotype in *Df(2L)VA23* embryos at stage 17 through misexpression of GFP-tagged DPxn. Expression of the construct was driven simultaneously with eve^{RNE}- and Q-Gal4. Two examples of NMJs labelled with anti-FasII from *Df(2L)VA23* embryos with (A) and without (B) DPxn misexpression are shown. The GFP-signal of the construct was enhanced using anti-GFP antibodies. The motor neuronal terminals expressing the rescue construct appear to have less filopodia-like protrusions and seem more compact as compared to the controls. However, a true rescue could not be achieved (see text). The cartoon to the right shows the area depicted in the confocal images. The black arrow points anterior.

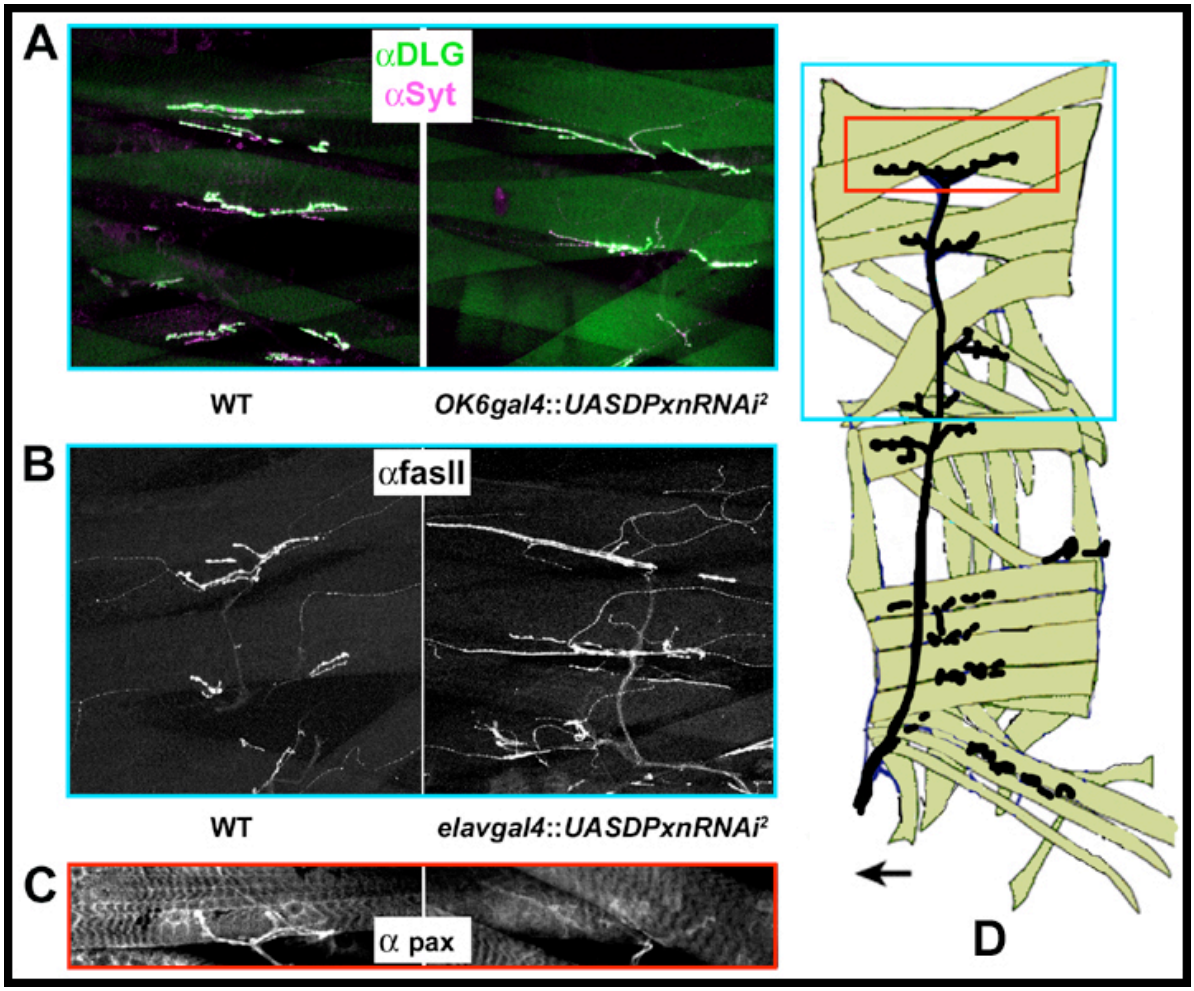
A
αDLG
αSyt
WT
OK6gal4::UASDPxnRNAi²
B
αfasII
WT
elavgal4::UASDPxnRNAi²
C
α pax
D

Figure 3.33: Reduced DPxn levels cause NMJ malformations. Targeted expression of DPxn-RNAi using the neuronal Gal4-driver lines OK6-gal4 (A) and elav-gal4 (B and C) cause elongation of the NMJs of third instar larvae (compare Table 3.5). The NMJs were labelled with anti-DLG (green), anti-Syt (magenta) and anti-FasII (in B). Application of anti-pax revealed that DPxn levels are reduced within NMJs as a result of RNA interference (C). This also confirms the specificity of anti-pax for DPxn in larval projections and NMJs. The scheme in D shows the areas depicted in the respective confocal images (blue box: A and B; red box: C). The black arrow points anterior.

3.6. Genetic strategy to uncover potential factors of the pathway of Shot function

As described in Chapter 3.5., a yeast two-hybrid approach was used to screen for potential Shot interaction partners. So far, one of them, DPxn, could be shown to represent a very likely direct Shot interactor shedding new light on mechanisms underlying the differentiation of synaptic terminals. A second, very different approach was used in order to find further genetic interactors of Shot. In the literature about pathfinding mechanisms in *Drosophila* several factors are mentioned which cause very similar motor axonal stall phenotypes as they occur in *shot* mutant embryos at early stages (stage 16; see Chapter 3.1.). Therefore it was tested whether they show also *shot*-like phenotypes at later stages, when synapses differentiate. Such similarities might reveal further components interacting with Shot either directly or indirectly in the same pathway.

The small GTPases of the Rho subfamily were reported to mediate morphological changes during axon growth and guidance and dendrite elaboration (Gao et al., 1999; Hall, 1998; Kaufmann et al., 1998; Kim et al., 2003; Luo et al., 1997; Luo et al., 1994). In particular, the misexpression of mutant isoforms (see below) of the Rho GTPase family members DRac1 (*Drosophila* Ras related C3 botulinum toxin substrate 1) and DCdc42 (*Drosophila* cell division cycle 42) were described to cause pathfinding defects and axonal stall phenotypes (Kaufmann et al., 1998; Kim et al., 2003; Luo et al., 1994). Mutant isoforms of DRhoA (*Drosophila* Ras homologous A) reduce dendrite branching (Lee et al., 2000a), a phenotype also observed in *shot* mutant embryos (see Chapter 3.1.). DRhoA has further been suggested to antagonise Shot function in the regulation of E-cadherin-associated cytoskeletal structures required for the localisation of apical determinants in tracheal branches (Lee et al., 2000b). These properties made the Rho-like GTPases ideal candidates for the purpose of this study.

In order to be able to study the role of the Rho GTPases in synapse formation the GAL4/UAS system (see Chapters 2.1.4., 3.1., 3.3. and 3.5.2.) was used to target expression of mutant protein forms of Rho GTPases selectively to neurones. The dominant mutant isoforms used were either constitutively active (CA; CA DRac1 isoform $DRac1^{V12}$ or CA DCdc42 isoform $DCdc42^{V12}$; amino acid Glycin has been exchanged for amino acid Valin at position 12, Luo et al., 1994) or dominant negative (DN; DN DRac1 isoform $DRac1^{N17}$, DN DCdc42 isoform $DCdc42^{N17}$ or DN isoform $DRhoA^{N19}$; Threonin for Asparagin exchange at position 17 or 19, respectively; see Figure 3.34). Before testing the effect of neuronally misexpressed

mutant isoforms of the respective RhoGTPases on synapse formation, the early motor neuronal stall phenotype was assessed in order to reconfirm earlier results reported in the literature (Kaufmann et al., 1998; Luo et al., 1994). The diverse isoforms were expressed using the *elav-Gal4* driver line. The analysis focused on the ventral motor neuronal projection of the segmental nerve b (SNb, compare Figure 3.1A, Chapter 3.1.). In wildtype embryos at stage 16 the SNb has reached its most dorsal target, the ventral lateral muscle VL1. In contrast, strong stall phenotypes of SNb were found for DRac1^{V12}, DCdc42^{V12} and DRac1^{N17}, weaker ones for DCdc42^{N17} (Figure 3.35). In Addition, axon guidance defects (wrong path selection) were observed in motor neurones expressing DRac1^{N17} and DCdc42^{V12} (not shown), which is in accordance with previously reported studies (Kaufmann et al., 1998; Kim et al., 2003). Misexpressed DN isoform of RhoA did not cause any growth defects in stage 16 embryos (not shown) and was excluded from further studies.

Having confirmed previously published results and thus functionality of the used transgenic flies, it was investigated whether neuronal expression of mutant isoforms of DRac1 and DCdc42, respectively, cause *shot*-like phenotypes at late stage 17. As described before (Chapter 3.1., Figure 3.2), the motor neuronal terminals were visualised with anti-Syn, anti-Syt (both presynaptic) and anti-DLG (predominantly postsynaptic), motor axons with anti-FasII. Synaptic terminals of DRac1^{V12} misexpressing neurones were severely reduced in size, mimicking the *shot* mutant phenotype at late stage 17 (Figure 3.36). Whereas Syn stayed restricted to putative presynaptic sites (Figure 3.36B^{i}), anti-Syt staining was spread along the axon (Figure 3.36A^{i}) as described earlier for *shot* mutant embryos (Figures 3.36B^{ii} and A^{ii}; see also Table 3.1). Furthermore, anti-DLG staining, which is normally found on the postsynaptic side of every NMJ, was lacking on many muscles (Figure 3.36C^{i}), indicating that these muscles were non-innervated (and that DLG-localisation obviously depends on innervation). Thus, pan-neuronal misexpression of CA DRac1 causes phenocopies of defects found in *shot* mutant NMJs.

To describe the phenotypes of misexpressed CA DRac1 mutant isoforms in more detail, Ulrike Mettler and Andreas Prokop carried out misexpression studies using further neuronal drivers (Mettler, 2002; for details see Chapter 7.2.). In brief, more overlaps between phenotypes of *shot* mutant embryos (see Chapter 3.1.) and those caused by misexpression of the CA DRac1^{V12} were found (Table 7.2): dendrites in the PNS and the CNS were reduced (see Figure 3.38C), the structure of scolopidial sensory neurones was impaired, and nerve roots in the CNS displayed mislocalisation of FasII and DLG (not shown). Hence, there is a

strong phenotypical overlap between *shot* mutant embryos and embryos misexpressing the CA mutant isoform of DRac1.

Misexpression of DCdc42^{V12} on the other hand did not cause any detectable structural NMJ defects when using the pan-neuronal driver *elav-Gal4* (Figure 3.37). NMJs seemed wildtypic and the synaptic antibodies did not reveal any mislocalisation of synaptic components. In order to allow a more precise analysis of DCdc42^{V12}-misexpression effects, the mutant isoform was expressed specifically in the motor neurones aCC and RP2 using the *eve^{RN2-E}-Gal4;UAS-Cd8GFP* strain (simultaneous expression of Cd8-GFP allows visualisation of the targeted neurones; see also Chapters 3.1. and 3.3.). NMJs of DCdc42^{V12}-expressing aCC and RP2 motor neurones seemed wildtypic, confirming the results obtained with *elav-Gal4* (not shown). However, these results are presently under reinvestigation, since use of an even stronger Gal4-driver line (*eve^{RND+O}*-Gal4) under more stringent conditions (29°C) caused aberrations of aCC/RP2 motor terminals (N. Sanchez-Soriano, personal communication). Yet, already in my experiments, the expression of DCdc42^{V12} caused a reduction of the dendritic side branches in the CNS (Figure 3.38B). At first glance, the phenotype appeared similar to the CNS phenotype observed in *shot* mutant alleles (Figure 3.38D; see also Chapter 3.1 and Prokop et al., 1998b) but further analysis is required. Although no defects could be detected for motor neuronal terminals upon misexpression of the CA mutant isoform of DCdc42 in the course of this thesis, the functions of DCdc42 and Shot were found to potentially overlap during dendrite formation in the CNS.

An essential question to be addressed was, whether these results with CA GTPases may provide insights into the molecular machinery underlying the synaptic differentiation of neurones. At first sight the phenotypes caused by CA GTPase misexpression could be viewed as dominant artefacts which do not reflect the function of native GTPases. Native GTPases might even not be expressed or activated in the investigated neurones during the time of synapse formation, so that the targeted CA form influences effectors which would normally not experience regulation through GTPase at this developmental stage. One strategy to test this possibility is to investigate neurones in which native GTPase function is affected:

1) If loss of GTPase function does not reveal any phenotypes, this would hint at a neglectable role of these GTPases during the differentiation of synaptic terminals.

2) The loss of GTPase function phenotypes could be very different or opposite to the ones caused by misexpressed CA forms, since the constitutively active GTPases can be expected to regulate effector genes at inappropriately high levels.

3) Another possibility is that loss- and gain-of-function phenotypes are comparable, since over-activation or suppression of effector function might impair their instructive influence on the associated molecular machinery alike (reviewed in Luo, 2000).

The first approach to remove native GTPase function was the use of their dominant negative forms. To this end, the driver lines *elav-Gal4* and *eve^{RN2-E}-Gal4* were used to misexpress DN DRac1^{N17} and DN DCdc42^{N17} and analyse potential effects on neuronal differentiation. However, no obvious defects of late neuronal differentiation were observed in these experiments (Figure 3.39). Before drawing premature conclusions, other approaches were tested to confirm this result. Thus, Gal4-mediated expression of wildtype or DN versions of *Drosophila* RacGAP (DRacGAP) was carried out. DRacGAP is a GTPase inactivating protein, which is thought to regulate DRac1 and DCdc42 activity in the fruit fly (see Figure 3.40; Sotillos and Campuzano, 2000). Expression of the wildtype form should reduce levels of activated DRac1 and DCdc42, because the misexpressed GAP increases the endogenous GTPase activity of DRac1 and DCdc42, thereby switching them off (compare Figure 3.40i.). Misexpression of the DN versions DRacGAP$^{\Delta EIE}$ and DRacGAP^{R417Q} should increase levels of DRac1 and DCdc42 activity, since the GTPases would no longer be able to leave their GTP bound active state (Figure 3.40ii). The latter case should be mimicking DRac1^{V12} misexpression. In order to test this and thus the functionality of the DN isoforms of DRacGAP, both isoforms were expressed in mesoderm using the *24B-Gal4* driver line, respectively. This treatment caused muscle fusion defects similar to (though much milder than) phenotypes described for *DRac1* mutants in mesoderm (Hakeda-Suzuki et al., 2002; Luo et al., 1994), confirming functionality of the constructs (not shown). The DN and wildtype isoforms of DRacGAP were subsequently misexpressed in neurones using the driver lines *elav-Gal4* and *eve^{RNE2}Gal4;UAS-Cd8GFP*, respectively. NMJs were labelled with anti-Syn, anti-Syt and anti-DLG. The motor neuronal projections were visualised with anti-FasII. In all misexpression experiments the NMJ pattern was wildtype, and the size of the boutons was normal (Figure 3.41). Synaptic proteins were localised properly and no defects could be detected in the FasII fascicle pattern of the CNS or the central dendritic projections.

Towards the end of my project and the writing up period of this thesis further experiments were carried out by members of the group. Thus, triple mutant embryos deleting the *DRac1*, *DRac2* and *Mtl* genes were analysed (Chapter 7.3.). It was shown previously, that these genes can partly compensate for each others function, and only the triple mutant constellation reveals a true DRac1 knock out phenotype (Hakeda-Suzuki et al., 2002). Interestingly, preliminary analyses of these triple Rac mutant flies cause no reduction of

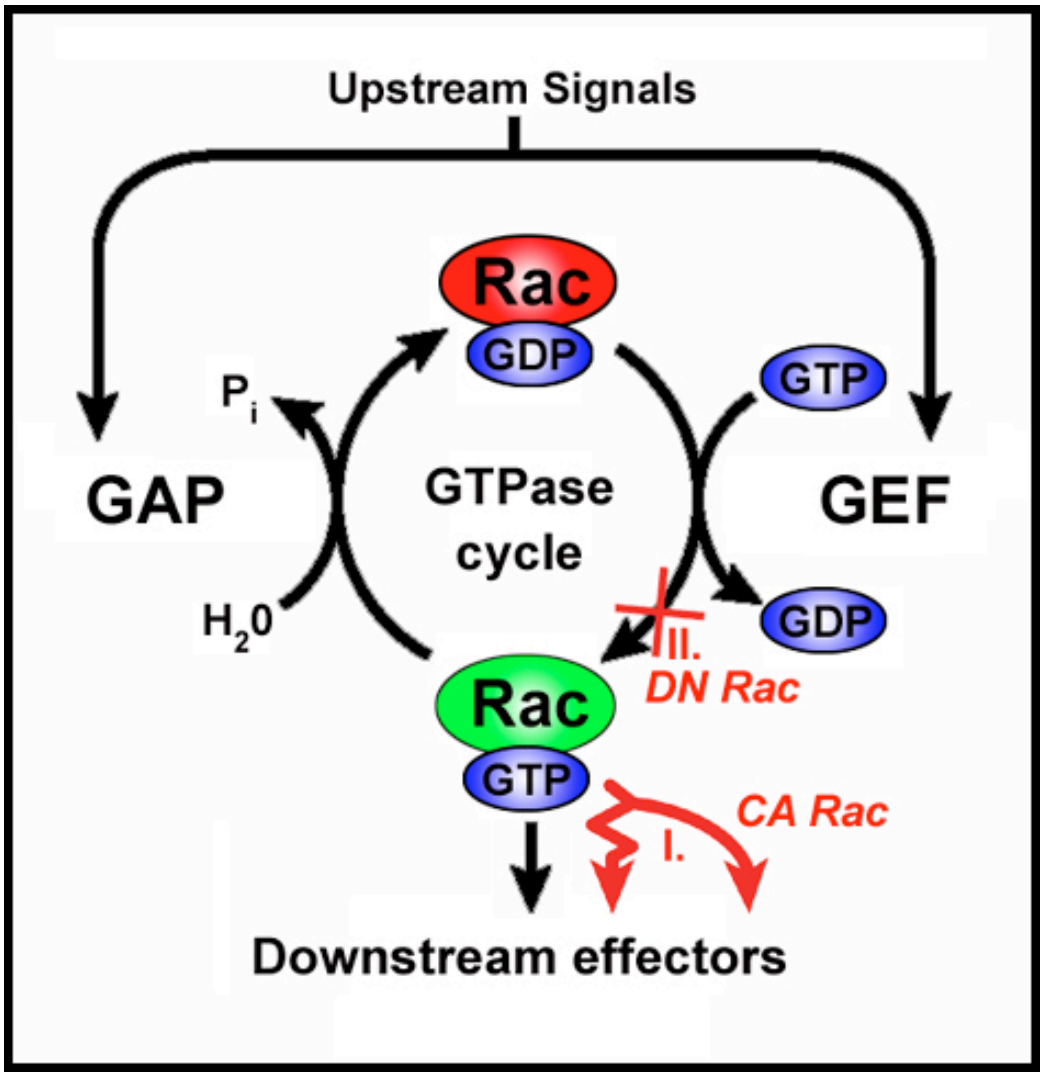
Upstream Signals
Rac
GDP
GTP
P_i
GAP
GTPase
cycle
GEF
H_20
GDP
II.
DN Rac
Rac
GTP
CA Rac
I.
Downstream effectors

synaptic spots, but instead terminal overgrowth with some similarity to that seen in DPxn mutant embryos (A. Prokop, personal communication). Such overgrowth could be interpreted as an inverse phenotype to that caused by DRac1^{V12} misexpression (see discussion for more details). Further confirmation for this observation comes from repetition of experiments with DN DRac1^{N17} using stronger driver lines than those used by me previously. Like analyses of triple DRac1 mutant embryos, also these experiments with DRac1^{N17} reveal aberrations of neuromuscular terminals with excessive overgrowth (Sánchez-Soriano, personal communication). These investigations are still ongoing, but indicate that native DRac1 plays a role during the differentiation of synaptic terminals which appears diametrically opposed to that of misexpressed DRac1^{V12} (see discussion). Both constellations, loss- and gain-of-function of GTPases are important in the context of this study. Gain-of-function mimics *shot* mutant phenotypes, loss-of-function seems to mimic DPxn phenotypes, which in turn are likely to have close links to Shot function (see Chapter 3.5.2.). In order to shed light on the genetic interactions of these components, a series of experiments are currently being carried out in Andreas Prokop's group. The concept of these investigations was essentially influenced by initial experiments carried out within this project, as explained in the following.

Figure 3.34: Rho-GTPases like *Drosophila* DRac1 act as molecular switches. They exist in two states: a GDP-bound inactive state (red eclipse) and a GTP-bound active state (green eclipse). Two classes of protein facilitate the switch between these two states. Guanine nucleotide exchange factors (GEFs) facilitate the exchange of GDP for GTP, thereby switching Rho-GTPases on. When bound to GTP, activated Rho-GTPases can bind to various downstream effectors and elicit different biological activities. By contrast, GTPase activating proteins (GAPs) increase the endogenous GTPase activity of Rho-GTPases, thereby helping to switch them off. In the experiments described in the text different mutant isoforms were misexpressed pan-neuronally or in subsets of motor neurones in order to impair the function of the specific Rho-GTPase during motor neuronal outgrowth or synapse formation. The mutant isoforms used were either constitutively active (CA) or dominant negative (DN). CA mutant proteins remain active independent of upstream signals (I.). In the case of the Rho GTPases, CA mutants are inhibited in their GTPase activity, thereby preventing them from being switched off (I.). DN proteins are non-functional mutant proteins that interfere with the functions of the endogenous wildtype proteins (II.) by titrating away regulatory proteins like GEFs, which would normally switch native GTPases on.

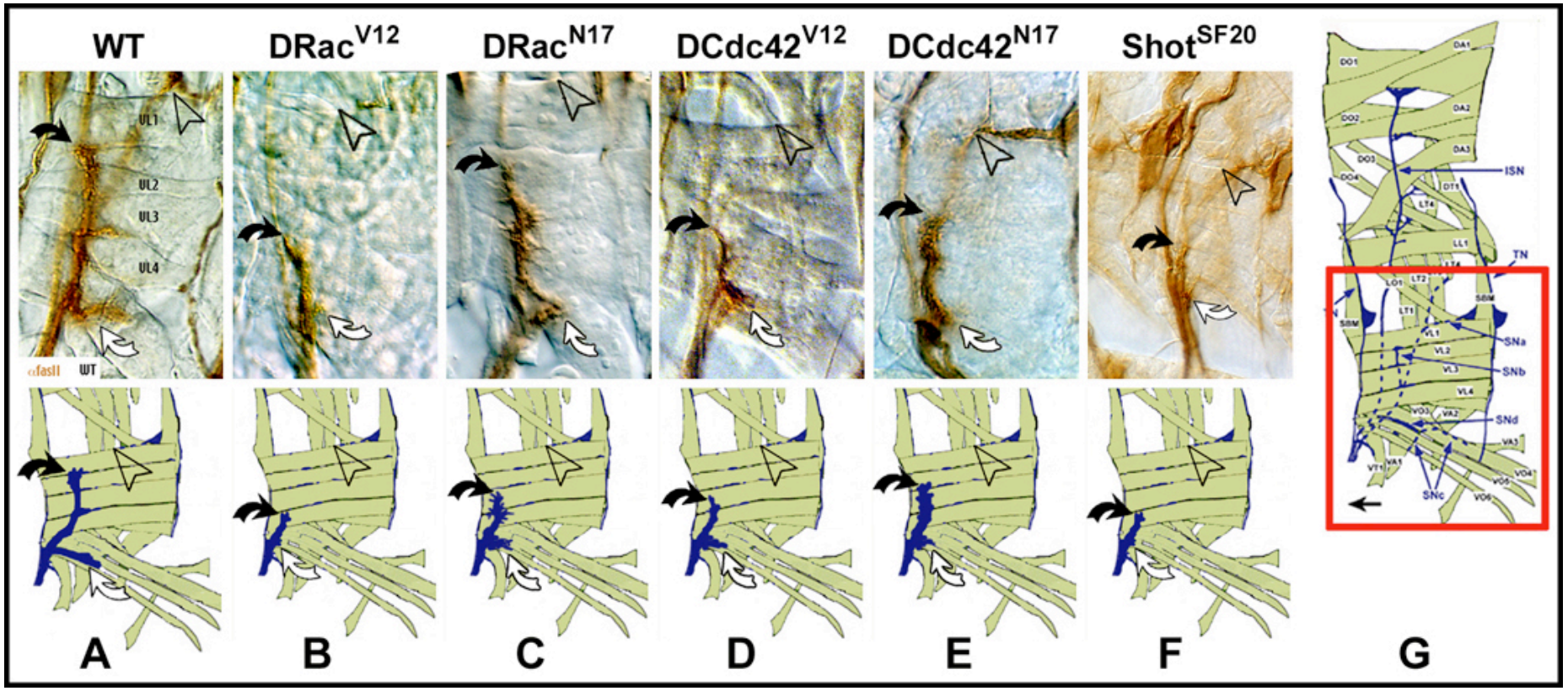
WT
DRac^V12
DRac^N17
DCdc42^V12
DCdc42^N17
Shot^SF20
UL1
UL2
UL3
UL4
αfasII WT
ISN
TN
SNa
SNb
SNd
SNc
A
B
C
D
E
F
G

Figure 3.35: Outgrowth phenotypes of motorneuronal projections in embryos at stage 16 misexpressing mutant isoforms of Rho-GTPases. The light microscopic pictures show projections of the segmental nerve b (SNb) on ventral longitudinal muscles VL1-VL4, and ventral oblique muscles (nomenclature as in Landgraf et al., 1997) in the central abdomen of wildtype control (A) and embryos pan-neuronally misexpressing CA DRac1^{V12} (B), DN DRac1^{N17} (C), CA DCdc42^{V12} (D) and DN DCdc42^{N17} (E). Misexpression of each mutant Rho-GTPase isoform causes stall phenotypes in all ventral projections. Strongest stall phenotypes were observed for CA DRac1^{V12}, CA DCdc42^{V12}, and DN DRac1^{N17}. The stall phenotypes are similar to those found in different *shot* mutant alleles (example is shown for *shot*^{SF20} in F, compare also Figure 3.1). Furthermore, axon guidance defects were observed in motor neurones expressing DN DRac1^{N17}and CA DCdc42^{V12} (not shown). Specimens were labelled with anti-FasII. The lower panel shows cartoons of the ventral muscle area (red box in overview cartoon, G) illustrating the phenotypes observed for the respective genotypes. Black bent arrows indicate growth cones of SNb motor neurones, open arrowheads indicate dorsal edges of muscle VL1, white bent arrows indicate projections of SNc and d. Black arrow in (G) points anterior.

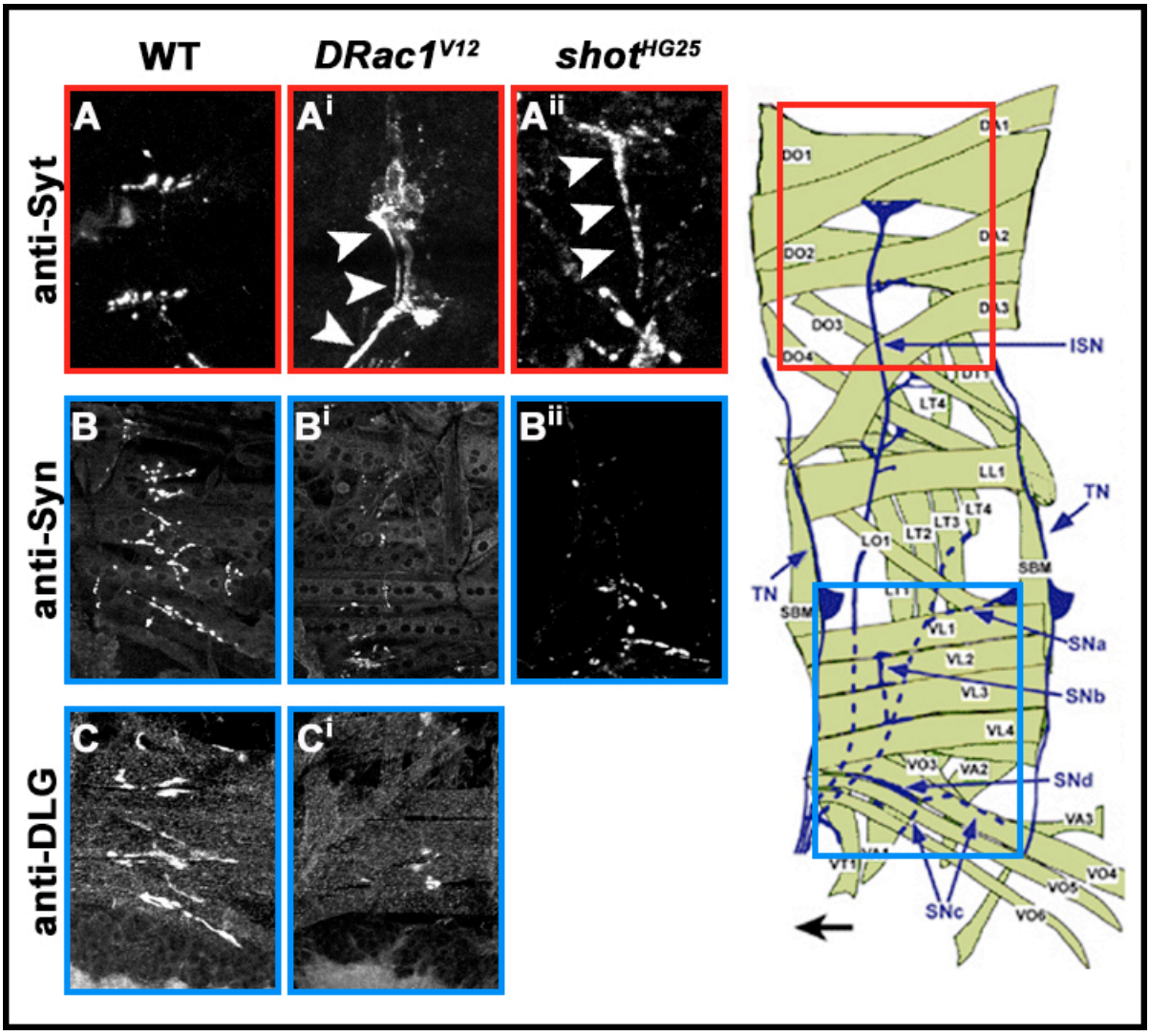
WT
DRac1V12
shotHG25
anti-Syt
anti-Syn
anti-DLG
A
Ai
Aii
B
Bi
Bii
C
Ci
DO1
DO2
DO3
DO4
ISN
LT4
LL1
TN
LT3
LT2
LO1
SBM
VL1
VL2
VL3
VL4
SNa
SNb
SNd
VO3
VA2
VA3
VT1
SNc
VO4
VO5
VO6

Figure 3.36: Misexpression of CA DRac1^{V12} causes phenocopies of *shot* mutant NMJ defects. CA DRac1^{V12} was misexpressed using the pan-neuronal driver *elav-Gal4*. NMJs of embryos at stage 17 were labelled with the antibodies against the synaptic proteins Syt (A-A^{ii}), Syn (B-B^{ii}) and DLG (C and C^{i}). Similar to *shot* mutant embryos (examples are shown for mutant allele *shot^{HG25}* in A^{ii} - B^{ii}, see also Figure 3.4) NMJs of motor neurones expressing CA DRac^{V12} are reduced in number and size as compared to wildtype (A-C). Moreover, an overlap in phenotype is found for the mislocalisation of the synaptic protein Syt (white arrowheads in A^{i} and A^{ii}). Confocal images of anti-Syn and anti-DLG stainings were taken from the ventral muscle area (blue box in overview cartoon), pictures showing anti-Syt stainings were taken from the dorsal muscle area (red box). The black arrow in the overview cartoon points anterior. Muscle nomenclature as in (Bate and Rushton, 1993).

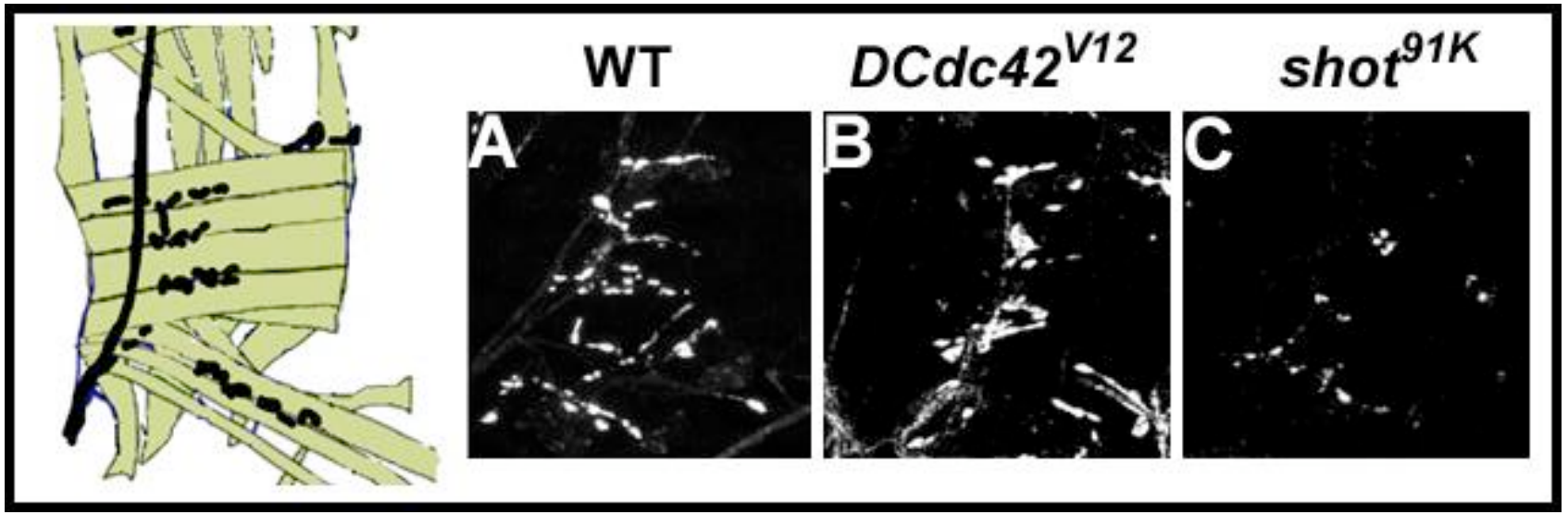
WT
DCdc42V12
shot91K
A
B
C

Figure 3.37: Neuronal misexpression of CA DCdc42 does not cause detectable structural defects at NMJs of embryos at late stage 17. Confocal images show NMJs at ventral longitudinal muscles (see cartoon) labelled with anti-Syn. Synapses of motor neurones expressing the CA mutant isoform of DCdc42^{V12} (B) appeared normal as compared to wildtype (A). A reduction in NMJ size as found in *shot* mutant embryos (shown for *shot^{91K}* mutant in C) could not be observed. Furthermore, neuronal misexpression of CA DCdc42^{V12} did not affect localisation of proteins such as Syt, DLG and FasII (not shown). Hence, there is no indication that CA DCdc42^{V12} causes NMJ defects similar to those found in *shot* mutant alleles (compare Figure 3.3).

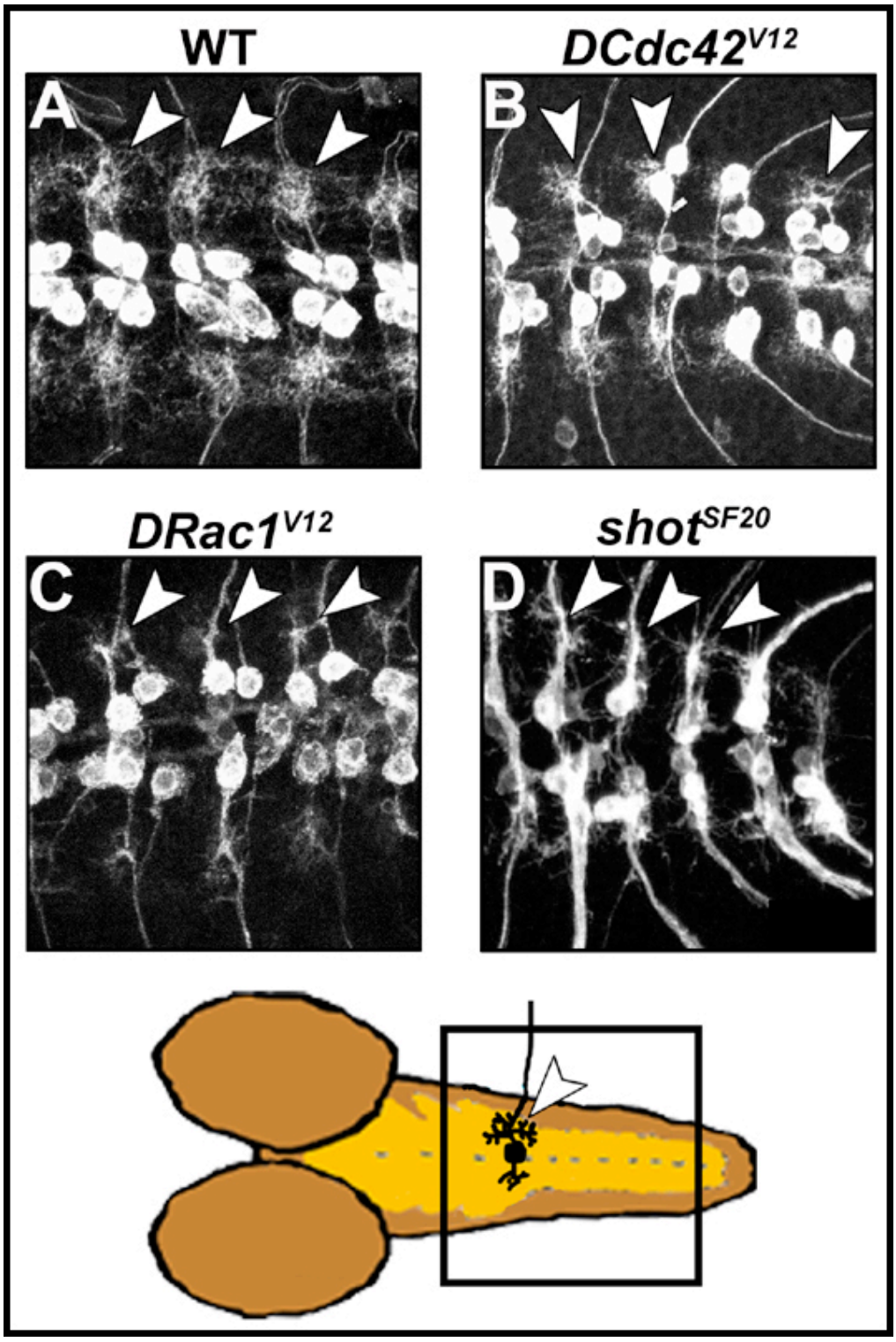
WT
DCdc42V12
A
B
DRac1V12
shotSF20
C
D

Figure 3.38: Neuronal misexpression of CA mutant isoforms of both DCdc42^{V12} and DRac1^{V12}, respectively, causes phenotypes reminiscent of *shot* mutant alleles in the CNS. Central dendritic projections (white arrowheads) of motor neurones aCC and RP2 were visualised by eve^{RNE2}-mediated misexpression of CD8-GFP. Simultaneous misexpression of either CA DCdc42^{V12} (B) or CA DRac1^{V12} (C) causes reduction of the dendritic projections as compared to control (misexpression of CD8-GFP alone, A). A similar phenotype has been shown previously for *shot* mutant alleles (shown in D for *shot^{SF20}*; compare Chapter 3.1.; Prokop et al., 1998b). The results suggest that the functions of DCdc42, DRac1 and Shot might converge in some developmental contexts, such as dendrite formation in the CNS. However, in other contexts such as the NMJ formation, DCdc42 seems to have separate or no functions as compared to DRac1 and/or Shot (compare Figure 3.36 and 3.37). The cartoon shows the area depicted in the confocal images. Image C was kindly provided by A. Prokop. Anterior is to the left.

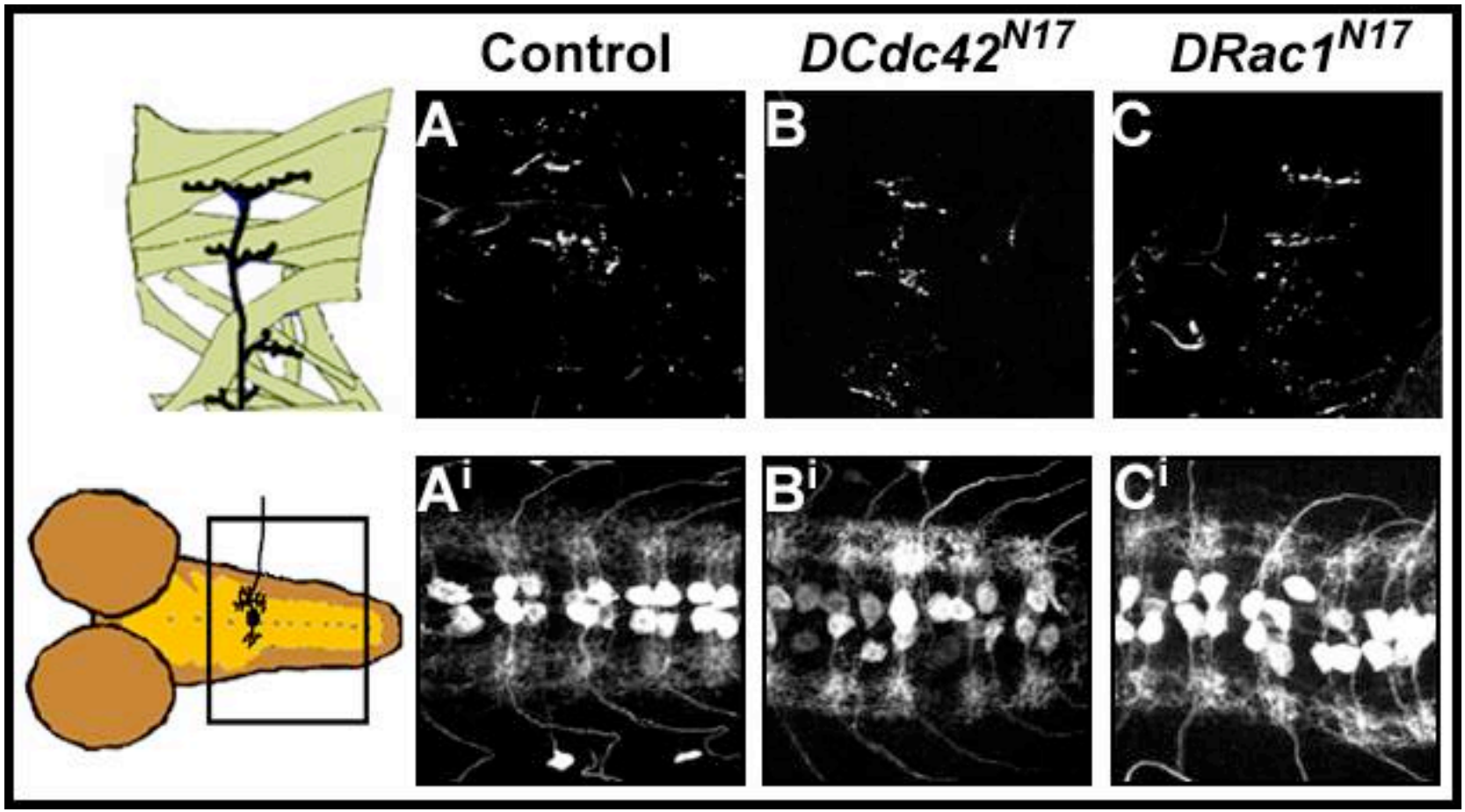
Control
DCdc42N17
DRac1N17
A
B
C
Ai
Bi
Ci

Figure 3.39: Neuronal misexpression of DN isoforms of DCdc42^{N17} or DRac1^{N17}, respectively, does not cause *shot*-like phenotypes in embryos at stage 17. No structural defects at NMJs (labelled with anti-Syt) were detected for motor neurones misexpressing DN DCdc42 (B) or DN DRac1 (C), respectively. The NMJs were normal in size as compared to the wildtype control (A) and no mislocalisation of the synaptic protein Syt could be observed. No defects were further observed for the localisation of the proteins Syn, DLG or FasII (not shown). Central dendritic projections of motor neurones aCC and RP2 were found to be wildtypic (see controle A^{i}) when misexpressing DCdc42^{N17} (B^{i}) or DRac1^{N17} (C^{i}) using the *eve$^{RN2\text{-}E}$-Gal4* driver line. The dendrites were visualised by simultaneous misexpression of CD8-GFP. The cartoons to the left show the area depicted in the confocal images. Anterior is to the left in all pictures.

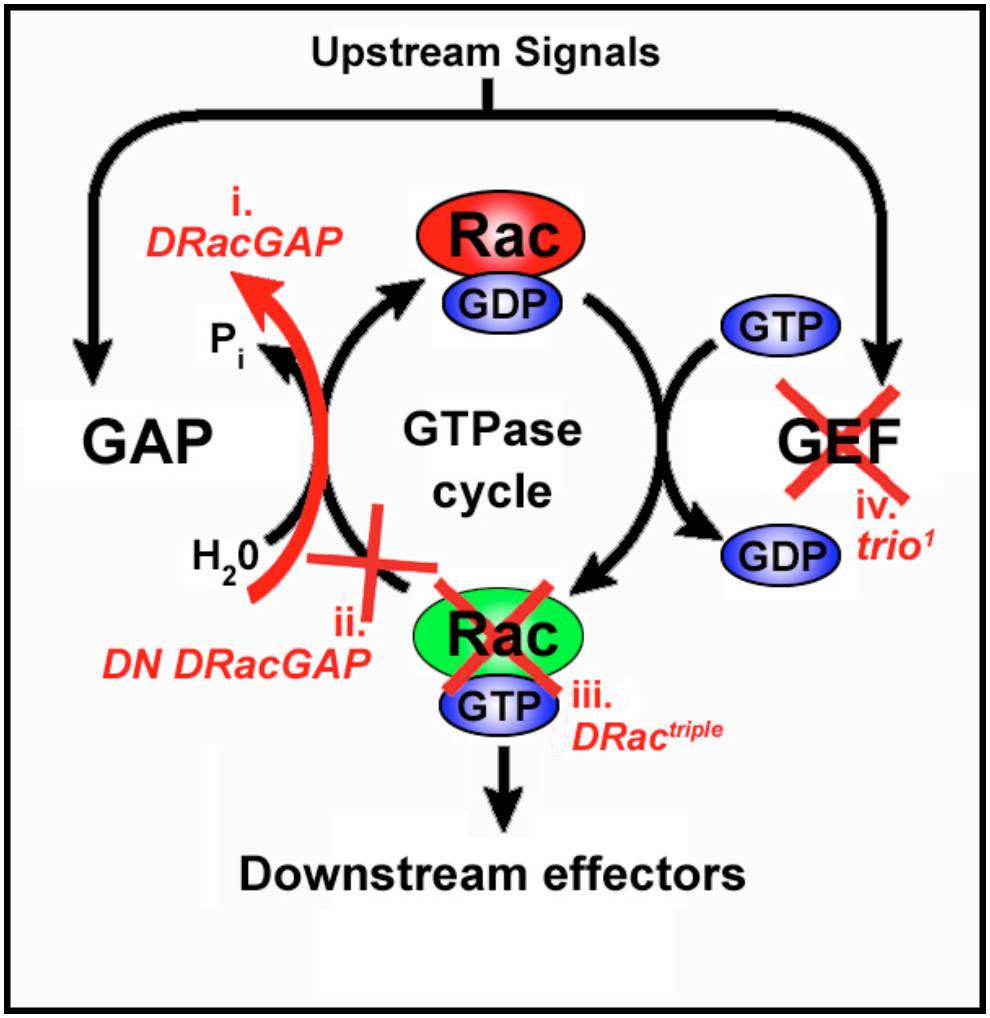
Upstream Signals
i.
DRacGAP
Rac
GDP
GTP
P
i
GAP
GTPase
cycle
GEF
iv.
trio1
H20
GDP
ii.
DN DRacGAP
Rac
GTP
iii.
DRactriple
Downstream effectors

Figure 3.40: Strategies undertaken to test for an intrinsic requirement of DRac1-function for synapse formation in *Drosophila* embryos. Different regulatory steps of the DRac1 functional pathway were knocked out. Through neuronal misexpression of a wildtype isoform of a GAP specific to DRac1 and DCdc42 (DRacGAP; Sotillos and Campuzano, 2000) it was tried to cause dominant mutant phenotypes by permanently activating the GTPase activity of DRac1, switching the GTPase off (i.). Neuronal misexpression of DN isoforms of the GAP specific to DRac1 and DCdc42 (DN DRacGAP) was undertaken in order to interfere with the deactivation of DRac1 (ii.), which was considered to result in phenotypes reminiscent of CA DRac1 misexpression defects. *DRac1* triple mutants deleting native *DRac* genes were analysed by A. Prokop (iii.). Finally, embryos were studied that were mutant for the GEF *trio*^{1} (iv.; carried out by A. Prokop), which is considered to cause phenotypes similar to loss of *DRac* defects, possibly because DRac1 cannot be switched into its active form (Hakeda-Suzuki et al., 2002).

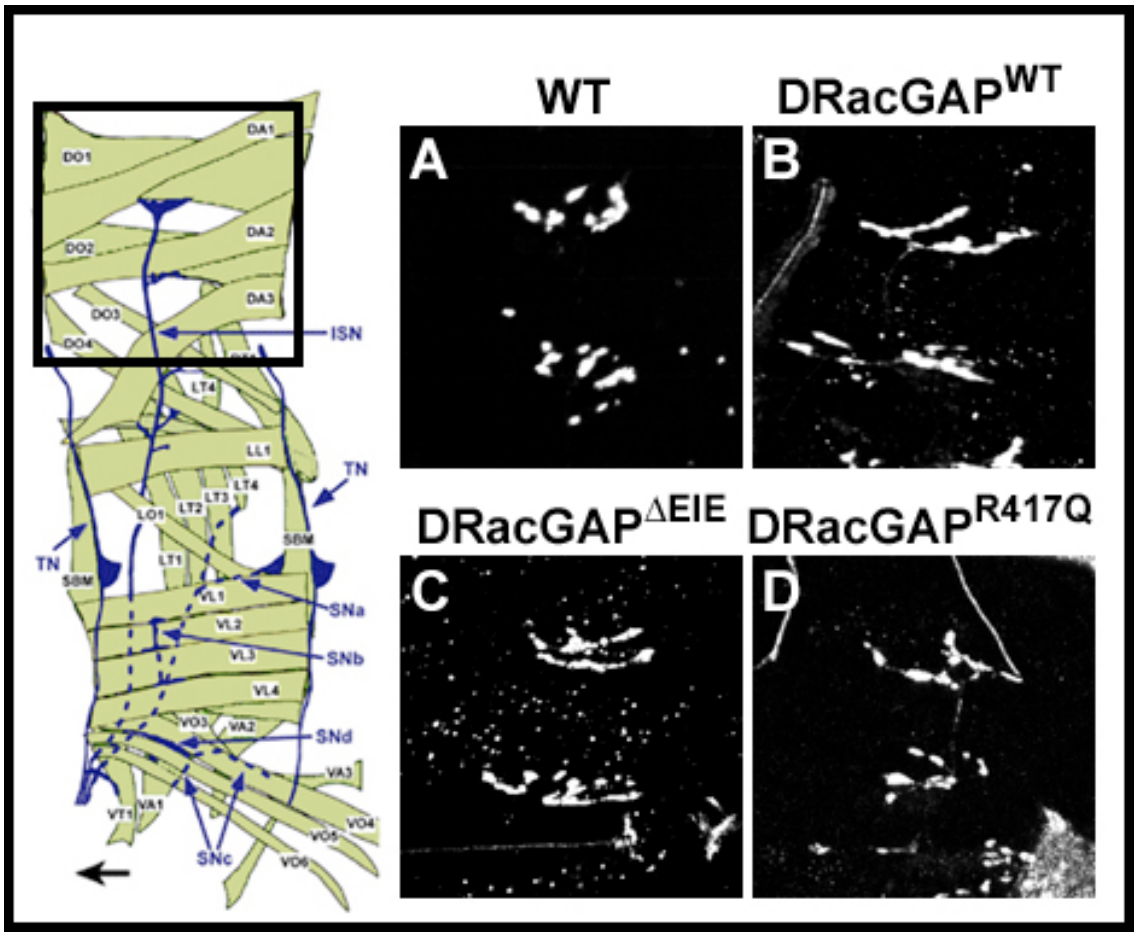
WT
DRacGAP^WT
A
B
DRacGAP^ΔEIE
DRacGAP^R417Q
C
D
DO1
DO2
DO3
DO4
DA1
DA2
DA3
ISN
LT4
LL1
TN
LT3
LO1
LT2
SBM
LT1
VL1
VL2
VL3
VL4
SNa
SNb
SNd
VO3
VA2
VA3
VT1
VA1
VO4
VO5
VO6
SNc

Figure 3.41: Misexpression study of wildtype and dominant mutant isoforms of DRac1GAP. Neuronal misexpression of the wildtype isoform of DRac1GAP (B) and of both DN isoforms DRac1GAP$^{\Delta EIE}$ (C) and DRac1GAP^{R417Q} (D), respectively, did not cause detectable phenotypes at the NMJ. Boutons were found to be wildtypic (compare wildtype control in A) in all cases studied as revealed by stainings with anti-Syt antibodies. No differences were further observed at the NMJ or for dendritic projections in the CNS in studies using antibodies specific to Syn, DLG and FasII (not shown). Hence it was not possible to show an intrinsic requirement for DRac1 during synapse formation at embryonic stage 17 using this approach. The cartoon to the left shows the area depicted in the confocal images. The black arrow points anterior.

3.6.1. Functions of Shot and activated Rho GTPases seem to converge on common factors

There are several scenarios, which could account for common phenotypes of Shot and activated Rho GTPases (Chapter 3.6.). First, Rho GTPases could act upstream of Shot regulating the localisation of Shot to specific compartments. Second, Rho GTPases could act on Shot, regulating its function. Third, Shot might localise activated Rho GTPases to specific neuronal compartments and thus coordinate their action. Fourth, Shot and Rho GTPases might bind to or converge on common effectors. As a first step, initiating the experimental series aiming to distinguish between such possibilities, the localisation of DCdc42 proteins in wildtype and *shot* mutant neurones was investigated by using GFP tagged versions of DCdc42 (the GFP-tagged wildtype version GFP-DCdc42^{WT} and the CA form GFP-DCdc42^{V12}, kindly provided by Akira Chiba). The tagged constructs were expressed using *eve^{RRK}-Gal4* (expression in the motor neurones aCC and RP2) as driver line. For increased signal intensity the GFP-tag was additionally labelled with anti-GFP antibody. As reported before by Akira Chiba and co-workers (personal communication), GFP-DCdc42^{WT} was found evenly distributed throughout the targeted motor neurones, i.e. in somata, dendrites and axons (Figure 3.42A). The misexpression of the GFP-tagged CA version of DCdc42 caused a reduction of central dendrites as observed for the non-tagged CA mutant isoform, indicating that the GFP-tag does not interfere with the functionality of the construct (Figure 3.42B). Interestingly, GFP-DCdc42^{V12} localisation was restricted to the somatodendritic area of targeted motor neurones, i.e. to the area where induced phenotypes (reduced dendrites) were observed. Such localisation could be explained through enhanced binding of CA DCdc42^{V12} to its somatodendritic effectors. Subsequently, both GFP-tagged DCdc42 isoforms where expressed using the same neuronal driver line (*eve^{RRK}-Gal4*) in *shot^{SF20}* mutant background (Chapter 2.1.4.1.). In *shot^{SF20}* mutant central nervous systems, both the wildtype- and CA isoforms of GFP-DCdc42 were found to be expressed at higher level than in wildtype background, a phenomenon that can not be explained so far. Therefore, the experiments were carried out by incubating the wildtype controls at 25°C whilst *shot^{SF20}* mutant embryos were kept at 18°C (temperature has an impact on Gal4-activity, Duffy, 2002). In *shot^{SF20}* mutant background GFP-DCdc42^{WT} was evenly distributed throughout the neurone as observed in wildtype background (Figure 3.42C). Similarly, GFP-DCdc42^{V12} was evenly distributed throughout the targeted motor neurone in *shot^{SF20}* mutant background (Figure 3.42D), which is in contrast to its somatodendritic restriction in wildtype background (Figure 3.42B). These

data suggest a scenario in which Shot localises the activated Rho GTPase DCdc42^{V12} either directly or indirectly, for example through the localisation of effectors to which DCdc42 binds in activated form. Although expression at 18°C was considerably lower than at 25°C, it can not be ruled out that the abolished compartmentalisation of CA DCdc42 in *shot*^{SF20} mutant embryos simply represents overspill due to higher protein levels. However, the interpretation of the data that Shot localises DCdc42 directly or indirectly would be consistent with the observation that mutant phenotypes of *shot* and the CA mutant isoform of the RhoGTPase are very similar.

Hence, similar to the results obtained from the study of DPxn localisation *in situ* (Chapter 3.5.1.) Shot was found to function potentially by localising regulatory elements to certain subcellular compartments. DPxn and Rho-like GTPases were identified as possible interactors of Shot. It was observed that GTPase gain-of-function mimics *shot* mutant phenotypes, while loss-of-function appears to mimic DPxn phenotypes, which again are likely to be related to Shot function (see Chapter 3.5.). These observations provide a basis for further analysis of mechanisms underlying synapse formation, and in particular of the genetic interactions between Shot, DPxn and the Rho-like GTPases in this developmental context.

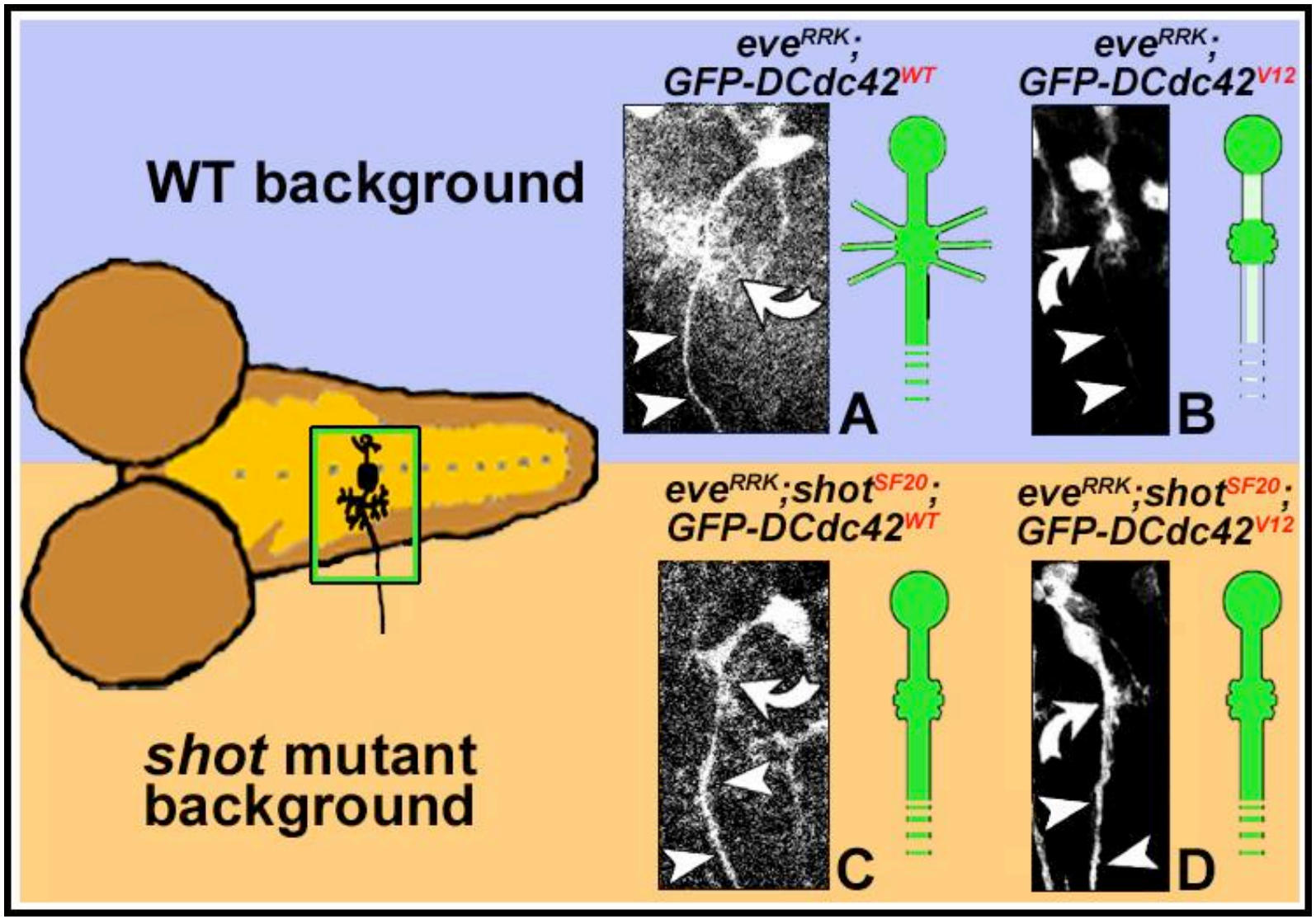
WT background
eve^RRK; GFP-DCdc42^WT
eve^RRK; GFP-DCdc42^V12
A
B
shot mutant background
eve^RRK;shot^SF20; GFP-DCdc42^WT
eve^RRK;shot^SF20; GFP-DCdc42^V12
C
D

Figure 3.42: The specific localisation of GFP-tagged CA DCdc42^{V12} in the somatodendritic area of motor neurones is impaired in *shot* mutant background. GFP-tagged wildtype (GFP-DCdc42^{WT}, A and C) and CA mutant (GFP-DCdc42^{V12}, B and D) isoforms of DCdc42, respectively, were misexpressed in motor neurones aCC and RP2 using the Gal4-driver line *eve^{RRK}*-Gal4. In wildtype background GFP-DCdc42^{WT} localised in cell bodies, axons (white arrowheads) and dendritic projections (white bents arrows; A). The misexpressed wildtype DCdc42 isoform did not cause any detectable structural defects in the central dendrites. In contrast, misexpression of GFP-tagged CA DCdc42^{V12} caused a reduction of dendritic projections (B). This confirms results of earlier misexpression studies with non-tagged CA DCdc42^{V12} isoforms (compare Figure 3.38B) and shows that the GFP-tag does not impair the functionality of the construct. Interestingly, GFP-tagged CA DCdc42^{V12} accumulates in the somatodendritic area. The specific localisation of CA DCdc42^{V12} might reflect site restricted distribution of DCdc42-GTPase-interacting partners. When misexpressing DCdc42^{WT} in *shot^{SF20}* mutant background using the same Gal4-driver-line, no change in the localisation of the construct was observed (C). The reduction of the dendritic projections is due to the *shot* mutation. The specific localisation of GFP-tagged CA DCdc42^{V12} was impaired in *shot^{SF20}* mutant background (D). GFP-DCdc42^{V12} was found evenly distributed throughout the motor neurones. Thus, the site restricted distribution of DCdc42 or DCdc42-interacting partners seems to be affected in *shot* mutants, suggesting Shot to potentially function by localising certain regulatory factors to specific cellular compartments. The cartoons to the right of each image summarise the localisation observed for the misexpressed construct (green). The cartoon to the left shows the area depicted in the confocal images. Anterior is to the left in all cases.

4. DISCUSSION

The formation of neuronal circuits during development is a stepwise process involving growth of neuronal processes into the right target areas, establishment of neuronal contacts with appropriate partner cells, and the differentiation of synapses at these contacts. Synapse formation involves consolidation and size adjustment of the cell junctional contact and the precisely aligned assembly of pre- and postsynaptic specialisations in appropriate quantities. Amongst the few mutations throughout animal kingdom disrupting synapse formation at the structural level are mutant alleles of *Drosophila shot*. More specifically, *shot* mutations affect late motoraxonal growth, shape acquisition of the presynaptic motor terminal at the NMJ, the assembly of presynaptic specialisations (active zones), and the formation of motorneuronal side branches in the CNS (Prokop et al., 1998b). In the work presented here, several approaches were undertaken to advance the understanding of Shot function in the context of synapse formation and to gain further insides into the molecular mechanisms underlying this developmental process. The results obtained and discussed in the following suggest the N-terminus of Shot to be essential for the formation of synaptic terminals and that Shot functions through diverse protein-protein interactions mediated by its different modular domains. As a result of a yeast two-hybrid screen *DPxn* was discovered to interact with the N-terminal Plakin domain of Shot. The interaction between DPxn and Shot was confirmed in independent experiments and it could be shown that the localisation of DPxn in muscle attachment cells is dependent on the presence of Shot. Furthermore, a function of DPxn at the NMJ was revealed upon removal of DPxn function via different genetic deletions or RNA interference. Thus, this study introduces DPxn as an interaction partner of Shot and as a new player of the genetic network underlying the formation of synaptic terminals in *Drosophila*. Additionally, in a genetic approach, a possible functional link between Shot and Rho-like GTPases was unravelled. These results provide the basis for further studies intending to describe a potential genetic interaction between Shot, DPxn and Rho-like GTPases, and additional yet unknown molecular mechanisms occurring during synapse formation.

4.1. The N-terminus of Shot is essential for the formation of synaptic terminals and its modular domains mediate different types of interactions

Shot belongs to the Spectraplakin family of proteins, sharing features with both the Spectrin and Plakin superfamilies (Röper et al., 2002). Spectrin members bind and crosslink Actin filaments and attach these to membrane receptors (Dubreuil and Grushko, 1998; Knust, 2000). Members of the Plakin superfamily connect adhesion receptors to intermediate filaments, but also crosslink different cytoskeletal elements (Ruhrberg and Watt, 1997). Spectraplakins have a series of five protein domains: 1. a choice of four N-termini, which may include the ABD (with two Calponin homologies), 2. a Plakin domain that appears to be present in all Spectraplakin isoforms, 3. a Plectin repeat containing segment, which may be at the C-terminus or within the protein, 4. a long rod composed of Spectrin repeats, and 5. a C-terminal interaction domain that contains two EF hands and a Gas2 domain (Gong et al., 2001; Gregory and Brown, 1998; Lee et al., 2000a; Leung et al., 1999; Okumura et al., 2002; Röper et al., 2002; Strumpf and Volk, 1998). The large size and modularity of Spectraplakins and the known functions of some of their domains suggest a multitude of possible interaction partners and, potentially, different sets of binding partners for different Spectraplakin isoforms. As shown previously, *shot* mutations affect neuromuscular terminals in the periphery and motor neuronal side branches in the CNS (Prokop et al., 1998b). Several findings strongly suggest, that mainly the N-terminus of Shot is required for the formation of such synaptic compartments: Only protein fractions containing N-terminal ABD and/or Plakin domains were localised at presynaptic sites upon targeted misexpression (Chapter 3.3., e.g. Figure 3.13). These findings were supported by the observations that only antibodies raised against the N-terminus of Shot can be detected at neuromuscular boutons (Chapter 3.4., Figure 3.22; Prokop et al., 1998b). Further support was obtained from the analysis of independently isolated *shot* mutant alleles (Chapter 3.1.). The mutant alleles $shot^{V104}$ and $shot^{V168}$, in which mutational events were previously reported to disrupt the C-terminus of Shot (Strumpf and Volk, 1998; $shot^{V168}$: T. Volk, personal communication), showed no obvious neuronal defects (Figures 3.1, 3.3 and 3.4). In contrast, mutant alleles $shot^{KakP2}$, $shot^{el3}$, $shot^{SF20}$, $shot^{HG25}$, $shot^{91K}$ and $shot^{3}$ had motor neuronal stall phenotypes at stage 16 and reduced NMJs at stage 17 to different degrees (Figure 3.10). The assumption that these neuronal phenotypes are caused by mutations affecting the N-terminus of Shot were

substantiated by information available for mutational events in *shot*^{kakP2}. In this allele, a P-element inserts in an intron 1917bps before the first exon encoding part of the first Calponin homology of the ABD (Gregory and Brown, 1998; Lee et al., 2000a; compare also Figure 1.3). The insertion is proposed to disrupt protein expression of the N-terminal region of the long isoforms of Shot (Lee et al., 2000a; see below). This information together with the neuronal phenotypes observed in this *shot* mutant allele (Figures 3.1, 3.2 and 3.10) argue in favour of a requirement of the N-terminus of Shot for neuronal growth and the formation of synaptic terminals.

In immunohistochemical experiments using antibodies specific to different regions of Shot, only partial overlap in the localisation of the different antibodies was observed (Figures 3.22 and 3.23). This suggests different Shot isoforms to be active in different cellular and developmental context. Indeed, multiple transcriptional start sites and alternative splicing throughout the *shot* gene generate protein isoforms predicted to differ in their Actin binding properties, rod domain length, and C-terminal domains (Gregory and Brown, 1998; Lee et al., 2000a; Röper et al., 2002; Strumpf and Volk, 1998). So far, four different N-terminal splice variants were identified (Lee et al., 2000a; Lee and Kolodziej, 2002b). Two isofoms (A and B) contain complete predicted ABDs, following unique sequences of 143 or 32 amino acids, respectively (see Figure 1.3). Isoform C contains a partial ABD, following a unique sequence of 210 amino acids, and isoform D contains no globular N-terminal domain. mRNAs of all isoforms are expressed in the epidermis at low levels and in muscle attachments at high levels. However, only mRNAs encoding the ABD containing isoforms A and B are expressed in the CNS and PNS, while mRNAs encoding isoforms C and D are not (Lee et al., 2000a). This difference in expression of ABD and non-ABD isoforms parallels the differences observed in the expression of neuronal Actin binding and epidermal non-Actin binding isoforms of the vertebrate homologues BPAG1 (Brown et al., 1995; Yang et al., 1996) and MACF1 (Gong et al., 2001; Karakesisoglou et al., 2000; Leung et al., 1999; Okuda et al., 1999), suggesting the specific requirements of the ABD within neuronal tissues to be conserved.

Evidence for a requirement of ABD activity in the context of axonal growth and synapse formation was provided by the analysis of Shot-antibody staining in the mutant allele *shot*^{kakP2} (Chapter 3.4.1., Figure 3.23). Anti-shot^{204} was still detected in *shot*^{kakP2}. The epitope used for production of anti-shot^{204} comprises amino acids 342 to 355 (Chapter 2.2.), a small region within the second Calponin homology of the ABD. Hence, anti-shot^{204} most likely binds to the Shot N-terminal isoforms A, B and C. In contrast, anti-Shot^{NB} was raised against

amino acids 2 to 341, including the first Calponin homology of the ABD. Therefore, this antibody should detect the Shot N-terminal isoforms A and B. However, anti-Shot^{NB} was reported to fail to stain *shot*^{kakP2} (Gregory and Brown, 1998). Both results together suggest that only N-terminal isoforms C (and D) are expressed in the *shot* mutant allele *shot*^{kakP2}. This was supported by observations made with the third Shot antibody, anti-shot^{Gas2}. Anti-shot^{Gas2} is specific for a C-terminal region of Shot and was postulated to bind all long isoforms of Shot, i.e. isoforms A to D (Lee et al., 2000a). In *shot*^{kakP2} anti-shot^{Gas2} was still detected in muscle attachment cells and scolopidial sensory neurones. However, anti-shot^{Gas2} failed to stain the CNS. Given that only Shot isoforms A and B are expressed in neuronal tissues (see above), the findings allow the conclusion that the P-element insertion in *shot*^{kakP2} results in the expression of only N-terminal isoforms C and D. Since *shot*^{kakP2} causes some phenotypes in the nervous system (see Chapter 3.1.), this would strongly indicate a requirement for a full-length ABD for the synaptogenic function of Shot.

The results from the misexpression study of distinct Shot domains implicate that the ABD and Plakin domain, but not the C-terminal Gas2 homology domain, are capable of driving localisation to neuromuscular terminals. However, the Plakin domain localised more specifically to presynaptic sites when expressed in conjunction with the ABD, suggesting the ABD to act possibly by targeting the Plakin domain to specific cellular compartments. This is in agreement with previous reports that proposed the ABD to be essential for the recruitment of Shot into the cytoplasmic faces of hemiadherens junctions (Subramanian et al., 2003). Such a compartmentalisation activity of the ABD could be mediated by interactions with the cytoskeletal element Actin, since interactions between Actin and the Calponin homologies of Shot ABD have been shown *in vivo* and proved to be essential for axon extension (Lee and Kolodziej, 2002b). Alternatively, the ABD could interact with other proteins, as indicated by the detection of different potential interaction candidates (amongst which Actin was not found) through the yeast two-hybrid analysis performed in this study (Chapter 3.5., Table 3.3). In vertebrates, part of the ABDs of BPAG1 and Plectin, a member of the Plakin family of proteins, mediate homo- and heterodimerisation, and the ABD of Plectin additionally binds to the cytoplasmic tail of β4-Integrin (Geerts et al., 1999). When the ABD alone of MACF1 is expressed in mouse keratinocytes, it associates with Actin, but a longer isoform of MACF1 containing this ABD associates with microtubules rather than Actin (Karakesisoglou et al., 2000).

Besides the ABD, the Plakin domain is found within the N-terminus of Shot. In the yeast two-hybrid screen for Shot interactors several independent interaction candidates were

obtained (Chapter 3.5., Table 3.3). The candidate received with highest frequency was the LIM-domain protein *Drosophila* Paxillin (DPxn; see also Chapter 4.2.). The interaction between DPxn and the Shot Plakin domain was confirmed (Chapters 3.5.1. and 7.1., Figures 3.27 and 7.1) and its requirement for the formation of synaptic terminals could be shown (Chapter 3.5.2.). Thus, interactions mediated by the Plakin domain appear essential for the function of Shot at the NMJ as well. This was further indicated by the localisation of misexpressed Plakin domains at NMJs (Figures 3.13 and 3.15). As mentioned before, the Plakin domain, which is found in all isoforms, shared localisation with both the ABD and the C-terminal domain, implying that the domain interacts with diverse targets depending on the cellular and developmental context. The Plakin domain of other proteins of the Plakin family of proteins, such as Plectin, Desmoplakin, Envoplakin, Periplakin and Epiplakin (Ruhrberg and Watt, 1997), were proposed to mediate direct or indirect binding to adhesion receptors. For example, the Plakin domain of BPAG1e binds directly to the transmembrane protein BPAG2 (Hopkinson and Jones, 2000) and that of Desmoplakin binds to Plakoglobin and Plakophilin, proteins that bind to desmosomal Cadherins (Smith and Fuchs, 1998). Hence, the Plakin domain appears to be responsible for different kinds of molecular interactions, some of which are strongly suggested to be required during growth of neuronal processes in *Drosophila*.

Multiple protein-protein interactions are also likely to take place at the C-terminal domain of Shot. A microtubule binding site consisting of a region including the Gas2 domain was shown to bind directly to α-Tubulin in a yeast two-hybrid analysis (Lee and Kolodziej, 2002b), and proposed to be required for Shot function during sensory and motor axon extension (Lee and Kolodziej, 2002b). Moreover, expression of proteins containing this microtubule binding site and the ABD in one molecule rescued axonal growth defects, whereas simultaneous expression of the two separate protein domains did not, indicating that the C-terminal Microtubule binding site is required in the same molecule together with the ABD (Lee and Kolodziej, 2002b). These results suggest a role of Shot in linking Actin to Microtubules, because this interaction is essential for structuring the axonal cytoskeleton (Houseweart and Cleveland, 1999; Kodama et al., 2003). However, it is quite possible that the Gas2 domain binds to other proteins, as does the ABD or Plakin domain (see above). For example, the C-terminal domain containing the EF hands and the GAS2 domains was proposed to associate with EB1 (Subramanian et al., 2003), an evolutionarily conserved protein that binds the plus ends of growing microtubules (Morrison et al., 2002; Tirnauer and Bierer, 2000). Furthermore, the Gas2 protein (growth arrest specific protein 2) was shown to

associate with the Actin cytoskeleton in cultured cells undergoing apoptosis (Brancolini et al., 1995). Thus, the C-terminus of Shot might mediate diverse protein-protein interactions. However an essential role for the formation of synaptic terminals could not be shown by the different experimental approaches carried out in this study.

The different protein-protein interactions carried out by distinct Shot isoforms may reflect cell- and stage-specific differences in Shot function. For example, in the context of muscle attachment/tendon cells, cytoskeletal cross-linking abilities of Shot confer mechanical resistance to pulling muscles, but also the localisation of the neuregulin-like growth factor Vein is altered in *shot* mutant tendon cells (Strumpf and Volk, 1998; Yarnitzky et al., 1997). This phenotype is proposed to be caused by disruption of Shot dependent clustering of a subset of membrane receptors and cytoskeletal binding proteins at sites of cell-cell contact. On the other hand, in the context of neurons, growth seems to depend on Shot-dependent crosslinking of cytoskeletal filaments or the localisation/regulation of EB1, a plus-end tracking protein of microtubules (Morrison et al., 2002; Subramanian et al., 2003; Tirnauer and Bierer, 2000). Furthermore, neuronal Shot seems to link the cytoskeleton to plasma membrane proteins, as suggested by the phenotype of mislocalised FasII in motor neurones of *shot* mutant alleles (Figure 3.9). This function of Shot may be similar to that underlying Vein localisation in tendon cells (see above) and could be compared to the activity of Spectrins and Dystrophin in organising the interaction between the cortical cytoskeleton and the plasma membrane proteins to generate cortical subdomains (Hopkinson and Jones, 2000). Similar functions have also been proposed for other members of the Spectrin and Plakin families, such as α-Actinin, Plectin and Desmoplakin (Fontao et al., 2001; Fyrberg et al., 1990; Hatzfeld, 1999; Steinbock and Wiche, 1999). Further function of Shot could be the scaffolding of signalling proteins to sites of cytoskeletal activity, as observed for the recruitment of nNOS mediated by Syntrophin-Dystrophin interaction (Brenman et al., 1996; Hashida-Okumura et al., 1999), a PDZ-LIM protein by α-Actinin (Vallenius et al., 2000) and the LAP (Leucine rich repeats and PDZ domain) family protein ERBIN by BPAG1 (Favre et al., 2001).

4.2. DPxn interacts with the Shot Plakin domain and is potentially required for the formation of synaptic terminals

In this study, the protein-protein interactions mediated by the distinct N-terminal Shot domains were addressed using a yeast two-hybrid screen. For both, the ABD and the Plakin domain several independent potential interaction partners were identified (see Chapters 3.5. and 4.1.). Several yeast-clones retrieved from the screen suggested a direct physical interaction of DPxn with the Shot Plakin domain. This was confirmed by biochemical data obtained from collaborating laboratories (Chapter 7.1.) and by data presented here, showing co-localisation of DPxn and Shot in diverse tissues (Figures 3.25-3.28) and suggesting that the DPxn association with the basal muscle tendon junction is Shot-dependent (Figure 3.27).

In vertebrates, Paxillin is expressed in cardiac muscles, skeletal muscles, liver and brain (Turner et al., 1991). Paxillin further localises at the rat diaphragm NMJ at the postsynaptic site, in the AChR-poor deep regions of the junctional folds (Turner et al., 1991). Other reports describe Paxillin to localise in astroglia of brain tracts in rat brains following lesion (Kalman and Szabo, 2001). In neuronal cell cultures a role for Paxillin has been demonstrated (Ivankovic-Dikic et al., 2000), and it was shown that phosphorylation of Paxillin by the protein kinase p38MAPK is involved in nerve growth-factor (NGF)-induced neurite extension (Huang et al., 2004). So far, no report is available on the localisation and function of DPxn in the nervous system of *Drosophila*.

In the work presented here, DPxn was shown to localise specifically to motorneuronal projections and synaptic terminals (Figures 3.25 and 3.28). Moreover, a requirement of DPxn for the formation of synaptic terminals is suggested by mutant phenotypes caused by *DPxn* deficiencies *Df(2L)VA23*, *Df(2L)TW158*, and *Df(2L)E55* (Chapter 3.5.2.), which can be mimicked with *DPxn-RNAi* expression (Figure 3.30). Additionally, the *DPxn-RNAi* experiments propose a further role for DPxn in the structural differentiation of larval NMJs (Figure 3.33). DPxn is hereby introduced as a new player of the genetic network underlying the formation of synaptic terminals in *Drosophila.* At the same time, the results prove the yeast two-hybrid screen performed to be successful, attributing the remaining interaction candidates of Shot high potential in contributing to the understanding of the machinery underlying synapse formation and the comprehension of Shot function during this developmental process.

Previously, the *DPxn gene* was identified in two independent approaches and shown to generate two transcripts coding for a protein with 57% overall identity to human Paxillin (DPxn, Wheeler and Hynes, 2001; Yagi et al., 2001) and a smaller isoform comprising a fraction of the C-terminal domains, partly encoded by its own specific exon (PDLP for *P*axillin *D*erived *L*IM-only *P*rotein, Yagi et al., 2001). DPxn has five LD motifs and four LIM domains (Figure 7.2). Three of the four tyrosine phosphorylation-sites of human Paxillin are conserved at comparable positions, only the tyrosine residue at position 31 is missing. When expressed in mammalian cells, DPxn localises to focal adhesions and is tyrosine-phosphorylated during cell adhesion. Although human Paxillin consists of three isoforms generated by alternative splicing (the alpha-, beta- and gamma isoforms; Mazaki et al., 1998), *Drosophila* only encodes a Paxillin homologue to the alpha isoform. Interestingly, the DPxn expression-profile appears to follow that of Shot, with highest levels detected at late embryonic stages and throughout larval life, i.e. at developmental stages where synapses form *de novo* or experience further structural changes (FlyBase, 1999).

Based on information available for vertebrate Paxillin, DPxn is a type of protein, which represents an ideal candidate for the interaction with Shot during NMJ formation. Human Paxillin is a 68kDa protein, which was identified as a component of sites of cell-substratum-contact (focal adhesions) in a variety of cell types grown in tissue culture (Turner et al., 1990). Paxillin has been suggested to function as a scaffolding or adaptor protein downstream of Integrins or growth factors, allowing the recruitment of various structural and signalling molecules to focal adhesions (for review see Turner, 2000a; Turner, 2000b). The LIM domains are thought to target the protein to focal contacts (Brown et al., 1996), whereas the LD motifs mediate binding to structural proteins that can bind to cytoskeletal elements such as Vinculin (Salgia et al., 1995; Turner and Miller, 1994) or Actopaxin (Nikolopoulos and Turner, 2000), or to mediators of signalling by Integrins and growth factors such as the Focal Adhesion Kinase (Fak; Hildebrand et al., 1995; Turner, 1994) or the C-terminal Src-kinase Csk (Sabe et al., 1994). The LD motifs appear to mediate also the interaction between DPxn and Shot, since it was shown here, that the association of DPxn with Shot involves the LD-motifs bearing N-terminus of DPxn (amino acids 1-347; see also Table 7.1). Multiple interactions with many proteins suggest Paxillin to play an essential role in many different signalling pathways that determine cell polarity, cell migration and cytoskeletal organisation (Huang et al., 2003; Nakamura et al., 2000; Petit et al., 2000; Yano et al., 2000). For example, Paxillin recruits the p21 GTPase activated kinase (Pak) to specific subcellular localisations either directly (Hashimoto et al., 2001) or through interactions with the ARF-GAP protein

Paxillin kinase linker p95PKL and the GEF PIX (a GEF to Rac1 and Cdc42; Brown et al., 2002; Daniels and Bokoch, 1999). Furthermore, Paxillin might facilitate the crosstalk between cytoskeletal elements directly as it was shown that besides binding to many Actin binding molecules (see above) the Paxillin LIM-domain interacts directly with α-Tubulin (Brown and Turner, 2002; Herreros et al., 2000). In addition, Paxillin may be linked to membrane vesicle trafficking through its association with Clathrin (Turner et al., 1999). The majority of studies on Paxillin protein interactions and function were carried out in cell culture experiments and results were found to be partially contradictory, depending on the cell culture system used (Brown et al., 2002; Turner, 2000a). Yet, Paxillin has the ability to bind to many structural proteins and enzymatic effectors of Integrin and growth factor signalling, suggesting DPxn to direct the organisation of the cytoskeleton in response to extracellular cues. Given the possibility that Shot might function by promoting growth, and that this activity is subject to changes of the extracellular environment, DPxn represents an optimal interactor of Shot for coordinating the structural differentiation of synaptic terminals.

There are several possibilities which could account for a functional link between Shot and DPxn:

1. Shot might be required at the NMJ for the localisation of DPxn. In muscle attachment cells the correct localisation of DPxn was shown to depend on the presence of Shot (Figure 3.27). At the NMJ, the multiple modular domains of Shot could allow the simultaneous binding of DPxn and several of its interaction partners at specific sites, thereby facilitating physical interactions and the transduction of information between them, for example through phosphorylation.

2. The interaction between Shot and DPxn influences the activity of DPxn. The association with Shot could for example interfere with the phosphorylation of DPxn through specific kinases in response to external cues, thereby inhibiting the transduction of information required for the regulation of the cytoskeleton arrangement.

3. DPxn interacts with Shot in order to regulate its activity. For example, DPxn could pass on signals from the cell surface through binding to Shot which could in turn result in the inactivation of the cytoskeleton crosslinking activity of Shot or suppress its interaction with the microtubule plus-end tracking molecule EB1 (Lee and Kolodziej, 2002b; Morrison et al., 2002; Röper et al., 2002; Subramanian et al., 2003; Chapter 3.2.). This way DPxn would act as a negative regulator of neuronal growth.

For several reasons I think the third possibility to be the most realistic one. First of all, the roles of Shot and MACF-1 as direct linkers and regulators of the cytoskeleton and of

Paxillin as signal-transducing mediator/modifier of protein interactions are well established (reviewed in Röper et al., 2002; Turner, 2000b; see above). Furthermore, the different phenotypes in *shot* and *DPxn* mutant embryos are in agreement with the third possibility: *shot* mutant terminals are reduced, lacking synaptic proteins (which can appear mislocalised in motor axons; Figures 3.3 and 3.4), whereas *DPxn* mutant terminals are enlarged, leaving synaptic proteins unaffected (Figures 3.30 and 3.33). The extended DPxn mutant phenotype depends on the presence of Shot. This is indicated by the observation that *DPxn;shot* double mutant embryos show a *shot* mutant phenotype (recent unpublished results by A. Prokop). Therefore, the *DPxn* mutant phenotype at the NMJ suggests DPxn to downregulate (cytoskeletal) processes mediated by Shot. Based on this scenario we would expect motor neurones overexpressing DPxn to show *shot* mutant NMJ phenotypes. Unfortunately, this was not observed (Figure 3.31), though the failed attempt to rescue the mutant phenotype in *Df(2L)VA23* gives reason to believe that the DPxn construct used in the experiments was not absolutely functional (Figure 3.32).

It is tempting to speculate that the signal for DPxn to inhibit Shot cytoskeleton crosslinking activity could be mediated by *PS-Integrins*. Many reports are available that describe Integrin signalling through Paxillin (see above; Turner, 2000a). In *Drosophila* it was shown that levels of *PS-Integrins* at NMJs regulate the degree of morphological growth and bouton differentiation (Beumer et al., 1999). Specifically, loss-of-function mutations of *PS-Integrins* cause structural overgrowth with increased number of boutons and branches in third instar larvae (Beumer et al., 2002), a phenotype which might share some similarity with that observed in third instar larvae with reduced DPxn expression. More detailed studies of the structural defects in *PS-Integrins* mutant NMJs will be required to evaluate a potential link between PS-Integrins, DPxn and Shot activity. It should be noted, that the interaction between DPxn and Shot could have different consequences depending on the developmental and cellular context. For example, Shot acts by recruiting DPxn in muscle attachment cells, while the interaction in motor neurones influences Shot activity.

It cannot be ruled out that DPxn carries out further functions which superimpose its regulational role in inhibiting Shot mediated terminal growth. For example, the interaction of DPxn with Vinculin could additionally contribute to the stabilisation of the axonal or terminal region, through manifestation of the Actin network mediated by Vinculin activity (Brandt, 1998; Polonchuk et al., 2000). The investigation of such possible interactions is promising to unravel further mechanisms required for the formation of synaptic terminals.

4.3. Genetic interaction between Shot, Rho-like GTPases and DPxn?

In the work presented here, a direct role of the small GTPases DRac1 and DCdc42 in the formation of motorneuronal synaptic terminals was revealed in the genetic approach carried out to uncover molecular partners of Shot (Chapter 3.6.). In particular, upregulation of DRac1 through misexpression of CA DRac1^{V12} mimicked basically all known *shot* mutant phenotypes (Chapters 3.6. and 7.2., Figure 3.36). Additionally, a functional link between Shot and the small GTPases was indicated by the impaired dendritic localisation of misexpressed GFP-tagged versions of CA DCdc42^{V12} in *shot* mutant background (Chapter 3.6.1., Figure 3.42). An intrinsic function of the small GTPases during formation of synaptic terminals is suggested by impaired morphology of motorneuronal terminals in *DRac* loss of function mutants (Chapter 7.3.) and preliminary results of ongoing misexpression experiments with the DN DRac1^{N17} isoform (N. Sanchez-Soriano, pers. communication). Surprisingly, these morphological changes, enlarged neuromuscular terminals with filopodia-like protrusions, are reminiscent of defects observed in *DPxn* mutant embryos, suggesting a potential genetical link between functions of Shot, the small GTPases, and DPxn.

The *shot* mutant phenotype affects neuronal growth and synaptic differentiation alike (Chapter 3.1.; Prokop et al., 1998b). Each of these processes requires dynamic remodelling of the Actin cytoskeleton (Brandt, 2001). The involvement of Shot in the organisation of the Actin network is suggested by its ability to interact with Actin *in vivo* (Lee and Kolodziej, 2002b; see also Chapter 4.1.), where the ABD of Shot is essential for motor and sensory axon extension (Lee and Kolodziej, 2002b) and formation of synaptic terminals (this work). Potential cooperative functions of Rho GTPases and Shot have been reported in processes required for tracheal tube formation (Lee and Kolodziej, 2002a). The Rho-like GTPases RhoA, Rac and Cdc42 are involved in the regulation of the Actin cytoskeleton to control changes in cell shape (Aspenström, 1999b; Etienne-Manneville and Hall, 2002; Hall, 1998; Luo, 2000; Ridley and Hall, 1992; Ridley et al., 1992). Moreover, DRac1 has been implicated in axon growth and guidance by the use of mutant isoforms DRac1 (Kaufmann et al., 1998; Luo et al., 1994) as well as *DRac1* loss-of-function analysis (Hakeda-Suzuki et al., 2002; Ng et al., 2002). The analysis of a neuronal GEF, Still life, suggested an involvement of Rho-like GTPases in the process of synapse formation (Sone, 1997). This was supported by

misexpression studies of mutant isoforms of DRac1 in the *Drosophila* giant fibre system (Allen et al., 2000), revealing that upregulation of DRac1 cause defective synapse formation, whereas downregulation of DRac1 resulted in overgrowth and the production of extra branches. However, the giant fibres represent a pair of large visually responsive interneurones, and the mechanisms underlying synapse formation in CNS seem to differ from those at NMJs and are independent from Shot function (Löhr et al., 2002).

On the basis of the work presented here and of other published results, different modes of interaction can be hypothesised: The mislocalisation of CA DCdc42^{V12} in *shot* mutant background suggests a possible functional link to be a Shot mediated localisation of the Rho-like GTPases either directly or indirectly, through recruitment of factors responsive or influential on GTPase activity. The latter case would be in agreement with previous reports that proposed the activation of GTPase regulatory elements to depend on their subcellular localisation (Sotillos and Campuzano, 2000; Van Aelst and D'Souza-Schorey, 1997). The localisation of different GTPase activators to certain cellular compartments in different developmental processes is required the more so as Rho-like GTPases act in multiple aspects of development, such as axon growth, guidance and branching (Hakeda-Suzuki et al., 2002; Ng et al., 2002). Thus, Shot mediated interactions could be involved in the differential activation of Rho-like GTPase signalling pathways.

Alternatively, signalling pathways that involve the activity of Rho-like GTPases could be required for the regulation of Shot function or its localisation. Rho-like GTPases link receptor stimulation to activation of cytosolic protein kinase cascades, which in turn orchestrate events, such as the organisation of the cytoskeleton (Bishop and Hall, 2000; Bourne et al., 1990; Hall, 1998). Shot could well be positioned downstream of such signalling cascades: Thus, one explanation for the almost complete phenocopy of *shot* mutant neuronal phenotypes through expression of CA DRac1^{V12} can be explained by the recent finding that GFP-tagged Shot is severely mislocalised in CA DRac1^{V12} mutant background (recent results by Mohiddin Lone; pers. communication). Of course, the CA DRac1^{V12} mutant condition is expected to express non-physiologically high levels of DRac1 activity and cause artificial dominant phenotypes. However, it would also be expected that the milder activity levels of intrinsic DRac1 would in principle carry out the same action and downregulate Shot activity during natural neuronal growth events, e.g. by suppressing its local interactions with proteins of the cytoskeleton or EB1.

Hence, Rho-like GTPases could act upstream or downstream of Shot, giving reason to assume a possibility of a hierarchical alignment of DRac, Shot and DCdc42 activity: DRac

could be required for the localisation or regulation of Shot function, which in turn influences the localisation of DCdc42 activity. This could be tested further by analysing the localisation of Shot and DCdc42 in motor neurones with up- or downregulated DRac levels.

If DRac acts upstream of Shot it could influence Shot for example through interfering with its cytoskeleton crosslinking activity by reorganising the Actin-filament network or through the coordination of other regulatory proteins. One such protein could be DPxn. *DPxn* mutant embryos display similar NMJ defects as do *DRac* loss-of-function mutant embryos or embryos expressing DN DRac isoforms. In the literature many reports are available that discuss potential involvements of both Rac-GTPase and Paxillin during particular developmental events, which could indicate functional links between the Rho-like GTPases, DPxn and Shot during the formation of synaptic terminals. For example, a genetical interaction between DPxn and Rho-GTPases has recently been suggested for the *Drosophila* eye system (Chen et al., 2001). Specifically, DPxn was found to negatively regulate the Rho pathway while positively regulating the Rac pathway. In vertebrate systems, several signalling pathways have been reported to converge on Rac and Paxillin: Rac has been shown to activate the c-Jun amino-terminal kinase (JNK; Minden et al., 1995), which in turn phosphorylates Paxillin to regulate cell adhesion and movement (Huang et al., 2003). An upstream kinase of JNK, the MAP kinase/ERK kinase kinase 1, is associated with Rac and is crucial to cell movement (Fanger et al., 1997a; Fanger et al., 1997b; Xia et al., 2000). Fak, which is required for cell movement (Ilic et al., 1995), and associates with Paxillin (Turner, 1994), has been shown to transmit Integrin stimulated signals to JNK via Ras/Rac1/Pak1/MAPK Kinase 4 pathway (Almeida et al., 2000; Oktay et al., 1999). As mentioned above (Chapter 4.2.) Paxillin binds p95PKL, which is proposed to function as a kinase linker connecting Paxillin to Pak (Turner et al., 1999). Pak binds to and is activated by Rac and Cdc42 (Aspenström, 1999a). GTP-activated Pak modifies the Actin cytoskeleton by a complex mechanism involving the activation of proximal regulators of Actin assembly such as LIM kinase (Dan et al., 2001). Paxillin might be crucial in the correct positioning of Pak at the plasma membrane, thereby facilitating its normal signalling to the Actin cytoskeleton (Brown et al., 2002). Thus, it is possible that these pathways all exert their influence on the synaptic activity of Shot through its connection with DPxn and the Rho-like GTPases DRac and DCdc42. Therefore, the results presented here build an essential platform for further analysis of mechanisms underlying synapse formation.

4.4. Shot function during synaptogenesis: Conclusions and future prospects

From my results it has become very clear that Shot, like other Spectraplakins, makes modular use of its different domains in different developmental contexts. To elucidate such interactions during the formation of synaptic terminals, DRac1, DCdc42, DPxn and another 12 candidate genes have been pinpointed here. This provides a sound basis for further investigations addressing the molecular details of the machinery underlying NMJ formation and differentiation.

The detailed analysis of the first selected candidate gene, DPxn, demonstrated that the performed yeast two-hybrid screen turned out to be successful. Therefore, the obtained candidate genes have great potential to provide further essential insights into the function of Shot at the forming synaptic terminal (i.e. what types of proteins are preferentially recruited by Shot at the NMJ). Future work will therefore focus on obtaining a selection of the most interesting among the remaining 12 candidate genes capitalising on *Drosophila* genetics and using potential synaptic phenotypes as read out. Furthermore, in order to gain insights into molecular details of these genes, work very similar to that shown here for DPxn can be carried out. In addition, continued data mining for potential homologues or other kind of updated information needs to be completed. The function of the candidate genes can further be addressed by describing their temporal and spatial expression patterns at the RNA and protein levels and by screening cDNA libraries to find out about potential splice versions/isoforms. Detailed genetic and microscopical analyses of their synaptic phenotypes can be carried out to evaluate their potential interaction with Shot.

A considerable list of signalling pathways act through or are recruited by Paxillin (Turner, 1998) and would be further candidates involved in NMJ formation. The potential regulatory role of DPxn on Shot could be tested by analysing the effect of mutations disrupting specific signalling molecules on the formation of synaptic terminals. For example NMJ morphology could be addressed in *PS-Integrin* mutants at stage 17. Not only does the *Integrin*-signalling in vertebrates involve Paxillin (Turner, 2000a), also mutations that strongly affect *PS-Integrin*-expression were reported to cause overgrowth of NMJs in third instar larvae (Beumer et al., 2002), a phenotype similar to that observed in *DPxn*-mutant larvae. JNK (Huang et al., 2003), Fak (Medley et al., 2003; Murakami et al., 1999) and the growth-factor stimulated Receptor Tyrosine Kinase (RTK; Voas and Rebay, 2004) are further

candidates for this approach. Genetic recombinations to create double or triple mutant animals for Shot, DPxn, Rho-like GTPases or molecules of the signalling pathways should allow the determination of the hierarchical arrangement of the involved factors.

Finally it will be of interest to advance the analysis of the diverse *shot* mutant alleles, particularly by immunohistochemical analysis using the available anti-Shot antibodies. This could be further complemented by the application of RNA-*in-situ* probes specific for certain isoforms or domains of Shot or by expressing rescue constructs bearing certain Shot domains in different *shot* mutant alleles. Together with the phenotype description, this approach should help to strengthen the working hypothesis, that the N-terminus of Shot is required for the formation of synaptic terminals.

5. SUMMARY

Functional neuronal networks require the appropriate establishment of synapses between neurons and their target cells. An essential gene in this context is Shot, a cytoskeletal interacting factor of the Spectraplakin family of proteins, which is required for the differentiation of presynaptic neuromuscular terminals and postsynaptic sidebranches of motor neurones in the CNS (Prokop et al., 1998, J. Cell Biol., 143: 1283)

This study investigates the function of the Spektraplakin protein Shot during the structural differentiation of synapses in *D. melanogaster* using different approaches: Through a comparative study of different *shot* mutant alleles it was tested whether the distinct modular domains of Shot are responsible for different kinds of molecular interactions. Because Shot is proposed to have an Actin-Microtubule crosslinking activity the comparative study was extended to studies of the organisation of cytoskeletal components in growth cones of different *shot* mutant alleles. In order to address the protein domains required for the formation of synaptic terminals different Shot domains were misexpressed in neuronal tissues using the UAS/Gal4-system. This approach revealed that specifically the N-terminal ABD and the Plakin domain of Shot are targeted to synapses, potentially interacting with proteins at that location. Based on these results the ABD and Plakin domains were used as baits in yeast-two hybrid screens in order to uncover interaction partners. One of the candidate proteins obtained is the small LIM-domain protein Paxillin (DPxn). The interaction of DPxn with Shot was confirmed via co-immunoprecipitation studies. Furthermore, co-localisation of DPxn with Shot *in vivo* at tendon cells and NMJs could be demonstrated. In tendon cells, DPxn and Shot co-localise exclusively on the basal side, and this localisation of DPxn is affected in the absence of Shot. A function of DPxn at the NMJ was shown upon removal of DPxn function via different genetic deletions or RNA interference. Both strategies consistently cause structural aberrations of motorneuronal terminals. Thus, this study introduces DPxn as an interaction partner of Shot and as a new player of the genetic network underlying the formation of synaptic terminals in *Drosophila*. Furthermore, in an alternative approach to unravel potential interaction partners of Shot, a possible functional link between Shot and the Rho-like GTPases was uncovered. These results provide a platform for further investigations addressing a potential genetic interaction between Shot, DPxn and Rho-like GTPases, and additional yet unknown molecular mechanisms occurring during synapse formation.

6. APPENDIX I

6.1. Chemicals

If not stated differently, chemicals used in the course of this work were purchased from Roth, Karlsruhe, Germany. Chemicals not mentioned elsewhere are: Acetone (VWR, Darmstadt, Germany), Acid-washed glass beads (425-600µm; Sigma, Osterode, Germany), Agarose (GENterprise, Mainz, Germany), Glycerol (50% and 70% in autoclaved PBS or H_2O; Sigma, Osterode, Germany), nail polish, Vectashield Mounting Medium H-1000 (Vectashield, Vector Laboratories, Burlingame, USA).

6.2. Kit-systems

GenElute Plasmid **Midiprep** Kit (Sigma, Osterode, Germany)

QIAquick **Gel extraction** Kit (Qiagen, Hilden, Germany)

QIAprep Spin **mini prep** Kit (Qiagen, Hilden, Germany)

TOPO TA Cloning Kit (Invitrogen, Carlsbad, USA)

TripleMaster **PCR** System (Eppendorf, Hamburg, Germany)

6.3. Enzymes and buffers

6.3.1. Restriction Enzymes

Restriction Enzymes:	**Restriction Enzyme Buffer**
BglII (MBI Fermentas, St. Leon-Rot, Germany)	Y^+Tango buffer
EcoRI (MBI Fermentas)	EcoRI or 2x Y^+Tango buffer
EcoRV (MBI Fermentas)	R^+Tango buffer
NdeI (MBI Fermentas)	R^+Tango buffer
SalI (MBI Fermentas)	O^+Tango buffer
SfiI (New England Biolabs, Frankfurt, Germany)	NEB buffer 2
XhoI (MBI Fermentas)	O^+Tango or 2x Y^+Tango buffer
XmaI (New England Biolabs)	NEB buffer 4

6.3.2. Other Enzymes

PCRs were run with TripleMaster Enzyme Mix containing 5U/µl *Taq* **Polymerase** (Eppendorf, Hamburg, Germany). Buffer used was 10x High Fidelity Buffer with Mg^{2+} (Eppendorf, Hamburg, Germany)

1mg/ml **RNase** (Boehringer, Ingelheim, Germany) was used to prevent contamination of the DNA plasmid preparations with RNAs

6.4. Equipment

Accurate scale Mettler PM4600 Delta Range (Mettler Instruments, Giessen, Germany)

Agarose Gel Unit Hoefer HE33 (VWR, Darmstadt, Germany)

CCD video camera Sony 3 CCD colour (Olympus, Hamburg, Germany)

Centrifuge Eppendorf 5417R (Eppendorf, Hamburg, Germany)

Centrifuge Eppendorf 5410 (Eppendorf, Hamburg, Germany)

Centrifuge Sigma 3K20 (Sigma, Osterode, Germany)

Camera Zeiss AxioCam (Zeiss, Jena, Germany)

Confocal Microscope Leica TCS (Leica, Bensheim, Germany)

Dissecting Microscope Leica MZ FLIII (Leica, Bensheim, Germany)

Dissecting Microscope Olympus SZX-ZB12 (Olympus, Hamburg, Germany)

EasyjecT Prima Electroporator (peqlab, Erlangen, Germany)

Heat plate and stirrer MB 3001 (Heidolph, Germany)

Incubator WTB Binder (VWR, Darmstadt, Germany)

Light Source ebq100 (LFS Leistungselektronik, Jena, Germany)

Light Source Olympus U-RFL-T-200 (Olympus, Hamburg, Germany)

Light Source Zeiss KL1500LCD (Schott, Mainz, Germany)

Microscope Zeiss Axiophot (Zeiss, Jena, Germany)

Microscope Olympus BX50WI (Olympus, Hamburg, Germany)

Monitor Monacor B+W video monitor (Intermercador GmbH+co, Bremen, Germany)

Phillips Digital Quartz Tuner (Saturn, Mainz, Germany)

pH-meter CG840 (Schott, Mainz, Germany)

Photometer Eppendorf Biophotometer RS232C (Eppendorf, Hamburg, Germany)

Power supply Biometra Power Pack P25 (Biotron, Göttingen, Germany)

Power supply Gene GPS200/400 (Pharmacia, Sweden)

Printer DPU-414 Seico Thermal printer (Eppendorf, Hamburg, Germany)

Printer Mitsubishi p91 video copy processor (VWR, Darmstadt, Germany)

Puller P-97 Sutter micropipette puller (Science Product GmbH, Hofheim, Germany)

Pump ILMVAC LVS301 (Ilmvac, Ilmenau, Germany)

Semidry-blotter Biometra Fast-Blot B34 (Biotron, Göttingen, Germany)

Siemens Simax Coffee Machine

Shaker GFL3015 (Gesellschaft für Labortechnik, Burgwedel, Germany)

Shaker IKA VIBRAX-VXR (IKA-Werk, Staufen, Germany)

Speedvac Savant (Thermo Life Sciences, Egelsbach, Germany)

Sterile banch Steril-VBH (Mahl Labortechnik, Kaarst. Germany)

Thermoblock Biometra TB1 (Biotron, Göttingen, Germany)

Thermocycler Biometra T-Gradient (Biotron, Göttingen, Germany)

Transilluminator MS Laborgeräte (Benda, Wiesloch, Germany)

Vortex Vibrofix VF1 Janke + Kunkel (IKA-Werk, Staufen, Germany)

Waterbath Certomat WR (Braun Biotech, Melsungen, Germany)

Waterbath GFL1002 (Gesellschaft für Labortechnik, Burgwedel, Germany)

Macintosh Powermac G-4 (Apple)

PC

6.5. Buffers, solutions and media

A&B phosphate Buffer was required to set up the fixation solution (see Chapter 6.6.):
Solution A: 28.39g Na_2HPO_4 in 1L H2O
Solution B: 27.6g NaH_2PO_4 in 1L H2O
A mixture of 36ml solution A and 14 ml solution B is filled up to 100ml with H2O. The resulting buffer is set to pH 7.2

Alkaline phosphatase (AP) detection buffer (Chapter 2.1.8.3.): 10ml 5M NaCl, 25ml 1M $MgCl_2$, 50ml 1M Tris (pH9.5), 0.5ml Tween20, 412ml H_2O, pH set to 9.5

Anode buffer I: 0.3 M Tris, 10% methanol, pH 10.4

Anode Buffer II: 25mM Tris, 10% methanol, pH10.4

Apple-agar filled petridishes: 27-28g of agar are dissolved in 1L commercially available apple juice. Mixture is poured into petridishes, which are stored upside down at 4°C

Broadie and Bate buffer (B&B; Broadie et al., 1992) was used for dissection of Drosophila embryos and larvae (Chapter 2.1.7.): 135mM NaCl, 5mM KCl, 4mM $MgCl_2$, 0.5mM $CaCl_2$, 5mM TES – N-tris[Hydroxymethyl]methyl-2-aminoethansulfonic acid (VWR, Darmstadt, Germany), 36mM sucrose, pH is set with NaOH to 7.15

5-Bromo-4-chloro-3-indolyl phosphate (**BCIP**)-solution for AP-staining (Chapter 2.1.8.3.): 50mg/ml BCIP in 100% N,N-Dimethylformamide

Cathode buffer: 25mM Tris base, 40mM 6-amino-n-caproic acid (VWR, Darmstadt, Germany), 10% methanol, pH 9.4

Coomassie staining solution: 1.25g Coomassie blue (brilliant blue R250; Sigma, Osterode, Germany), 227ml Isopropyl alcohol, 46ml glacial acetic acid in a total volume of 1L.

Coomassie destaining solution: 75ml glacial acetic acid, 50 ml Isopropyl alcohol in a total volume of 1L

DAB-Solution: 10mg 3,3'-Diaminobenzidine Tetrahydrochloride (Sigma, Osterode, Germany) are dissolved in 30ml PBT and subsequently aliquoted in volumes of 1ml and stored at -20°C.

10x Dropout solution: 300mg/L L-Isoleucine, 1500mg/L L-Valine, 200mg/L L-Arginine HCl, 300mg/L L-Lysine HCl, 200mg/L L-Methionine, 500mg/LPhenylalanine, 2000g/L L-Threonine, 300mg/L L-Tyrosine, 200mg/L L-Uracil (Bio 101, Inc., Carlsbad, USA), autoclaved and stored at 4°C

Lämmli solution: 50mM Tris-HCl (pH 6.8), 100mM Dithiothreitol, 2% SDS, 0.1% Bromine phenol blue, 10% Glycerol

LB agar and ampicillin plates: add 15g/L agar to freshly prepared LB broth (see below), autoclave and cool to 50°C, add ampicillin to 100µg/ml (VWR, Darmstadt, Germany), pour plates and store at 4°C

LB broth: 10g/L Bacto-tryptone, 5g/L Bacto-yeast extract, 5g/L NaCl (adjust pH to 7.0 with 5N NaOH, autoclave

Lysis buffer for DNA Miniplasmid preparation: 4.3ml ddH_2O, 0.5ml 10% SDS, 0.2ml 5N NaOH. Make fresh before any usage with sterile solutions.

Neutralisation buffer for DNA Miniplasmid preparation: 4.3ml ddH_2O, 0.5ml 10% SDS, 0.2ml 5N NaOH. Buffer was made freshly before each application using sterile solutions.

Nitro-blue-tetrazolium (**NBT**) solution (Chapter 2.1.8.3.): 50mg/ml NBT in 70% N,N-Dimethylformamide

PBS with Tween detergent (**PBT**): 0.3% Tween-20 in PBS

Phenol-Chloroform-Isoamyl alcohol: Phenol, chloroform and isoamyl alcohol are added together in a ratio of 25:24:1 (v/v)

Phosphate-buffered saline (**PBS**): 137mM NaCl, 2.7mM KCl, 4.3mM $Na_2HPO_4 \cdot 7H_2O$, 1.4mM KH_2PO_4, pH 7.3; autoclaved

Polyacrylamide stacking gel (5%) in a total volume of 10ml: 7.54ml H_2O, 1ml 1.25M Tris-HCl (pH 6.8), 0.1ml 10% SDS, 1.28ml Acrylamide, 50µl APS, 30µl TEMED

Polyacrylamide separation gel (8%) in a total volume of 15ml: 7.73ml H_2O, 3ml 1.875M Tris-HCl (pH 8.8), 0.15ml 10% SDS, 4ml Acrylamide, 75µl APS, 45µl TEMED

Polyacrylamide gel running buffer: 3.03g Tris, 14.4g Glycin and 1g SDS in a total volume of 1L (ddH_2O)

Ponceau-S-Red staining solution: 0.5% Ponceau-powder in 1% acetic acid

Resuspension buffer for DNA Miniplasmid preparation: 50mM Glucose, 10mM EDTA (pH 8.0), 25mM Tris (pH 8.0), autoclaved, stored at 4°C

Synthetic dropout (**SD**) medium: 6.7g/L Difco yeast nitrogen base without amino acids (kind gift from A. Ahle), 20g/L agar. H_2O is added to 850ml, then 100ml of sterile 10x dropout solution are added and the pH is adjusted to 5.8. The medium is autoclaved, and dextrose is added to 2% after medium has cooled down to approximately 50°C

Tris-Acetate-EDTA (**TAE**) 50x stock solution (pH 8.3): 2M Tris-Acetate and 50mM EDTA (pH8.0)

Tris-EDTA (**TE**)**-buffer** (pH 7.4): 10mM Tris-HCL (pH 7.4), 1mM EDTA (pH 8.0)

Tris buffered saline (TBS): 37.5ml 2M Tris-HCl (pH9.5), 2.9g NaCl, 25ml 1M $MgCl_2$ in a total volume of 500ml

X-Gal (**5-bromo-4-chloro-3-indolyl-b-D-galactopyranoside**) stock solution: X-Gal was dissolved in N,N-Dimethylformamide at a concentration of 20mg/ml and stored in the dark at -20°C

Yeast lysis solution: 2% Triton X-100, 1% SDS, 100mM NaCl, 10mM Tris (pH8.0), 1mM EDTA

Z-buffer for β-galactosidase filter assays: 16.1g/L $Na_2HPO_4 \cdot 7H_2O$, 5.5g/L $NaH_2PO_4 \cdot H_2O$, 0.75g/L KCl, 0.246g/L $MgSO_4 \cdot 7H_2O$, pH 7.0, autoclaved

Z-buffer/X-Gal solution: 100ml Z-buffer, 0.27ml β-mercaptoethanol (Sigma, Osterode, Germany), 1.67ml X-Gal stock solution

6.6. Fixative Solutions

4% paraform aldehyde fixative solution: 4% paraform aldehyde are dissolved in A&B phosphate buffer. The fixation solution can be stored at -20°C. Before usage, the solution is thawed at 60°C for 20 minutes.

Bouin's fixative solution (Featherstone et al., 2002): 7.5ml saturated picrinic acid (keep in dark), 2.5ml formaldehyde (37%), 0.5ml glacial acetic acid (VWR, Darmstadt, Germany)

6.7. Other materials

6.7.1. Sharpened tungsten wires

Sharpened tungsten rods (0.005x3 inch, TW5-3, Science Products, Hofheim, Germany) were used to cut open the embryos (along either the dorsal, lateral or ventral midline, respectively): One terminal of a MTR27 power supply (Leitz, Wetzlar, Germany) was connected to a carbon electrode and the other terminal to the tungsten rod. The rod was sharpened by dipping it repeatedly in a KOH/$NaNO_2$ solution (34g/71g in 100 ml of dH_2O).

6.7.2. Sylgard

Dissections of stage 17 embryos or third instar larvae (Chapter 2.1.7.) were carried out on Sylgard coated coverslips and petridishes, respectively. Sylgard was produced by mixing 5 volumes of Sylgard 184 silicone elastomer base with 1 volume Sylgard 184 curing agent (both from Dow Corning, Wiesbaden, Germany). After thorough mixing at room temperature the liquid Sylgard was stored at -20°C. For polymerisation of Sylgard coated coverslips or petridishes were kept at 68°C overnight.

6.7.3. Dissection glass needles

Dissection glass needles were produced using Vitrex capillary tubes (0.780-1-00x80mm, GB100T8P, Science Products, Hofheim, Germany) and a P-97 micropipette horizontal puller (Sutter Instruments, Science Products, Hofheim, Germany). Parameters were set as follows (these are approximates after ramp test of the capillary tubes):

Step	Heat	Pull	Velocity	Time
1	460	0	40	190
2	420	0	40	190
3	420	0	80	190

6.7.4. Membranes for Western Analysis

Immobilon P polyvinylidene fluoride (PVDF) microporous membrane 0.45µm 26CMX3.75M (Millipore GmbH, Eschborn, Germany)

Protran nitrocellulose transfer membrane (Schleicher and Schuell, Dassel, Germany)

6.7.5. Microdissection tools

Forceps Dumont INOX Nr.5 (neoLab, Heidelberg, Germany)

Microscissors 15004-08 (Fine Science Tools GmbH, Heidelberg, Germany)

6.8. Bacterial strains

E.coli strain **XL1-Blue** (electrocompetent): *recA1 endA1 gyrA96 thi-1 hsdR17 supE44 relA1 lac [F'proAB lacIqZDM15 Tn10 (Δ)]*

E.coli strain **DH5[alpha]** (chemocompetent): *F'phi80dlacZ δ (lacZYA-argF)U169 deoR recA1 endA1 hsdR17 (rk-, m k+) phoA supE44 λ-thi-1 gyrA96 relA1/F' proAB+ lacIqZδM15 Tn10(Δ)*

E.coli strain **RRI** (electrocompetent): *HB101 RecA+*

6.9.Yeast strains

Saccharomyces cerevisiae strain **Y187** (transformed with bait; transformation: A. Ahle and T. Böckers, Institute for Anatomy, University of Münster, Germany): *MATα, ura3-52, his3-200, ade2-101, trp1-901, leu2-3, 112, gal4Δ, met-, gal80Δ, URA3::GAL1$_{UAS}$-GAL1$_{TATA}$-lacZ, MEL1* (Harper et al., 1993)

Saccharomyces cerevisiae strain **AH109** (pretransformed *Drosophila melanogaster* library: A. Ahle and T. Böckers, Institute for Anatomy, University of Münster, Germany): *MATa, trp1-901, leu2-3, ura3-52, his3-200, gal4Δ, gal80Δ, LYS2::GAL1$_{UAS}$-GAL1$_{TATA}$-HIS3, GAL2$_{UAS}$-GAL2$_{TATA}$-ADE2, URA3::MEL1$_{UAS}$-MEL1$_{TATA}$-lacZ* (James et al., 1996)

6.10.Vectors

pAS2-1 plasmid map (Harper et al., 1993)

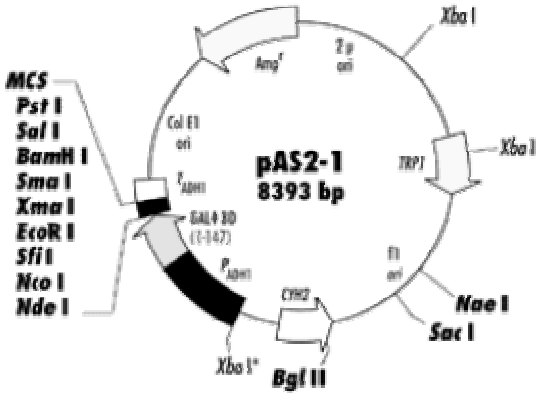

pAS2-1 generates a hybrid that contains amino acids 1-147 of the Gal4 DNA-binding domain. Unique restriction sites are located in the multiple cloning site (MCS)-region at the 3' end of the ORF

for the Gal4 peptide. The hybrid protein is expressed from the constitutive *ADH1* promoter (P), transcription is terminated at the *ADH1* transcription termination signal (T). In addition to the yeast nutritional marker *LEU2* pAS2-1 carries *CYH*^{s}*2* for cycloheximide sensitivity. pAS2-1 can replicate autonomously in *E. coli* and *S. cerevisiae*.

pACT2 plasmid map (Harper et al., 1993)

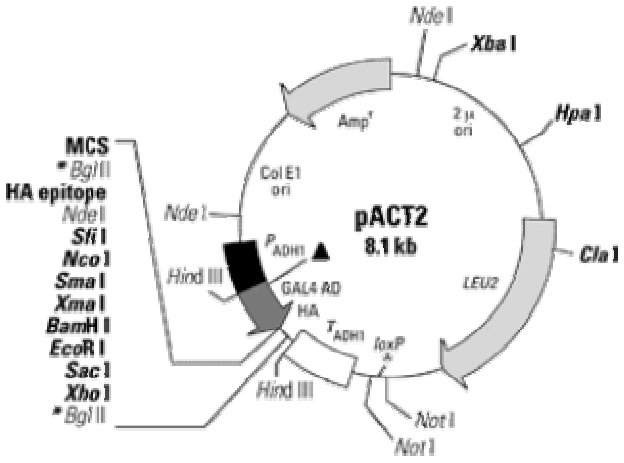

pACT2 generates a hybrid that contains amino acids 768-881 of the Gal4 activating domain. Unique restriction sites are located in the multiple cloning site (MCS)-region at the 3' end of the ORF for the Gal4 peptide. The hybrid protein is expressed from the constitutive *ADH1* promoter (P), transcription is terminated at the *ADH1* transcription termination signal (T). pACT2 carries the yeast nutritional marker *TRP1*. pACT2 can replicate autonomously in *E. coli* and *S. cerevisiae*.

pCRII TOPO plasmid map (Invitrogen, Carlsbad, USA)

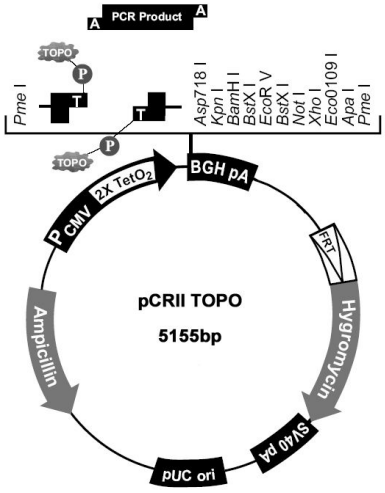

Taq polymerase has a nontemplate-dependent terminal transferase activity that adds a single deoxyadenosine (A) to the 3´ ends of PCR products. The linearized vector supplied in the TOPO cloning Kit (Invitrogen, Carlsbad, USA) has single, overhanging 3´ deoxythymidine (T) residues. This allows PCR inserts to ligate efficiently with the vector.
Topoisomerase I from *Vaccinia virus* binds to duplex DNA at specific sites and cleaves the phosphodiester backbone after 5′-CCCTT in one strand. The energy from the broken phosphodiester

backbone is conserved by formation of a covalent bond between the 3′ phosphate of the cleaved strand and a tyrosyl residue (Tyr-274) of topoisomerase I. The phospho-tyrosyl bond between the DNA and enzyme can subsequently be attacked by the 5′ hydroxyl of the original cleaved strand, reversing the reaction and releasing topoisomerase. For further details see http://www.invitrogen.com.

6.11.Oligonucleotides

Primers for *shot* **ABD** (BioSpring, Frankfurt, Germany):

Forward primer, incorporating SfiI: ggccnnnn/nggcc (n-core in pAS2.1 is atgga)

5'-ggccatggaggccGACGAACGCGATGCC-3'
(28ntds; 15ntds binding original sequence [capital letters]; Tm 47°C)

Reverse primer, incorporating XmaI: c/ccggg

3'-GGAGATAGGTAGGTGAgggccc-5'
(22ntds; 16ntds binding original sequence [capital letters]; Tm 43°C)

Primers for *shot* **PAT** (BioSpring, Frankfurt, Germany):

Forward primer, incorporating SfiI: ggccnnnn/nggcc (n-core in pAS2.1 is atgga)

5'-ttatatggccatggaggccGGGTACCGCAAGATGACATCG-3'
(40ntds; 21ntds binding original sequence [capital letters]; Tm 56°C)

Reverse primer, incorporating XmaI: c/ccggg

3'-CTGTTTAACGACTCGCTCCCCACgggcccctaggc-5'
(35ntds; 23ntds binding original sequence [capital letters]; Tm 59°C; this primer was also used as reverse primer for shot PT.

Primers for *shot* **PT** (BioSpring, Frankfurt, Germany)**:**

Forward primer, incorporating SfiI: ggccnnnn/nggcc (n-core in pAS2.1 is atgga)

5'-ttatatggccatggaggccCCCAAGATGGAGTCACAACGTCGC-3'
(43ntds; 24ntds binding original sequence [capital letters]; Tm 59°C)

Reverse primer, incorporating XmaI: c/ccggg; See reverse primer for *shot* PAT.

Primers for *shot* **GT** (BioSpring, Frankfurt, Germany):

Forward primer, incorporating NdeI: ca/tatg

5'-aacgcatatgCTCAAGTACATGAACCACAAGAAGTC-3'
(36ntds; 26ntds binding original sequence [capital letters]; Tm 54°C)

Reverse primer, incorporating SalI: g/tcgac

3'-CTTAAAGTACCGGCAGAGTCGcagctggacaacat-5'

(35ntds; 21ntds binding original sequence [capital letters]; Tm 54°C)

Sequencing primers (GenTech, Mainz, Germany):

Forward primer for sequencing Bait-Inserts in pAS2-1:

5'-TCATCGGAAGAGAGTAGT-3'

Reverse Primer for sequencing Bait-inserts in pAS2-1:

5'-CGTTTTAAAACCTAAGAGTCAC-3'

Forward primer for sequencing Prey-Inserts in pACT2:

5'-TACCACTACAATGGATG-3'

Reverse Primer for sequencing Prey-inserts in pACT2:

5'-GTGAACTTGCGGGGTTTTTCAGTATCTACGAT-3'

Forward primer GT at position[iii] 414:

5'-GGTGCGCGTGGGTGGCGGTTGGG-3'

Forward primer GT at position 912:

5'-CGCTGTCGCTGGATAGCACGG-3'

Reverse primer GT at position 436:

5'-CCCAACCGCCACCCACGCGCACC-3'

Forward primer PAT at position 504:

5'-GGCCAATCGTCGTGTGGTGG-3'

Forward primer PAT/PT at position 984:

5'-GGAGACGGCCTTCCACATTGTGG-3'

Forward primer PAT/PT at position 1422:

5'-CATCGAGAAGGCCTGGTATCGC-3'

Forward primer PAT/PT at position 1963:

5'-CAATTGCTTGCCGCTGACTATGGC-3'

Forward primer PAT/PT at position 2431:

5'-GAAGCCCATCTGACAGCCATG-3'

Forward primer PAT/PT at position 2901:

[iii] Position refers to sequence of respective Shot domain within original pP[UAST] constructs received from A. Subramanian

5’-GGGCGCTTGCCTGCTATTGCC-3’

Reverse primer PAT at position 523:

5’-CCACCACACGACGATTGGCC-3’

6.12. DNA/protein markers and quantifying standards

λDNA HindIII digest DNA marker (MBI Fermentas, St. Leon-Rot, Germany)

GeneRuler^{TM} 100 bp Ladder Plus DNA marker (MBI Fermentas, St. Leon-Rot, Germany)

Low Molecular Weight Calibration Kit for SDS-electrophoresis (Amersham Biosciences, Braunschweig, Germany)

High Molecular Weight Calibration Kit for SDS-electrophoresis (Amersham Biosciences, Braunschweig, Germany)

7.APPENDIX II

7.1. Biochemical confirmation of the interaction between the Shot Plakin domain and DPxn as revealed by yeast two-hybrid assay

In collaboration with Arul Subramanian and Talila Volk (Weizmann Institute of Genetics, Rehovot, Israel) co-immunoprecipitation (co-IP) studies were carried out. To this end, DPxn was co-transfected with any of the three Shot domains PAT, PT, or GT, in *Drosophila Schneider* SR^{2+}-cells. Using antibodies against DPxn and the TAP-tag (tandem affinity purification-tag) of the distinct Shot domains, respectively, they observed co-localisation of DPxn with both N-terminal domains PAT and PT (both containing the Plakin domain), but not with the C-terminal Shot domain (Figure 7.1A). Hence, there is a considerable probability that DPxn is interacting with the Shot Plakin domain in the *Drosophila* cell system. Subsequently, the respective Shot domain TAP fusion proteins and associated components were recovered from the cell extracts by affinity selection on an IgG matrix (specific to the TAP-tag of the Shot constructs; Rigaut et al., 1999). Washed and eluted material was subjected to Western analysis, testing the blotted membrane with antibodies to DPxn and the TAP-tag. As shown in Figure 7.1B DPxn co-immunoprecipitated with both N-terminal constructs. This suggests that DPxn is indeed interacting with the Shot-Plakin domain, confirming the results obtained in the yeast two-hybrid assay. A. Subramanian observed that PAT yielded more DPxn than PT. This is possibly due to a more accurate folding of the first construct. An additional interaction of DPxn with the ABD within the PAT construct is rather unlikely since the ABD did not show any interaction with DPxn in the yeast assay. Further, Arul Subramanian could yield best precipitation results when adding the phosphatase repressor Na-Vanadate to the protein extraction buffer. He therefore tested the Western blots with antibodies specific to phosphorylated tyrosine residues, revealing that co-precipitated DPxn was indeed phosphorylated (Figure 7.1B) and suggesting that phosphorylation of DPxn is possibly facilitating its interaction with the Shot Plakin domain.

DPxn has distinct protein interaction motifs, including three major tyrosine phosphorylation sites, five Leucine rich sequences termed LD motifs, and four LIM domains (Cystein and Histidin rich, Zinc coordinating domains composed of two tandemly repeated Zinc fingers)[iv]. While the C-terminus of DPxn comprises the LIM domains, the LD-motifs and the tyrosine phosphorylation sites are located within its N-terminus (Figure 7.2). Yeast two-hybrid prey constructs bearing the nucleotides 145-1185 (encoding amino acids 1-347 of DPxn, i.e. the N-terminal region including the LD motifs and tyrosine phosphorylation sites; the numbers refer to the cDNA sequence representing GenBank accession number AB048194) and nucleotides 1174-1983 (encoding the amino acids 344-581 of the DPxn C-terminal LIM domains), respectively, were available from Ryohei Yagi (Department of Molecular Biology, Osaka Bioscience Institute, Japan). These constructs offered an opportunity to carry out refined yeast two-hybrid assays, testing for the requirement of the specific DPxn regions for the interaction with the Shot Plakin domain. The constructs were amplified by the author following standard cloning and plasmid isolation techniques (Chapters 2.3.2. and 2.3.3.6.) and sent to the collaborating laboratory of T. Böckers (Institute for Anatomy, University of Münster, Germany) for co-transformation with the Shot Plakin bait construct into yeast cells and subsequent testing for reporter gene activation (see Chapter 2.3.3.). The direct yeast two-hybrid tests resulted in the interaction of the Shot Plakin domain with the N-terminal domain but not with the C-terminal domain of DPxn (Table 7.1).

	DPxn	DPxn-N	DPxn-C
Shot-Plakin	+	+	-

Table 7.1: Direct Yeast Two-Hybrid tests of the Shot Plakin domain with full length *Drosophila* Paxillin (DPxn) N-terminal DPxn and C-terminal DPxn, respectively. The Shot Plakin domain was found to interact with full length and N-terminal DPxn (+), but not with C-terminal DPxn (-) as revealed by the expression of the reporter genes His, Ade and β-Gal (see Chapter 2.3.3.). All individual *DPxn* clones retrieved from the yeast two-hybrid screen represented full length *DPxn*-sequences: the direct testing of the distinct DPxn termini against the Shot Plakin domain allowed to narrow down the interaction to the N-terminus of DPxn.

[iv] www.mshri.on.ca/pawson

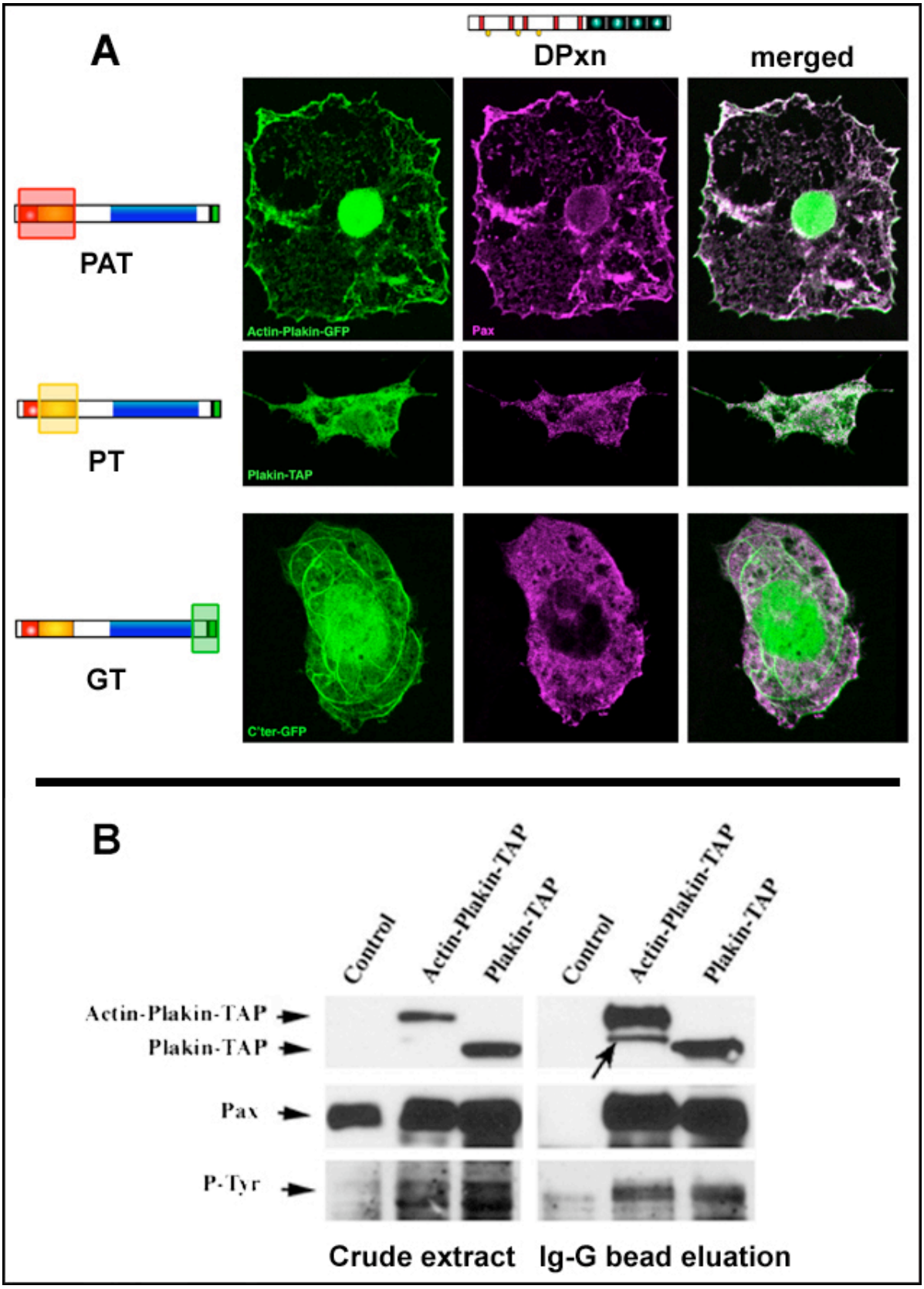
A
DPxn
merged
PAT
PT
GT
Actin-Plakin-GFP
Pax
Plakin-TAP
C'ter-GFP
B
Control
Actin-Plakin-TAP
Plakin-TAP
Control
Actin-Plakin-TAP
Plakin-TAP
Actin-Plakin-TAP
Plakin-TAP
Pax
P-Tyr
Crude extract
Ig-G bead eluation

The results are in agreement with findings of the co-immunoprecipitation analysis that suggested the interaction between DPxn and Shot to require phosphorylation of DPxn. Conserved Tyrosine phosphorylation sites are found within the N-terminus of DPxn (Figure 7.2). If the interaction between DPxn and the Shot Plakin domain is facilitated by phosphorylation, then it is very likely to include the N-terminus of DPxn.

Figure 7.1: Localisation- and co-imunoprecipitation studies of DPxn and different Shot domains. DPxn was co-expressed with the Shot constructs PAT, PT, and GT, respectively, in *Drosophila Schneider SR*$^+$-cells (A; colour code of the bar diagrams follows that of Figures 1.3 and 7.2, respectively). DPxn was labelled with anti-DPxn (magenta), PAT and PT were detected with rabbit IgG, GT with anti-GFP (all shown in green). The merged pictures show that DPxn follows the localisation of the Plakin-domain containing constructs PAT and PT, but does not co-localise with the C-terminal construct GT. Results of the co-immunoprecipitations are shown in B. Protein extracts of *SR*$^+$-cells expressing DPxn and PAT or PT, respectively, were blotted and tested with rabbit IgG (top rows), anti-DPxn (middle rows) and anti-Phospho-Tyrosin (P-Tyr; bottom rows). Co-immunoprecipitation was carried out with IgG beads (recognise the TAP-tag of the Shot constructs; right panel). DPxn was found to co-precipitate with the Plakin domain containing constructs. Anti-P-Tyr staining reveals that the interaction possibly requires phosphorylation of the DPxn-protein. Additional band of the Aktin-Plakin-TAP (i.e. PAT) protein is due to degradation.

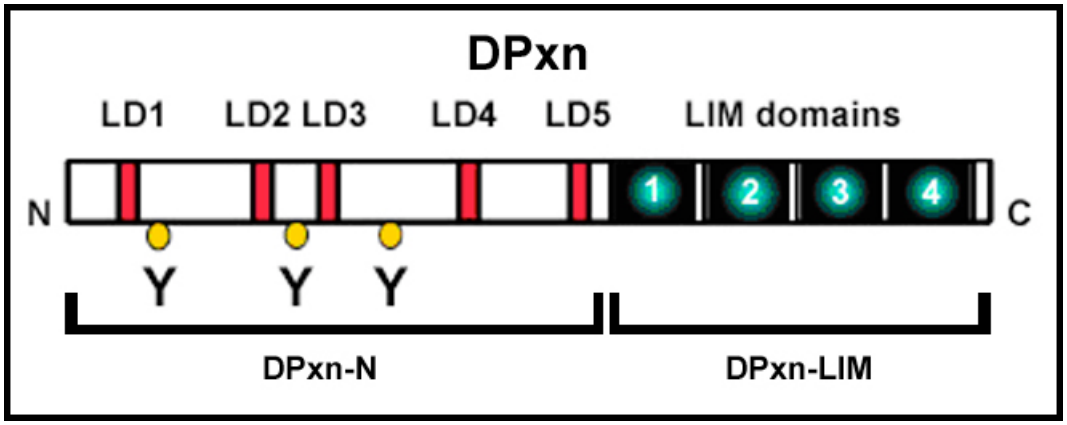
DPxn
LD1
LD2 LD3
LD4
LD5
LIM domains
N
C
1
2
3
4
Y
Y
Y
DPxn-N
DPxn-LIM

Figure 7.2: Schematic representation of *Drosophila* DPxn protein. LD-motifs are shown in red, LIM domains are indicated in black. Putative tyrosine phosphorylation sites (Y) are shown in yellow. The N-terminal sequence used for the direct yeast two-hybrid assay against the Shot Plakin domain comprised all five LD-motifs and three tyrosine phosphorylation sites (DPxn-N, amino acids 1-347), the C-terminal sequence covered all four LIM domains (DPxn-LIM, amino acids 344-581). DPxn is 581 amino acids long and shares 57% amino acid identity for the entire protein and 78% amino acid identity for the LIM domain region with human Paxillin α (Yagi et al., 2001).

7.2. Misexpression studies of Rac1^{V12} as performed by U. Mettler and A. Prokop (Mettler, 2002)

U. Mettler and A. Prokop studied the phenotypical overlap between CA DRac1^{V12} misexpressing and *shot* mutant embryos in more detail: Targeted motor neuronal misexpression of CA DRac1^{V12} by the *eve^{RNE2}Gal4* and *MzVum-Gal4* driver lines showed severely reduced branches in the CNS. Further, especially *MzVum-Gal4* mediated expression of CA DRac1^{V12} caused obvious pattern defects of anti-Fasciclin II, which failed to stay in the nerve, but spread into the nerve roots. Mislocalisation of another marker was also observed: anti-DLG, usually found in higher levels at the nerve roots than in the neuropile, looses its specific localisation in *shot* or *elav-Gal4::DRac1^{V12}* embryos. In contrast to their reduced NMJs, *elav-Gal4::DRac1^{V12}* embryos showed a fairly normal differentiation of presynaptic structures in the CNS: the neuropile was astonishingly little reduced, despite severe growth defects in the CNS (see below). Also stainings against the presynaptic proteins Synapsin and Synaptotagmin showed an astonishingly voluminous neuropile filled with presynaptic puncta comparable to the wild type. This was similarly observed in *shot* mutant embryos (Löhr et al., 2002). Like in *shot* mutant embryos, *elav-Gal4::DRac1^{V12}* embryos dendrites and multidendritic neurones were almost abolished and the microtubule associated protein Futsch revealed impairment of chordotonal neurones. Also in non-neuronal tissue CA DRac1^{V12} phenocopied *shot* mutant embryos. Expression of CA DRac1^{V12} with the tendon cell specific driver line *Stripe-Gal4* disturbed the association of muscle with tendon cells. CA DRac1^{V12}-induced defects were not exclusively restricted to those of *shot*. For example, the reproducible Fasciclin II pattern of longitudinal fascicles in the CNS (Landgraf et al., 2003), was found to be impaired in CA DRac1^{V12}-expressing embryos, which is in contrast to observation in *shot* mutants (Prokop et al., 1998b). Given the severity of CA DRac1^{V12} induced phenotypes it had to be checked whether these phenotypes are caused by true regulation through DRac1-signalling or whether they reflect secondary defects due to gradual onset of cell death. To test this, *eve^{RNE2}Gal4::DRac1^{V12}* individuals were investigated at the third instar larval stage. It was found that CA DRac1^{V12} expressing aCC and RP2 motor neurones still existed at this stage. Their axons terminated at similar positions as observed in embryos. Furthermore, their axonal endings as well as central side branches were severely reduced. Thus, late embryonic neuronal differentiation defects seemed to be caused directly through DRac1 signalling and, in addition, postsynaptic growth of synaptic compartments is suppressed by CA DRac1^{V12}.

Ulrike Mettler and Andreas Prokop could further show that distinct Fasciclin II positive fascicles in the CNS were found reduced or missing when driving mutant GTPase isoforms DN Cdc42^{N17} and CA Cdc42^{V12} with *MzVum-Gal4*. Further, using the driver *DDC-Gal4*, they revealed reduced efferent projections caused by the isoforms CA DCdc^{V12}, DN DRac1 ^{N17} and CA DRac1^{V12} dendrites. However, *DDC-Gal4* drives expression in only one motor neurone, innervating the ventral lateral muscle 6, in the third instar larvae, i.e. at a development point when initial contacts have been made and the synapses had time to mature.

Gal4-driver	**RhoGTPase**	Reduced dendrites CNS (PNS)	Reduced NMJs	Defect CNS fascicle pattern	Mislocalised	
					FasII	Syt
Elav-Gal4	Cdc42^{N17}	(O)	O	+	O	O
	Cdc42^{V12}	(++)	O	++	O	O
	Rac1^{N17}	(O)	O	+	O	O
	Rac1^{V12}	(++)	++	++	++	++
eve^{RNE2}Gal4; UAS-Cd8GFP	Cdc42^{N17}	O	O	n.d.	n.d.	n.d.
	Cdc42^{V12}	++	O	n.d.	n.d.	n.d.
	Rac1^{N17}	O	O	n.d.	n.d.	n.d.
	Rac1^{V12}	++	++	n.d.	n.d.	n.d.
MZVum-Gal4	Cdc42^{N17}	O (O)	O	++	O	O
	Cdc42^{V12}	++(++)	O	++	O	O
	Rac1^{N17}	++(n.d.)	O	O	O	O
	Rac1^{V12}	++(++)	++	O	++	++
DDC-Gal4	Cdc42^{N17}	O	O	O	n.d.	n.d.
	Cdc42^{V12}	++	++	+	n.d.	n.d.
	Rac1^{N17}	O	+	O	n.d.	n.d.
	Rac1^{V12}	++	++	+	n.d.	n.d.
shot^{SF20}		++	++	O	++	++

Table 7.2: Summary of phenotypes observed upon targeted misexpression of different mutant RhoGTPase isoforms using distinct neuronal Gal4-drivers (for *MzVum*- and *DDC-Gal4* see Mettler, 2002) as compared to defects found *shot* mutant background (*shot^{SF20}*; see Chapter 3.1.). O, no mutant phenotype; +, weak mutant phenotype; ++, strong mutant phenotype; n.d., not determined.

7.3. Genetical approach to investigate the requirement for DRac1 function at the NMJ

In order to study loss of DRac function genetically *trio*^{1} mutant embryos and *Rac1*^{J11}, *Rac2*$^{\Delta}$, *Mtl*$^{\Delta}$ triple mutant embryos were studied at late stage 17 (Andreas Prokop). Since functions of the closely related *Rac1*, *Rac2* and *Mtl* genes are partly redundant, only the *Rac* triple-mutant constellation results in complete loss of Rac function (Hakeda-Suzuki et al., 2002). *trio*^{1} mutant embryos carry a loss of function allele of the GEF Trio. Trio is essential for DRac function in axon growth and guidance: Mutations in *trio* cause phenotypes reminiscent of loss of *DRac* defects, which is believed to be due to the fact that DRac GTPases can not be switched into their active form (see Figure 3.40iv.; Hakeda-Suzuki et al., 2002). In this study, both *trio* and *DRac* triple mutant embryos showed severe patterning defects of motor axons and longitudinal fascicles in the CNS, which is in agreement with findings in earlier embryos (Hakeda-Suzuki et al., 2002). By contrast, other late neuronal differentiation phenotypes occurred fairly normal: Large boutons were formed, Fasciclin II, DLG and Synaptotagmin expression in the nerve roots was rather normal, multidendritic sensory neurones formed sensory protrusions, and scolopidial organs showed no obvious structural defects. However, the Fasciclin II staining revealed that motor neuronal terminals of *DRac* triple mutant embryos were extended, showing structural defects reminiscent of *DPxn* mutant embryos (see Figure 3.30) and embryos expressing DN DRac1^{N17} under stringent conditions (N. Sanchez-Soriano, personal communication). Thus, CA DRac1 mimics *shot* mutant phenotypes, while loss of DRac function (DN DRac1^{N17} misexpression or *DRac1* triple mutants) mimics *DPxn* mutant phenotypes. Results presented in Chapter 3.5. suggest the functions of Shot and DPxn during the structural differentiation of NMJs to be related. Accordingly, there is a high probability for the different components to interact genetically. Experiments are presently undertaken to test this notion.

8. LITERATURE

Adams, M. D. Celniker, S. E. Holt, R. A. Evans, C. A. Gocayne, J. D. Amanatides, P. G. Scherer, S. E. Li, P. W. Hoskins, R. A. Galle, R. F. et al. (2000). The genome sequence of *Drosophila melanogaster*. *Science* 287, 2185-95.

Ahmari, S. E., Buchanan, J. and Smith, S. J. (2000). Assembly of presynaptic active zones from cytoplasmic transport packets. *Nat. Neurosci.* 3, 445-451.

Alberts, B., Bray, D., Lewis, J., Raff, M., Roberts, K. and Watson, J. D. (1994). Molecular biology of the cell. New York London: Garland Publishing Inc.

Albright, T. D., Jessell, T. M., Kandel, E. R. and Posner, M. I. (2000). Neural science: a century of progress and the mysteries that remain. *Cell* 100 Suppl, S1-55.

Albright, T. D., Jessell, T. M., Kandell, E. R. and Posner, M. I. (2001). Progress in the neural sciences in the the century after Cajal (and the mysteries that remain). *Ann N Y Acad Sci* 929, 11-40.

Allen, M. J., Shan, X. and Murphey, R. K. (2000). A role for *Drosophila* Drac1 in neurite outgrowth and synaptogenesis in the giant fiber system. *Mol. Cell. Neurosci.* 16, 754-765.

Allwardt, B. A., Lall, A. B., Brockerhoff, S. E. and Dowling, J. E. (2001). Synapse formation is arrested in retinal photoreceptors of the zebrafish *nrc* mutant. *J. Neurosci.* 21, 2330-2342.

Almeida, E. A., Ilic, D., Han, Q., Hauck, C. R., Jin, F., Kawakatsu, H., Schlaepfer, D. D. and Damsky, C. H. (2000). Matrix survival signaling: from fibronectin via focal adhesion kinase to c-Jun NH(2)-terminal kinase. *J Cell Biol* 149, 741-54.

Altschul, S. F., Gish, W., Miller, W., Myers, E. W. and Lipman, D. J. (1990). Basic local alignment search tool. *J. Mol. Biol.* 215, 403-410.

Ansorge, W., Voss, H., Wirkner, U., Schwager, C., Stegemann, J., Pepperkok, R., Zimmermann, J. and Erfle, H. (1989). Automated Sanger DNA sequencing with one label in less than four lanes on gel. *J Biochem Biophys Methods* 20, 47-52.

Araque, A., Parpura, V., Sanzgiri, R. P. and Haydon, P. G. (1999). Tripartite synapses: glia, the unacknowledged partner. *Trends Neurosci* 22, 208-15.

Ashburner, M. (1989). *Drosophila*: a laboratory handbook (two volumes). Cold Spring Harbor New York: Cold Spring Harbor Laboratory Press.

Aspenström, P. (1999a). Effectors for the Rho GTPases. *Curr Opin Cell Biol* 11, 95-102.

Aspenström, P. (1999b). The Rho GTPases have multiple effects on the actin cytoskeleton. *Exp Cell Res* 246, 20-5.

Baines, R. A., Robinson, S. G., Fujioka, M., Jaynes, J. B. and Bate, M. (1999). Postsynaptic expression of tetanus toxin light chain blocks synaptogenesis in *Drosophila*. *Curr. Biol.* 9, 1267-1270.

Bärlocher, F. (1999). Biostatistik. Praktische Einführung in Konzepte und Methoden. Stuttgart: Thieme.

Bate, M. and Broadie, K. (1995). Wiring by fly: The neuromuscular system of the *Drosophila* embryo. *Neuron* 15, 513-525.

Bate, M. and Martínez-Arias, A. (1993). The development of *Drosophila melanogaster* (2 Vol.). Cold Spring Harbor, New York: Cold Spring Harbor Laboratory Press.

Bate, M. and Rushton, E. (1993). Myogenesis and muscle patterning in *Drosophila melanogaster*. *Comptes Rendus Acad. Sci.* 316, 1055-1061.

Bernier, G., Brown, A., Dalpe, G., De Repentigny, Y., Mathieu, M. and Kothary, R. (1995). Dystonin expression in the developing nervous system predominates in the neurons that degenerate in dystonia musculorum mutant mice. *Mol Cell Neurosci* 6, 509-20.

Bernstein, E., Caudy, A. A., Hammond, S. M. and Hannon, G. J. (2001a). Role for a bidentate ribonuclease in the initiation step of RNA interference. *Nature* 409, 363-6.

Bernstein, E., Denli, A. M. and Hannon, G. J. (2001b). The rest is silence. *Rna* 7, 1509-21.

Beumer, K., Matthies, H. J. G., Bradshaw, A. and Broadie, K. (2002). Integrins regulate DLG/FAS2 via a CaM kinase II-dependent pathway to mediate synapse elaboration and stabilization during postembryonic development. *Development* 129, 3381-3391.

Beumer, K. J., Rohrbough, J., Prokop, A. and Broadie, K. S. (1999). A Role for PS Integrins in morphological growth and synaptic function at the postembryonic neuromuscular junction of *Drosophila*. *Development* 126, 5833-5846.

BioTechniques. (2000). Yeast Hybrid Technologies. Natick, MA, USA: Eaton, F.W.

Bishop, A. L. and Hall, A. (2000). Rho GTPases and their effector proteins. *Biochem. J.* 348, 241-255.

Blake, D. J. and Kröger, S. (2000). The neurobiology of duchenne muscular dystrophy: learning lessons from muscle? *Trends Neurosci.* 23, 92-99.

Bodmer, R. and Jan, Y. N. (1987). Morphological differentiation of the embryonic peripheral neurons in *Drosophila*. *Roux's Arch. Dev. Biol.* 196, 69-77.

Bosher, J. M. and Labouesse, M. (2000). RNA interference: genetic wand and genetic watchdog. *Nat Cell Biol* 2, E31-6.

Bourne, H. R., Sanders, D. A. and McCormick, F. (1990). The GTPase superfamily: a conserved switch for diverse cell functions. *Nature* 348, 125-32.

Bowie, J. E. and Young, I. T. (1977). An analysis technique for biological shape-II. *Acta Cytol* 21, 455-64.

Brancolini, C., Benedetti, M. and Schneider, C. (1995). Microfilament reorganization during apoptosis: the role of Gas2, a possible substrate for ICE-like proteases. *Embo J* 14, 5179-90.

Brand, A. and Perrimon, N. (1993). Targeted gene expression as a means of altering cell fates and generating dominant phenotypes. *Development* 118, 401-415.

Brand, A. H. and Dormand, E. L. (1995). The GAL4 system as a tool for unravelling the mysteries of the Drosophila nervous system. *Curr Opin Neurobiol* 5, 572-8.

Brandt, R. (1998). Cytoskeletal mechanisms of axon outgrowth and pathfinding. *Cell Tissue Res* 292, 181-9.

Brandt, R. (2001). Funktionen des Zytoskeletts bei der Entwicklung von Nervenzellen. *Neuroforum (Neurowiss. Ges.)* 2.01, 47-56.

Brenman, J. E., Chao, D. S., Gee, S. H., McGee, A. W., Craven, S. E., Santillano, D. R., Wu, Z., Huang, F., Xia, H., Peters, M. F. et al. (1996). Interaction of nitric oxide synthase with the postsynaptic density protein PSD-95 and α1-syntrophin mediated by PDZ domains. *Cell* 84, 757-767.

Broadie, K., Sink, H., Van Vactor, D., Fambrough, D., Whitington, P. M., Bate, M. and Goodman, C. S. (1993). From growth cone to synapse: the life history of the RP3 motor neuron. *Development* (Suppl.), 227-238.

Broadie, K., Skaer, H. and Bate, M. (1992). Whole embryo culture of *Drosophila*: development of embryonic tissues in vitro. *Roux's Arch. Dev. Biol.* 201, 364-375.

Broadie, K. S. (1999). Development of electrical properties and synaptic transmission at the embryonic neuromuscular junction. *Int Rev Neurobiol* 43, 45-67.

Broadie, K. S. (2000). Electrophysiological approaches to the neuromusculature junction. In *Drosophila Protocols*, (ed. W. Sullivan M. Ashburner and R. S. Hawley), pp. 273-295. Cold Spring Harbor, New York: Cold Spring Harbor Laboratory Press.

Broadie, K. S. and Bate, M. (1993a). Development of the embryonic neuromuscular synapse of *Drosophila melanogaster*. *J. Neurosci.* 13, 144-166.

Broadie, K. S. and Bate, M. (1993b). Innervation directs receptor synthesis and localization in *Drosophila* embryo synaptogenesis. *Nature* 361, 350-353.

Broadie, K. S. and Richmond, J. E. (2002). Establishing and sculpting the synapse in Drosophila and C. elegans. *Curr Opin Neurobiol* 12, 491-8.

Brockie, P. J. and Maricq, A. V. (2003). Ionotropic glutamate receptors in Caenorhabditis elegans. *Neurosignals* 12, 108-25.

Brown, A., Bernier, G., Mathieu, M., Rossant, J. and Kothary, R. (1995). The mouse dystonia musculorum gene is a neural isoform of bullous pemphigoid antigen 1. *Nat Genet* 10, 301-6.

Brown, M. C., Perrotta, J. A. and Turner, C. E. (1996). Identification of LIM3 as the principal determinant of paxillin focal adhesion localization and characterization of a novel motif on paxillin directing vinculin and focal adhesion kinase binding. *J Cell Biol* 135, 1109-23.

Brown, M. C. and Turner, C. E. (2002). Roles for the tubulin- and PTP-PEST-binding paxillin LIM domains in cell adhesion and motility. *Int. J. Biochem. Cell Biol.* 34, 855-863.

Brown, M. C., West, K. A. and Turner, C. E. (2002). Paxillin-dependent paxillin kinase linker and p21-activated kinase localization to focal adhesions involves a multistep activation pathway. *Mol. Biol. Cell* 13, 1550-1565.

Brown, N. H. and Kafatos, F. C. (1988). Functional cDNA libraries from Drosophila embryos. *J Mol Biol* 203, 425-37.

Budnik, V. and Gramates, L. S. (1999). Neuromuscular junctions in *Drosophila*. San Diego London Boston NewYork Sydney Tokyo Toronto: Academic Press.

Budnik, V., Koh, Y. H., Guan, B., Hartmann, B., Hough, C., Woods, D. and Gorczyca, M. (1996). Regulation of synapse structure and function by the *Drosophila* tumor suppressor gene *dlg*. *Neuron* 17, 627-40.

Campagna, J. A., Rüegg, M. A. and Bixby, J. L. (1995). Agrin is a differentiation-inducing "stop signal" for motorneurons in vitro. *Neuron* 15, 1365-1374.

Campos-Ortega, J. A. and Hartenstein, V. (1997). The embryonic development of *Drosophila melanogaster*. Berlin: Springer Verlag.

Chalfie, M., Tu, Y., Euskirchen, G., Ward, W. W. and Prasher, D. C. (1994). Green fluorescent protein as a marker for gene expression. *Science* 263, 802-5.

Challacombe, J. F., Snow, D. M. and Letourneau, P. C. (1997). Dynamic microtubule ends are required for growth cone turning to avoid an inhibitory guidance cue. *J. Neurosci.* 17, 3085-3095.

Chen, G.-C., Turano, M., Hagel, M., Thomas, S. M. and Settleman, J. (2001). Genetic interactions between the cytoskeletal adaptor, Paxillin, and Rho GTPase signalling pathway. A. Dros. Res. Conf. 43 2002 :444C. In *43rd Annual Drosophila Research Conference*, (ed. San Diego.

Chiba, A. (1999). Early Development of the Drosophila Neuromuscular Junction: A Model For Studying Neuronal Networks in Development. In *Review of international neurobiology*, vol.

43 (ed. R. J. Bradley R. A. Harris and P. Jenner), pp. 283. San Diego London Boston NewYork Sydney Tokyo Toronto: Academic Press.

Chien, C. T., Bartel, P. L., Sternglanz, R. and Fields, S. (1991). The two-hybrid system: a method to identify and clone genes for proteins that interact with a protein of interest. *Proc Natl Acad Sci U S A* 88, 9578-82.

Dalva, M. B., Takasu, M. A., Lin, M. Z., Shamah, S. M., Hu, L., Gale, N. W. and Greenberg, M. E. (2000). EphB receptors interact with NMDA receptors and regulate excitatory synapse formation. *Cell* 103, 945-56.

Dan, C., Kelly, A., Bernard, O. and Minden, A. (2001). Cytoskeletal changes regulated by the PAK4 serine/threonine kinase are mediated by LIM kinase 1 and cofilin. *J Biol Chem* 276, 32115-21.

Daniels, R. H. and Bokoch, G. M. (1999). p21-activated protein kinase: a crucial component of morphological signaling? *Trends Biochem Sci* 24, 350-5.

Dent, E. W., Callaway, J. L., Szebenyi, G., Baas, P. W. and Kalil, K. (1999). Reorganisation and movement of microtubules in axonal growth cones and developing interstitial branches. *J. Neurosci.* 19, 8894-8908.

Dubreuil, R. R. and Grushko, T. (1998). Genetic studies of spectrin: new life for a ghost protein. *BioEssays* 20, 875-8.

Duffy, J. B. (2002). GAL4 system in Drosophila: a fly geneticist's Swiss army knife. *Genesis* 34, 1-15.

Emery, A. E. (2002). Muscular dystrophy into the new millennium. *Neuromuscul Disord* 12, 343-9.

Ernsberger, U. and Rohrer, H. (1999). Development of the cholinergic neurotransmitter phenotype in postganglionic sympathetic neurons. *Cell Tissue Res.* 297, 339-361.

Etienne-Manneville, S. and Hall, A. (2002). Rho GTPases in cell biology. *Nature* 420, 629-35.

Fabini, G., Freilinger, A., Altmann, F. and Wilson, I. B. (2001). Identification of core alpha 1,3-fucosylated glycans and cloning of the requisite fucosyltransferase cDNA from Drosophila melanogaster. Potential basis of the neural anti-horseadish peroxidase epitope. *J Biol Chem* 276, 28058-67.

Fanger, G. R., Gerwins, P., Widmann, C., Jarpe, M. B. and Johnson, G. L. (1997a). MEKKs, GCKs, MLKs, PAKs, TAKs, and tpls: upstream regulators of the c-Jun amino-terminal kinases? *Curr Opin Genet Dev* 7, 67-74.

Fanger, G. R., Johnson, N. L. and Johnson, G. L. (1997b). MEK kinases are regulated by EGF and selectively interact with Rac/Cdc42. *Embo J* 16, 4961-72.

Favre, B., Fontao, L., Koster, J., Shafaatian, R., Jaunin, F., Saurat, J. H., Sonnenberg, A. and Borradori, L. (2001). The hemidesmosomal protein bullous pemphigoid antigen 1 and the integrin beta 4 subunit bind to ERBIN. Molecular cloning of multiple alternative splice variants of ERBIN and analysis of their tissue expression. *J Biol Chem* 276, 32427-36.

Featherstone, D. E., Rushton, E. and Broadie, K. (2002). Developmental regulation of glutamate receptor field size by nonvesicular glutamate release. *Nature Neurosci.* 5, 141-146.

Featherstone, D. E., Rushton, E. M., Hilderbrand-Chae, M., Phillips, A. M., Jackson, F. R. and Broadie, K. (2000). Presynaptic glutamic acid decarboxylase is required for induction of the postsynaptic receptor field at a glutamatergic synapse. *Neuron* 27, 71-84.

Fields, S. and Song, O. (1989). A novel genetic system to detect protein-protein interactions. *Nature* 340, 245-6.

FlyBase. (1999). The FlyBase database of the *Drosophila* genome projects and community literature. *Nucleic Acids Res.* 27, 85-88; http://flybase.bio.indiana.edu/.

Fontao, L., Geerts, D., Kuikman, I., Koster, J., Kramer, D. and Sonnenberg, A. (2001). The interaction of plectin with actin: evidence for cross-linking of actin filaments by dimerization of the actin-binding domain of plectin. *J Cell Sci* 114, 2065-76.

Fuchs, E. and Karakesisoglou, I. (2001). Bridging cytoskeletal intersections. *Genes Dev* 15, 1-14.

Fyrberg, E., Kelly, M., Ball, E., Fyrberg, C. and Reedy, M. C. (1990). Molecular genetics of Drosophila alpha-actinin: mutant alleles disrupt Z disc integrity and muscle insertions. *J Cell Biol* 110, 1999-2011.

Gao, F.-B., Brenman, J. E., Jan, L. Y. and Jan, Y. N. (1999). Genes regulating dendritic outgrowth, branching, and routing in *Drosophila*. *Genes Dev.* 13, 2549-2561.

Garner, C. C., Zhai, R. G., Gundelfinger, E. D. and Ziv, N. E. (2002). Molecular mechanisms of CNS synaptogenesis. *Trends Neurosci* 25, 243-51.

Geerts, D., Fontao, L., Nievers, M. G., Schaapveld, R. Q., Purkis, P. E., Wheeler, G. N., Lane, E. B., Leigh, I. M. and Sonnenberg, A. (1999). Binding of integrin alpha6beta4 to plectin prevents plectin association with F-actin but does not interfere with intermediate filament binding. *J Cell Biol* 147, 417-34.

Gietz, R. D. and Woods, R. A. (2002). Screening for protein-protein interactions in the yeast two-hybrid system. *Methods Mol Biol* 185, 471-86.

Goda, Y. and Davis, G. W. (2003). Mechanisms of synapse assembly and disassembly. *Neuron* 40, 243-64.

Gong, T. W., Besirli, C. G. and Lomax, M. I. (2001). MACF1 gene structure: a hybrid of plectin and dystrophin. *Mamm. Genome* 12, 852-861.

Greenspan, R. J. (1997). Fly pushing: The theory and practice of *Drosophila* genetics. Cold Spring Harbor New York: Cold Spring Harbor Laboratory Press.

Gregory, S. L. and Brown, N. H. (1998). *kakapo*, a gene required for adhesion between cell layers in *Drosophila*, encodes a large cytoskeletal linker protein related to plectin and dystrophin. *J. Cell Biol.* 143, 1271-1282.

Grenningloh, G., Rehm, E. J., and Goodman, C.S. (1991). Genetic analysis of growth cone guidance in Drosophila: Fasciclin II functions as a neuronal recognition molecule. *Cell* 67, 45-57.

Grieder, N. C., de Cuevas, M. and Spradling, A. C. (2000). The fusome organizes the microtubule network during oocyte differentiation in Drosophila. *Development* 127, 4253-64.

Grueber, W. B., Jan, L. Y. and Jan, Y. N. (2002). Tiling of the *Drosophila* epidermis by multidendritic sensory neurons. *Development* 129, 2867-78.

Guo, L., Degenstein, L., Dowling, J., Yu, Q.-C., Wollmann, R., Perman, B. and Fuchs, E. (1995). Gene targeting of BPAG1: Abnormalities in mechanical strength and cell migration in stratified squamous epithelia and severe neurologic degeneration. *Cell* 81, 233-243.

Hakeda-Suzuki, S., Ng, J., Tzu, J., Dietzl, G., Sun, Y., Harms, M., Nardine, T., Luo, L. and Dickson, B. J. (2002). Rac function and regulation during *Drosophila* development. *Nature* 416, 438-442.

Hall, A. (1998). Rho GTPases and the actin cytoskeleton. *Science* 279, 509-514.

Hall, A. C., Lucas, F. R. and Salinas, P. C. (2000). Axonal remodelling and synaptic differentiation in the cerebellum is regulated by WNT-7a signalling. *Cell* 100, 525-535.

Hall, Z. W. and Sanes, J. R. (1993). Synaptic structure and development: The neuromuscular junction. *Cell/Neuron (Suppl.)* 72/10, 99-121.

Halpern, M. E., Chiba, A., Johansen, J. and Keshishian, H. (1991). Growth cone behaviour underlying the development of stereotypic synaptic connections in *Drosophila* embryos. *J. Neurosci.* 11, 3227-3238.

Harper, J. W., Adami, G. R., Wei, N., Keyomarsi, K. and Elledge, S. J. (1993). The p21 Cdk-interacting protein Cip1 is a potent inhibitor of G1 cyclin-dependent kinases. *Cell* 75, 805-16.

Hartenstein, V. (1988). Development of *Drosophila* larval sensory organs: spatiotemporal pattern of sensory neurones, peripheral axonal pathways and sensilla differentiation. *Development* 102, 869-886.

Hashida-Okumura, A., Okumura, N., Iwamatsu, A., Buijs, R. M., Romijn, H. J. and Nagai, K. (1999). Interaction of neuronal nitric-oxide synthase with alpha1-syntrophin in rat brain. *J Biol Chem* 274, 11736-41.

Hashimoto, S., Tsubouchi, A., Mazaki, Y. and Sabe, H. (2001). Interaction of paxillin with p21-activated Kinase (PAK). Association of paxillin alpha with the kinase-inactive and the Cdc42-activated forms of PAK3. *J Biol Chem* 276, 6037-45.

Hatzfeld, M. (1999). The armadillo family of structural proteins. *Int Rev Cytol* 186, 179-224.

Herreros, L., Rodriguez-Fernandez, J. L., Brown, M. C., Alonso-Lebrero, J. L., Cabanas, C., Sanchez-Madrid, F., Longo, N., Turner, C. E. and Sanchez-Mateos, P. (2000). Paxillin localizes to the lymphocyte microtubule organizing center and associates with the microtubule cytoskeleton. *J. Biol. Chem.* 275, 26436-26440.

Hildebrand, J. D., Schaller, M. D. and Parsons, J. T. (1995). Paxillin, a tyrosine phosphorylated focal adhesion-associated protein binds to the carboxyl terminal domain of focal adhesion kinase. *Mol Biol Cell* 6, 637-47.

Hopkinson, S. B. and Jones, J. C. (2000). The N terminus of the transmembrane protein BP180 interacts with the N-terminal domain of BP230, thereby mediating keratin cytoskeleton anchorage to the cell surface at the site of the hemidesmosome. *Mol Biol Cell* 11, 277-86.

Houseweart, M. K. and Cleveland, D. W. (1999). Cytoskeletal linkers: new MAPs for old destinations. *Curr. Biol.* 9, R864-R866.

Huang, C., Borchers, C. H., Schaller, M. D. and Jacobson, K. (2004). Phosphorylation of paxillin by p38MAPK is involved in the neurite extension of PC-12 cells. *J Cell Biol* 164, 593-602.

Huang, C., Rajfur, Z., Borchers, C., Schaller, M. D. and Jacobson, K. (2003). JNK phosphorylates paxillin and regulates cell migration. *Nature* 424, 219-23.

Ilic, D., Furuta, Y., Kanazawa, S., Takeda, N., Sobue, K., Nakatsuji, N., Nomura, S., Fujimoto, J., Okada, M. and Yamamoto, T. (1995). Reduced cell motility and enhanced focal adhesion contact formation in cells from FAK-deficient mice. *Nature* 377, 539-44.

Ito, K., Urban, J. and Technau, G. M. (1995). Distribution, classification, and development of *Drosophila* glial cells in the late embryonic and early larval ventral nerve cord. *Roux's Arch. Dev. Biol.* 204, 284-307.

Ivankovic-Dikic, I., Gronroos, E., Blaukat, A., Barth, B. U. and Dikic, I. (2000). Pyk2 and FAK regulate neurite outgrowth induced by growth factors and integrins. *Nat Cell Biol* 2, 574-81.

James, P., Halladay, J. and Craig, E. A. (1996). Genomic libraries and a host strain designed for highly efficient two-hybrid selection in yeast. *Genetics* 144, 1425-36.

Johansen, J., Halpern, M. E., Johansen, K. and Keshishian, H. (1989). Stereotypic morphology of glutamatergic synapses on identified muscle cells of *Drosophila* larvae. *J. Neurosci.* 9, 710-725.

Joiner, M. A. and Griffith, L. C. (2000). Visual input regulates circuit configuration in courtship conditioning of *Drosophila melanogaster*. *Learn Mem* 7, 32-42.

Kalman, M. and Szabo, A. (2001). Immunohistochemical investigation of actin-anchoring proteins vinculin, talin and paxillin in rat brain following lesion: a moderate reaction, confined to the astroglia of brain tracts. *Exp Brain Res* 139, 426-34.

Karakesisoglou, I., Yang, Y. and Fuchs, E. (2000). An epidermal plakin that integrates actin and microtubule networks at cellular junctions. *J. Cell Biol.* 149, 195-208.

Kaufmann, N., Wills, Z. P. and Van Vactor, D. (1998). *Drosophila* Rac1 controls motor axon guidance. *Development* 125, 453-461.

Keshishian, H., Broadie, K., Chiba, A. and Bate, M. (1996). The *Drosophila* neuromuscular junction: A model system for studying synaptic development and function. *Annu. Rev. Neurosci.* 19, 545-575.

Kim, M. D., Kamiyama, D., Kolodziej, P., Hing, H. and Chiba, A. (2003). Isolation of Rho GTPase effector pathways during axon development. *Dev Biol* 262, 282-93.

Klagges, B. R. E., Heimbeck, G., Godenschwege, T. A., Hofbauer, A., Pflugfelder, G. O., Reifegerste, R., Reisch, D., Schaupp, M., Buchner, S. and Buchner, E. (1996). Invertebrate Synapsins: a single gene codes for several isoforms in *Drosophila*. *J. Neurosci.* 16, 3154-3165.

Knust, E. (2000). Control of epithelial cell shape and polarity. *Curr Opin Genet Dev* 10, 471-5.

Kodama, A., Karakesisoglou, I., Wong, E., Vaezi, A. and Fuchs, E. (2003). ACF7: an essential integrator of microtubule dynamics. *Cell* 115, 343-54.

Küppers, B., Sánchez-Soriano, N., Letzkus, J., Technau, G. M. and Prokop, A. (2002). In developing *Drosophila* neurons GABA production is tightly regulated downstream of Gad translation and can be influenced by calcium. *J. Neurochem.*, submitted.

Landgraf, M., Bossing, T., Technau, G. M. and Bate, M. (1997). The origin, location, and projection of the embryonic abdominal motorneurons of *Drosophila*. *J. Neurosci.* 17, 9642-9655.

Landgraf, M., Sanchez-Soriano, N., Technau, G. M., Urban, J. and Prokop, A. (2003). Charting the Drosophila neuropile: a strategy for the standardised characterisation of genetically amenable neurites. *Dev Biol* 260, 207-25.

Lee, S., Harris, K.-L., Whitington, P. M. and Kolodziej, P. A. (2000a). *short stop* is allelic to *kakapo*, and encodes rod-like cytoskeletal-associated proteins required for axon extension. *J. Neurosci.* 20, 1096-1108.

Lee, S. and Kolodziej, P. A. (2002a). The plakin Short Stop and the RhoA GTPase are required for E-cadherin- dependent apical surface remodeling during tracheal tube fusion. *Development* 129, 1509-1520.

Lee, S. and Kolodziej, P. A. (2002b). Short Stop provides an essential link between F-actin and microtubules during axon extension. *Development* 129, 1195-1204.

Lee, T. and Luo, L. (1999). Mosaic analysis with a repressible neurotechnique cell marker for studies of gene function in neuronal morphogenesis. *Neuron* 22, 451-461.

Lee, T., Winter, C., Marticke, S. S., Lee, A. and Luo, L. (2000b). Essential roles of *Drosophila* RhoA in the regulation of neuroblast proliferation and dendritic but not axonal morphogenesis. *Neuron* 25, 307-316.

Leung, C. L., Green, K. J. and Liem, R. K. (2002). Plakins: a family of versatile cytolinker proteins. *Trends Cell Biol.* 12, 37-45.

Leung, C. L., Sun, D., Zheng, M., Knowles, D. R. and Liem, R. K. H. (1999). Microtubule actin cross-linking factor (MACF): A hybrid of dystonin and dystrophin that can interact with the actin and microtubule cytoskeleton. *J. Cell Biol.* 147, 1275-1285.

Li, H., Chaney, S., Forte, M. and Hirsh, J. (2000). Ectopic G-protein expression in dopamine and serotonin neurons blocks cocaine sensitization in *Drosophila melanogaster* (Erratum: Curr. Biol.10, R393, 2000). *Curr. Biol.* 10, 211-214.

Lin, C. H. and Forscher, P. (1995). Growth cone advance is inversely proportional to retrograde F-actin flow. *Neuron* 14, 763-771.

Lin, D. M. and Goodman, C. S. (1994). Ectopic and increased expression of Fasciclin II alters motoneuron growth cone guidance. *Neuron* 13, 507-523.

Lindsley, D. C. u. Z., G. G. The genome of Drosophila melanogaster. (1992). The genome of Drosophila melanogaster. San Diego New York Boston London Sydney Tokyo Toronto: Academic Press Inc.

Littleton, J. T., Bellen, H. J. and Perin, M. S. (1993a). Expression of synaptotagmin in *Drosophila* reveals transport and localization of synaptic vesicles to the synapse. *Development* 118, 1077-1088.

Littleton, J. T., Stern, M., Schulze, K., Perin, M. and Bellen, H. J. (1993b). Mutational analysis of Drosophila synaptotagmin demonstrates its essential role in Ca^{2+}-activated neurotransmitter release. *Cell* 74, 1125-1134.

Löhr, R., Godenschwege, T., Buchner, E. and Prokop, A. (2002). Compartmentalisation of central neurons in *Drosophila*: a new strategy of mosaic analysis reveals localisation of pre-synaptic sites to specific segments of neurites. *J. Neurosci.*, in press.

Lu, M., Witke, W., Kwiatkowski, D. J. and Kosik, K. S. (1997). Delayed retraction of filopodia in gelsolin null mice. *J. Cell Biol.* 138, 1279-1287.

Luo, L. (2000). Rho GTPases in neuronal morphogenesis. *Nat. Rev. Neurosci.* 1, 173-180.

Luo, L., Jan, L. Y. and Jan, Y. N. (1997). Rho family small GTP-binding proteins in growth cone signalling. *Curr. Opin. Neurobiol.* 7, 81-86.

Luo, L., Liao, Y. J., Jan, L. Y. and Jan, Y. N. (1994). Distinct morphogenetic functions of similar small GTPases: *Drosophila* Drac1 is involved in axonal outgrowth and myoblast fusion. *Genes Dev.* 8, 1787-1802.

Mazaki, Y., Uchida, H., Hino, O., Hashimoto, S. and Sabe, H. (1998). Paxillin isoforms in mouse. Lack of the gamma isoform and developmentally specific beta isoform expression. *J Biol Chem* 273, 22435-41.

Medley, Q. G., Buchbinder, E. G., Tachibana, K., Ngo, H., Serra-Pages, C. and Streuli, M. (2003). Signaling between focal adhesion kinase and trio. *J Biol Chem* 278, 13265-70.

Mettler, U. (2002). Untersuchungen zur möglichen Funktion der kleinen GTPasen und anderer Gene bei der Synapsenbildung in der Fruchtfliege Drosophila melanogaster. *Diplomarbeit, FB Biologie, Johannes Gutenberg Universität Mainz*.

Minden, A., Lin, A., Claret, F. X., Abo, A. and Karin, M. (1995). Selective activation of the JNK signaling cascade and c-Jun transcriptional activity by the small GTPases Rac and Cdc42Hs. *Cell* 81, 1147-57.

Morrison, E. E., Moncur, P. M. and Askham, J. M. (2002). EB1 identifies sites of microtubule polymerisation during neurite development. *Brain Res Mol Brain Res* 98, 145-52.

Murakami, H., Iwashita, T., Asai, N., Iwata, Y., Narumiya, S. and Takahashi, M. (1999). Rho-dependent and -independent tyrosine phosphorylation of focal adhesion kinase, paxillin and p130Cas mediated by Ret kinase. *Oncogene* 18, 1975-82.

Murthy, V. N. and De Camilli, P. (2003). Cell biology of the presynaptic terminal. *Annu Rev Neurosci* 26, 701-28.

Nakamura, K., Yano, H., Uchida, H., Hashimoto, S., Schaefer, E. and Sabe, H. (2000). Tyrosine phosphorylation of paxillin alpha is involved in temporospatial regulation of paxillin-

containing focal adhesion formation and F-actin organization in motile cells. *J Biol Chem* 275, 27155-64.

Ng, J., Nardine, T., Harms, M., Tzu, J., Goldstein, A., Sun, Y., Dietzl, G., Dickson, B. J. and Luo, L. (2002). Rac GTPases control axon growth, guidance and branching. *Nature* 416, 442-447.

Nikolopoulos, S. N. and Turner, C. E. (2000). Actopaxin, a new focal adhesion protein that binds paxillin LD motifs and actin and regulates cell adhesion. *J. Cell. Biol.* 151, 1435-1448.

Noakes, P. G., Gautam, M., Mudd, J., Sanes, J. R. and Merlie, J. P. (1995). Aberrant differentiation of neuromuscular junctions in mice lacking s-laminin/laminin ß2. *Nature* 374, 258-262.

Oktay, M., Wary, K. K., Dans, M., Birge, R. B. and Giancotti, F. G. (1999). Integrin-mediated activation of focal adhesion kinase is required for signaling to Jun NH2-terminal kinase and progression through the G1 phase of the cell cycle. *J Cell Biol* 145, 1461-9.

Okuda, T., Matsuda, S., Nakatsugawa, S., Ichigotani, Y., Iwahashi, N., Takahashi, M., Ishigaki, T. and Hamaguchi, M. (1999). Molecular cloning of Macrophin, a human homologue of *Drosophila* Kakapo with a close structural similarity to Plectin and Dystrophin. *Biochem. Biophys. Res. Comm.* 264, 568-574.

Okumura, M., Yamakawa, H., Ohara, O. and Owaribe, K. (2002). Novel alternative splicings of BPAG1 (bullous pemphigoid antigen 1) including the domain structure closely related to MACF (microtubule actin cross-linking factor). *J. Biol. Chem.* 277, 6682-6687.

Patel, N. H. (1994). Imaging neuronal subsets and other cell types in whole-mount Drosophila embryos and larvae using antibody probes. *Methods Cell Biol* 44, 445-87.

Patton, B. L., Chiu, A. Y. and Sanes, J. R. (1998). Synaptic laminin prevents glial entry into the synaptic cleft. *Nature* 393, 698-701.

Person, W. R., Wood, T., Zhang, Z. and Miller, W. (1997). Comparison of DNA sequences with protein sequences. *Genomics* 46, 24-36.

Petit, V., Boyer, B., Lentz, D., Turner, C. E., Thiery, J. P. and Valles, A. M. (2000). Phosphorylation of tyrosine residues 31 and 118 on paxillin regulates cell migration through an association with CRK in NBT-II cells. *J Cell Biol* 148, 957-70.

Polonchuk, L., Elbel, J., Eckert, L., Blum, J., Wintermantel, E. and Eppenberger, H. M. (2000). Titanium dioxide ceramics control the differentiated phenotype of cardiac muscle cells in culture. *Biomaterials* 21, 539-50.

Prokop, A. (1999). Integrating bits and pieces - synapse formation in *Drosophila* embryos. *Cell Tissue Res.* 297, 169-186.

Prokop, A., Landgraf, M., Rushton, E., Broadie, K. and Bate, M. (1996). Presynaptic development at the *Drosophila* neuromuscular junction: The assembly and localisation of presynaptic active zones. *Neuron* 17, 617-626.

Prokop, A., Martín-Bermudo, M. D., Bate, M. and Brown, N. (1998a). Absence of PS integrins or laminin A affects extracellular adhesion, but not intracellular assembly, of hemiadherens and neuromuscular junctions in *Drosophila* embryos. *Dev. Biol.* 196, 58-76.

Prokop, A., Uhler, J., Roote, J. and Bate, M. C. (1998b). The *kakapo* mutation affects terminal arborisation and central dendritic sprouting of *Drosophila* motorneurons. *J. Cell Biol.* 143, 1283-1294.

Ranjan, R., Bronk, P. and Zinsmaier, K. E. (1998). Cysteine string protein is required for calcium secretion coupling of evoked neurotransmission in drosophila but not for vesicle recycling. *J Neurosci* 18, 956-64.

Rao, A., Cha, E. M. and Craig, A. M. (2000). Mismatched appositions of presynaptic and postsynaptic components in isolated hippocampal neurons. *J. Neurosci.* 20, 8344-8353.

Richmond, J. E. and Broadie, K. S. (2002). The synaptic vesicle cycle: exocytosis and endocytosis in Drosophila and C. elegans. ***Curr Opin Neurobiol*** **12, 499-507.**

Ridley, A. J. and Hall, A. (1992). The small GTP-binding protein rho regulates the assembly of focal adhesions and actin stress fibers in response to growth factors. ***Cell*** **70, 389-99.**

Ridley, A. J., Paterson, H. F., Johnston, C. L., Diekmann, D. and Hall, A. (1992). The small GTP-binding protein rac regulates growth factor-induced membrane ruffling. ***Cell*** **70, 401-10.**

Rigaut, G., Shevchenko, A., Rutz, B., Wilm, M., Mann, M. and Seraphin, B. (1999). A generic protein purification method for protein complex characterization and proteome exploration. ***Nat Biotechnol*** **17, 1030-2.**

Rodesch, C. K. and Broadie, K. (2000). Genetic studies in ***Drosophila*****: vesicle pools and cytoskeleton-based regulation of synaptic transmission.** ***Neuroreport*** **11, R45-53.**

Rohrbough, J., Pinto, S., Mihalek, R. M., Tully, T. and Broadie, K. (1999). latheo, a Drosophila gene involved in learning, regulates functional synaptic plasticity. ***Neuron*** **23, 55-70.**

Röper, K., Gregory, S. L. and Brown, N. H. (2002). The 'spectraplakins': cytoskeletal giants with characteristics of both spectrin and plakin families. ***J Cell Sci*** **115, 4215-25.**

Rüegg, M. A. and Bixby, J. L. (1998). Agrin orchestrates synaptic differentiation at the vertebrate neuromuscular junction. ***Trends Neurosci.*** **21, 22-27.**

Ruether, K., Grosse, J., Matthiessen, E., Hoffmann, K. and Hartmann, C. (2000). Abnormalities of the photoreceptor-bipolar cell synapse in a substrain of C57BL/10 mice. ***Invest. Ophthalmol. Vis. Sci.*** **41, 4039-4047.**

Ruhrberg, C. and Watt, F. M. (1997). The plakin family: versatile organizers of cytoskeletal architecture. ***Curr. Opin. Genet. Dev.*** **7, 392-397.**

Sabe, H., Hata, A., Okada, M., Nakagawa, H. and Hanafusa, H. (1994). Analysis of the binding of the Src homology 2 domain of Csk to tyrosine-phosphorylated proteins in the suppression and mitotic activation of c-Src. ***Proc Natl Acad Sci U S A*** **91, 3984-8.**

Salgia, R., Li, J. L., Lo, S. H., Brunkhorst, B., Kansas, G. S., Sobhany, E. S., Sun, Y., Pisick, E., Hallek, M., Ernst, T. et al. (1995). Molecular cloning of human paxillin, a focal adhesion protein phosphorylated by P210BCR/ABL. ***J Biol Chem*** **270, 5039-47.**

Sambrook, J., Russell, D. W. and Sambrook, J. (2001). Molecular Cloning: A Laboratory Approach. Cold Spring Harbor, New York, USA: Cold Spring Harbor Laboratory Press.

Sanes, J. R. and Lichtman, J. W. (1999). Development of the vertebrate neuromuscular junction. ***Annu Rev Neurosci*** **22, 389-442.**

Scheiffele, P., Fan, J., Choih, J., Fetter, R. and Serafini, T. (2000). Neuroligin expressed in nonneuronal cells triggers presynaptic development in contacting axons. ***Cell*** **101, 657-669.**

Schmitz, F., Konigstorfer, A. and Sudhof, T. C. (2000). RIBEYE, a component of synaptic ribbons: a protein's journey through evolution provides insight into synaptic ribbon function. ***Neuron*** **28, 857-872.**

Sepp, K. J. and Auld, V. J. (2003). RhoA and Rac1 GTPases mediate the dynamic rearrangement of actin in peripheral glia. ***Development*** **130, 1825-35.**

Sherrington, C. (1906). The integrative action of the nervous system. New Haven: Yale University Press.

Sink, H. and Whitington, P. M. (1991). Location and connectivity of abdominal motoneurons in the embryo and larva of ***Drosophila melanogaster*****.** ***J. Neurobiol.*** **22, 398-311.**

Smith, E. A. and Fuchs, E. (1998). Defining the interactions between intermediate filaments and desmosomes. ***J Cell Biol*** **141, 1229-41.**

Sone, M. (1997). Still life, a protein in synaptic terminals of *Drosophila* homologous to GDP-GTP exchangers. *Science* 275, 543-547.

Sotillos, S. and Campuzano, S. (2000). DRacGAP, a novel Drosophila gene, inhibits EGFR/Ras signalling in the developing imaginal wing disc. *Development* 127, 5427-38.

Stanyon, C. A. and Finley, R. L., Jr. (2000). Progress and potential of Drosophila protein interaction maps. *Pharmacogenomics* 1, 417-31.

Steinbock, F. A. and Wiche, G. (1999). Plectin: a cytolinker by design. *Biol Chem* 380, 151-8.

Strumpf, D. and Volk, T. (1998). Kakapo, a novel *Drosophila* protein, is essential for the restricted localization of the neuregulin-like factor, Vein, at the muscle-tendon junctional site. *J. Cell Biol.* 143, 1259-1270.

Subramanian, A., Prokop, A., Yamamoto, M., Sugimura, K., Uemura, T., Betschinger, J., Knoblich, J. A. and Volk, T. (2003). Shortstop recruits EB1/APC1 and promotes microtubule assembly at the muscle-tendon junction. *Curr Biol* 13, 1086-95.

Suter, D. M. and Forscher, P. (1998). An emerging link between cytoskeletal dynamics and cell adhesion molecules in growth cone guidance. *Curr. Opin. Neuorbiol.* 8, 106-116.

Thomas, U., Ebitsch, S., Gorczyca, M., Koh, Y. H., Hough, C. D., Woods, D., Gundelfinger, E. D. and Budnik, V. (2000). Synaptic targeting and localization of discs-large is a stepwise process controlled by different domains of the protein. *Curr. Biol.* 10, 1108-1117.

Thomas, U., Kim, E., Kuhlendahl, S., Koh, Y. H., Gundelfinger, E. D., Sheng, M., Garner, C. C. and Budnik, V. (1997). Synaptic clustering of the cell adhesion molecule fasciclin II by discs-large and its role in the regulation of presynaptic structure. *Neuron* 19, 787-799.

Tirnauer, J. S. and Bierer, B. E. (2000). EB1 proteins regulate microtubule dynamics, cell polarity, and chromosome stability. *J Cell Biol* 149, 761-6.

Turner, C. E. (1994). Paxillin: a cytoskeletal target for tyrosine kinases. *BioEssays* 16, 47-52.

Turner, C. E. (1998). Paxillin. *Int J Biochem Cell Biol* 30, 955-9.

Turner, C. E. (2000a). Paxillin and focal adhesion signalling. *Nat. Cell Biol.* 2, E231-E236.

Turner, C. E. (2000b). Paxillin interactions. *J. Cell Sci.* 113 Pt 23, 4139-4140.

Turner, C. E., Brown, M. C., Perrotta, J. A., Riedy, M. C., Nikolopoulos, S. N., McDonald, A. R., Bagrodia, S., Thomas, S. and Leventhal, P. S. (1999). Paxillin LD4 motif binds PAK and PIX through a novel 95-kD ankyrin repeat, ARF-GAP protein: A role in cytoskeletal remodeling. *J Cell Biol* 145, 851-63.

Turner, C. E., Glenney, J. R., Jr. and Burridge, K. (1990). Paxillin: a new vinculin-binding protein present in focal adhesions. *J Cell Biol* 111, 1059-68.

Turner, C. E., Kramarcy, N., Sealock, R. and Burridge, K. (1991). Localization of paxillin, a focal adhesion protein, to smooth muscle dense plaques, and the myotendinous and neuromuscular junctions of skeletal muscle. *Exp Cell Res* 192, 651-5.

Turner, C. E. and Miller, J. T. (1994). Primary sequence of paxillin contains putative SH2 and SH3 domain binding motifs and multiple LIM domains: identification of a vinculin and pp125Fak-binding region. *J Cell Sci* 107 (Pt 6), 1583-91.

Vallenius, T., Luukko, K. and Makela, T. P. (2000). CLP-36 PDZ-LIM protein associates with nonmuscle alpha-actinin-1 and alpha-actinin-4. *J Biol Chem* 275, 11100-5.

Van Aelst, L. and D'Souza-Schorey, C. (1997). Rho GTPases and signaling networks. *Genes Dev* 11, 2295-322.

vanVactor, D. V., Sink, H., Fambrough, D., Tsoo, R. and Goodman, C. S. (1993). Genes that control neuromuscular specificity in *Drosophila*. *Cell* 73, 1137-1153.

Verkhusha, V. V., Tsukita, S. and Oda, H. (1999). Actin dynamics in lamellipodia of migrating border cells in the Drosophila ovary revealed by a GFP-actin fusion protein. ***FEBS Lett*** **445, 395-401.**

Voas, M. G. and Rebay, I. (2004). Signal integration during development: insights from the Drosophila eye. ***Dev Dyn*** **229, 162-75.**

Weber, K., Riemer, D. and Dodemont, H. (1991). Aspects of the evolution of the lamin/intermediate filament protein family: a current analysis of invertebrate intermediate filament proteins. ***Biochem. Soc. Trans.*** **19, 1021-1023.**

Weigmann, K., Klapper, R., Strasser, T., Rickert, C., Technau, G., Jackle, H., Janning, W. and Klambt, C. (2003). FlyMove--a new way to look at development of Drosophila. ***Trends Genet*** **19, 310-1.**

Wheeler, G. N. and Hynes, R. O. (2001). The cloning, genomic organization and expression of the focal contact protein paxillin in ***Drosophila*****.** ***Gene*** **262, 291-299.**

Wolf, B., Seeger, M. and Chiba, A. (1998). Commissureless endocytosis is correlated with neuromuscular synapse initiation. ***Development*** **125, 3853-3863.**

Wucherpfennig, T., Wilsch-Brauninger, M. and Gonzalez-Gaitan, M. (2003). Role of Drosophila Rab5 during endosomal trafficking at the synapse and evoked neurotransmitter release. ***J Cell Biol*** **161, 609-24.**

Xia, Y., Makris, C., Su, B., Li, E., Yang, J., Nemerow, G. R. and Karin, M. (2000). MEK kinase 1 is critically required for c-Jun N-terminal kinase activation by proinflammatory stimuli and growth factor-induced cell migration. ***Proc Natl Acad Sci U S A*** **97, 5243-8.**

Yagi, R., Ishimaru, S., Yano, H., Gaul, U., Hanafusa, H. and Sabe, H. (2001). A novel muscle LIM-only protein is generated from the paxillin gene locus in ***Drosophila*****.** ***EMBO Rep.*** **2, 814-820.**

Yang, Y., Dowling, J., Yu, Q. C., Kouklis, P., Cleveland, D. W. and Fuchs, E. (1996). An essential cytoskeletal linker protein connecting actin microfilaments to intermediate filaments. ***Cell*** **86, 655-65.**

Yano, H., Uchida, H., Iwasaki, T., Mukai, M., Akedo, H., Nakamura, K., Hashimoto, S. and Sabe, H. (2000). Paxillin alpha and Crk-associated substrate exert opposing effects on cell migration and contact inhibition of growth through tyrosine phosphorylation. ***Proc Natl Acad Sci U S A*** **97, 9076-81.**

Yarnitzky, T., Min, L. and Volk, T. (1997). The ***Drosophila*** **neuregulin homolog vein mediates inductive interactions between myotubes and their epidermal attachment cells.** ***Genes Dev.*** **11, 2691-2700.**

Yeh, E., Gustafson, K. and Boulianne, G. L. (1995). Green fluorescent protein as a vital marker and reporter of gene expression in ***Drosophila*****.** ***Proc. Natl. Acad. Sci. U S A*** **92, 7036-7040.**

Versicherung gemäß §11 Abs. 3d der Promotionsordnung vom 22.12.2002

1) Ich habe die jetzt als Dissertation vorgelegte Arbeit selbst angefertigt und alle benutzten Hilfsmittel (Literatur, Apparaturen, Material) in der Arbeit angegeben.

2) Ich habe und hatte die jetzt als Dissertation vorgelegte Arbeit nicht als Prüfungsarbeit für eine staatliche oder andere wissenschaftliche Prüfung eingereicht.

3) Ich hatte weder die jetzt als Dissertation vorgelegte Arbeit noch Teile einer Abhandlung davon bei einer anderen Fakultät bzw. einem anderen Fachbereich als Dissertation eingereicht.

Mainz, den **----------**

(Michael Mende)

ABBREVIATIONS

ABD	actin binding domain
aCC	anterior corner cell
ACF7	actin and microtubule crosslinking factor 7
AD	activating domain
AP	alkaline phosphatase
B&B	Broadie and Bate buffer
BCIP	5-bromo-4-chloro-3-indolyl phosphate
bd	bipolar dendrite
BD	binding domain
BPAG1	Bullous Pemphigoid Antigen 1
CA	constitutive active
Cdc42	cell division cycle 42
CNS	central nervous system
cDNA	complementary DNA
DAB	diaminobenzidine
DCdc42	*Drosophila* Cdc42
DDC	*Dopa decarboxylase*
ddNTPs	dideoxynucleotides
Df	deficiency
DLG	Disc large
DN	dominant negative
DNA	deoxyribonucleotide acid
DPxn	*Drosophila* Paxillin
DRac1	Drosophila Rac
dsRNA	double stranded RNA
DTT	dithiothreitol
EB1	End-binding protein 1
EGF/NGF	epidermal/nerve growth factor
elaV	*embryonic lethal, abnormal vision*
es	external sensory neurones
eve	*even skipped*
FAK	Focal adhesion kinase
FasII/III	Fasciclin II/III
GEF	guanine nucleotide exchange factor
GFP	green fluorescent protein
GT	TAP-tagged Gas2 homology protein domain of Shot
GUK	guanylate kinase
HRP	horse radish peroxydase
ISN	intersegmental nerve
JNK	c-Jun amino terminal Kinase
Kak	Kakapo
Kbp	Kilo base pairs
kDA	kilo Dalton
LD	leucine rich domain
LIM	acronym for characteristic cysteine and histidine rich, zinc-coordinating domain, first described in transcription factors Lin-1, Isl-1 and Mec-3
MACF1	human microtubule and actin crosslinking factor 1 (formerly ACF7)
mACF7	mouse actin and microtubule crosslinking factor 7
MAGUKs	membrane associated guanylate kinases
md	multiple dendrite
mef2	*myocyte enhancer factor 2*
mRNA	messenger RNA
MT	Microtubules
MTJ	myotendineous junction

mys	*myspheroid*
NBT	nitro blue tetrazolium chloride
N-CAM	neural cell adhesion molecule
NMJ	neuromuscular junction
OP	optical density
ORF	open reading frame
P95 PKL	Paxillin Kinase Linker, 95kDA
PAGE	polyacrylamide gel electrophoresis
PAT	TAP-tagged ABD and Plakin protein domain of Shot
PAK	p21 activated kinase
pax	paxillin
PBS	phosphate buffered saline
PBT	PBS with Tween-20
PCR	polymerase chain reaction
PDZ	acronym for PSD95, DLG, and ZO1
PNS	peripheral nervous system
PS	position specific
PSD95/SAP90	post synaptic density 95/synapse associated protein 90
PT	TAP-tagged Plakin protein domain of Shot
PVDF	polyvinylidene fluoride
Rac1	Ras related C3 botulinum toxin substrate 1
Rho	Ras homologue A
RNA	ribonucleotide acid
RNAi	RNA interference
RP2	Royal Prawn 2
rpm	rounds per minute
RTK	receptor tyrosine kinase
sc	scolopidial sensory neurones
SD	synthetic dropout
SDS	sodium dodecyl sulphate
Shot	short stop
SNa/b/c/d	segmental nerve a/b/c/d
Syn	synapsin
Syt	synaptotagmin
Taq	*Thermus aquaticus*
TBS	Tris buffered saline
TE	Tris-EDTA buffer
TAE	Tris-Acetate-EDTA buffer
Tris	Tris Hydroxymethylaminoethane
tub	tubulin
UAS	upstream activating site
VL	ventral lateral muscles
VUM	*ventral unpaired median*
WMW-test	Wilcoxon-Mann-Whitney-test
ZO1	zonula occludens 1

ACKNOWLEDGEMENTS

This work was funded by the German Israeli Foundation for Scientific Research and Development (I073-203.05/98).